From RF-microsystem technology to RF-nanotechnology

Fabio Coccetti

Habilitation à Diriger des Recherches
Institut National Polytechnique de Toulouse

Préparée au
Laboratoire d'Analyse et d'Architecture des Systèmes du CNRS

Par

Fabio COCCETTI

Chercheur Associé au LAAS/CNRS Toulouse
Ingénieur de Recherche chez Fialab – Toulouse

From RF-Microsystem Technology to RF-Nanotechnology

Date de soutenance, 6 décembre 2013 devant la commission d'examen composée de :

Président :	Prof. Gilles DAMBRINE (IEMN –Université de Lille1)
Rapporteurs :	Prof. Pierre BLONDY (XLim –Université de Limoge) Prof. Philippe FERRARI (IMEP-LAHC – INPG-UJF) Prof. Roberto SORRENTINO (Università di Perugia)
Examinateurs:	Dr. Jean Louis CAZAUX (ThalesAleniaSpace) Prof. Luca PIERANTONI (Università Politecnica delle Marche) Prof. Robert PLANA (ALSTOM – UPS)
Invités:	Dr. Xavier LAFONTAN (Intesens) Dr. Patrick PONS (CNRS-LAAS)
Garant :	Prof. Hervé AUBERT (INP Toulouse – CNRS-LAAS)

to my beloved

Parents

and

Lisa

TITLE

From RF-Microsystem Technology To RF-Nanotechnology

the way toward « nano » - enabled RF- intelligence
…exploiting the « room at the bottom »[1]

Subtitle:

Limits and opportunity of multiphysics / multidisciplinarity in MST

MST's legacy toward RF Nanotechnology

From top-down miniaturization to bottom-up nanosystems.

Toward the CNT molecular radio.

Bridging the THz gap and energy efficient autonomous integrated systems for future nano-enabled cognitive systems

Inspired by:

** « ***There's Plenty of Room at the Bottom, an invitation to enter a new field of physics*»** is the title of a lecture given by physicist Richard Feynman at an American Physical Society meeting at Caltech on December 29, 1959[1].

[1] « **There's Plenty of Room at the Bottom, an invitation to enter a new field of physics»** is the title of a lecture given by physicist Richard Feynman at an American Physical Society meeting at Caltech on December 29, 1959.
Feynman considered a number of interesting ramifications of a general ability to manipulate matter on an atomic scale. He was particularly interested in the possibilities of denser computer circuitry, and microscopes which could see things much smaller than is possible with scanning electron microscopes. These ideas were later realized by the use of the scanning tunneling microscope, the atomic force microscope and other examples of probe microscopy and storage systems such as Millipede, created by researchers at IBM.
Feynman also suggested that it should be possible, in principle, to make nanoscale machines that "arrange the atoms the way we want", and do chemical synthesis by mechanical manipulation. He also presented the "weird possibility" of "swallowing the doctor," an idea which he credited in the essay to his friend and graduate student Albert Hibbs. This concept involved building a tiny, swallowable surgical robot by developing a set of one-quarter-scale manipulator hands slaved to the operator's hands to build one-quarter scale machine tools analogous to those found in any machine shop. This set of small tools would then be used by the small hands to build and operate ten sets of one-sixteenth-scale hands and tools, and so forth, culminating in perhaps a billion tiny factories to achieve massively parallel operations. He uses the analogy of a pantograph as a way of scaling down items. This idea was anticipated in part, down to the microscale, by science fiction author Robert A. Heinlein in his 1942 story *Waldo*.
As the sizes got smaller, one would have to redesign some tools, because the relative strength of various forces would change. Although gravity would become unimportant, surface tension would become more important, Van der Waals attraction would become important, etc. Feynman mentioned these scaling issues during his talk. Nobody has yet attempted to implement this thought experiment, although it has been noted that some types of biological enzymes and enzyme complexes (especially ribosomes) function chemically in a way close to Feynman's vision.

There's plenty of room at the bottom, says noted scientist as he reveals—

How to Build an Automobile

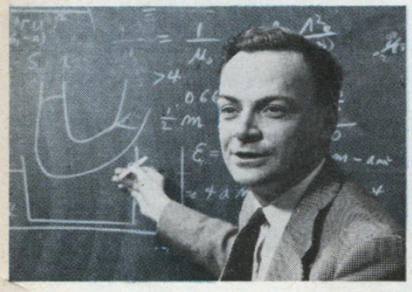

At 42, Richard Phillips Feynman, Ph.D., enjoys world renown as a theoretical physicist, local fame as a "marvelous" performer on the bongo drums, and campus admiration as a man with a pixyish humor that turns a lecture on quantum electrodynamics into a ball. You'll see why when you read his impassioned and witty plea to think small.

This tall, slim, dark-haired scholar helped importantly in developing the atomic bomb and watched its first test explosion. In 1954 he won the $15,000 Albert Einstein Award, one of the nation's highest scientific honors.

He is capable both of exuberant fellowship and of rather stern withdrawal, especially when pondering intricate problems. Even his heavy thinking has a light touch, however. In deepest thought, while pacing the floor, he slowly flips a silver dollar back and forth across the fingers of his right hand by carefully controlled movements of the knuckles. It's no easy trick even when you have nothing else to think about.

Born in New York City in 1918, he graduated from MIT in 1939 and got his Ph.D. at Princeton in 1942. He was a member of the Laboratory of Nuclear Studies at Cornell from 1945 to 1950. In 1950, he began his present job as professor of theoretical physics at Caltech.

Dr. Feynman loves music, children, camping in the wilds, and unpremeditated jaunts to faraway places. He boned up on Portuguese to become a visiting lecturer for two seasons in Brazil, and learned Spanish under forced draft to go to Peru and poke around Inca ruins.

The accompanying article is condensed from a speech (addressed to an American Physical Society meeting, not the Pasadena Rotary luncheon). The full transcript appeared in "Engineering and Science Magazine," published at the California Institute of Technology.

Exploring the fantastic possibilities of the very small should pay off handsomely—and provide a lot of fun, too

By Richard P. Feynman

Professor of Theoretical Physics, California Institute of Technology

PEOPLE tell me about miniaturization, about electric motors the size of the nail on your small finger. There is a device on the market by which you can write the Lord's Prayer on the head of a pin. But that's nothing. That's the most primitive, halting step.

Why not write the entire 24 volumes of the "Encyclopaedia Britannica" on the head of a pin?

Let's see what would be involved. The head of a pin is a sixteenth of an inch across. If you magnify it 25,000 diameters, the area of the head of the pin is equal to the area of all pages of the encyclopedia. All it is necessary to do is to reduce the writing in the encyclopedia 25,000 times. Is that possible? One of the little dots on the fine halftone reproductions in the encyclopedia, when you demagnify it by 25,000 times, still would contain in its area 1,000 atoms. So, each dot can easily be adjusted in size as required, and there is no question that there is enough room on the head of a pin to put all of the "Encyclopaedia Britannica."

IMAGINE that it is written in raised letters of metal that are 1/25,000 ordinary size. How would we read it?

We would press the metal into plastic and make a mold; peel the plastic off very carefully; evaporate silica into the plastic to get a very thin film; then shadow it by evaporating gold at an angle against the silica so that all the little letters appear clearly; dissolve the plastic away from the silica film; and then look through it with an electron microscope.

Extract of the "Popular Science November 1960"

Table of Contents

I. Abstract

The RF microsystem technology is believed to introduce a paradigm switch in the wireless revolution. Although only few companies are to date doing successful business with RF-MEMS, and on a case-by-case basis, important issues need yet to be addressed in order to maximize yield and performance stability and hence, outperform alternative competitive technologies (e.g. ferroelectric, SoS, SOI,…). Namely the behavior instability associated to: 1) internal stresses of the free standing thin layers (metal and/or dielectric) and 2) the mechanical contact degradation, be it ohmic or capacitive, which may occur due to low forces, on small areas, and while handling severe current densities.

The investigation and understanding of these complex scenario, has been the core of theoretical and experimental investigations carried out in the framework of the research activity that will be presented here. The reported results encompass activities which go from coupled physics (multiphysics) modeling, to the development of experimental platforms intended to tackles the underlying physics of failure.

Several original findings on RF-MEMS reliability in particular with respect to the major failure mechanisms such as dielectric charging, metal contact degradation and thermal induced phenomena have been obtained. The original use of advanced experimental setup (surface scanning microscopy, light interferometer profilometry) has allowed the definition of innovative methodology capable to isolate and separately tackle the different degradation phenomena under arbitrary working conditions. This has finally permitted on the one hand to shed some light on possible optimization (e.g. packaging) conditions, and on the other to explore the limits of microsystem technology down to the nanoscale.

At nanoscale indeed many phenomena take place and can be exploited to either enhance conventional functionalities and performances (e.g. miniaturization, speed or frequency) or introduce new ones (e.g. ballistic transport). At nanoscale, moreover, many phenomena exhibit their most interesting properties in the RF spectrum (e.g. micromechanical resonances). Owing to the fact that today's minimum manufacturable features have sizes comparable with the fundamental technological limits (e.g. surface roughness, metal grain size, …), the next generation of smart systems requires a switching paradigm on how new miniaturized components are conceived and fabricated. In fact endowed by superior electrical and mechanical performances, novel nanostructured materials (e.g. carbon based, as carbon nanotube (CNT) and graphene) may provide an answer to this endeavor. Extensively studied in the DC and in the optical range, the studies engaged in LAAS have been among the first to target microwave and millimiterwave transport properties in carbon-based material paving the way toward RF nanodevices. Preliminary modeling study performed on original test structures have highlighted the possibility to implement novel functionalities such as the coupling between the electromagnetic (RF) and microelectromechanical energy in vibrating CNT (toward the nanoradio) or the high speed detection based on ballistic transport in graphene three-terminal junction (TTJ). At the same time these study have contributed to identify the several challenges still laying ahead such as the development of adequate design and modeling tools (ballistic/diffusive, multiphysics and large scale factor) and practical implementation issues such as the effects of material quality and graphene-metal contact on the electrical transport. These subjects are the focus of presently on-going and future research activities and may represent a cornerstone of future wireless applications from microwave up to the THz range.

II. List of Acronyms

AFM	Atomic Force Microscopy
BFN	Beam Forming Network
BST	Barium Strontium Titanate
C/DCT	Charge/Discharge Current Transient
CEM	Computational Electromagnetic
CLRH	Composite Left Right Handed
CPW	Coplanar waveguide
CTE	Coefficient of Thermal Expansion
DGS	Defect Ground Structure
EBG	Electromagnetic Bandgap
ESD	Electro-Static Discharge
FDC	Force Distance Curve microscopy
FET	Field Effect Transistors
FM	Failure mechanisms
FMEA	Failure Mechanisms Effect Analysis
FTIR	Fourier transform Infra-Red spectroscopy
FWHM	Full Width Half Maximum
HBM	Human Body Model
IR	Infra Red
IDC	Interdigital Capacitor
KPFM	Kelvin Probe Force Microscopy
MEMS	Micro-Electro-Mechanical Systems
MIM	Metal-Insulator-Metal
MM	Meta-Materials
MST	Micro-Systems Technology
NEMS	Nano-Electro-Mechanical Systems
RF	Radio Frequency (according to IEEE from KHz up to the optical range)
RH	Relative Humidity
SIW	Substrate Integrated Waveguide
SCT	Scale Changing Technique
TF	Thin Film (test vehicle)
TLM	Transmission Line Method
TLP	Transmission Line Pulsing
TSDC	Thermally Stimulated Discharge Current
XPS	X-ray photoelectron spectroscopy

III. Preamble

Hereby I will take the opportunity (and the freedom) to introduce myself with a short and hopefully not boring fly-by biography. I do it for two main reasons: first, since I do not intend to write an actual biography, nor I think this will ever happen in the future, this is probably the only opportunity to share with you, the (on duty, or curious) reader, more about the "person" behind this manuscript. Second, a fast forward biography covering the most decisive part of my life will clarify and make more consistent the profile of the "professional" behind this work.

Said that, what follows is going to drive you through a quite atypical journey of what I consider to be "an individual animated by technology driven curiosity and good will".

Atypical, because I recognized that after a quarter of professional activity (depending from current pension regulations) none of my former and present colleague's career resembles even closely to mine. As matter of fact I like to locate myself in the "limbo", which divides industrial-profit-driven reality from the academic-knowledge driven realm. Being much closer to this latter and belonging officially to the former, I realized that it was the perfect environment to develop my curiosity and good will.

The best way for "untangling the nets" is to sort out the events by following a chronological order. Let's start.

Since my early studies I always privileged technical matter, and above all, anything that had to do with electricity. Let's skip the details but some significant fact represented already a good premonition of what unfolded later on. This includes my first experimental demonstrator at the end of the elementary school grade (a photovoltaic driven electrical engine toy) through out the more sophisticated piece of hardware issued from spontaneous homework at high school, as the digitally programmable FM radio or the very rudimental 4 bit CPU done by simple logic port and discrete components. This latter outcome was the results of the high school spare time spent with my colleague and friend Daniele Tajolini in his garage transformed in an electronic workshop (apparently little later and with not as much success as other couples did earlier in other garages in the US). Anyway, only at the university (Università di Perugia) I received the true and official baptism in electrical engineering. Was at that time that thanks to an opening position (with Prof. Mauro Mongiardo), I participated to one of the most brilliant and successful endeavor of present European Union, the Erasmus Program.

Launched from Perugia the Erasmus rocket projected me at Technische Universität München (TUM) in Munich Germany. That was the first crucial step of the journey. Welcomed in an early Oktoberfest morning by another expatriate Dr. Pierantoni good friend and colleague ever since, I landed into a truly vibrant international environment and into a prestigious organization, the Institute for High Frequency Engineering (or Lehrstuhl für Hochfrequenztechnik - HFT), led by Prof. Peter Russer. During the time I spent with Prof. Russer, I completed my MSc thesis (to be exact the Italian equivalent "Tesi di Laurea", then defended back in Italy), the PhD degree and always thank to the Peter's impressive network of contacts, I literally received an experience boost by visiting influential universities (in the US at the University of Michigan working with Prof. Linda Katehi, and exchanging very interesting time also with Prof. G. Rebeiz and his students), or leading industrial groups (internship at Daimler in Ulm Germany, at that time Daimler-Chrysler, and at Rohde&Schwarz always in Munich).

During the period spent in Munich I have had the opportunity to assist Prof. Russer in building up the Master in High Frequency Engineering (newly introduced in 1999) and give master and lab classes to the very international students we gathered worldwide. This part of the work at TUM made clear the importance of breeding a new class of engineer in a very specialized field such as high frequency and electromagnetic. The building up of this MSc was a real headache for the complexity of the curricula and the variety of student's background, but ensured the institute the supply of very high level international post graduated. Moreover thanks to the TUM visiting professor program I had the great opportunity and pleasure to meet other great professionals such

as Prof. Zoya Popovic (University of Colorado Boulder), Prof. Andreas Cangelaris (University of Illinois, Champain), Prof. Manos Tentzeris (Georgia Tech), and Prof. Stephen Maas (UCLA).

On the technical and scientific side, although the TUM high frequency institute was deeply involved in numerical techniques, which eventually became the argument of my PhD, I had the chance to start, since my day one, a research activity on a very recent and exotic technology called RF-MEMS. It was October 1998 exactly the time when the famous special issue on RF-MEMS edited by (Rebeiz, Katehi, Nguyen)[2] came out.

That was it.

Another rocket that propelled me into an unexplored field with plenty of unknowns but also promises of opportunity ahead.

I immediately realized that those bright tiny elements barely visible on thin silicon slice (they were capacitive RF switches issued by an experimental RF-MEMS Daimler process) represented "the challenge" for all those mathematic physics engineering knowledge we had gathered so far at university. Finally a clear mission, which explained years of hard learning work. As we know a posteriori the task wasn't easy, but it allowed me to shed some light on crucial issues. The most representative being the *dilemma of high aspect ratio electromagnetic modeling*, the *riddle of multiphysics modeling and characterization* and the *mysteries of micromachining*. These fundamental aspects of RF-MEMS allowed me to consolidate a multidisciplinary background of knowledge and to develop a comprehensive network of professional contacts and expertise.

This network became something more consistent with the name of AMICOM[3] a European initiative called Network of "Excellence", which clustered around the topic of "RF-MEMS for advanced RF Architectures" some among the most "knowledgeable" organizations in Europe.

TUM was part of it. CNRS-LAAS was its heart.

At LAAS this network had been thought, conceived and coordinated, by Prof. Robert Plana. As consequence of this further successful initiative of the European Union (called the Framework Program for Research and Development), a couple of opening postdoctoral positions were made available. It happened to be France and more exactly Toulouse (LAAS) or Limoge (XLim or better IRCOM at that time) the possible locations. In spite of the cultural and geographical shock (though alleviated by a sort of come back to Latin ground), I did not hesitate to leave my comfortable German nest for embarking another European mission. I accepted the position in Toulouse. I picked up LAAS's because it was the cockpit of what it was announced to be an amazing professional endeavor which unprecedentedly combined (it was one of the first European specialized network ever made) an impressively large number of scientists of international repute, with as many competences, personalities and experience, all converging toward an intriguing "hot technology".

After the Erasmus Program with the following experience at TUM, that was the second rocket-opportunity that propelled me into the stardom of technology and its ecosystem of knowledge and capabilities.

My post doc at LAAS was transformed in a crash course in management when I took over the responsibility of the AMICOM project. That was one of the toughest time I have ever had. Noteworthy is that it was also the reason of my permanence in Toulouse to these days.

Although trained to multitasking between teaching-research-management activities at TUM, this time the task was announced to be colossal, at least from a new recruit perspective. In spite of this I "recklessly" accepted it. I wasn't alone though. On the contrary, I could count on Robert's remote advice and "even" on his physical presence, at those few but critical circumstances were it was indispensable. In addition to it another colleague and another "Robert"o came on assistance. Besides Sorrentino the "Professor" that introduced me to electromagnetic fields back in the 90's in Perugia, I discovered "the colleague" that mentored me through the tough realm of larger responsibilities. The supporting team was moreover completed by the guidance of a very

[2] G.Rebeiz, L. Katehi, C. Nguyen Proceedings of IEEE Special Issue 1998 Vol. 86, Nr8.

[3] AMICOM Network of Excellence - Funded under the 7th Framework program of the European Commission during the period 2004-2008 (27 organisations from 13 EU countries for a total budget of 7.5M€) – www.amicom.info

experienced group of colleagues forming the "AMICOM Board" such as Hermann (Prof. Schumacher from Ulm University), Harrie (Dr. Tilmans from IMEC), Alex (Dr. Muller from IMT) and other great professionals and individuals involved in AMICOM.

My professional journey took a swift acceleration forward by gaining momentum in scientific maturity and vision.

The heritage left by the AMICOM experience was then instrumental in dealing with the complex RF-MEMS world. At that time (2005-06) became clear that an emerging technology does not mean a ready to use product, far from that. The word "reliability" became the buzzword and in few years the focus of several large national and international projects. At LAAS I had the opportunity to work in these projects and manage some of them. This time, not much RF nor electromagnetic was involved, but rather solid state and fundamental physics. Again plenty of experience and new knowledge I did not hesitate to learn about thanks to experts with whom I had the chance to work with one among all Prof. George Papaioannou.

As clearly depicted by technology analyst (e.g. Dr. Jeremie Bouchaud Director and Principal Analyst, MEMS & Sensors, at iSuppli with whom I had the opportunity to work during the EU project ARRRO), as any other emerging technology, RF-MEMS follows the well known *Gartner "hype" curve*[4]*. In case of RF-MEMS this model announced* a so called *peak of inflated expectation* (around 2003) when the technology went viral and several organizations, industry and research lab alike, jumped in to try out the RF-MEMS experience. This was followed by the *trough of disillusioned* (around 2005) where many of the aforementioned organizations gave up under the burden of low profitability or shortcoming in performances. Nowadays we are experiencing the *slope of "enlightenment"* where only few companies succeeded in doing serious business on a case-by-case basis, while trying to maximize yield and performances stability in order to outperform alternative competitive technologies (ferroelectric, SoS, and SOI).

As matter of fact it is clear that after almost two decades of frenetic R&D activities the RF-MEMS business, dominated by switches and variable capacitance, was crying out for a return on investment. It has reached a decisive turnpike where only stable high yield manufacturing process could guarantee profitability and durable mass-market insertion (e.g. Wyspry, and Cavendish-Kinetics), relegating dedicated RF-MEMS processes to nice markets (e.g. RADANT, OMRON).

This situation helped to locate my activity at LAAS, where the RF-MEMS technology was introduced in 1995 (by Dr P. Pons, Prof. R. Plana) and where the focus was moved around 2009, from developing a complete RF-MEMS technological process, to undermining the fundamental failure mechanisms.

All these activities in understanding RF-MEMS from a fundamental physics point of view brought me closer to what was the most recent decisive point of my technical scientific evolution. Macroscopic electrical behavior was strongly dependent from nanoscopic phenomena which, thanks to the progresses in nanoscience (in characterization, modeling, fabrication), became more accessible. It was has been at that time (2010) exactly, 50 years after his publication, that I came across the famous speech from Prof. Richard Feynman entitled "There's a lot of room at the bottom"[1]. In it the foundations of nanotechnology was laid down. Dr. Feynman anticipated with an impressive realism and extraordinary intuition, what progress in nanoscience would have brought to humanity in the coming future. That speech is considered as the groundbreaking prophecy in the field of information technology "miniaturization" and source of inspiration for the bottom-up approach in nanoelectronics.

Meanwhile a new class of material was emerging and being explored by physics and electrical engineers. The carbon based materials, were since the early 90's being used by the mechanical engineers with extraordinary results but only more recently microelectronics and RF engineers have been moved their interest on individual use of special form of carbon nanostructures as carbon nanotube CNT (1991) and graphene (2004). Although theoretically potentialities were well know to physicists the experimentally and practical exploitation was still absent. The extraordinary mechanical and electrical properties attributed to these nanoscopic objects combined

[4] J. Bouchaud « RF MEMS Market II 2005-2009 Analysis, Forecasts and Technology Review » – WTC Munich October 2005

with my past experience in dealing with limitation of material conventionally used for RF-MEMS, attracted my curiosity and my interest. Again I was accompanied in this unexplored field by a colleagues and good friend of mine as Luca (Dr. Pierantoni now at the Università Politecnica dell Marche - Italy) expert in theoretical multiphysics modeling and the "eccentric" Dr. Mircea Dragoman (from IMT Bucharest and frequent visitor at LAAS) who used to guide us through the comprehension of the complex phenomena taking place in CNT and graphene.

With both of them started another part of my journey where the fascinating science of nanotechnology merged with the considerable body of knowledge and applications in microwave/RF, I was more familiar with. In spite of the fact that we were just starting to scratch the surface of this fascinating field, our force of persuasion on the importance of merging RF and nanotechnology paid off with an international recognition. With Luca we ended up creating a brand new Technical Committee within the IEEE-MTT Society. Called RF-Nanotechnology it represents to date, a major achievement in the community since it permitted to create a focus on en emerging topics, only sporadically addressed before by the MTT society[5]. It was January 2010.

With this endeavor we indented to create a professional recipient aiming to fill the gap between physicists, traditionally used to deal with fundamental physic problems, and engineers, used to a more pragmatic approach toward application. In other words, this was the attempt to joint advanced fundamental physics (such as quantum mechanic) and the body of knowledge owned by RF engineers.

In the past these competences could live apart from each other since conventional RF problems, such as Maxwell's equations, did not need any quantum physics, and vice versa. The introduction of a new class of nanoscale materials into the RF realm imposed a switching paradigm in how problem should have been solved, imposing a new set of modeling, manufacturing and characterization tools with respect to what typically used in RF engineering.

Today my journey in the research realm continues with a twofold approach. On the one hand capitalizing on the expertise I gathered on RF MEMS technology through collaborative project and more specifically with activities based on more mature technology (i.e. the BEOL CMOS MEMS technology from IHP in Germany) and on the other by exploring the possibility offered by graphene based nanodevices. This activities are in line with the objective of the Micro and Nanosystems for Wireless Communication group (funded by Robert in 2006 and led by Patrick since 2012), in which I have the opportunity to work and more at higher level, with the scientific program on "cyber-physical systems" called ADREAM which represents one of the two research pillars (along with ALIVE on bio-engineering) defined at LAAS. The quest for miniaturized and more performing RF devices is a marvelous adventure I hope to carry out with my closer colleagues such as Hervé (Prof. Aubert, the closer to my background on electromagnetic), Patrick (Dr. Pons, with whom I share my background on microsystem engineering) and George (Dr G. Deligeorgis whose expertise's in nanotechnology and solid state physics are instrumental for dealing with new research directions such as ballistic electronics). Not to mention all the other several colleagues close and far I have the chance to know and the privilege to collaborate with.

The path is long and many are the competences that I still need to acquire, but I am certain that the conditions are there to have still lots of fun ahead of me.

Last, but as important as anything mentioned just above, is my engagement in training, education and dissemination activities. As matter of fact the continuous line connecting all my research activity with these latter, be it as advisor for MSc and PhD students or by teaching in international schools and regular university classes, represents an integral part of my profession. Since the TUM time, I have always had the opportunity to work with individuals (teachers or students) with whom, I shared the most precious driving force above all, the curiosity and hunger for knowledge. This is something I definitely count to keep alive through my involvement into education at local institutions (e.g. the Université de Toulouse - in particular at ENEEIHT) and other international activities (e.g. the European Course on Microwave of the EUMA).

[5] L. Pierantoni, F. Coccetti, P. Russer, (Invited guest editors) "Nanoelectronics: The Paradigm Shift [From the Guest Editors' Desk]" IEEE Microwave Magazine, Vol.11, N°7, December 2010, pp.: 8-10.

At the “bottom”, there is indeed plenty of room for innovation enabled by high frequency and nanotechnology. I hope to be part of it by remaining at the middle of the marvelous triangle of innovation, formed by education-research-industry.

1 Introduction: Getting the full picture

Aiming toward miniaturized and energy efficient RF (sensing localization, harvesting and communications) intelligence (for IoT/Cognitive Systems/Cyberphysical Systems and more)

The main objective of nowadays information communication technology is to introduce yet more functionality in the daily life of individuals and the surrounding environment in order to increase the level of wealth. Growing socio-economical demand for the "anything at anytime and anywhere" has pushed technical progresses to develop "technological smartness" which can be embedded in objects and deployed in the environment.

Certainly one of the most relevant factor of the ITC revolution unfolding since few decades is the exploitation of electromagnetic energy to carry out fundamental actions such as detection, localization, sensing, harvesting and above all communication in a completely contactless and wireless fashion. The exploitation of the RF spectrum to this aim is for sure one of the most emblematic challenge behind the emerging concepts of what is currently called Ambient Intelligence, Internet of Things, cyberphysical systems or cognitive systems. This increase of distributed intelligence based on the exploitation of shared resources such as energy (J) and spectrum (Hz) indeed, is doomed to reach a physical limit. Many are the evidences of these phenomena, and enormous are the hidden implications.

Regarding the energy, « as systems continue to shrink, less energy is available on board which is creating a power challenge that prompts several important questions. … », « To overcome this trend, another energy paradigm is needed » in order to generate (harvest and supply) and use (convert and transfer) energy.[6]

According to estimations carried out form large European technology workgroups[7] the energy target for the different major functions in sustainable future autonomous systems, should be scaled down by factor 1000. So that for instance in the coming decade is expected a consumption of 10-100 k_BT (or 0.1aJ) per binary operation in computation, 100 nW/integrated sensing event (including the first stage of the readout circuit) and 10 pJ/useful bit in communication (including transmitter and receiver processing energy, RF front end energy and transmitted energy. Finally the harvesting part will rely on the combination of o multitude of energy sources in order to reach the power density target of 1-10 mW/cm^2.

Regarding the spectrum, according to Edholm's Law[8] of bandwidth the need for wireless communication bandwidth increases with a trend similar to the Moore's law, with nomadic and mobile data rate intersecting the wired date rate by 2030.

"The amount of wireless data that has been transmitted by the growing legions of smartphones and wirelessly connected tablets has doubled every year for the last four years. "… there would be as many as 50 billion devices transmitting and receiving wireless data by 2020, leading many in the wireless industry to forecast a spectrum crisis" … "a recent European study found that freeing 400 megahertz of radio spectrum to be shared using new technologies would be equivalent to an economic financial stimulus of 800 billion euros."[9,10].

---

[6] Energy Autonomous Systems: Future Trends in Devices, Technology, and Systems,» CATRENE Working Group on Energy Autonomous Systems, 2 0 0 9 - CATRENE - Cluster For application technology Research in Europe on Nanotechnology.

[7] EU Guardian Angel Flagship Project on "Zero-power technology platform for system autonomy," – Final Report - April 2012

[8] IEEE Spectrum article, "Edholm's Law of Bandwidth" Telecommunications data rates are as predictable as Moore's Law," By STEVEN CHERRY / JULY 2004

[9] NYT Article: "Presidential Panel Urges More Flexible Use of Spectrum," By J. Markoff, Published: May 25, 2012

[10] Quote from a US presidential advisory committee Report on "Realizing the Full Potential of Government-Held Spectrum to Spur Economic Growth" by Eric E. Schmidt, Mark P. Gorenberg and David E. Liddle - 2012

The quest for yet more spectrum and energy efficient wireless systems has indeed greatly pushed the development of technologies and techniques to optimize both of them.

On the one hand the digital electronics has reached astonishing level in in terms of computational calculus and data storage, following the impressive trend in circuit integration dictated by the Moore's law. On the other hand a large variety of conventional analog functionalities (RF, biochip, sensing, actuation, …) have been scaled down by the progresses in microsystems technology and enhanced the level of diversification. The combination of these two realms by means of heterogeneous integration is expected to pave the way toward future smart microsystem.

The International Technology Semiconductor Roadmap (ITRS)[11]and the key technology-working group at the European Commission[12] are certainly among the most authoritative strategic think tank in the field of ICT. According to those the innovation for future high-end products will pass through the combination of the digital processing CMOS based electronics along with the multiple functionalities introduced by the analog processing, brought together by means of a heterogeneous integration approach (Figure 1.1). If the CMOS evolution that follows the well-known Moore's law pushes miniaturization to the extreme limits of integration, the analogic counterpart brings in diversification at the cost of fixed sizes imposed by the underling physics. Example of very advanced smart systems based on this combination are already commercially available with sophisticated and accurate MEMS sensors (gyroscope and accelerometers) combined with readout and control CMOS electronics.

Among the MEMS technology the RF's is the one that bears the largest promises to introduce a paradigm switch in the wireless revolution. This technology has the potential to responds to the spectrum and energy optimization challenge by introducing frequency agility while maintaining low power consumption and minimum losses. The RF-MEMS will be the pivotal part of the past and ongoing research topics presented later on in this document.

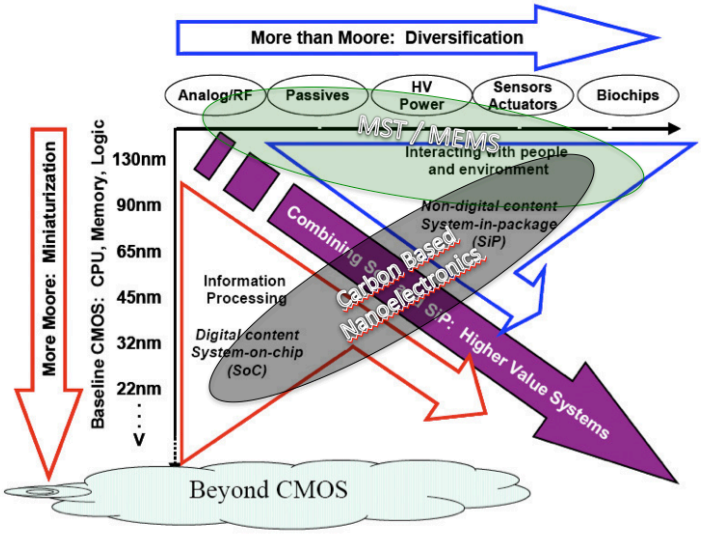

Figure 1.1: The heterogeneous integration of digital and non-digital functionality according to ITRS (Modified from version wrt ITRS white paper[13])

[11] International Technology Semiconductor Roadmap – ITRS (2011) - http://www.itrs.net/

[12] High-Level Group on Key Enabling Technologies – Final Report – European Commission June 2011.

[13] « More-than-Moore » ITRS White Paper - Editors: Wolfgang Arden, Michel Brillouët, Patrick Cogez, Mart Graef, Bert Huizing, Reinhard Mahnkopf

RF-MEMS technology has become increasingly important in the last two decades and it is now accounted in the major technology roadmap for smart systems integration.

MEMS devices (e.g. accelerometer) combined to CMOS logic, have been revolutionizing the human-to-machine communications (e.g. tilt the device to rotate the screen). A similar degree of evolution is expected in combining the RF-MEMS with the CMOS circuitry to achieve new functions such as the automated closed loop antenna impedance matching module, and the dynamically tunable filter module. Both of them have the capability to introduce considerable benefits to the wireless mobile communications business, with lower consumption at the handheld terminal, hence longer battery life, better link budget efficiency hence less cumbersome base stations, less radiated power, better use of the available spectrum hence better quality of service.

RF-MST and in particular RF-MEMS is the emblematic example of enabling technology toward smart miniaturized RF microsystems. RF-MEMS itself represents the convergence of mechanical and electrical functionalities. In the general definition they emerge as a subclass of RF microsystems, which are also issued by micromachining processes, but contrarily from this larger family, they feature movable functional parts. A synopsis for this class of components is given in Figure 1.2. The electromechanical nature of MEMS components identifies a core group that is essentially made of vibrating devices (resonators) and device based on displacement (varicap and switches). Due to their intrinsic superior performances in linearity, low loss and low power consumption (among other) they are on the way to revolutionize RF front end with more useful bandwidth and energy efficiency as mentioned earlier.

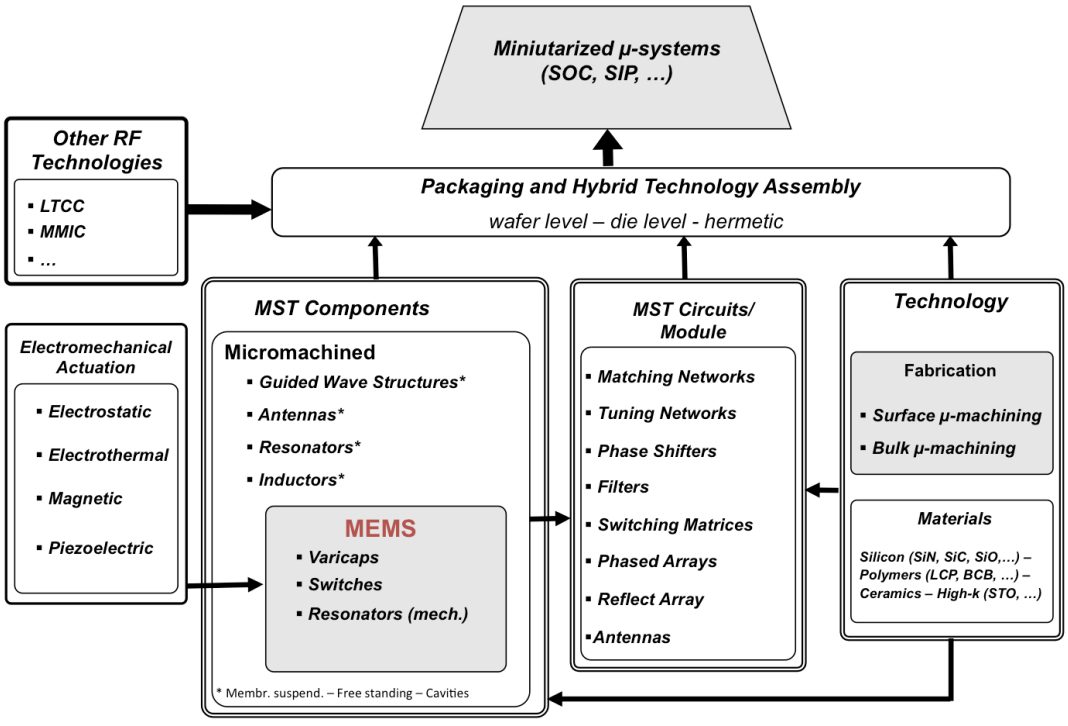

Figure 1.2: The RF-MST roadmap toward smart miniaturized microsystems (modified version with respect from Ref Stephan Lucysyn 2005)

At the moment of this writing however (2013), we are two years away from the first mass market application of RF-MEMS[14]. The targeted market segment is the omnipresent mobile terminal communication, and more in particular one of the worldwide largest consumer

[14] Source IHP iSupply November 2011

electronics manufacturer who "dared" the first RF-MEMS inside one of their flagship smartphone. The RF-MEMS provider is one of the early and most perseverant RF-MEMS fabless company (WiSpry[15]), manufacturing its devices on 8 inches wafer size and 180nm CMOS process line (IBM Microelectronic).

This happens more than two decades *after* the RF-MEMS technology went viral in the R&D. As matter of facts the first pioneering work from K. Petersen in 1979[16] was certainly a breakthrough but also too in advance with respect to the need of the time, and it went unnoticed. This until n the quest for yet more agile yet less power hungry "*wireless"* solutions, pushed RF engineers to look for a new class of components such to introduce a technology rupture and enable a more advanced RF front-end. It was the beginning of the 90s, the dawn of Internet revolution and wireless mass communication. The need for more and better-exploited band was became apparent and several research groups, be it university or industry, engaged the RF-MEMS endeavor. What happened in these two past decades is now history, and it was anticipated and monitored by several technology market analysts. Among this, worth of note, was Wich Technology Consulting (WTC now acquired by iSupply[17]), and Yole[18]. WTC analysis based on the principal RF-MEMS industrial and academic players, followed the *Gartner "hype" curve[19] reported in Fig. 3.3). This graph typically describes the market maturity evolution of new technologies for the specific case of RF-MEMS[20] (*Figure 1.3*). This model announced that the* so-called *peak of inflated expectation* (around 2003) when the technology popularity reached its apex. This moment was followed by the *trough of disillusioned* (around 2005) where many of the aforementioned organizations gave up under the burden of low profitability or shortcoming in performances.

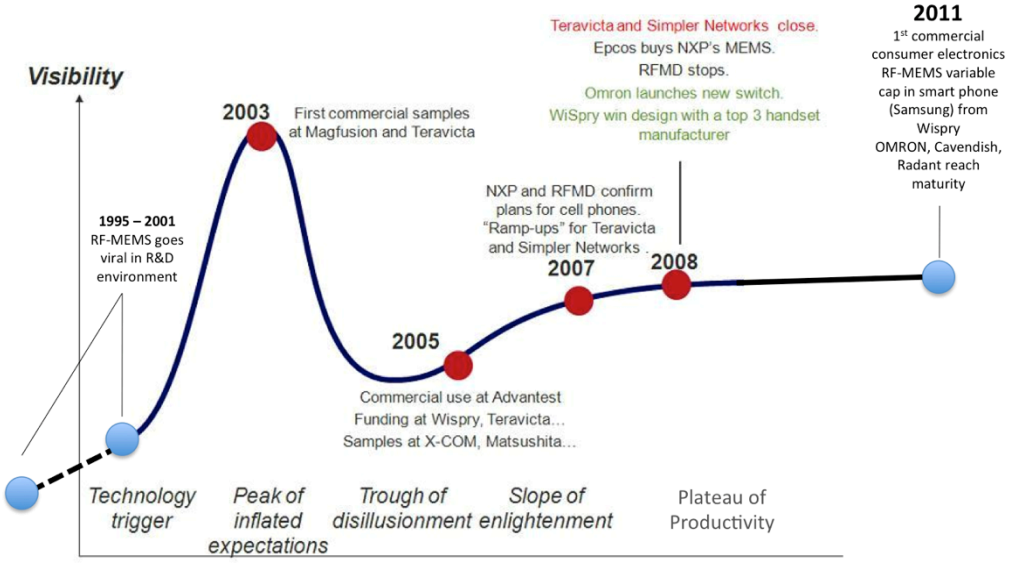

Figure 1.3: The Gartner's curve for RF-MEMS technology (red dots from source figure by J. Bouchuad – principal MEMS analyst at iSuppli, while blue dot are an adaptation from the author)

Nowadays in 2012 RF-MEMS technology is experiencing the *slope of enlightenment* and entering the *plateau of productivity* with only few companies doing successful business on a

[15] WiSpry Irvine, CA 92618 - www.wispry.com

[16] K. E. Petersen, "Micromechanical Membrane Switches on Silicon," *IBM J. Res. Develop., vol. 23, no. 4, pp. 376-385,* July 1979

[17] IHP iSuppli marker research: http://www.isuppli.com/

[18] Yole Development group: http://www.yole.fr/

[19] Gartner Research Methodologies - http://www.gartner.com/technology/research/methodologies/hype-cycle.jsp

[20] J. Bouchaud « RF MEMS Market II 2005-2009 Analysis, Forecasts and Technology Review » – WTC Munich October 2005.

case-by-case basis and trying to maximize yield and performances stability in order to outperform alternative competitive technologies (ferroelectric, SoS, and SOI). Manufacturing process stability and performances optimization remain to date the biggest challenges toward the 1B$ RF-MEMS market.

According to the experience collected in these years of personal activity in RF-MEMS technology two important and distinctive elements have emerged as dominating the maturity level:

- **Free standing thin layers** (metal and/or dielectric) which internal stresses are extremely sensitive to manufacturing process condition and procedure

- **Mechanical contact** between metal or dielectric layers which occurs at low force regime and on very small areas

Both of these elements are also very sensitive to working ambient conditions, such as RH temperature, gas composition, and working profiles such as RF and/or DC current. In particular **electrical current flow between two MEMS parts in mechanical contact represents a very singular feature, which specifically characterizes MEMS switches**. In fact in **none of the MEMS devices successful commercialized to date this scenario takes place**. The totality of commercial MEMS devices (inkjet printer head, gyroscope, accelerometer, micro-mirror, …) are based on proximity sensing and/or actuation and do not include parts which enter in physical contact with each other. Typically these parts are coming out from IC-like manufacturing processes, which are characterized by a surface roughness comparable (~ nm) to some of the device minimum features (area of the contact spot). This is not the case in macro-contact switches or relays where forces and contact area are much larger, resulting in large contact surfaces. Moreover due to the very low forces, which are applied to this contact (between few hundred uN to few mN), quite complex phenomena take place in the several but limited locations where the contact spots are formed. This turns out to strongly reduce the overall contact area due to the actual contact force exerted on it. In this scenario of weak force, point-like multiple contacts any electrical energy transferred through it, gives rise to extreme working conditions dominated by strongly coupled phenomena (thermal, mechanical, chemical, …).

On top of this also manufacturing tolerances and technological dispersions should be accounted. Their effect on geometry and material translates in a deviation from nominal value and introduce a further element of complexity.

The relevant R&D efforts devoted to the RF-MEMS[21] technology during the last two decades have strongly suffered from the missing understanding of this complex behavior and consequently caused, a quite late insertion of this technology in the application value chain.

The accurate control and exploitation of these features, which represents the very essence of MEMS, contact based devices (e.g. switches) needs necessarily to be addressed with **multiphysics** investigation tools.

This is what will be described in the next chapter where the focus will be on the numerical tools used to face a typical multiphysics scenario of arising in MEMS undergoing high level of RF power handling (>5W). This subject has a been an important research topic for all those devices addressing applications such as radars, based station, satellite, ... etc. Both numerical and experimental tools have been developed at LAAS during the early stage of my staying (post-doc). The obtained results have been able to draw important guidelines for yet more robust power handling design and to establish a very original experimental investigation platform.

[21] The total R&D investment on RF-MEMS in the US is estimated to be not far from 1 B$ (source G. Rebeiz at IMS 2012).

On the other hand, the multiple-scale and multiple-variable problem of MEMS modeling suggested another interesting research area which combining the computational power of distribute computing resources (grid computing technology) and the flexibility of some open source electromagnetic solver has allowed to explore the path toward fast global optimization. Distribute computing has been applied to carry out parallel (one problem decomposed in pieces and solved at the same time of many different nodes) or parametric (many different variable configuration of the same original problem. This part has been faced in the framework of collaborative projects, and it is briefly described in the appendix (Appendix 4.2.1)

This study introduced my research activity to wider reliability issues of RF-MEMS, not only or not at all related to RF. It quickly became the major research field for me at LAAS in the period 2007-2012.

At the end of the first wave of interest for this technology around beginning of the 00's the impact of failure mechanisms started to become a major concerns. In particular as mentioned earlier dielectric charging, contact degradation and thermal induced phenomena where the most severe, for which little knowledge existed.

The major limitation was that up to that time nobody had followed the approach to isolate the single failure mechanisms and study it apart. Effort in LAAS and Novamems did that for the first time. The approach of the "divide et impera" was applied to the three aforementioned failure mechanisms.

In particular the case study based on the use of AFM based investigation methodology will be detailed since it has been particularly effective in studying the dielectric charging taking place at the metal to dielectric contact interface. This approach has generated a quite considerable body of knowledge on electrostatically induced stiction mechanisms, which included environmental effects as well. These results contributed a lot in the understanding of electrostatic actuation at the microscale and shed some light on how optimal working condition for micro and nano actuation should be designed. Other failure mechanisms study associated to metal-to-metal contact (done at Novamems) and to stress in thin membrane will be also outlined.

For what regards the maturity and industrial adoption of RF-MEMS technology the consensus today is that success is essentially related to the presence of an ***actual NEED*** (unmatched by other technologies). Only under this condition the critical mass can be reached. The most critical part consists in addressing the ***reliability versus variability*** challenge which implies to establishment of a manufacturing platform upon which transfer the R&D results and bring them to match industrial qualification standards.

The second part of the manuscript is dedicated to future research activities. The experience and work done on RF MEMS technology made clear that the components developed today are often reaching the limit of classical/conventional manufacturing capabilities. In order to push even further the performances and smartness (more enhanced functionalities) a switching paradigm in conceiving new miniaturized components is needed. This thinking turned my research interest toward novel generation of emerging materials, which intrinsic physical and structural properties open the way to a new class of devices and manufacturing process. Carbon based materials such as carbon nanotube (CNT) and graphene came up quite recently to the large scientific public and have become ever since a center of gravity for researchers. Their peculiar latex structure endow them with superior electrical and mechanical performances, which have been extensively studied from the DC up to the optical range. The research direction which is propose in chapter 3 is based on the assumption that **miniaturized smart systems can be made upon functionalities that take place at nanometer scale** (e.g. ballistic transport, or the CNT self oscillation) and **through their collective exploitation which allows to alleviate the impedance mismatching existing between the nano and the application realm**.

In spite of the great promises hold by this material toward nanoelectronics and nanosysytems, several obstacles lie ahead. They are essentially linked with the difficulties to handle, understand and control these nanostructures and the underlying physics. Owing to the completely new transport mechanisms and to their sensitivity with the surrounding environment these nanoobjects require a completely new modeling and characterization approach. The modeling simulation tools are scarce since coupled physics, this time classical's (e.g. Maxwell's equations) and quantum's (either Schroedinger's or Dirac's) are at stake. Regarding the characterization or even just the observation, they relies on a combination of sophisticated equipment for the local material structural investigation (e.g. Hall's, Rahman ineterferometer, SEM, …) and more conventional ones for the extraction of the electrical measurements (e.g. Hall effect, DC, Scattering parameters). On top of this the manufacturing processes need to be redefine by scratch. It is in this context that soft lithography, CVD growth and inkjet transfer have become increasingly interesting techniques to do accurate nanostructuring over large-scale production. Some example of device currently being developed (Y junction detector) will be presented as example of ongoing research activities while some considerations on oscillating NEMS will give a personal outlook on possible more long term research directions.

This will close an overview where past research on RF-MEMS reliability currently being exploited in research project based on mature external foundries, merges with new perspective based on carbon based nanoelectronics and fundamental investigation, at the center of prospective research activities.

Other activities in the area of RF microsystem conducted in the same time frame (always in the past ten years) but rather apart from the main flow of topics given in main body of this document are quickly mentioned for sake of completeness and record in the appendix 4.2.

2 Past research activities: Overview

Riding the RF-MEMS technology "hype"

Introduction

This part will be devoted to personal research activities that have been carried out in the period 2004 – 2013. In this tens years spent at LAAS-CNRS the focus has been essentially on RF-MEMS but not only. Being in particular RF-MEMS reliability one of the hot topics in the CISHT (former name of the group from which the MINC was born in 2007) a good part of the experience in electromagnetic and multiphysics modeling gathered during my past experience at TUM in Germany was readily available and exploited in the post doc period 2004-2005. At that time the major unsolved issue was the investigation RF power handling in microelectromechanical switches (PAMIR DGA project – see Annex). Progress in new commercial numerical tools allowed me to reach interesting results. Moreover also advanced instruments were available at LAAS. In particular the IR imaging resources and expertise, which allowed us to develop an original and innovative experimental set up, combining IR thermal imaging with RF probe testing. This will be the first par of this chapter.

The main flow of my research activity kept going with an increasing involvement in RF-MEMS reliability. The focus however moved quite swiftly from RF and multiphysics theoretical and experimental investigations, to the study of more fundamental failure physics such as metal contact degradation, and dielectric charging. Considered by far as the major limitations of any RF-MEMS, most of the efforts and resources (the project FAME (ANR), SYMIAE (RTRA), REDS (ESA), Polynoe (DGA) and the PhD students F. Pennec, U. Zaghloul, J. Ruan, A. Broue, N. Torres) were addressed to these studies. The knowledge background required to face this task however, had to do more with material science and solid state physics than RF. For this reason the several collaborations established in the past allowed to integrate the group at LAAS with well reputed expert in the field such as Prof. G. Papaioannou 2008-2010 and Prof. B Bhushan 2009-2012). Their support allowed me to enlarge my knowledge in the field and acquire a distinctive multidisciplinary background.

The second and larger part of this chapter is therefore dedicated to the principal findings on RF-MEMS reliability, which are essentially on the degradation of metal-to-dielectric contact in MEMS electrostatic actuators (topic of the U. Zaghloul's PhD and in part of J. Ruan's PhD), and more briefly on the metal-to-metal contact in resistive switches (topic of A. Broue's PhD and F. Pennec's PhD with whom I collaborate), for concluding with the last part devoted to the investigation of MEMS technology based on BiCMOS (by IHP Germany). In this last part (topic of N. Torres-Matabosch's PhD the design for reliability approach was applied to IHP capacitive switched in order to study the effect of stress on thin membrane and the effect of process tolerances on it. In some how this last this part represents the apogee of a personal experience embracing the multifacets of RF-MEMS reliability.

According to Gartner's curve for emerging technologies the so called peak inflated expectations represents the point where R&D activities reach the maximum of the "hype" before to leave the room the few that will succeed to commercialization. For RF-MEMS this has been also the case. Out of the several groups that worked on this topic only very few company succeeded to cross the valley of death. In spite of this, an enormous amount of knowledge has

been generated and shared. In the following of this chapter the results from the development done at LAAS and Fialab (former Novamems) will be outlined. They are organized in two main parts, which concern numerical modeling and simulation and the experimental investigation toward reliability assessment.

2.1 Research activity in modeling:

This section will be devoted to the modeling of the **coupled physics** and will summarize the approach toward a multiphysics modeling and validation platform established during the very beginning research activities at LAAS (within the DGA-PAMIR and FP6-AMICOM project).

2.1.1 The challenge of coupled-physics

The physics involved in a MEMS device imply the coexistence of different physics in the same place and at the same time. The overall behavior strongly depends on how these interactions take place. In Figure 2.1 is given a schematic representation of the possible coupling along with main the parameters involved.

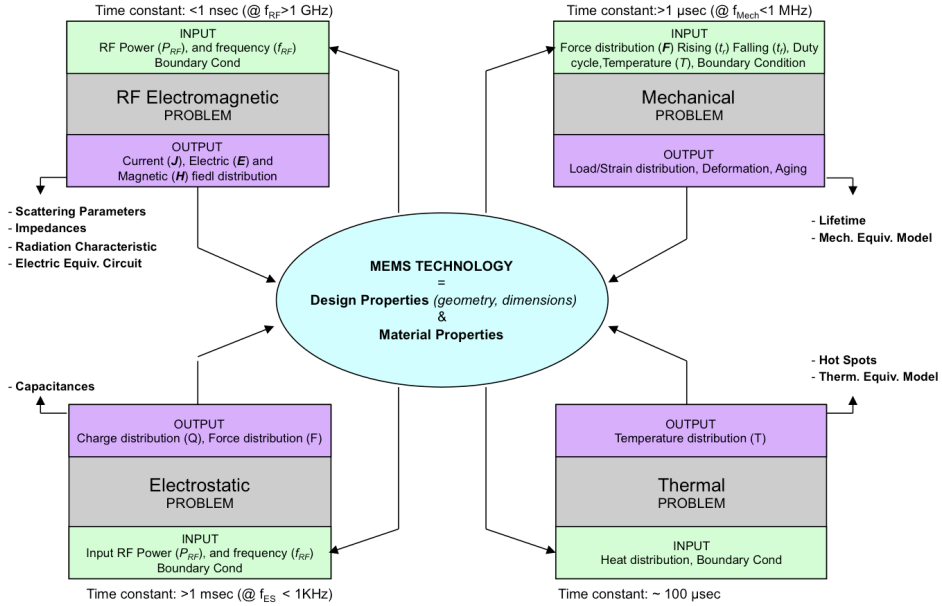

Figure 2.1: Representation of main physics involved in an RF-MEMS device with highlighted input and output parameters.

The critical factor is therefore the underlying coupling mechanism, the time constant associated to them, and the intensity of the stimuli. There are several example where these coupling can be neglected since either the stimuli is too low or the time constant of the two phenomena is very different. MEMS devices represent a perfect case study for this problematic. In particular with respect to the time constants the different physics involved therein are characterized by even very different values going from the slowest process taking place at electrostatic (DC and LF) and thermal level (above the 10^{-3} sec range) to the mechanical which depending from vibrational or displacement mode can even reach the (10^{-6} sec), to finally end with the electromagnetic phenomena which can range in the 10^{-6} down to the 10^{-12} sec for electrical RF signal in the microwave and millimeter wave range.

Under this scenario the modeling can be simplified by considering only the coupling between phenomena, which takes place in the same time constant range. This is the case for the

electrostatic thermal and the mechanical's while it is not the case for the electromagnetic one, which can be separately considered and does not have significant influence on the formers.

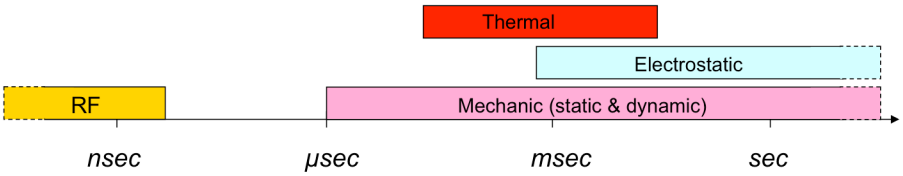

Figure 2.2: Typical distribution of time constants for the different physics involved in a MEMS device.

Electro-thermo-mechanical coupling for RF MEMS: power handling case study

The RF power handling of an RF-MEMS device strongly depends on the voltages and currents distribution which may yield unwanted phenomena such as self actuation, stiction and contact wearing, self heating and electromigration. With device sizes of approximately a few square millimeters or less and made of suspended movable metal and/or dielectric parts, it becomes evident that RF power handling optimization must be based on a comprehensive modeling approach, covering the underlying coupled thermo-electromechanical phenomena. Throughout the following paragraphs, the focus will be on capacitive switches, varactors and metal contact switches.

Self-heating typically due to Joule's effect is a major reliability concern for RF-MEMS devices where air-suspended structures (transmission-line, fixed-fixed membrane or cantilever beams), suffer from high temperature rise due to the large thermal resistance toward natural heat sinks as the substrate. The high frequency nature of the electric signals yields standing waves with current peaks localized in specific area of the structure. Moreover due to skin effects, currents crowding takes place on the conductor surfaces. These aspects are responsible for significant temperature increase as compared to direct current DC operation and represent the main cause of typical failure mechanisms such as melting, creep, and thermal-strain-induced buckling. Wang et al[22] have shown that buckling occurs at a lowest temperature and is therefore the most significant among the thermal failure modes. Buckling yields permanent shape changes, which can alter electrical parameters such as the capacitance, hence affecting RF performances as characteristic impedance and resonance frequency. Thermal issues need therefore to be first identified and then carefully addressed already at design phase.

In the following sections a comprehensive modeling flow introduced to perform a robust multiphysics co-design will be described and the techniques used to carry out experimental investigation and validation of the simulation results will complete this part.

Numerical investigation of self-heating due to RF power

A number of theoretical studies have been carried out in the field of self-heating within RF MEMS devices. Analytical or numerical tools provide accurate information already at design level, enabling cost-effective optimized solutions. Closed-form expressions have been found for

[22] Z. Wang, B. D. Jensen, L. L. W. Chow, J. L. Volakis, K. Saitou and K. Kurabayashi, "Full-wave electromagnetic and thermal modeling for prediction of heat-dissipation-induced RF MEMS switch failure", *J. Micromech. Microeng.*, vol. 16, pp. 157-164, 2006.

more common structures, such as double-clamped beams[23] or suspended CPW transmission lines[24] providing simple but accurate estimations of expected temperature rises. In general, however, RF MEMS technology is characterized by complex geometries, with features in the micro and sub-micrometer scales, with large aspect ratios and the use of very different materials (e.g. semiconductors, metals, dielectrics). This scenario rules out the use of analytical approaches, and imposes that of numerical ones. Moreover as already mentioned, besides the complexity of the model, there is a clear need to couple the different physics involved, hence the need for thermo-electromechanical co-design approaches. Examples for the numerical investigation of temperature rise due to self heating within RF MEMS have been reported[25,26], where a numerical electromagnetic tool based on finite-difference time-domain (FDTD) and integral methods, respectively, have been coupled to FEM thermal solvers. Other investigations have covered the electromechanical aspect by coupling electrostatic and mechanical solvers[27]. Very little had been reported at that time (2005) on a more comprehensive thermo-electromechanical analysis.

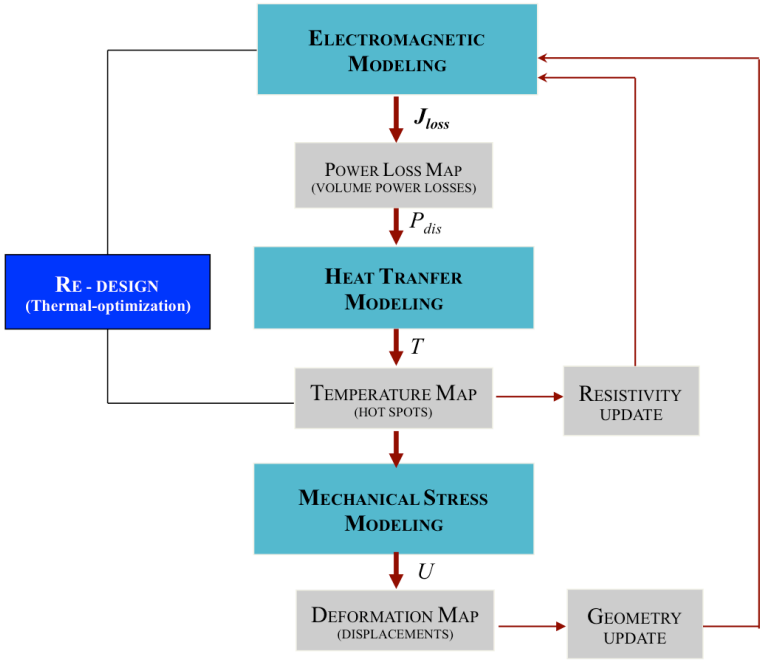

Figure 2.3: Multi-physics modeling and co-design flow for analysis and optimization of RF MEMS

The block diagram proposed in Figure 2.3 shows how such an approach was envisioned. In this scheme, the flow diagram is recursive, with respect to the optimization (re-design) and the

[23] J. B. Rizk, E. Chaiban and G. M. Rebeiz, "Steady state thermal analysis and high-power reliability considerations of RF MEMS capacitive switches", *IEEE MTT-S Symposium Digest*, pp. 239-242, Jun. 2002.

[24] L. L. W. Chow, Z. Wang, B. D. Jensen, K. Saitou, J. L. Volakis, K. Kurabayashi, "Skin-effect self-heating in air-suspended RF MEMS transmission-line structures", *Journal of Microelectromechanical Systems*, vol. 15, no. 6, pp. 1622-1631, Dec. 2006.

[25] W. Thiel, K. Tornquist, R. Reano and L. P. B. Katehi, "A study of thermal effects in RF-MEM-switches using a time domain approach", *IEEE MTT-S*, pp. 235-238, Jun. 2002.

[26] B. D. Jensen, K. Saitou, J. L. Volakis and K. Kurabayashi, "Fully integrated electrothermal multi-domain modeling of RF MEMS switches", *IEEE Microw. Wireless Compon. Lett.*, vol. 13, no. 9, pp. 364-366, Sep. 2003.

[27] S. G. Tan, E. P. McErlean, J. S. Hong, Z. Cui, L. Wang, R. B. Greed, D. C. Voyce, "Electromechanical modeling of high power RF MEMS switches with ohmic contact", *13th Gallium Arsenide and other Compound Semiconductors Application Symposium (GaAs'2005)*, Paris, pp. 505-508, Oct. 2005

simulation loop. In the first loop, the simulated variables (e.g. current densities, temperature rises and mechanical stresses) can help to enhance the design whereas they assume critical values (*such as current density values larger than threshold allowed for instance by electromigration*[28]). This can be done by introducing, features such as thicker or larger conductors, or more efficient thermal sinks. The effectiveness of these solutions however needs eventually to be validated. For this purpose the design parameters (geometries and material) need to be updated by taking into account phenomena such as thermally-induced deformations. Once the update is done it needs to be re-simulated in order to check the compliance with the given specifications.

Since the final goal is to obtain an optimized RF component, the investigation starts from the electromagnetic design and model. The heat source for the coupled thermal problem coincides with the volume power losses P_{dis}, computed from the resulting electromagnetic fields solution $\boldsymbol{E}$, $\boldsymbol{H}$, $\boldsymbol{J}$ as the contribution of the losses from conductors, dielectrics and magnetic materials. This is given by the following expression:

$$P_{dis} = \frac{1}{2}\Re\left\{\int_V \vec{E}\cdot\vec{J}\,dV\right\} + \frac{\omega}{2}\left\{\int_V \varepsilon''\left|\vec{E}\right|^2\,dV + \int_V \mu''\left|\vec{H}\right|^2\,dV\right\} \qquad (2.1)$$

where the volume integrals are extended over the entire domain V, and ε'', μ'' represent the imaginary components of the permittivity and permeability, respectively, for the different materials and ω is the angular frequency.

The use of good thermal conductors (e.g. gold, aluminum, etc.) and the small surface areas allow to neglect the convective and radiated heat transfer mechanisms, which typically account for less than 1% of the total temperature rise[23]. Hence, the thermal problem can be described only by the conducting heat transfer equation:

$$\rho c_p \frac{\partial T}{\partial t} = k\,\nabla^2 T + P_{dis} \qquad (2.2)$$

where T is the time dependent temperature at each point of the volume V, ρc_p is the thermal inertia, k is the thermal conductivity and P_{dis} is the heat source given by (2.1). As mentioned earlier, since the time constant of the RF transients are several orders of magnitude smaller (typically below 100 ns for microwave and millimeter wave signals) the time constants of thermal transients (i.e. typically in the range of 100 ms for these applications), the two problems can be considered separately. Hence, the steady-state electromagnetic simulation results can be used for the thermal transient analysis.

On the contrary, mechanical analyses cannot in general be separated from the thermal ones. Commercial tool available for this purpose (here was Ansoft e-phisics[29]) are typically limited to small deformation case (linear mechanical deformations). Under this condition the equation simplify a lot since the second order terms can be neglected). Whereas "small" is in relation to the dimensions of the problem size and the characteristic length of the spatial variation of the external force. In this case the mechanical model can be restricted to static and linear deformations analysis. Under this approximation of small mechanical displacement, the kinematics of the deformation can be described through the linear strain tensor $\overline{\overline{e}}$ and the deformation u, by means of the following expression[30]:

[28] Examples of DC current limits for electromigration at 25°C are: *25 GA/m²* for Cu; *5~20 GA/m²* for Au; *2 GA/m²* for Al. Moreover due to the self healing phenomena occurring when AC is applied these limits increase by a factor 10 (from the $J_{max(AC)} > 31.6 J_{max(DC)}$).

[29] E-physics from Ansoft corporation, "e-Physics Technical Note" 2005, www.ansoft.com (e-physics is no longer available since Ansoft was purchased by ANSYS in 2010)

[30] Pei Chi Chou,Nicholas J. Pagan « Elasticity: Tensor, Dyadic, and Engineering Approaches » Princeton N.J Van Nostrand 1967.

$$\overline{\overline{e}} = \nabla^{(s)} u \tag{2.3}$$

where $\nabla^{(S)}$ is the symmetric gradient and:

$$\overline{\overline{e}} = \begin{pmatrix} e_{xx} & e_{xy} & e_{xz} \\ e_{yx} & e_{yy} & e_{yz} \\ e_{zx} & e_{zy} & e_{zz} \end{pmatrix} \text{ with } e_{ik} = \frac{1}{2}\left(\frac{du_i}{dx_k} + \frac{du_k}{dx_i}\right), \text{ (i,k) = x,y,z} \tag{2.4}$$

is the strain tensor.

The coupling of thermal analysis with a stress solver is done by introducing the temperature distribution in the constitutive equation, which for isotropic elastic materials is given by:

$$\overline{\overline{\sigma}} = \overline{\lambda}\, trace(\overline{\overline{e}})I + 2\overline{\mu}\overline{\overline{e}} - \frac{E}{1-2\nu}\alpha(T - T_0)I \tag{2.5}$$

where T is the temperature solution of (2.2), T_0 is the room temperature, I represents the unit tensor, $\overline{\lambda}$ and $\overline{\mu}$ are the Lamé constants that are a function of the Young's modulus E and Poisson's ratio ν as:

$$\overline{\mu} = \frac{E}{2(1-\nu)}, \quad \overline{\lambda} = \frac{E\nu}{(1+\nu)(1-2\nu)} \tag{2.6}$$

Deformations due to RF-induced heat are computed by solving in u from (2.3) through the (2.6). An example of this modeling strategy is given in

Figure 2.4. In this case it becomes evident how the effect of the thermo-dilatation induced by self-heating and mapped back to the electromagnetic model as mechanical deformation, induces a severe degradation of the RF performance. The results for the specific case study (6 W of CW RF input power) shows how the membrane bends upward with a significant maximum deformations as large as 0.8 µm (the membrane width and thickness are 100 µm and 1.5 µm, respectively, and actuated on a 0.2 µm thick dielectric). This translates to a reduction in the isolation (IL) of almost 18 dB at 24 GHz. Clearly, this shows the thermally induced effect on the device working conditions. At the time when these results were first published[31] full comprehensive coupling of the electro-thermo-mechanical phenomena was not possible on the same simulation platform. The geometry update on the original design (structures) and the transfer between the significant variable (E-field, T, and deformations) was therefore carried out manually between available commercial tools.

[31] F. Coccetti, B. Ducarouge, E. Schied , D. Dubuc , K. Grenier , R. Plana, "Thermal analysis of RF-MEMS switches for power handling front-end",13th Gallium Arsenide and other Compound Semiconductors Application Symposium (GaAs'2005), Paris (France), 3-4 October 2005, pp.513-516.

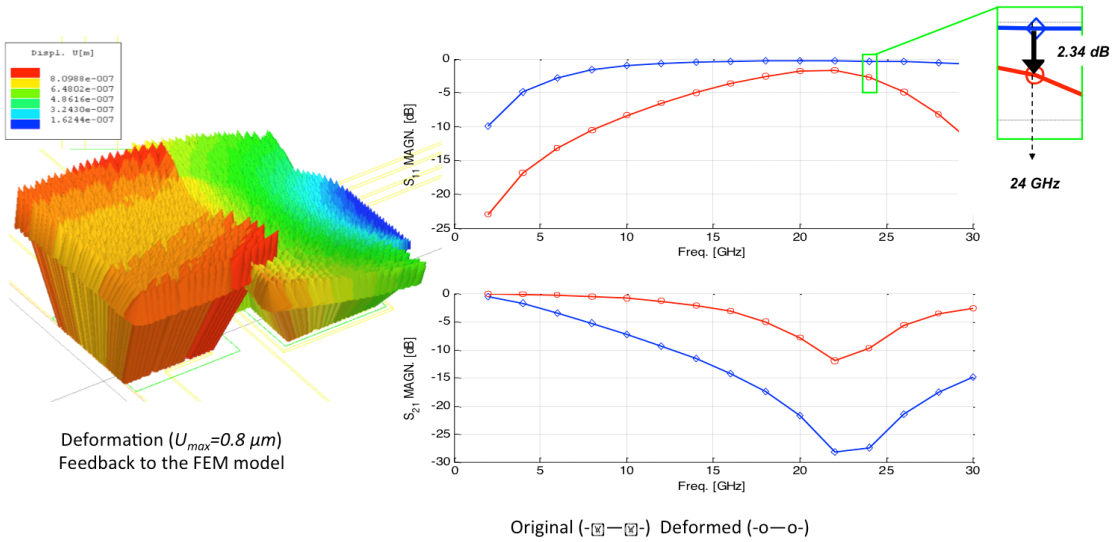

Figure 2.4: Example of simulated RF performances for a deformed membrane (deformation is taken into account by updating the geometries in the electromagnetic simulation with the value provided by the mechanical solver)

The experimental validation of this phenomenon was challenging as well. As matter of fact the observation of RF performance, temperature rise and mechanical deformation is extremely hard at the same time due to difficulties in combining very costly and cumbersome equipment on the same test bench. In spite of this state of the art results have been obtained as described in the following section.

Validation through experimental observation of self-heating due to RF power.

The experimental characterization of electromagnetic induced heat for RF MEMS devices and circuits, aims to identify and quantify critical temperature rise (hot-spots) in order to validate or monitor design robustness with respect to power handling. As matter of fact a characterization tool able to provide reliable experimental results directly on working devices could enable a very fast analysis of front-end modules such for instance, reconfigurable antennae, phase shifters and impedance matching and or switching networks. There are a number of techniques (see Table 2.1) known for the thermal characterization of microelectronics and which are possible candidate also for MEMS scale thermal investigation.

Among these techniques some as the four wires measurement have already been successfully used on RF MEMS structures[32]. In that work, the average temperature rise for a suspended CPW-TL inner conductor *(616 µm x 15 µm x 2.7 µm)* have been measured for three frequencies at varying input RF power. The results showed that a 0.5 W RF power yields an average temperature rise of *75°C* at *18 GHz*, *65°C* at *13.5 GHz*, and *20°C* at *2 GHz*. The 2- and 18-GHz results are in good agreement with the analytical predictions derived from the steady state heat conduction governing equation for this specific case. This technique needs a careful sample design and fabrication in order to be carried out and it can provide only the average temperature rise (no temperature map distribution).

[32] L. L. W. Chow, Z. Wang, B. D. Jensen, K. Saitou, J. L. Volakis, K. Kurabayashi, "Skin-effect self-heating in air-suspended RF MEMS transmission-line structures", *Journal of Microelectromechanical Systems*, vol. 15, no. 6, pp. 1622-1631, Dec. 2006.

Table 2.1: List of techniques typically used for thermal characterization of MEMS.

TECHNIQUE	ADVANTAGE(S)	DRAWBACK(S)
THERMOCOUPLE/RTD	FAST PRECISE REASONABLE COST	DIRECT CONTACT NEEDED ERROR DUE TO UNKNOWN CONTACT RESISTANCE
LASER THERMO-REFLECTANCE METHOD	QUALITATIVELY ACCURATE	ADDITIONAL CALIBRATION NEEDED SENSITIVE OPTICAL ALIGNMENT REQUIRED EXPENSIVE BULKY
SCANNING THERMAL MICROSCOPE	MOST PRECISE ACCURATE	DIRECT CONTACT REQUIRED ERROR DUE TO UNKNOWN CONTACT RESISTANCE SLOW SCANNING SPEED EXPENSIVE EQUIPMENT
ELECTRO-OPTO-THERMAL PROBE	PRECISE ACCURATE NON CONTACT	DIFFICULT CALIBRATION DUE TO ELECTRO-OPTO-THERMAL COUPLING EFFECTS
FOUR WIRE MEASUREMENT	FAST ACCURATE EASILY IMPLEMENTED	CAREFUL SAMPLE DESIGN AND FABRICATION NEEDED
INFRA-RED MICROSCOPE	FAST NON CONTACT EASILY IMPLEMENTED	EMISSIVITY DEEMBEDDING REQUIRED HIGH COSTS FOR HIGH RESOLUTION (~5µM)

On the contrary another technique, which has been applied to investigate thermal phenomena in RF MEMS, enables detailed thermal read out by means of infrared (IR) microscope[33]. A similar set up was used in the experimental platform established at LAAS and shown in Figure 2.5.

The thermal imaging was provided by the IR camera from Jade MW (CEDIP Infrared Systems)[34], mechanically mounted on top of the probe station by means of a customized carrier, allowing x-y movements above the entire area of the wafer sample. The camera was characterized by a very cold detector, (*93K*) which enabled a very high thermal sensitivity. This aspect represents a critical parameter especially in case of very low emission material as gold (which emissivity ranges between *0.02* and *0.04*, depending whether it is polished or electroplated). The camera works in the spectral range of 2-5.2 μm, and in the temperature range -20°C to 1300°C. A customized objective with focal length of 30 mm enables a resolution down to $20x20\mu m^2$ per pixel (at least four times the wavelength of the IR radiation around room temperature). In the study described hereby, a calibration at a single temperature and manual emissivity compensation was applied.Two types of measurements are possible, transient time evolution at specific spots (given their *x-y* coordinates) and steady state temperature maps over a rectangular areas (given Δx and Δy range). In the following part the experimental results for both working modes will be reported in the case of a RF-MEMS capacitive switches. The RF MEMS components under test consist of devices realized in gold on a silicon and Benzocyclotene Butene, (Si/BCB, 400/20μm) wafer support. Fabrication process and design have been entirely done at LAAS-CNRS[35].

[33] R. Fillit, B. Ivira, J. Boussey, R. Fortunier, P. Ancey, "Structural and thermal investigation for FBAR reliability in wireless application", *Proc. 43rd Annual Reliability Physics Symposium*, pp. 342-346, Apr. 2005.

[34] Cedip Infrared Systems, (purchased by Flir Systems Inc. in 2008)

[35] B. Ducarouge, "Conception et Caracterisation de Micro-commutateurs Electromechaniques Hyperfrequences de Puissance: Application a un circuit de commutation d'Emission/Reception Large Bande", PhD Dissertation Thesis, Laboratoire d'Analyse et d'Architecture des Systemes du CNRS, 2005.

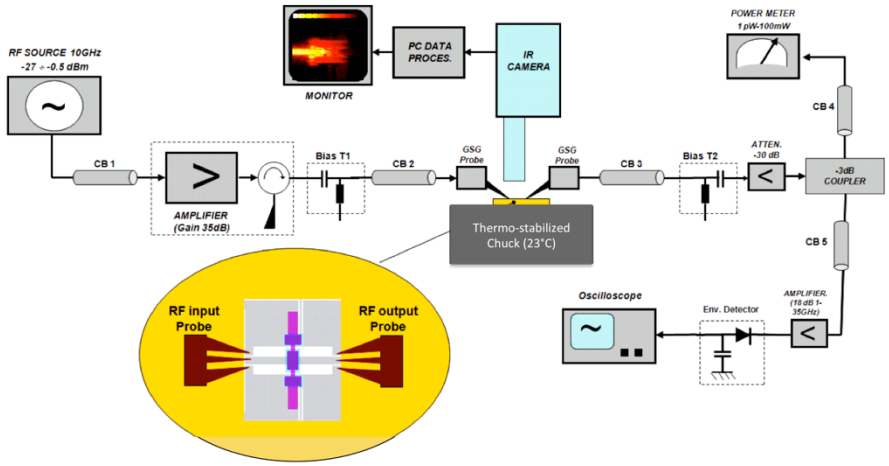

a)

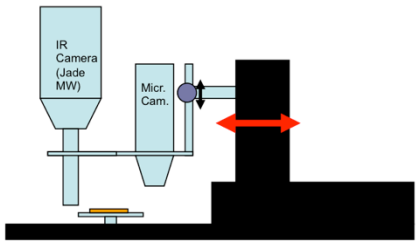

Adaptation of the IR CAMERA on the Probe station
(together with the microscope for the probe positioning)

JADE MW CEDIP Infrared Systems – France Characteristics:

- Very cold detector (93 K) for low emission materials (gold)
- *20x20 μm²* pixel resolution measurements (and *10x10 μm²* for qualitative observation HOT SPOTS)
- Measurement tollerance (after calibration) of 1°C.

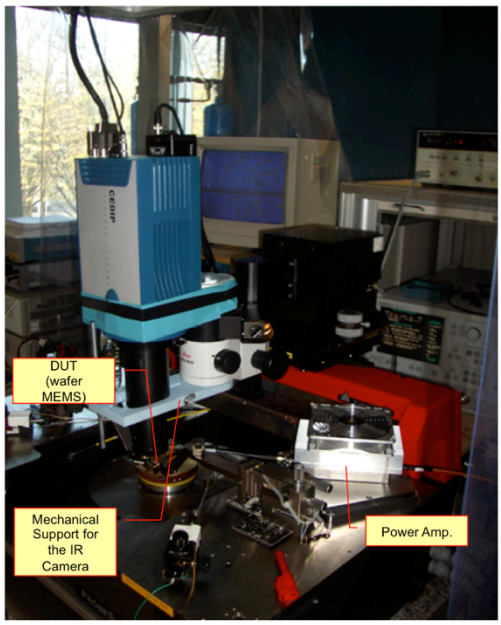

b)

Figure 2.5: Setup used for the thermal imaging of RF-MEMS devices under working power handling conditions: Schematic of the test setup (a) and view of the bench with blow up of the mechanical mounting adopted for the IR camera. The RF source delivers a CW signal (from -27 dBm up to -0.5 dBm), followed by a solid state power amplifier (35-40 dB gain in the frequency range 9.5-10.5 GHz). The measured values of 6.3 W (max delivered power at the DUT) takes into account the 50 Ohm GSG probes, the other lossy element along the chain (circulator, bias-T, coupler), the 35 dB power amplifier at the input branch and the 30dB attenuator at the output's. A power meter, (sensitivity 1 pW-100mW), constituted the final element of the output part of the measurement setup. The DUT is hold by a thermo-stabilized chuck at the constant temperature of *23°C*. The IR camera is PC-assisted in order to carry out the numerical calibration (de-embedding of the emissivity) and the processing of the results.

Temperature time transient: The temperature time transient measurements have been performed at a frequency of 10 GHz. In this case 4 different representative points have been chosen (of which 3 above the movable membrane) and monitored over a time window of 10 sec. After 1 sec the RF power has been instantaneously turned on to the two final constant values of 3.6 W and 6.3 W respectively. The measurements results for the 0 to 6.3W time transient

temperature behavior in down condition is given in Figure 2.6, while in the table are listed the maximum temperature rise for the two working conditions (ON-OFF States) in all selected spots.

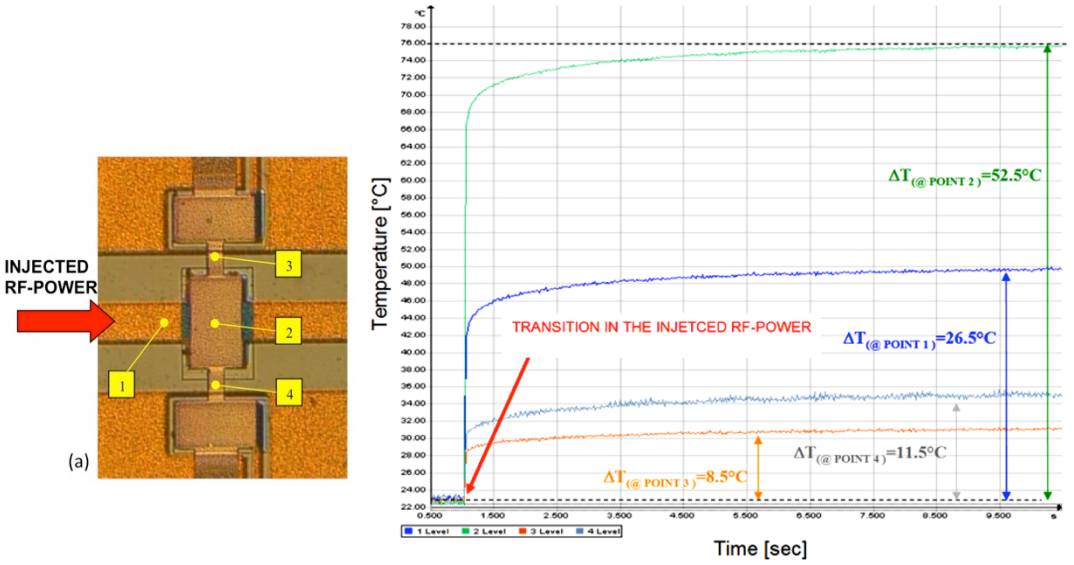

Working State	Temperature Rise P_{in}=3.6W [C°]				Temperature Rise P_{in}=6.3W [C°]			
	Point 1	Point 2	Point 3	Point 4	Point 1	Point 2	Point 3	Point 4
ON (Up)	2.5	2.5	2.4	2.4	5	3.6	5	5
OFF (Down)	11.3	26	10	6	26.5	52.5	11.5	8.5

Figure 2.6: Transient behavior of the temperature rise for the four considered points (showed on the device picture on the left) for the DOWN state. The RF incident power is turned on to 6.3W after 1 sec. The device is originally at a room temperature of 23°C. The temperature rise for both working states and in each point are reported the table below for two RF power levels.

For the device in ON-state (membrane in rest position - up), the RF power signal transits through the MEMS structure, with an overall maximum power loss given by $L_{ON} = P_{in}\left(1 - |S_{11ON}|^2 - |S_{21ON}|^2\right) = 152\ mW$ (for a $P_{in}=6.3\ W$, and measured scattering parameters at 10GHz, $|S_{11ON}| = -16.8\ dB$, and $|S_{21ON}| = -0.2\ dB$ and neglecting the radiated power). The heat induced by Joule effect yields a quite uniformly temperature rise of only 5°C all over the observed domain.

In the OFF-state working condition, (membrane actuated - down), the losses calculated for the MEMS discontinuity are much larger as expected, with $L_{OFF} = 514\ mW$, (for the same incident power level $P_{in}=6.3\ W$ and for measured scattering parameters at 10 GHz, equal to $|S_{11OFF}| = -0.4\ dB$, and $|S_{21ON}| = -22\ dB$). From the measurement results it is evident (see graph in Figure 2.6) that the maximum temperature rise takes place in correspondence of the point 2, the membrane middle point, where the increment of temperature is of 52.5°C. This can be justified by considering that the current distribution, responsible of the induced heat, has a maximum in correspondence of that point (Point 2 in Figure 2.6a). It is there indeed that the capacitive virtual short takes place.

Worth noting is that Point 3 and Point 4, corresponding to two symmetric positions on the gold membrane, present measured temperatures which differ for 4°C and 3°C each other, for 3.6W and 6.3W respectively. This is likely due to the fact that in the reality the structure presents slight asymmetries (due to actuation conditions), which may yield temperature distribution unbalance.

From this experimental observation could be drawn on the overall behavior. For the tested MEMS device the OFF-state (actuated membrane) results the most critical in terms of power

handling, with a final hot spot temperature of 75°C at 6.3W. The temperature rise transient shows moreover a double time constant behavior with a first rise, taking place in few 100 msec, and a slower one that is evolving over few sec up to the end of the 10 sec observation window. A possible explanation for these two mechanisms can be attributed to the different thermal time constants for the MEMS part the first, and to the bulkier substrate the second. Moreover the very sharp gradient of temperature observed on the membrane is the evidence of relatively high thermal impedance presented by the thin metal membrane. In spite of the fact that it is made of very good thermal conductor (Gold) the very small thickness (1-1.5μm) seems to hamper the heat distribution (this will be evident also in the following part about the steady state condition). In conclusion the dynamic thermal behavior of the RF MEMS component under transient RF power condition has provided a number of important physical insights[36].

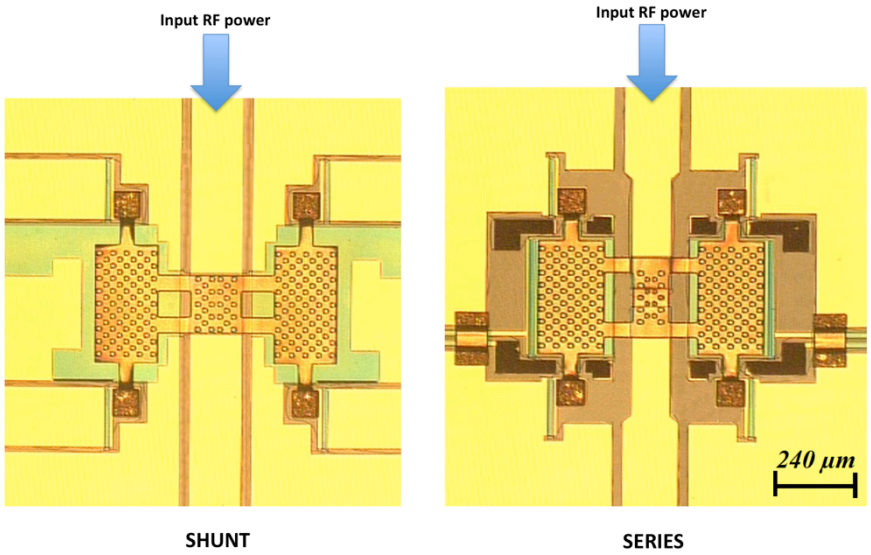

Figure 2.7: Picture of the DUT for the thermal steady state analysis (RF-MEMS capacitive shunt and series switches[35]).

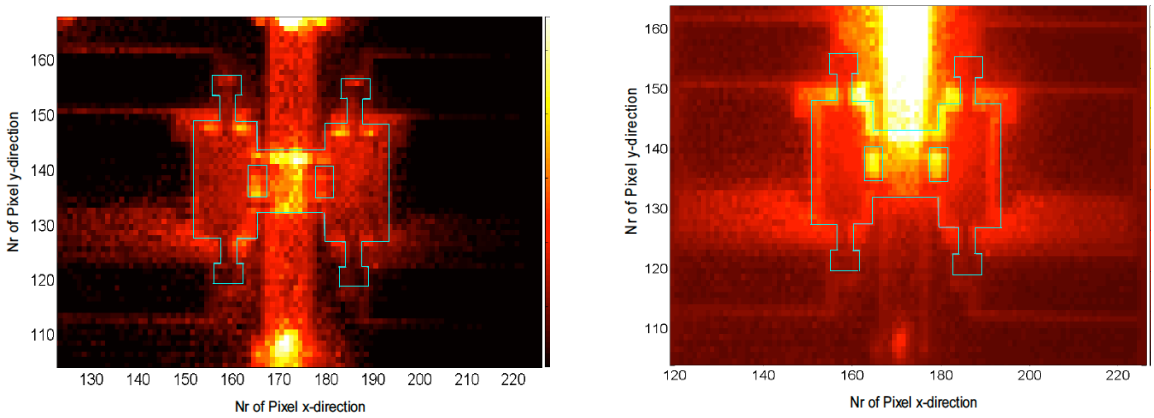

Figure 2.8: Temperature map at the thermal steady-state (P_{in} = 6.3 W) for the **shunt configuration** in: (left) ON-state (membrane up) and (right) OFF configuration (membrane down). For clarity the membrane shape contour is reported.

[36] F. Coccetti and R. Plana, "RF MEMS reliability under high power stress: characterization and modelling," at the RF-MEMS workshop on industrial applications : RF power MEMS: Reliability and Applications during the MEMSWAVE 2007 in Barcellona June 2007.

Steady state thermal mapping (Hot Spot identification): In this case the temperature distribution has been measured all over the MEMS regions for the two working states and for 6.3 W of continuous power at 10 GHz[37]. The DUT investigated is a RF MEMS shunt capacitive switch issued by a similar technology as the previous one and depicted in Fig. 4.7.

In this case the device was specifically optimized for power handling application and realized by means of the same technology as the previous one in two different configuration, series and shunt[35].

The readout with the IR camera is carried out upon an area of circa *1200 x 2000 μm^2* with *20x20 μm^2* pixel resolution at the thermal steady state, i.e. once the temperature has reached a stable distribution. Since, as shown in the previous section (transient study) this delay can be estimated in few hundreds of *msec*, the measurement was taken after few tents of *second* from the moment the RF power was applied.

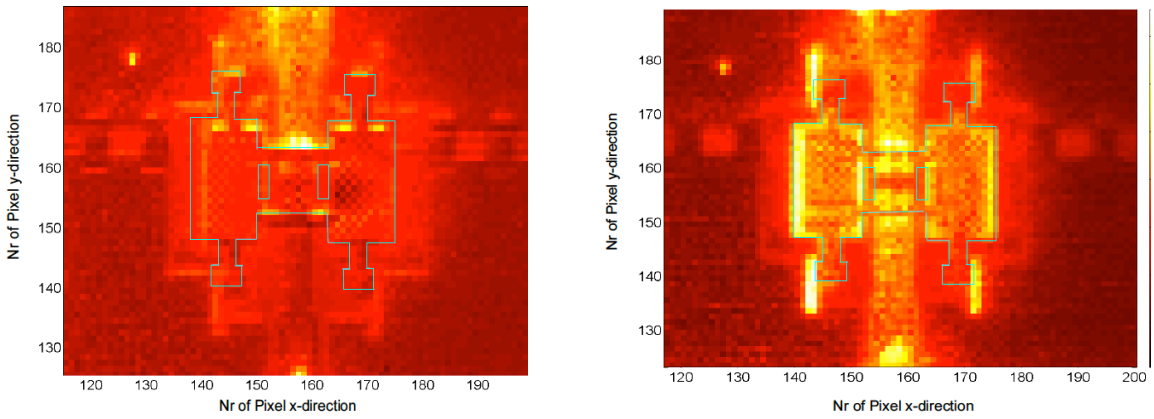

Figure 2.9: Temperature map at the thermal steady-state (P_{in} = 6.3 W) for the **series configuration** in: (left) ON-state (membrane up) and (right) OFF configuration (membrane down). The membrane shape contour is reported.

For the shunt configuration (given picture in Figure 2.7 and IR results in Figure 2.8) the temperature map of the ON-state (membrane up) shows a very limited rise of only 16.1 °C reaching 39.1 °C in the inner conductor and at the input-output probe access. When the membrane is actuated (OFF-state membrane down) a much different scenario occurs, with a rise in temperature of almost 50 °C in the inner conductor side, where the power is injected. There the temperature reaches 72.9 °C. A temperature rise is evident also along the membrane profile in the same side, showing the heating due to the current short circuited by the membrane itself.

Passing to the series configuration (given picture in Figure 2.7 and IR results in Figure 2.9), the thermal behavior induced by the RF power presents a dual phenomenon with respect to the previous one. In fact for the OFF-state (membrane up), since the gap on the signal line yield an open circuit, no current flow through the MEMS structure, hence the temperature rise is very low and remains below 34.4 °C all over the device (see Figure 2.9 left).

A slight heating takes place at the edge of the membrane where RF signal may spill through due the small but still visible capacitance between inner conductor and the membrane. On the other hand in the ON-state, when the membrane is actuated (membrane down) the temperature rises at 42.2 °C quite uniformly on the membrane and the inner conductor. This is the consequence of the current flowing through the device (see Figure 2.9 right). In contrast to the shunt configuration in this working condition the membrane is not actuated upon a continuous

37 F. Coccetti, R. Plana, "Simultaneous electro-thermal experimental analysis of RF-MEMS switches for high microwave power handling", Physica Status Solidi (a). Applications and Material Science, Vol.205, N°11, pp.: 2647-2650, December 2008.

ground plates, which behaves as heat sink, but rather on the smaller actuation pads. This explains the uniform distribution of the temperature upon the membrane.

In general the lesson learned from these experiments can be resumed in the following conclusions:

- The IR camera calibration is quite difficult in the case of very low emissivity (very reflective) materials (e.g. emissivity for polished/electroplated gold 0.02/0.04) where the level of radiated heat, is masked by background noise. A solution could be to apply a uniformity calibration at different T.
- Dielectric materials such as Si_xN_y and SiO_2 are transparent to IR and won't be seen by the camera. Hence only the temperature of underling object will be visible. The same happens to very thin (thickness < IR wavelength) membrane of low emissivity material.
- IR camera resolution is limited (here to 20x20 μm^2 in calibrated condition for the measurement of the temperature, and 10x10 μm^2 for qualitative estimation or hot spot localization). A possible solution adopted by Fillit et al.[33], is to use wavelength filtering which however implies much smaller focus depth (objective sample distance <10 mm) and hence very hard RF probing conditions.
- The power amplifier limits the maximum level of input power and the frequency band. For power level above 10 W measurements on probe become prohibitive due to the thermo-mechanical phenomena arising at the probe contact. For that range of power only connected packaged DUT can be used.

These shortcomings are still present today in spite of the progresses in IR imaging.

General remarks on the experimental investigation by IR imaging

The experimental investigation with the IR camera has allowed to collect a number of important findings about not only on the in-house MEMS devices as shown above, but also on third parties ones (RF MEMS switches by EADS[38]). The preliminary comparisons with the numerical modeling described earlier have been very encouraging with agreement well below 5% between the maximum detected and predicted temperatures (see

Figure 2.10). The lack of mechanical detection (e.g. profilometer) while the switch is operated (i.e. while CW RF power applied), did not allow to monitor possible mechanical failure (deformations). However the stability on the RF performances (no changes vs temperature) allows to rule out such possibility bringing to the conclusion that the investigated devices where robust with respect to the RF power handling.

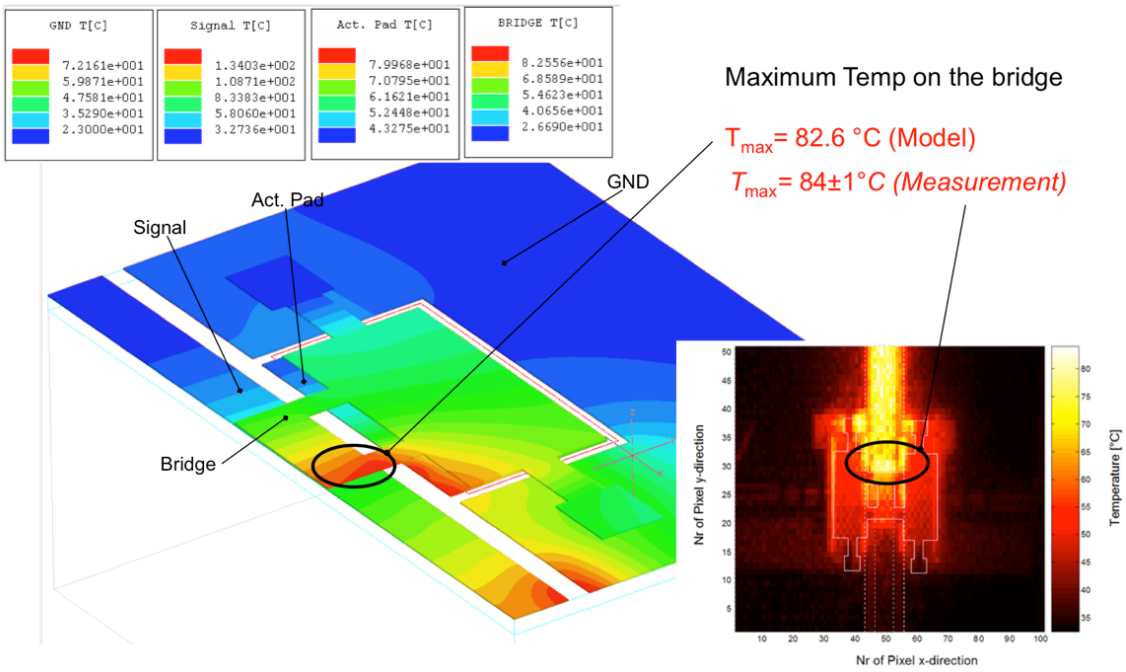

Figure 2.10: Comparison between the numerical multiphysics model (half structure) and the experimental validation technique based on IR imaging (the device is the one described in B.Ducarouge PhD Thesis[35]).

[38] A. Stehle, C. Siegel, V. Ziegler, B. Schönlinner, U. Prechtel, H. Seidel and U. Schmid, "High-power handling capability of low complexity RF-MEMS switch in Ku-band," Electronics Letters 22nd November 2007 Vol. 43 No. 24.

2.1.2 Conclusions on Numerical modeling for RF Microsystems Technology

The numerical modeling of RF microsystems is very challenging for a number of reasons.

- First because of their arbitrary shapes and the large variety of constitutive material the electromagnetic solver must be full wave and capable to handle full three-dimensional geometries.
- Second owing to the extremely small features (dielectric or metal thicknesses), which need to be accounted within a much larger global problem, the modeling is characterized by extremely high aspect ratio (even $>10^4$ as could be in RF-MEMS switches), which moreover, are distributed over multiple scale (example of an RF-MEMS variable capacitor mounted in a phase shifter which is then replicated over an array to form a reflectantennas).
- Third since each MEMS device can have multiple working state (2 in the basic case of a switch) the number of possible configurations that need to be explored may quickly explode (e.g. a 11 bit matching network yields 2048 different configurations).
- Finally the multiple physics involved and their strong coupling requires as saw in the previous section a multiphysics approach.

In spite of the fact that first guess modeling can be done with fairly simple and fat tools (Method of Moment based), the challenge to accurately embrace all these aspects in one single platform is still a long term objective of the research on numerical modeling. The evolution of numerical tools in the last half-century has been impressive (Figure 2.11). Triggered by the appearance of the first computer hardware and made clearly visible by the proliferations of a multitude of original algorithms and methods (FDTD, MoM, TLM, …) their level of maturity has been continuously increasing by adding sophisticated features (meshing, boundary conditions, excitations,…). Since a couple of decades however, owing to the fall of hardware and equipment costs, the trend in research was moved to software optimization for customized CPU/Memory architectures, giving rise to application specific integrated circuit (hardware implement of a numerical processing as for instance the FDTD ASIC) or by dedicated hardware architectures as the vector computing on GPU. At the end of 90's with the appearance of high speed communication network, the advantages of distributed computing became viable. Be it on computer cluster and/or on grid platforms, this phenomenon are still ongoing and culminated with the omnipresent cloud computing. In spite of the large availability of computational and memory storage, these latter is less prone to complex and heavy calculus as those necessary in electromagnetics.

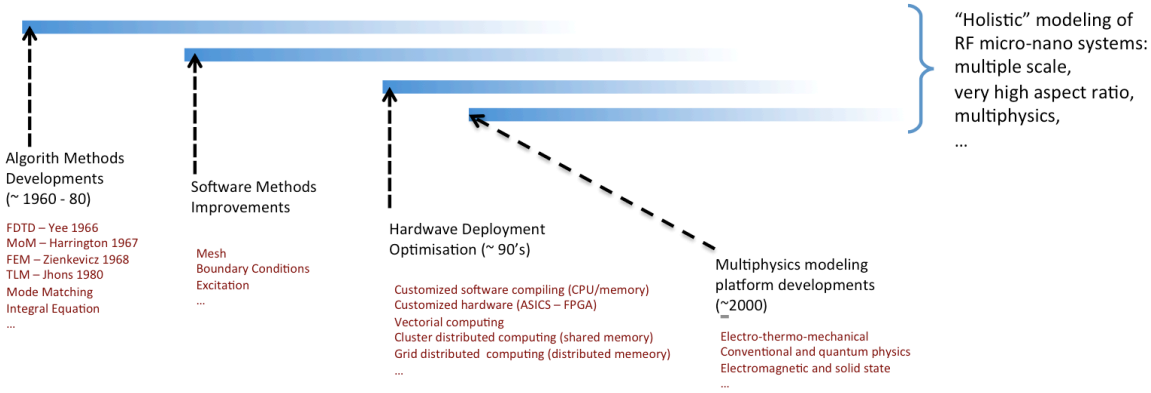

Figure 2.11: Overview of the evolution numerical modeling of RF micro and nanosystem technology.

On the contrary the most recent trend in numerical modeling is the convergence of different solvers, so to provide a single multiphysics platform. This trend is being implemented by almost all major software developers (at least those to my knowledge such as ANSYS, Comsol, CST, …), where the electro-thermo mechanical coupling start to be included. At the moment, due to the strong non linearity (example mechanical instability) a comprehensive and fully iterative coupling is still out of reach. Similar problems hamper the integration of further solvers such as the solid state physics and possibly the quantum physics which have been used so far separately but which coupling become increasingly important in facing nanoscale phenomena.

The quest for an holist numerical tool able is certainly still open but its achievement is only question of time.

2.2 Research activity assessing RF-MEMS reliability

The RF MEMS reliabilities started to become an increasingly large concern at the end of the 90's. At that time this technology was becoming very popular and the research community dealing with it was for a large extend made of electrical engineers, excited by the astonishing announced high frequency performance. In these years the appearance of fundamental failure modes became apparent across a multitude of technologies based on even very different processes and materials choice proliferating on those days. It was only few years later that a convergence of competences in mechanical, electrical so as in material science and process engineering alike, allowed to reach a critical mass and produce the first results in understanding and counteracting these limitations.

Another important element in this development was to recognize that these failure mechanisms depended from the specific application (mission profile), so that they could be sorted and addressed selectively according to the specific need.

As result of this maturation effort in large part carried out and coordinated by IMEC (I. De Wolf) within the AMICOM NoE, a consensus over an application driven failure mode effect analysis (FMEA) ranking was established (2007). Populated by the major failure mechanisms, this table gave clear priority to dielectric charging, contact degradation and thermally induced elasto-plastic deformations.

Two important and distinctive features distinguish RF-MEMS from previous technologies, most prominently represented by the CMOS and the MEMS's. Although they share a quite significant technological heritage with the former, differently from CMOS, RF-MEMS devices are made of **free standing** thin parts (metal and/or dielectric), driven into motion by dedicated actuation circuitry. Moreover if the most emblematic among all RF-MEMS devices is considered, the switch, RF-MEMS are the only MEMS category implementing a **mechanical contact** between thin (metal or dielectric) films (fixed and/or free standing) through very weak forces (in general well below 1 mN).

Both features, ***mechanical contact*** and ***movable free thin-film***, are extremely sensitive to ambient conditions, such as RH, temperature, gas composition, and working requirements, such as signal amplitude (voltage and or current), frequency, waveform (duty-cycle). As matter of fact, in none of the MEMS devices successful commercialized to date these two features take place at once. The totality of commercial MEMS devices[39] (inkjet printer head, gyroscope, accelerometer, micro-mirror, …), are based on proximity sensing and/or actuation and do not have parts which enter in "physical contact" with each other and undergoes electrical currents. Moreover since these parts are issued from IC-like manufacturing processes, which do not foresee any special surface treatment, their **roughness heavily affects the contact physics**. Noteworthy is that this is not the case in macro-contact switches or relays, where contact forces are large enough to overcome roughness limitations and yield more stable and larger contact area (typically through the operation called contact burn-in). Therefore due to the very low forces and the consequent uncertainty at the contact (physical contact at random spot locations/size and proximity effects at close but contactless facing spots), quite complex electrical and thermal transport physics take place. Locally (contact spots) this gives rise to extreme working conditions dominated by severe electro-thermo-mechanical phenomena and chemical reactions.

[39] According to a USA study ("The 2011 MEMS industry commercialization report card" by R. Grace Associates - 2012) most of the MEMS products nowadays available on the market have had an average discovery to full-commercialization elapse time ranging from 20 to 25 years (with the only exception of MEMS pressure sensors which suffered from the early development which on the contrary profited the later product such as accelerometers gyroscopes). On the contrary RF-MEMS switches took 27 to 34 years to reach the market.

On top of this also manufacturing tolerances and technological dispersions need to be accounted for. Their effect on geometry and material translates in a deviation from nominal value and hence in further parameters dispersion.

It is therefore clear that maximize reliability of RF-MEMS is a task which implies a threefold approach:

- the availability of **stable manufacturing processes** (high repeatability and yield);
- the understanding of the **underlying physics of failure** down to the nanoscale and for typical working condition (which must be well know);
- **advanced/innovative design solutions** which minimize the effects of manufacturing tolerances/dispersion and prevent/alleviate failure mechanisms (design for reliability).

The understanding of the failure mechanisms by tackling the underlying physics of failure is definitely the most critical aspect, since it is likely to unveil actual breakthrough in the way a device, can be manufactured and/or can be designed to attain yet superior performances. In order deal with the physics of failure of RF-MEMS however, failure mechanisms need to be first isolated and carefully observed. This has been exactly the approach followed at LAAS and Fialab. By focusing on the main failure mechanisms (see Fig), these studies covered several aspects:

- Determination and control of main mechanical parameters for thin metal membranes: Y. Icham (LAAS - 2007-10), C. Seguineau (Fialab 2009), C. Villeneuve (LAAS – 2009-2011) and N. Torres (LAAS 2009-2012);
- Metal contact degradation experimental characterization and numerical modeling: A. Broue (LAAS-Fialab 2009-12), F. Pennec (LAAS 2007-10), L. Hong (LAAS 2010-13), and N. Torres (LAAS 2009-2012);
- Dielectric charging theoretical and experimental investigation: J. Ruan (LAAS 2007-10), M. Lahmandi (2005-2009) and U. Zaghloul (LAAS 2008-2011).

Noteworthy is that the aforementioned studies have been carried out on “non packaged” test vehicles and actual devices. This choice was justified by the need to guarantee the physical access to the MEMS part and perfectly control working ambient condition during the experiments[40].

[40] To date there are not direct or indirect experimental method to measure the “exact” conditions (e.g. below 1% limit for the relative humidity) in micro cavities as those typically used for MEMS packaging.

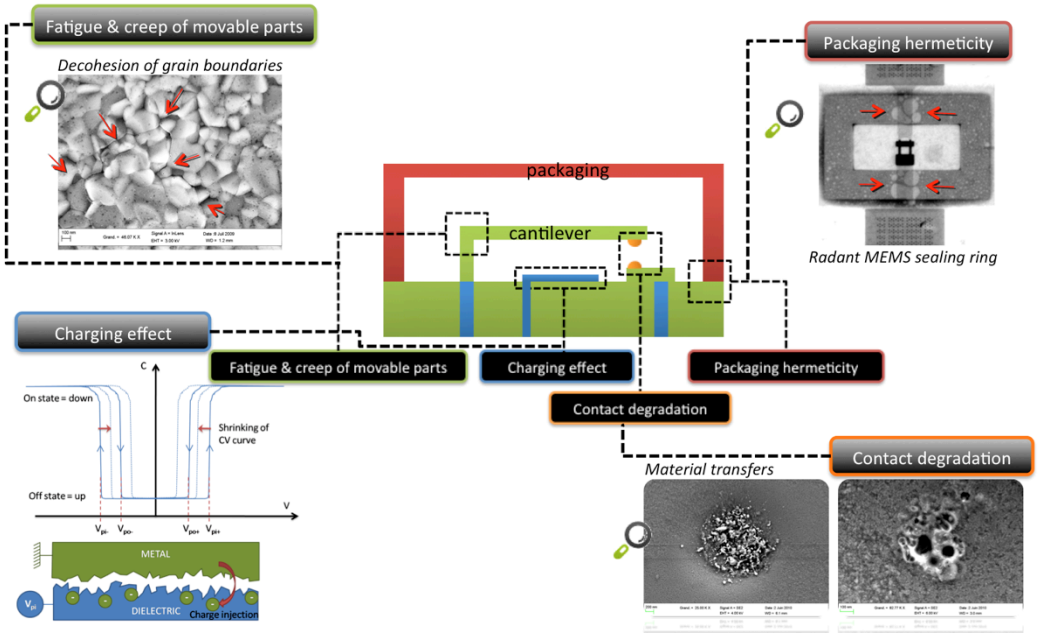

Figure 2.12 [Source: A. Broue PhD 2012]: Schematic view of major failure mechanisms studied at LAAS and Fialab.

It is on the aforementioned three failure mechanisms that the research activity reported hereby will focus, with a special emphasis on dielectric charging. The presented results are a very synthetic view of the results obtained through out a large number of projects[41] and as many collaboration exchange programs and PhD thesis.

2.2.1 The RF-MEMS reliability puzzle

In spite of the last two decades of the tremendous R&D efforts on RF-MEMS this technology is still considered in its juvenile age, similar to the IC technology 40 or 50 years ago. Several reliability concerns are the major hindering factors that prevent the commercialization and utilization of numerous MEMS devices[42].

Reliability can generally be defined as 'the probability that an item will perform a required function under stated conditions for a stated period of time'[43]. The term 'probability' points out that probabilistic models and statistical methods apply. Also, the term 'required function' indicates that a well defined specifications of satisfactory operation, and therefore a definition of failure needs to be defined. The 'stated conditions' term includes the entire physical environment (electrical, mechanical, thermal, and environmental conditions). Finally, the term 'stated period of time' defines a concept of the required lifetime. When a failure occurs, i.e. the device does not perform anymore the required function during functional or reliability testing or in the field, a failure analysis (FA) is normally carried out to investigate and determine the cause. FA can involve electrical testing, fail-site isolation, deprocessing, defect characterization and corrective actions[44]. There is often confusion on the terminology used for failure analysis where four terms

[41] Project on RF-MEMS reliability at LAAS: Local funding (MEMSFIT, RTRA-SYMIAE), national (ANR-FAME) and international (FP6-AMICOM NoE, EDA-POLYNOE) (see in Annex 4.3 for more details)

[42] Hartzell, A. L., M. Silva, and H. Shea (2011), *MEMS Reliability*, Springer, New York, USA.

[43] Tabata, O., and T. Tsuchiya (2008), *Reliability of MEMS: Testing of Materials and Devices*, Wiley-VCH, Weinheim, Germany.

[44] EDFAS Desk Reference Committee (2011), *Microelectronics Failure Analysis Desk Reference*, sixth edition, ASM International, Cleveland, Ohio, USA.

are used inconsistently: *'failure mode', 'failure defect', 'failure mechanism', and 'failure cause'* [45]. The '*failure mode'* is what is first identified, i.e. measured or observed as a deviating or failing behaviour with respect to the specs. For example, a shift in the C-V characteristics of a MEMS switch is a failure mode. The *'failure defect'* is what is observed after identifying the failure mode, and in some cases no failure defect is seen. A MEMS cantilever stuck to the susbtrate is an example of a failure defect. The *'failure mechanism'* is the physics and/or chemistry causing the failure, for example, charging, creep, fatigue, etc. Finally, the *'failure cause'* is what is causing the failure mechanism, for example, the relative humidity causing capillary stiction.

For conventional microelectronic devices, for example ICs, there is a large knowledge available on the reliability testing and failure analysis. The key failure modes are well identified, and the reliability test methodologies are available and described in standards such as IEC[46] or MIL[47] As mentioned earlier though a considerable portion of this knowledge could be applied to MEMS, there are numerous key issues which are unique to MEMS and stand against that.

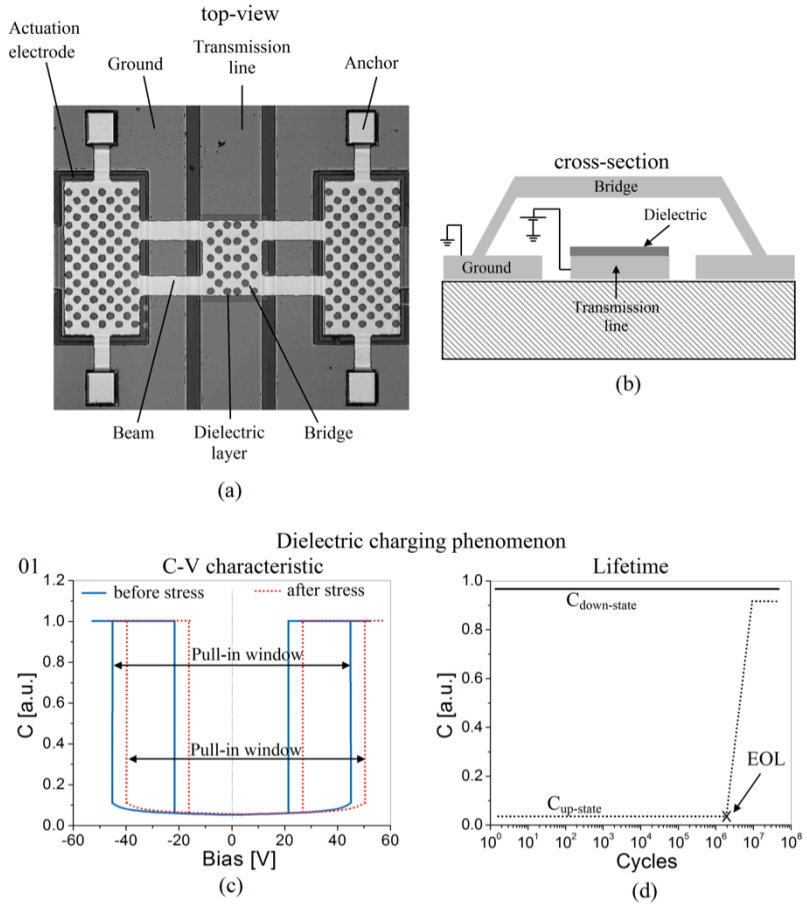

Figure 2.13: Dielectric charging in electrostatic MEMS Switches: a) a magnified image of a finished switch from LAAS48, b) vertical cross section of the same device, c) shift in the C-V characteristic and d) example of lifetime test result.

For example, the reliability issues related to the mechanical part of MEMS structures and to the particular packaging prototype, and deal with failures such as creep, fatigue, fracture, wear,

[45] De Wolf, I. (2006), "Reliability of MEMS," Proc. of the 7th Int. Conf. on Thermal, Mechanical and Multiphysics Simulation and Experiments in Micro-Electronics and Micro-Systems (EuroSime 2006), pp. 1-6.

[46] http://www.iec.ch/.

[47] http://www.landandmaritime.dla.mil/programs/milspec/ListDocs.asp?BasicDoc=MIL-STD-883

[48] V. Puyal, D. Dragomirescu, C. Villeneuve, J. Ruan, P. Pons and R. Plana, "Frequency Scalable Model for MEMS Capacitive Shunt Switches at Millimeter-Wave Frequencies," *IEEE Trans. Microw. Theory Tech.* **57**, 2009, pp. 2824-2833.

stiction, outgassing, hermeticity, etc occurs only in MEMS and has no equivalent relliability concerns in conventional microelectronics. In addition, MEMS devices have a large variety of different applications involving interfacing with various kinds of signals (electrical, optical, chemical, fluidic, pressure, acceleration, etc). For theses reasons, the involved reliability tests of MEMS are typically defined on an application-specific basis, and there are not much generic test methods or standardization available in particulat for RF-MEMS'.

Using techniques like failure mode and effects analysis (FMEA) helps to assess the reliability in all development stages of a MEMS device. Basically, FMEA is defined as 'a systematic and structured study of the potential failures that might occur in any part of the MEMS to determine the probable effect of each on all other parts of the system and on probable operational success, with the aim of improvement in the design, product and process development. Therefore, it involves brainstorming of potential failure modes, identifying suspected root causes, assigning levels of risk, and following through with corrective and protective actions[49]. FMEA starts with identifying the failure modes, defects, mechanisms and causes and estimating their severity (S), occurrence (O) and detectability (D) for a specific MEMS device and for a certain application in a certain environment. The latter three parameters are given weighting points between for example 1 and 10, where S = 1 means that this failure mechanism does not cause any damage to the MEMS, while S = 10 indicates that it causes an immediate irremediable death of the device[50]. Also, O = 1 means that the failure is very unlikely to occur, while O = 10 indicates the very high probability for its occurrence. D = 1 means that the defect is detectable, while D = 10 points out that that defect detection is almost impossible. This is followed by determining a risk priority number (RPN = S x O x D) for each failure mechanism. Thus, the higher the RPN is, the more critical is the failure mechanism.

Some of these reliability issues are the creep resulting from high temperature used during the packaging process[51], outgassing of the packaging material[52] and adhesion or commonly referred to as stiction due to dielectric charging[53] and/or the presence of condensed water vapor from the environment[54]. In DC-contact switches, the main failure is due to the degradation of the ohmic contacts with repeated actuations[55], while for electrostatic capacitive switches the main failure is due to the dielectric charging of the switch insulating film[56].

An example of an FMEA study performed for electrostatic capacitive MEMS switches is presented in Table 2.1[57]. The failure mechanisms are ranked in the table based on the RPN numbers where the failure mechanism with the highest RPN (i.e. the most critical) is listed first. The first three failure mechanisms are briefly discussed in this section. The dielectric charging of

[49] Tanner, D. M. (2009), "MEMS reliability: Where are we now?," *J. Microelectron. Reliab.* **49,** 937–940

[50] De Wolf, I. (2006), "Reliability of MEMS," Proc. of the 7th Int. Conf. on Thermal, Mechanical and Multiphysics Simulation and Experiments in Micro-Electronics and Micro-Systems (EuroSime 2006), pp. 1-6.

[51] Modlinski, R., A. Witvrouw, P. Ratchev, A. Jourdain, V. Simons, H. Tilmans, J. Den Toonder, R. Puers and I. De Wolf (2004), "Creep as a reliability problem in MEMS," *J. Microelectron. Reliab.* **44**, 1733-1738

[52] Oya, Y., A. Okubora, M. Van Spengen, P. Soussan, S. Stoukatch, X. Rottenberg, P. Ratchev, H. Tilmans, W. De Raedt and E. Beyne (2004), "A reliable and compact polymer-based package for capacitive RF-MEMS switches," *International Electron Devices Meeting*, pp. 31-34, IEEE, New York

[53] J. Wibbeler, G. Pfeifer and M. Hietschold (1998), "Parasitic charging of dielectric surfaces in capacitive microelectromechanical systems (MEMS)," *Sens. Actuator A-Phys.* **71**, 74-80.

[54] B. Bhushan, (2011), *Nanotribology and Nanomechanics I - Measurement Techniques and Nanomechanics*, third edition, Springer-Verlag, Heidelberg, Germany.

[55] C. Goldsmith, J. Ehmke, A. Malczewski, B. Pillans, S. Eshelman, Z. Yao, J. Brank and M. Eberly (2001), "Lifetime characterization of capacitive RF MEMS switches," *2001 IEEE MTT-S Int. Microwave Symp. Proc.*, pp. 227-230, IEEE, New York.

[56] K. Man, (1999), "MEMS reliability for space applications by elimination of potential failure modes through testing and analysis," *Proc. of SPIE MEMS reliability for Critical and Space applications, Vol. 3880*, (eds. R. A. Lawton, W. M. Miller, G. Lin and R. Ramesham), pp. 120-129, SPIE, Bellingham, Washington.

[57] ESA Endorfins project, Contract no 18613/05/NL/1A, EC-FP6 AMICOM Network of Excellence 2004-07.

the insulating film is the **first ranked failure mechanism**, and therefore it has been intensively studied during the last two decades[55,58,59].

Table 2.1: FMEA study of electrostatic MEMS switches, the RPN of each failure mechanism is not included.

	Failure mechanism	Failure defect	Failure mode	Failure cause
1	Dielectric charging of the insulator	Non-permanent stiction	-Drift in C-V, V_{pi}, V_{po} -Dead device	• Electric field charge • Radiation • Air-gap breakdown • Electron emission
2	T-induced elastic deformation of the bridge	Non-permanent deformation of the bridge (restored when T-source is removed), possibly stiction	-Drift in C-V, V_{pi}, V_{po} -Dead device	• Environment T • Different CTE • Power RF signal induced T • Non uniform T
3	Plastic deformation of the bridge	Permanent deformation, possibly stiction	-Drift in C-V, V_{pi}, V_{po} -Dead device	• Creep • Thermal induced charges in material properties (for $T > T_c$)
4	Structural Short (electrical and non-electrical connections)	Particles, shorted metals, contamination, remains of sacrificial layer, stuck bridge	Anomalous or dead device	• Contamination, particles, remaining sacrificial layer • Wear particles • Fracture • Lorenz forces • Shock
5	Capillary Forces	Stiction	Dead device	• Humidity (Package leaks)
6	Fusing	Opens, roughness increase	Dead device	• High RF power pulses, ESD
7	Fracture	Broken bridges or hinges	Dead device	• Fatigue • Brittle materials and shock • High local stresses and shock
8	Dielectric breakdown	Dead device, possibly stiction	Short between the bridge and the actuation electrodes	• ESD • Excessive charging of the insulator
9	Corrosion	Dendrites formation, oxidation, changes in color	-Drift in Rc C-V, V_{pi}, V_{po} -Dead device	• Humidity, enhanced by bias • Corrosive gases induced chemical reaction (ex. oxidation)
10	Wear, Friction, Fretting corrosion	Surface modifications, debris, stiction	-Drift in Rc C-V, V_{pi}, V_{po} -Dead device	• Rough Surfaces in sliding contact
11	Creep	Deformation of the bridge in time	-Drift in C-V, V_{pi}, V_{po} -Dead device	• High metal stress and high temperature, creep sensitive
12	Equivalent DC voltage	Self biasing stiction	-Drift in C-V, V_{pi}, V_{po} -Dead device	• High RF power including spontaneous collapsing or stiction of mobile part
13	Lorenz forces	Self biasing stiction	Anomalous switching behavior	• High RF power in two adjacent lines • External magnetic field
14	Whisker formation	Bumps in metal, holes in insulator on top of metal layers, etc	Anomalous down capacitance	• High compressive stress in metal resulting in grains extrusions, might be enhanced
15	Fatigue	Broken bridges and hinges, cracks, microcracks	Shifts in electrical and mechanical properties	• Large local stress variations due to motion of parts • Enhanced probability of cracks
16	Electromigration	Cracks, opens, thickness changes in metal lines	Increase of resistance, opens, shorts	• High current density
17	Van der Waals forces	Stiction	Dead device	• Smooth and flat surfaces in close contact
18	Electric field-induced meniscus	Stiction	Anomalous or dead device	• Residual layer of water (due to residual RH)

[58] X. Rottenberg, I. De Wolf, B. K. J. C. Nauwelaers, W. De Raedt, and H. A. C. Tilmans, "Analytical model of the DC actuation of electrostaticMEMSdevices with distributed dielectric charging and nonplanar electrodes," *IEEE/ASME J. Microelectromech. Syst.*, **16**, (2007) 1243-1253.

[59] D. Mardivirin, A. Pothier, A. Crunteanu, B. Vialle, P. Blondy, "Charging in dielectric less capacitive RF-MEMS switches," EEE Transactions on Microwave Theory and Techniques Vol.57, Issue 1 (2009) pp.231-236.

The failure defect of this mechanism is a non-permanent stiction of the suspended electrode (bridge) to the dielectric. It is not permanent since the injected charges are removed from the dielectric film after a *certain time*. The associated failure mode is a shift of the C–V characteristic of the switch[60] with a constant pull-in window evolving the same way as shown in Figure 2.13c or narrowing of the C–V characteristic[58,61]. A typical lifetime experiment involves stressing the RF-MEMS switch with unipolar actuation cycles with the up and down-state capacitances monitored during cycling. Due to charge build-up in the dielectric during the lifetime test, high adhesion or stiction occurs between the bridge and the dielectric. This is detected through the reduction in the measured up-state capacitance and is used to determine end-of-life (EOL) of the switch as shown in Figure 2.13d. Therefore, the failure mode of the dielectric charging mechanism can also be a non functional device. There are several different failure causes behind this mechanism. First, the charging during the down-state position due to the high electric field applied to the thin insulating film. The charging due to radiation (ex. for MEMS switches in space applications), air-gap breakdown, and electron emission are other failure causes for this mechanism.

The temperature induced elastic deformation of the bridge is the second ranked failure mechanism in Table 2.1. The failure defect of this mechanism is a non-permanent deformation of the bridge if it is restored after removing the T-source. If the deformation is so large that the deformed bridge touches the dielectric or the cap of the package, the failure defect might be also stiction. The failure mode of this mechanism is a narrowing of C-V characteristic and changes in the pull-in and pull-out voltages, or a non-functional device similar to the dielectric charging failure mechanism. There are different possible failure causes for the elastic deformation. One is the change in the environmental temperature, which causes a deformation of the bridge either because of an expansion or because of a difference in thermal expansion coefficient (CTE) between the materials used for the bridge. Another possible cause is the non-uniform temperature in the bridge caused by the power of the RF signal (see previous section).

The Third failure mechanism listed in Table 2.1 is the plastic deformation of the bridge. The failure defect is a permanent deformation of the bridge, and also a possible stiction if the deformation is too large. The failure mode is similar to the one of the first and second failure mechanisms, but is in this case irreversible. Actually, the device is not necessary to be malfunction, but its electrical parameters will show a permanent offset. Possible failure causes are creep in the metal layer of the bridge and temperature-induced changes in the material properties while the latter could results during the device packaging. The remaining failure mechanisms are responsible for failure modes that may occur in capacitive (metal-to-dielectric) as well as in resistive (mechanical metal-to-metal) contacts devices. In these latter, phenomena of capillarity, welding, corrosion (as pitting or any chemical reaction yielding the formation of dielectric or organic thin film material) introduce a degradation of the contact resistance which stands to resistive switches as the capacitance contact degradation stands to the former. This part will be briefly mentioned later on in this chapter (A. Broue's PhD thesis) with the platform developed within the ANR project FAME[62]. The following section will be devoted to the new methodology introduced to study the dielectric charging in electrostatic actuation of MEMS.

2.2.2 Dielectric polarization/charging

First of all the basic polarization/charging mechanisms in dielectrics are presented in order to obtain a better insight on the effect of ionic or covalent bonds as well as different conduction mechanisms which occur in most commonly used MEMS thin film dielectrics.

[60] X. Yuan, J. Hwang, D. Forehand and C. Goldsmith (2005), "Modeling and characterization of dielectric-charging effects in RF MEMS capacitive switches," *2005 IEEE MTT-S Int. Microwave Symp. Dig.*, pp. 753-756, IEEE, New York.

[61] Z. Olszewski, R. Duane, and C. O'Mahony, (2008) "A study of capacitance-voltage curve narrowing effect in capacitive microelectromechanical switches," *Appl. Phys. Lett.* **93**, Art. #094101.

[62] ANR PNANO Program "RF MEMS Switch Failure Mechanisms Analysis (FAME project) 2008-11.

Polarization/Charging mechanisms

The polarization of a solid dielectric submitted to an external electric field occurs through a number of mechanisms involving microscopic or macroscopic charge displacement. These mechanisms could be divided according to the time scale of polarization build-up in two categories, the instantaneous and the delayed time dependent polarization. The time dependent polarization mechanisms[63], which are responsible for the dielectric charging phenomena, are characterized by a time constants that may be as low as 10^{-12} s or as large as years. In the latter, no relaxation could be observed under normal experiment time windows. These mechanisms are called slow and include dipolar, space charge, and interfacial polarization. These polarization mechanisms could take place in contact as well as contactless scenarios. In contactless charging the time varying electric field can interact with the dielectric material under two processes: dipolar polarization (reorientation of defects having an electric dipole moment), and space charge polarization (arising from redistribution of preexisting and/or field generated charge carriers). In contact charging, charges are injected into the dielectric film through various charge injection mechanisms.

The dipolar or orientational polarization Figure 2.14a, occurs in materials containing permanent molecular or ionic dipoles. The time required for this process can vary between picoseconds to even years depending on the frictional resistance of the medium. The dipolar polarization of inorganic crystals may be caused by structural properties of the crystal lattice or it may be due to lattice imperfection or doping.

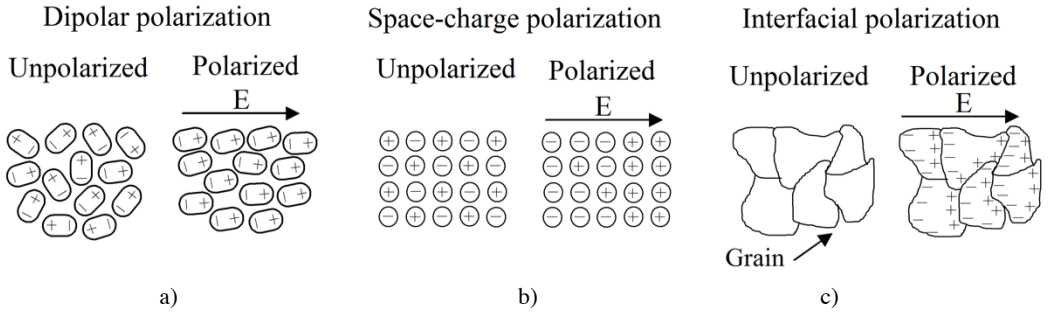

Figure 2.14: Different polarization mechanisms.

The structural interpretation of the dielectric processes occurring in many polar materials, is usually approached by assuming impaired motions or limited jumps of permanent electric dipoles. In molecular compounds for example, relaxation can be considered as arising from hindered rotation of the molecule as a whole, of small units of the molecule or some flexible group around its bond to the main chain. On the other hand, relaxation is mainly associated with ionic jumps between neighboring sites in ionic crystals.

The space charge or translational polarization (Figure 2.14b) is observed in materials containing intrinsic free charges such as ions or electrons or both. It arises from macroscopic charge transfer towards the electrodes that may act as total or partial barriers. Moreover, the charging of space-charge electrets may be achieved by injecting charge carriers. Other methods include the generation of carriers within the dielectric by light, radiation or heat and simultaneous charge separation by a field. The space charge polarization causes the material to be spatially not neutral, hence is a much more complex phenomenon than the dipolar polarization. Dipolar and space charge polarizations often coexist and the electric field and polarization are averaged over the dielectric film thickness. In addition, the simultaneous displacement of free charges and dipoles during the polarization process may lead to a particular

[63] Kao, K. C. (2004), "Dielectric Phenomena in Solids, With Emphasis on Physical Concepts of Electronic Processes," *Elsevier Academic Press*.

situation where the internal electric field is nearly zero, so that no preferred orientation of dipoles occurs.

The interfacial polarization (Figure 2.14c), referred also as Maxwell-Wagner-Sillars (MWS) polarization, is a characteristic of systems with heterogeneous structure. It results from the formation of charged layers at the interfaces due to unequal conduction currents within the various phases. In structurally heterogeneous materials, such as complicated mixtures or semi-crystalline products, it can be expected that field-induced ionic polarization will obey more closely an interfacial model of the MWS type than a space-charge model of the barrier type. The electric field can achieve a migration charge by (a) bulk transport of charge carriers within the higher conductivity phase, and (b) surface migration of charge carriers. As a consequence surfaces, grain boundaries, and interphase boundaries may charge. Charges "blocked" at the interface between two phases with different conductivity give a contribution to the net polarization of the body exposed to the electric field.

Charge injection mechanisms

The conduction mechanisms in dielectrics are divided in two categories; the steady state and transient current. The steady state does not contribute to dielectric charging while the transient current does. In electrostatic MEMS switches the dielectric films are usually a few hundred nm thick and because of the high fields (~10^6 V/cm) applied across these films during actuation, conduction is typically nonohmic and dominated by transport via traps in the dielectric and by charge injection and tunneling. In order to describe the charge injection mechanisms in MEMS, the leakage current models from metal-insulator-metal (MIM) capacitors could be employed[64]. By analyzing leakage current transients in MIM, the dielectric charging can be monitored and then linked to MEMS reliability[65]. However, there has been no direct evidence of relation between the dielectric film DC leakage current and the dielectric charging, except the fact that the leakage current masks the slow charging and discharging processes[66]. The main electronic processes that were identified to take place in MEMS switches are the Poole-Frenkel (PF) and the Trap Assisted Tunneling (TAT) conductions[67].

Poole-Frenkel (PF) process

The classical Poole-Frenkel (PF) effect is the thermal emission of charge carriers from Coulombic (i.e., charged) traps in the bulk of a dielectric or semiconductor, enhanced by the application of an electric field[68]. When an electric field is applied, the barrier height is reduced on one side of the trap, thereby increases the probability of the electron escaping from the trap. As the field increases, the potential barrier further decreases, making it easier for the electron to vacate the trap by thermal emission and enter the quasi-conduction band of the host material.

Trap Assisted Tunneling (TAT)

Trap assisted tunneling (TAT) is determined by the spatial and energetic distribution of trap states, the offset between the Fermi energy of the electrode and the conduction band of the dielectric and the lower limit of the tunneling relaxation times. It has[69] been widely investigated

[64] R. Ramprasad, (2003), "Phenomenological theory to model leakage currents in metal-insulator-metal capacitor systems," *Phys. Status Solidi B-Basic Solid State Phys.* **239**, 59-70.

[65] U. Zaghloul, G. Papaioannou, F. Coccetti, P. Pons and R. Plana (2009), "Dielectric charging in silicon nitride films for MEMS capacitive switches: Effect of film thickness and deposition conditions," *J. Microelectron. Reliab.* **49**, 1309-1314

[66] M. Lamhamdi, J. Guastavino, L. Boudou, Y. Segui, P. Pons, L. Bouscayrol and R. Plana (2006), "Charging-Effects in RF capacitive switches influence of insulating layers composition," *J. Microelectron. Reliab.* **46**, 1700-1704.

[67] S.M. Sze Physics of Semiconductor Devices Wiley-Interscience 1969

[68] J. Frenkel, (1938), "On pre-breakdown phenomena in insulators and electronic semiconductors," *Physical Review* **54**, 647-648.

[69] C. Cherki, R. Coelho and R. Nannoni (1972), "Influence of interfacial tunnel exchange on dielectric losses in thin amorphous insulating films," *Physica Status Solidi (a)*, **2**, 785-796.

in thin dielectric films applicable to MOS capacitors and memory devices[70]. Defects in the dielectric layer give rise to tunneling processes based on two or more steps.

Investigated dielectric materials in electrostatic MEMS

Several dielectric materials were investigated in electrostatic MEMS switches on the way to solving the dielectric charging problem. This includes SiO_2[71], Si_3N_4[72], AlN[73], Al_2O_3[74], Ta_2O_5[75], and HfO_2[76].

SiO_2 and Si_3N_4 are the most intensively investigated dielectric materials for electrostatic MEMS switches due to the fact they are among the most widely used in RFIC electronics. In spite of the extensive knowledge gathered on their electrical properties and stemmed from the semiconductor technology, a comprehensive understanding of the charging phenomenon of these materials implemented in electrostatic MEMS switches is still missing. This is attributed to the deposition of dielectric films on rough metal surfaces and at low temperatures (≤ 300 ºC), which are normally required by the fabrication technology of MEMS switches. The underlying metal roughness influences the dielectric film surface morphology. Also, the low temperature deposition results in a considerable deviation of material stoichiometry, and leads to SiO_x and SiN_x films with $x < 2$ and $x < 1.33$, respectively. Additionally, the low temperature gives rise to the formation of silicon nanoclusters and/or nanocrystals in both materials which are expected to lead to a random distribution of dipolar polarization as well as interfacial polarization. In SiO_x the stored charge density was reported to be thermally activated. Also, the time constants were found to be temperature independent. On the other hand, in SiN_x, it was shown that the stored charge increases with the film thickness and the deposition temperature[77]. The "holes injection" introduces metastable traps which affect the charge transport in the dielectric film, and give rise to asymmetrical current-voltage characteristics in MIM capacitors with electrode-dielectric symmetry[78].

There is a little known on the influence of other investigated dielectric materials on MEMS reliability. Ta_2O_5 and HfO_2 were used for MEMS switches due to their high dielectric constant, but both materials exhibit ionic conduction.

The charging behavior of Al_2O_3 and AlN materials has not been deeply investigated. The O–Al bonds in Al_2O_3 compound exhibit highly ionic nature. Also AlN piezoelectric material was already employed in MEMS switches[79]. Reliability measurements have shown that under low pull-in voltage or certain polarity the device degradation may be extremely low. Assessment of MIM capacitors with crystalline AlN dielectric has indicated that this behavior is attributed to

[70] R.A. Perera, Ikeda, R. Hattori and Y. Kuroki (2003), "Trap assisted leakage current conduction in thin silicon oxynitride films grown by rapid thermal oxidation combined microwave excited plasma nitridation," *J. Microelectronic Engineering,* **65**, 357–370.

[71] X. Yuan, S. Cherepko, J. Hwang, C. L. Goldsmith, C. Nordquist, and C. Dyck (2004), "Initial Observation and Analysis of Dielectric-Charging Effects on RF MEMS Capacitive Switches," *International Microwave Symposium*, pp. 1943-1946.

[72] G. Papaioannou, M. Exarchos, V. Theonas, G. Wang and J. Papapolymerou (2005), "Temperature study of the dielectric polarization effects of capacitive RF MEMS switches," *IEEE Trans. Microw. Theory Tech.* **53**, 3467-3473.

[73] E. Papandreou, G. Papaioannou, and T. Lisec (2009), "A correlation of capacitive RF-MEMS reliability to AlN dielectric film spontaneous polarization," *International Journal of Microwave and Wireless Technologies* **1**, 43-47

[74] P. Blondy, A. Crunteanu, A. Pothier, P. Tristant, A. Catherinot, and C. Champeaux (2007), "Effects of Atmosphere on the Reliability of RF-MEMS Capacitive Switches," *European Microwave Integrated Circuits Conf.*, pp. 548-551

[75] X. Rottenberg, H. Jansen, P. Fiorini, W. De Raedt, and H. Tilmans (2002), "Novel RFMEMS capacitive switching structures," *32nd European Microwave Conf.*, pp. 1-4.

[76] J.K. Luo, M. Lin, Y.Q. Fu, L. Wang, A.J. Flewitt, S.M. Spearing, N.A. Fleck, and W.I. Milne (2006), "MEMS based digital variable capacitors with a high-k dielectric insulator," *Sensors and Actuators A*, **132**, 139–146.

[77] R. Daigler, E. Papandreou, M. Koutsoureli, G. Papaioannou and J. Papapolymerou (2009), "Effect of deposition conditions on charging processes in SiNx: Application to RF-MEMS capacitive switches," *J. Microelectron. Eng.* **86**, 404-407

[78] J. Vandershueren, and J. Casiot in: P. Braunlich, Ed. (1979), *Topics in Applied Physics: "Thermally stimulated relaxation in solids"*, Springer-Verlag, Heidelberg, Germany.

[79] J.A. Ruffner, P.G. Clem, B.A. Tuttle, D. Dimos, and D.M. Gonzales (1999), "Effect of substrate composition on the piezoelectric response of reactively sputtered AlN thin films," *Thin Solid Films*, **354**, 256-261.

the presence of a spontaneous polarization arising from dislocations that may induce a surface charging.

The space charge polarization due to presence of free charges or injected charges as well as the dipolar polarization constitutes the major charging mechanisms in all aforementioned dielectric films. Given the extreme diversity in composition and behavior that each of these dielectrics may have even by slightly changing the deposition methods, the development of a systematic investigation platform can be carried out only if a specific material is chosen as reference. The choice at LAAS for a reference-investigated dielectric felt on plasma-enhanced chemical vapor deposition (PECVD) SiN_x. This material has been largely exploited in many different processes and its study represented an important common interest in the laboratory.

Available characterization techniques for the dielectric charging

Due to the complexity of dielectric charging mechanisms, these phenomena cannot be investigated through a simple and univocal assessment method. Various characterization techniques based on different test vehicles, such as actual MEMS switches, metal-insulator-metal (MIM) capacitors, or bare thin dielectric films, need to be considered (see Table 2.2).

Table 2.2: Comparison between the investigated techniques with respect to applicable test vehicles where reference dielectrics is SixNy deposed under several different recipes.

	CV	C/DCT	TSDC	KPFM	FDC
TF				√	√
MIM	√	√	√	√	√
MEMS	√	√		√	√

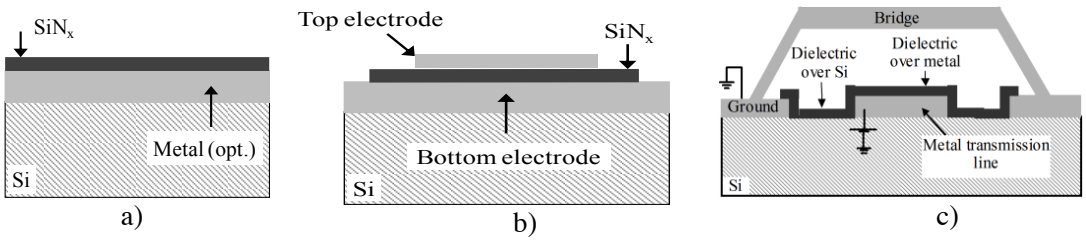

Figure 2.15: Typical test vehicles used for the investigation of the dielectric charging: a) thin film dielectric (TF) on substrate (but also on metals); b) metal-insulator-metal (MIM); c) actual capacitive MEMS switch with dielectric deposed on metal so as the substrate.

As concluded from the abovementioned discussion, each assessment method provides partial information about the charging phenomenon. A critical issue is to establish a phenomenological correlation between the results coming from different investigation methods. Thus, the methods associated to MIM capacitors (C/DCT and TSDC) have been considered as efficient tools to assess the bulk properties of the dielectric films. The same is however limited in providing information about the actual MEMS device.

In the following the focus will be mainly devoted to the **new methodology introduced in these studies** (U. Heiba Zaghloul PhD Thesis 2008-11), which are **based on the extensive exploitation of *surface scanning microscopy technique*** such as the Kelvin Probe Force microscopy (KPFM) and the Force Distance Curve (FDC) microscopy. Before to do it however hereby follows a brief overview of more conventional techniques.

Characterization based on Micro Electro Mechanical (MEMS) test vehicles:

Several characterization methods were reported to study dielectric charging using the actual MEMS switches. Among those, the basic assessment methods rely on monitoring the shift of

bias for minimum capacitance, V_{min}, or pull-in and pull-out voltages of the C-V characteristic of a MEMS switch. The shift in V_{min} method is based on the fact that when the switch dielectric is charged, the C-V characteristic below pull-in is asymmetrical. The unique advantage of V_{min} based methodology is that the shift is a quantity that accurately provides information on the dielectric charging and does not depend on the mechanical parameters of the switch metal bridge. For this reason, it has been widely used[53,80], to assess the charging due to cycling and ESD stress at room as well as at elevated temperatures. Yet, the charge calculated through this method is obtained under low electric field conditions. Since the performance of a capacitive MEMS switch is determined by the shift of pull-in and pull-out voltages, which occur under high electric fields, the importance of V_{min}-based characterization technique is limited. This further explains why the influence of dielectric charging on the shift of pull-in and pull-out voltages and the evolution of their windows under electrical stress has been the most intensively investigated method to study charging in electrostatic MEMS switches[81,82,83,84].

Monitoring the switch-ON and switch-OFF transients or discharge current transients (DCT) is another method to study the dielectric charging in MEMS switches[72,85,86]. In this technique, the dielectric charging and discharging kinetics and the mechanisms that contribute to them could be investigated. The modification of the electrostatic force between the switch bridge and the dielectric film by trapped charges resembles the concept behind this method. This effect is emphasized by the fact that **in a real MEMS switch the surfaces of the switch bridge and the dielectric film are not perfectly flat during contact**. So, **the charge injection occurs through asperities and the surface roughness**. In the case of discharge currents, the C-V characteristic is required in order to determine the charge sign. On the other hand, the presence of thermally activated mechanisms in dielectrics requires characterizing MEMS switches under different temperatures.

Characterization methods based on Metal-Insulator-Metal (MIM) test vehicles:

Although MIM capacitors do not substitute MEMS switches in the ‘up’ and ‘down’ states, they proved to be valuable test structures for studying the electrical properties of dielectric materials. The dielectric charging in MIM capacitors were investigated through two experimental methods; the charge/discharge current transients (C/DCT) and the thermally stimulated depolarization currents (TSDC). Both methods are based on the application of an electric field for a long time so that to produce saturation of dipole orientation and trapping of injected charges. In the C/DCT method, the charging and discharging currents of a MIM capacitor are measured. The TSDC provides a complete picture of the temperature-dependent relaxations, and allows the parameters of activation energy, E_A, and relaxation time, τ_0, to be obtained from a single measurement.

The C/DCT method was extensively applied to study dielectric charging in SiO_2[87] and Si_3N_4[88] films. In all cases, the results revealed that both the charging and discharging transients

[80] J. Ruan, G. J. Papaioannou, N. Nolhier, N. Mauran, M. Bafleur, F. Coccetti and R. Plana (2008), "ESD failure signature in capacitive RF MEMS switches," *J. Microelectron. Reliab.*, **48**, 1237-1240.

[81] C. Goldsmith, J.Ehmke, A.Malczewski, B.Pillans, S.Eshelman, Z.Yao, L.Brank, M.Eberly, “Lifetime characterization of capacitve RF MEMS switches”, *IEEE International Microwave Symposium*, vol.1, May 2001.

[82] S. Melle, D. De Conto, D. Dubuc, K. Grenier, O. Vendier, J. Muraro, J. Cazaux and R. Plana, "Reliability modeling of capacitive RF MEMS," *IEEE Trans. on Microw. Theory Tech.* **53**, (2005) 3482-3488.

[83] X. Rottenberg, I. De Wolf, B. K. J. C. Nauwelaers, W. De Raedt, and H. A. C. Tilmans, "Analytical model of theDCactuation of electrostaticMEMSdevices with distributed dielectric charging and nonplanar electrodes," *IEEE/ASME J. Microelectromech. Syst.*, **16**, (2007) 1243-1253.

[84] D. Mardivirin, A. Pothier, A. Crunteanu, B. Vialle, P. Blondy, “Charging in dielectric less capacitive RF-MEMS switches,” EEE Transactions on Microwave Theory and Techniques Vol.57, Issue 1 (2009) pp.231-236.

[85] W. Van Spengen, P. Czarnecki, R. Poets, J. Van Beek and I. De Wolf (2005), "The influence of the package environment on the functioning and reliability of RF-MEMS switches," *Proc. 2005 IEEE Int. Reliability Physics Symposium*, pp. 337-341, IEEE, New York.

[86] Nieminen, H., J. Hyyrylainen, T. Veijola, T. Ryhanen and V. Ermolov (2005), “Transient capacitance measurement of MEM capacitor,” *Sensors and Actuators A* **117**, 267–272.

[87] X. Yuan, J. Hwang, D. Forehand and C. Goldsmith (2005), "Modeling and characterization of dielectric-charging effects in RF MEMS capacitive switches," *2005 IEEE MTT-S Int. Microwave Symp. Dig.*, pp. 753-756, IEEE, New York.

are multi exponential with temperature independent relaxation time constants. Also, the presence of thermally activated mechanisms in SiN_x was reported based on the C/DCT measurements. The decay was fitted using the stretched exponential law and the Arrhenius plot of relaxation time allowed the calculation of the activation energy (E_A) and relaxation time constants (τ_0) at room temperature[89]. On the other hand, the advantages of employing the TSDC method are twofold. First, the measured TSDC current at different temperature is analyzed and leads to the different involved charging mechanism for which E_A and τ_0 can be determined. A direct example for that was reported by Papandreou et al.[90], where the relaxation times in SiN_x were found to be distributed around specific activation energies with values of 0.17 eV, 0.35 eV and 0.55 eV. The other important benefit is that the TSDC method could measure a wide range of relaxation times which exits in amorphous dielectric films where the relaxation times are normally distributed over several decades.

The abovementioned assessment methods applied for either actual MEMS switches or MIM capacitors, although extremely useful, lead to results that depend strongly on the nature of the device under test. Thus, in MIM capacitors the discharge takes place under a short circuit condition and the trapped charges are collected by (both) injecting electrodes. On the contrary, in MEMS the injected charges are collected only by the bottom electrode while the top electrode, the bridge, is in the up-state. Additionally, MEMS failure mechanisms are often related to multiphysics phenomena. For example, the FEMA results (Table 2.1) highlights that several failure mechanisms, rather than the dielectric charging, result in a shift of the C-V characteristics, and pull-in and pull-out voltages. This includes the elastic and plastic deformation of the bridge, corrosion, wear, friction, fretting corrosion, and creep failure mechanisms. Therefore, the characterization techniques which make use of the actual MEMS switches, *cannot study separately* the dielectric charging phenomenon since other failure mechanisms contribute to the measurements. Besides, these methods are quite expensive and time consuming since the fabrication of the complete MEMS devices, including many levels of photolithography, is required.

Characterization method based on Thin-Films (TF) test vehicles:

The characterization method of thin dielectric films is base upon the surface scanning microscopy which was originally introduced at LAAS in 2007[91]. In this investigation the charging in bare SiN_x thin films (TF) deposited over hosting underlying surfaces be them metal (electrodes or transmission lines), or dielectric (as passivation SiO_2 layers) or semiconductor (as bare silicon substrate). In these studies the observation of the thin-film material and its interaction with underneath material is at stake.

The three different characterization test vehicles mentioned above (Table 2.2) have been studies with conventional technique (CDT, TSDC,…) but here the emphasis will be given to the newly introduces dielectric studies approaches based on surface scanning microscopy based on the innovative use of the AFM equipment.

Surface scanning microscopy (AFM) technique applied to dielectric charging

[88] M. Lamhamdi, P. Pons, U. Zaghloul, L. Boudou, F. Coccetti, J. Guastavino, Y. Segui, G. Papaioannou and R. Plana (2008), "Voltage and temperature effect on dielectric charging for RF-MEMS capacitive switches reliability investigation," *J. Microelectron. Reliab.* **48**, 1248-1252

[89] M. Exarchos, V. Theonas, P. Pons, G.J. Papaioannou, S. Melle, D. Dubuc, F. Coccetti, and R. Plana (2005), "Investigation of charging mechanisms in Metal-Insulator-Metal structures," *J. Microelectronics Reliability*, **45**, 1782–1785

[90] E. Papandreou, M. Lamhamdi, C. M. Skoulikidou, P. Pons, G. Papaioannou and R. Plana (2007), "Structure dependent charging process in RF MEMS capacitive switches," *J. Microelectron. Reliab.* **47**, 1812-1817.

[91] M. Lamhamdi, L. Boudou, P. Pons, J. Guastavino, A. Belarni, M. Dilhan, Y. Segui and R. Plana, "Si3N4 thin films proprerties for RF-MEMS reliability investigation," *Proc. of the International Solid-State Sensors, Actuators and Microsystems Conference (TRANSDUCERS 2007)*, (2007) pp. 579-582, IEEE, New York

There are several advantages for the AFM-based assessment methods. First, it efficiently simulates the **charging *through* asperities** and the charge collection through the bottom electrode of MEMS switches providing qualitative information on dielectric free surface charge distribution and decay. Second, the AFM-based technique allows **studying the dielectric charging physics *separately***, and hence building a comprehensive understanding of the charging phenomenon without interferences with other failure mechanisms. Finally, it represents a **low cost and quite fast solution** compared to the currently available assessment methods since the required samples for this approach are bare dielectric films, hence no photolithography steps are required during the sample preparation[92].

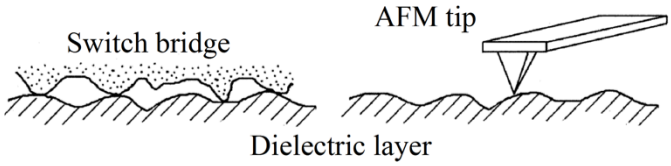

Figure 2.16: Multi-asperity at the interface between the switch bridge and the dielectric film and the use of the AFM tip to emulate the single asperity contact.

In spite of the aforementioned advantages, the AFM based characterization suffers from several weaknesses. First, the AFM tip simulates charging through only a single asperity, while in MEMS switch charging takes place through thousands or millions of asperities simultaneously. Also, the published work related to dielectric charging assessment using AFM, was performed in ambient air, and hence the effect of relative humidity has not been addressed. Moreover, the used samples have not been thermally treated before the AFM experiments. Jacobs et al. reported that at low humidity (≈10%) trapped surface charges could be detected in the KPFM measurements while such charging effects become less prominent at high humidity levels (≈80%)[93]. In addition, the adsorbed water layer on the sample surface is considered to shield the surface potential[94]. The removal of the water-related layer from both surfaces of the sample and the AFM tip was found to be very important to improve the reliability of AFM-based measurements[95]. For these reasons, the available previous results (anterior to this study - 2007) based on AFM characterization related to the charging phenomenon have to be considered carefully since their experimental conditions have not been addressed properly. In addition, there has been no report on the dielectric charging under different electric fields comparable to the existing ones in driving MEMS switches using AFM.

Before to see more in details these techniques is essential to stress the **importance of physical material characterization**. In fact, in order to carry out the investigation of thin film dielectrics (SiN_x films), the use of physical material characterization techniques such as Fourier transform Infra-Red spectroscopy (FT-IR) and (X-ray photoelectron spectroscopy) XPS has been extensively used (H. Wang Post-Doc 2009-2010) to well characterize the material under test. FT-IR spectroscopy in particular was performed to provide information about the chemical bonds of the dielectric film and their variations[96]. The reflection and transmission modes were

[92] U. Zaghloul, F. Coccetti, G. Papaioannou, P. Pons and R. Plana (2010), "A novel low cost failure analysis technique for dielectric charging phenomenon in electrostatically actuated MEMS devices," *2010 IEEE Int. Reliability Physics Symp.*, pp. 237-245, IEEE, New York.

[93] H. Jacobs, H. Knapp and A. Stemmer (1999), "Practical aspects of Kelvin probe force microscopy," *Rev. Sci. Instrum.* **70**, 1756-1760.

[94] H. Sugimura, Y. Ishida, K. Hayashi, O. Takai and N. Nakagiri (2002), "Potential shielding by the surface water layer in Kelvin probe force microscopy," *Appl. Phys. Lett.* **80**, 1459-1461.

[95] S. Ono, M. Takeuchi and T. Takahashi (2001), "Kelvin probe force microscopy on InAs thin films grown on GaAs giant step structures formed on (110) GaAs vicinal substrates," *Appl. Phys. Lett.* **78**, 1086-1088.

[96] The infrared spectra were acquired in the 400 – 4000 cm^{-1} range with a BIORAD FTS60A spectrometer with the samples under nitrogen flow to avoid the effect of humidity and ambient

employed for SiN_x layers deposited on metal and silicon, respectively. On the other hand the XPS experiments were used to provide information about the different chemical bonds and valence state in surface and bulk SiN_x[97]. Here it should be pointed out that the XPS measurement is not sensitive to hydrogen or helium.

These studies have allowed us to correlate the dielectric charging investigation methodology to the constitutive structural properties of the materials.

KPFM-based characterization technique

The Kelvin Probe Force microscopy (KPFM) is also known as surface potential microscopy is a "non-contact" variant of the AFM and was invented in 1991[98]. The KPFM, allow measure the contact potential difference (CPD) by observing the work function of a surfaces at atomic or molecular scales. The work function relates to many surface phenomena, including catalytic activity, reconstruction of surfaces, doping and band-bending of semiconductors, charge trapping in dielectrics and corrosion. The map of the work function produced by KPFM gives information about the composition and electronic state of the local structures on the surface of a solid. Since the work function or surface potential strongly affect the chemical and physical phenomena taking place at the surface, KPFM reveals critical information on the physical and chemical changes of the surface condition, needed for understanding physical and chemical phenomena on metal/semiconductor surfaces and devices[99,100]. In the following section, the theory behind surface potential measurements using KPFM is presented. A discussing about the procedure of different KPFM-based characterization techniques employed to study the charging phenomenon will be outlined by stressing the role of critical KPFM measurement parameters and their optimization with respect to MEMS reliability investigation.

KPFM theory

A block diagram of the KPFM surface potential measurement system is shown in Figure 2.17a. There are three spectral components for the electrostatic force between the AFM tip and the sample surface that exist at DC, ω and 2ω, and are given by H. Jacobs et al. [101], and B. Bhushan et al. [102] as:

$$\left.\begin{aligned} F_{DC} &= -\frac{1}{2}\frac{dC}{dz}((\Delta\Phi - U_{DC})^2 + \frac{1}{2}U_{AC}^2) \\ F_{\omega} &= -\frac{dC}{dz}(\Delta\Phi - U_{DC})U_{AC}\sin(\omega t) \\ F_{2\omega} &= \frac{1}{4}\frac{dC}{dz}U_{AC}^2\cos(2\omega t) \end{aligned}\right\} \qquad (2.7)$$

where ω is the mechanical resonance frequency of the AFM tip, C is the capacitance between the tip and the sample surface, z is the tip-sample separation, ΔΦ is the contact potential difference between the tip and the sample materials, UDC is the applied DC voltage to the AFM

[97] A VG ESCALAB 220-iXL spectrometer was used to perform the XPS measurements. The deposited SiN_x layers were excited by MgKα (1253.6 eV), and the kinetic energies of the electrons emitted were collected at a constant energy resolution of 1 eV. Since the SiN_x films are rather nonconductive, electron compensation was needed during the measurement

[98] M. Nonnenmacher, M. P. O'Boyle, and H. K. Wickramasinghe (1991). "Kelvin probe force microscopy" (free-download pdf). *Appl. Phys. Lett.* **58** (25): 2921. Bibcode 1991ApPhL..58.2921N. doi:10.1063/1.105227.

[99] W. Melitz, J. Shena, A.C. Kummela, S. Lee, "Kelvin probe force microscopy and its application," Elsevier, Surface Science Reports 66 (2011) 1–27.

[100] Kelvin Probe Force Microscopy on Wikipedia

[101] H. Jacobs, H. F. Knapp, S. Müller and A. Stemmer (1997), "Surface potential mapping: A qualitative material contrast in SPM," *Ultramicroscopy* **69**, 39-49.

[102] B. Bhushan and A. Goldade (2000), "Measurements and analysis of surface potential change during wear of single-crystal silicon (100) at ultralow loads using Kelvin probe microscopy," *App. Surf. Sci.* **157**, 373-381.

tip from the KPFM feedback loop, and UAC is the voltage amplitude of the sinusoidal signal applied from the oscillator to drive the AFM tip at or very close to ω during the surface potential measurements. Since the cantilever responds only to forces at or very close to its resonance frequency, the DC and F2ω force components do not cause any significant oscillation of the cantilever, and F_ω becomes the dominant one. The main goal of the KPFM feedback loop is to adjust the potential of the tip, U_{DC}, until the term $\Delta\Phi$-U_{DC} becomes 0, at which point the cantilever oscillation amplitude is supposed to be zero ($F_\omega = 0$). At this point, the measured tip potential, U_{tip}, which corresponds to the contact potential difference between the tip and the sample, $\Delta\Phi$, is equal to the sample surface potential, and is used to generate a potential map for the sample surface. The presence of the induced charges on a charged dielectric surface produces an additional electrostatic force, which contributes to the total electrostatic force between the AFM tip and the sample surface. In other words, **the trapped charge alters the contact potential difference between the tip and the dielectric materials**, $\Delta\Phi$, and therefore it can be determined by the local measured tip potential, U_{DC}.

The KPFM surface potential measurements are normally performed using the lift-mode (Figure 2.17b). In this mode, the surface topography and the potential signals are subsequently recorded over the sample surface. First the surface topography is acquired in tapping mode along a single line profile (1 in Figure 2.17b)[103]. Next, the mechanical excitation of the cantilever is turned off and the tip ascends to a fixed distance from the sample surface H (2 in Figure 2.17b). Finally, a second scan is executed along the same line following the same topographic profile recording local variations in the surface potential (3 in Figure 2.17b). In this study, conductive scanning capacitance microscopy-Platinum Iridium Tapping (SCM-PIT) AFM tips from NanoWorld® were used for the KPFM measurements.

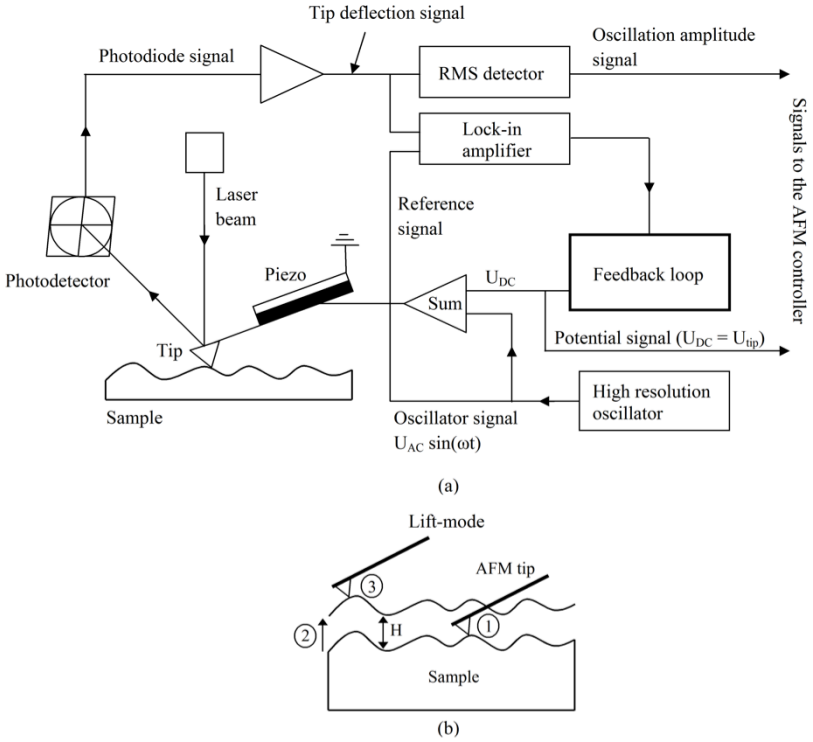

Figure 2.17: KPFM surface potential measurement procedure: a) block diagram, b) the lift-mode.

[103] Liscio, A., V. Palermo, D. Gentilini, F. Nolde, K. Müllen, and P. Samorí (2006), "Quantitative measurement of the local surface potential of p-conjugated nanostructures: a Kelvin Probe Force Microscopy study," *Adv. Funct. Mater.*, **16**, 1407-1416.

These tips are Antimony n-doped Si, coated with platinum/iridium to provide high conductivity, and have a typical tip radius of less than 25 nm. The metallic coating as well as the low spring constant (K = 1-5 N/m) and the low resonance frequency (f_o = 60-100 KHz) of these tips make them well suited for sensitive surface potential measurements.

As mentioned, three different characterization methodologies based on KPFM surface potential measurements have been introduced to study the charging phenomena. This includes the application of KPFM to investigate the charging in bare dielectric thin films (KPFM-TF), MIM capacitors (KPFM-MIM), and MEMS switches (KPFM-MEMS).

KPFM-TF technique

The KPFM-TF characterization method is used to study the charging in bare SiN_x thin films (TF) deposited over planar substrates. The measurement procedure is made of two consecutive steps as shown in Figure 2.18. First, charges are injected in single points over the SiN_x surface by applying voltage pulses of defined amplitude, U_p, and duration, T_p, to the AFM tip during scanning the sample surface in tapping mode (Figure 2.18a). **The tapping mode was used for charge injection since it is the most reliable mode for obtaining reproducible KPFM results**. Charge injection in contact mode often led to a damaged tip shape, which affects the KPFM measurements negatively. After completing the charge injection, KPFM surface potential measurement is performed.

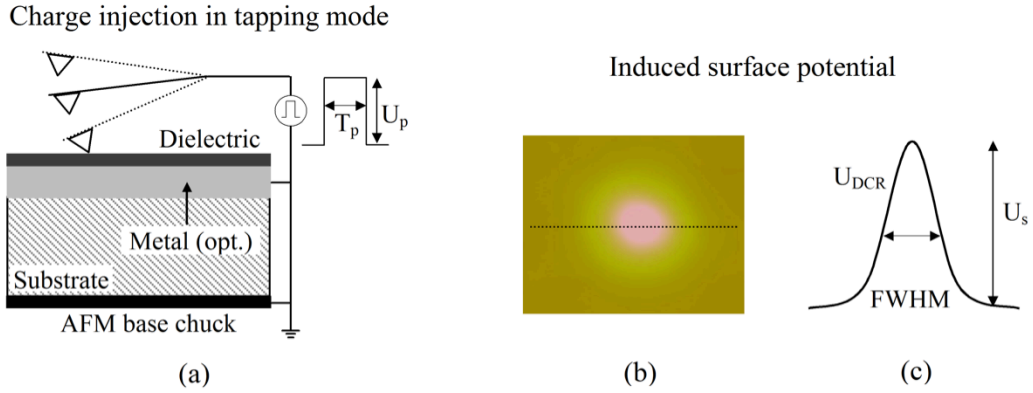

Figure 2.18: Dielectric charging assessment using KPFM-TF technique: a) charge injection in tapping mode, b) resulting surface potential map from injection in a single point, c) the extracted relative potential profile represented by Us and FWHM.

For each injected position over the dielectric surface, the measured surface potential, U_{DC}, has a maximum at the position which was directly under the AFM tip apex during the charge injection step, and it decreases gradually at the edges of injected position as shown in Figure 2.18b, c. The peak value of the induced surface potential is located in the KPFM map, and a horizontal cross section is taken at this position resulting in the absolute surface potential profile. In order to eliminate the impact of the tip material, the background surface potential of the SiN_x film is measured first before performing the charge injection step. Afterwards, the background potential is subtracted from the absolute potential profile resulting in the relative surface potential profile, U_{DCR} (Figure 2.18c), which is a direct indication of the injected charge density in the dielectric film. Therefore, the analysis of KPFM-TF results is performed using the surface potential peak amplitude, U_s, full width at half maximum (FWHM), and the integral of the relative potential profile (Figure 2.18c). For better accuracy, each KPFM-TF measurement is performed three times, and a statistical evaluation is made by averaging over these three measurements. The evolution of U_s and FWHM with time also monitored and analyzed in order to study the discharging process in dielectric films.

An example of KPFM-TF surface potential maps measured for charges injected under different pulse amplitude, U_p, using positive and negative voltage is presented in Figure 2.19a, b, respectively. The figure also shows the potential maps obtained at different time points after the charge injection step for studying the charge relaxation. The decay of the measured surface potential with time due to charge collection is obvious from the figure. Figure 2.19**c** presents the resulting potential profile for charges injected under different pulse amplitude, U_p. It is clear from the figure that U_s, FWHM (Figure 2.19d) and consequently the potential profile integral (Figure 2.19e) increases remarkably with increasing the applied pulse amplitude.

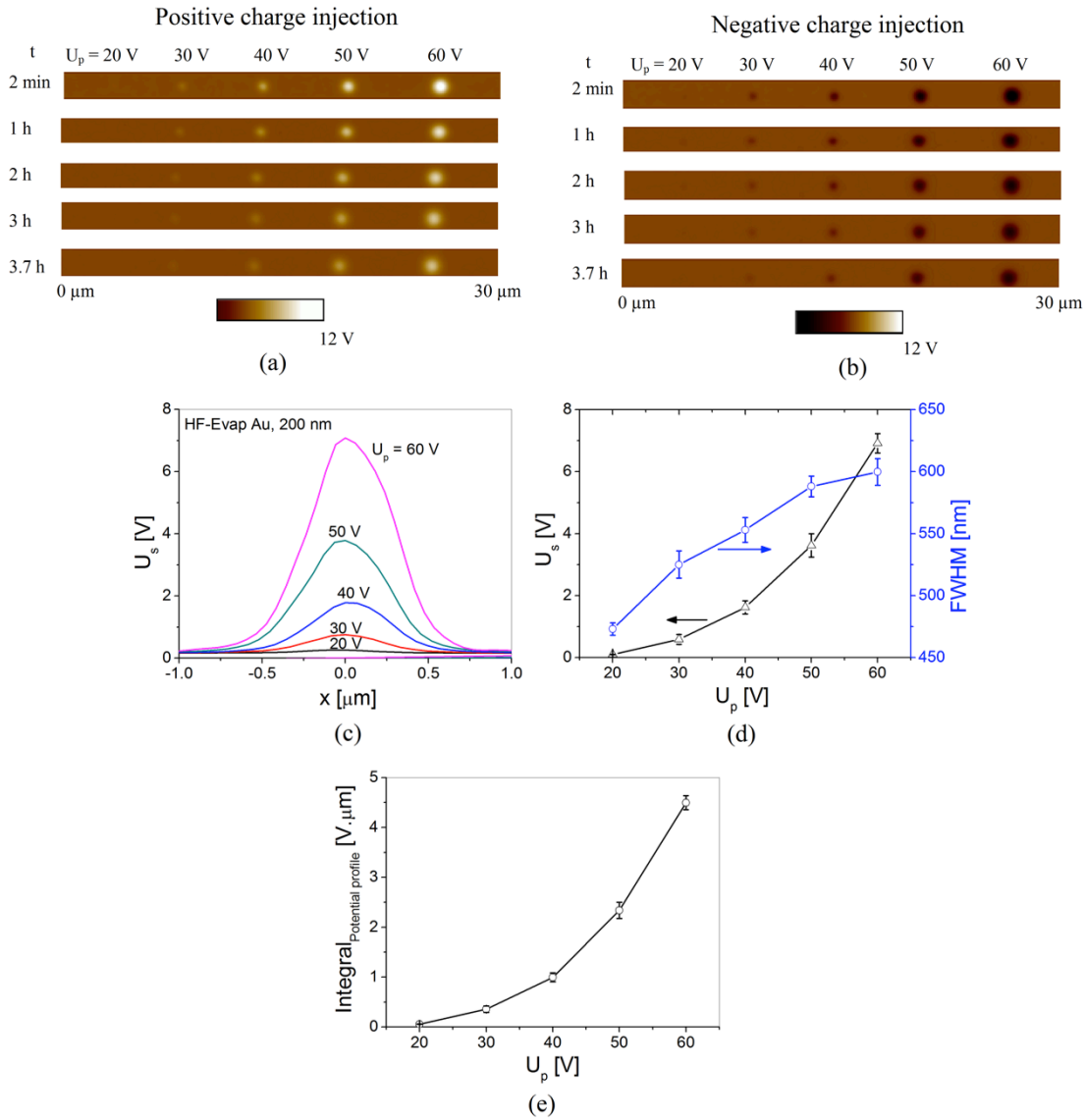

Figure 2.19: Example of KPFM-TF results for charges injected using different Up: the surface potential is obtained at different time points after injection for positive (a) and negative (b)charge injection; c) potential profile for positive charge injection at t=0, (d) the corresponding FWHM and (e)potential profile integral.

Extensive studies on the effect of tip-sample separation and tip shape degradation during measurement have been done by fine tuning of the AFM feedback systems and monitoring the

effect of them on the final read out (surface potential and FWHM)[104]. This combined with the use of reference samples (materials) has allowed an accurate calibration the measurement setup.

Noteworthy is that this technique does not allow the quantitative estimation of the accumulated/injected charge since in order to do this a very accurate knowledge of the tip-sample electrostatic capacitance is needed.

KPFM-MEMS, KPFM-MIM characterization techniques

Although the KPFM-TF characterization method simulates efficiently the charging and discharging scenarios in electrostatic MEMS switches, it suffers from some drawbacks. First, the charge injection using the AFM tip in single points simulates a single asperity while in MEMS switches charging takes place through thousands or even millions of asperities locations simultaneously due to the roughness of both the dielectric film and the switch bridge. Second, the charge injection in single points results in inhomogeneous sample surface and therefore the measured KPFM potential is an average value as explained earlier, and hence it does not reflect accurately the real induced surface potential. Finally, due to the influence of the dielectric charging on surface topography measurements, additional techniques are required to avoid noise or artifacts in the KPFM signals[105], leading to more complex measurements.

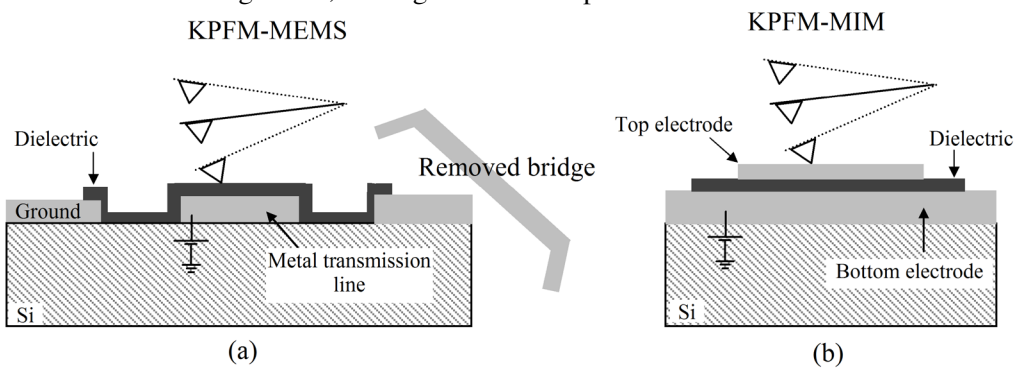

Figure 2.20: Schematic representation describing the procedure of (a) KPFM-MEMS and (b) KPFM-MIM characterization technique.

In order to overcome these drawbacks, other KPFM-based characterization techniques have been proposed in this study. The first technique (KPFM-MEMS) makes use of KPFM to study the discharging process on a microscopic scale for a charged dielectric film implemented in MEMS switch. The switch is actuated first using the desired stress voltage and duration to charge the SiN_x film. Next, the switch suspended electrode is mechanically removed, and KPFM is used to monitor the induced surface potential over the charged dielectric with time (Figure 2.20a). The second technique (KPFM-MIM), was proposed for the first time in these studies and is used to observe the discharging process in MIM capacitors. Similar to KPFM-MEMS, the SiN_x film is charged first by electrically stressing the MIM capacitor. Then, the surface potential of the top MIM electrode, which reflects the potential of the charged SiN_x film, is measured in time by KPFM (Figure 2.20b). Since the MIM top electrode has a homogeneous surface

[104] U. Zaghloul, B. Bhushan, F. Coccetti, P. Pons, and R. Plana (2011), "Kelvin probe force microscopy-based characterization techniques applied for electrostatic MEMS/NEMS devices and bare dielectric films to investigate the dielectric and substrate charging phenomena," J. Vac. Sci. Technol. A 29, Art.# 051101

[105] D. Ziegler, N. Naujoks, and A. Stemmer (2008), "Feed-forward compensation of surface potential in atomic force microscopy," *Rev. Sci. Instrum.* **79**, Art. #063704.

potential, the measured KPFM signal is independent of tip related issues (i.e. the tip shape, tip-sample separation, tip position over the sample, etc). Moreover, the measured KPFM-MIM potential is closer to the real surface potential of the charged dielectric compared to KPFM-TF, since it is averaged over an equipotential surface. Finally, the impact of the dielectric charging on surface topography, which usually exists in the KPFM-TF method, can be completely eliminated using the KPFM-MIM technique. At this point the KPFM surface potential can be measured over any location of the MIM top electrode. Hence, the additional techniques employed to reduce the effect of charging on topography like the one presented in D. Ziegler et al.[105] are not anymore required.

FDC-based characterization methodology

Induced adhesive force and surface potential measurements using FDC

An example of the force-distance curve for the investigated SiN_x samples is presented in Figure 2.21a. The force-distance measurement starts at a large separation from the sample surface (point A) where there is no deflection of the cantilever. As the piezo moves towards the sample, a sudden mechanical instability occurs between point B and point C, and the tip jumps into contact with the adsorbed water film and wicks up around it to form a meniscus. The cantilever bends downwards because of the attractive meniscus force acting on the tip. As the piezo further approaches the SiN_x surface, the deflection of the cantilever increases while the tip travels in the water film and eventually contacts the underlying SiN_x surface at point C, and then the cantilever starts to bend upwards. Once the piezo reaches the end of its designated ramp size at point D, it is retracted to its starting position. The tip goes beyond zero deflection (point E) and enters the adhesion region. At point E, the elastic force of the cantilever becomes equivalent to the adhesive force, causing the cantilever to snap back to point F. The adhesive force, which is the force needed to pull the tip away from the sample, can be calculated from FDC by multiplying the vertical distance between E and F with the stiffness of the cantilever, k, as given by B. Bhushan[54]:

$$F_{adh} = (F - E)\,k \qquad (2.8).$$

When voltage is applied between the AFM tip and the sample, the cantilever deflection increases due to the increase in the attractive electrostatic force, as shown in Figure 2.21b. The difference between the points E and F increases too with increasing the applied voltage as shown from the figure, and according to Eq. 2.8 this leads to an increase in the adhesive force between the AFM tip and the sample. A similar response exits when measuring the adhesive force between the AFM tip and a charged SiN_x film. **Due to trapped charges in a charged dielectric, the induced surface potential over the dielectric results in increasing the voltage difference between the tip and the dielectric, leading to larger adhesive force**. Basically, this is the principle behind which the FDC measurements were employed to study the dielectric charging phenomenon. The force-volume method was used in order to map the adhesive force between the sample and the tip in three dimensions. A single force-distance curve records the force imposed on the tip as it approaches and retracts from a point on the sample surface, as explained in Figure 2.21a. Force-volume imaging associates each (X, Y) position with a force- distance curve in Z. For each sample, the force-volume method was used to obtain adhesive force maps over a selected dielectric area. The adhesive force for each position in the map is then calculated from the obtained force-distance curves using Eq. 2.8. This is followed by a statistical evaluation for each map by averaging over all the measured positions.

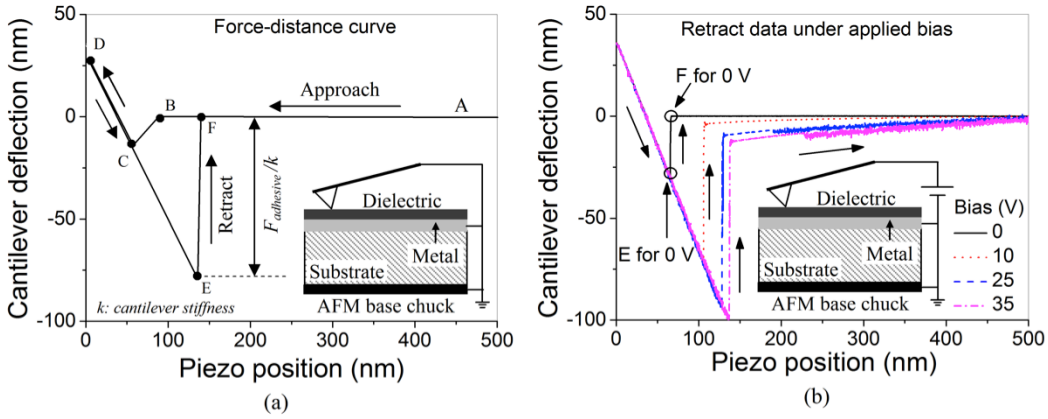

Figure 2.21: Dielectric charging characterization based on FDC measurements: (a) an example of the force-distance curve plot for the investigated SiNx samples, and (b) the retract data of force-distance curve plot at different voltage levels applied between the AFM tip and the sample.

As shown from Figure 2.21b, when a voltage difference exists between the AFM tip and the sample, the cantilever does not return directly to its original position, and instead its return path has an intermediate stag. Based on that, for charged dielectric films an external voltage is applied to the AFM tip and is modified gradually in order to set off the induced surface potential over the dielectric surface. When the applied bias equals the induced surface potential over the dielectric film, force distance curve returns to its original shape and the intermediate stages shown in Figure 2.21b disappears. At that point, the external applied voltage is equal in amplitude and opposite in sign to the induced surface potential over the dielectric surface.

FDC-based characterization techniques: FDC-TF, FDC-MIM and FDC-MEMS.

The first technique applies the FDC methodology to study the charging in bare SiN_x thin films (FDC-TF), similar to the KPFM-TF method. The second and third techniques apply the FDC method to study the dielectric charging in SiN_x films implemented in MIM capacitors (FDC-MIM) and MEMS switches (FDC-MEMS), similar to KPFM-MIM and KPFM-MEMS methods, respectively. In the FDC-TF technique, the charging of the SiN_x film is performed through scanning the SiN_x surface in contact mode using the force-volume method while a voltage difference is applied between the tip and the Au layer underneath the SiN_x film (see inset in Figure 2.21b). After completing the charging experiment, the voltage difference between the AFM tip and the sample was removed.

An example of the obtained adhesive force maps using the FDC-TF technique after charging the SiN_x film using a single scan is shown in Figure 2.22a. The figure highlights that the adhesive force in the charged (dark brown) area is much larger compared to the non-charged (light brown) area over the dielectric surface. Charge injection over the dielectric surface results in a large induced surface potential that causes a considerable voltage difference between the AFM tip and the SiN_x sample. Consequently, the electrostatic attractive force between the AFM tip and the dielectric surface will increase, causing the net adhesive force to be larger than the non-charged areas. The adhesive force maps obtained from charge injection using different applied electric field is presented in Figure 2.22b, while the measured surface potential using the FDC method and the measured adhesive force for these maps are presented in Figure 2.22c. It is clear from the figures that the measured surface potential and adhesive force increase with the electric field applied during the charging step due to larger injected charge density in the dielectric film.

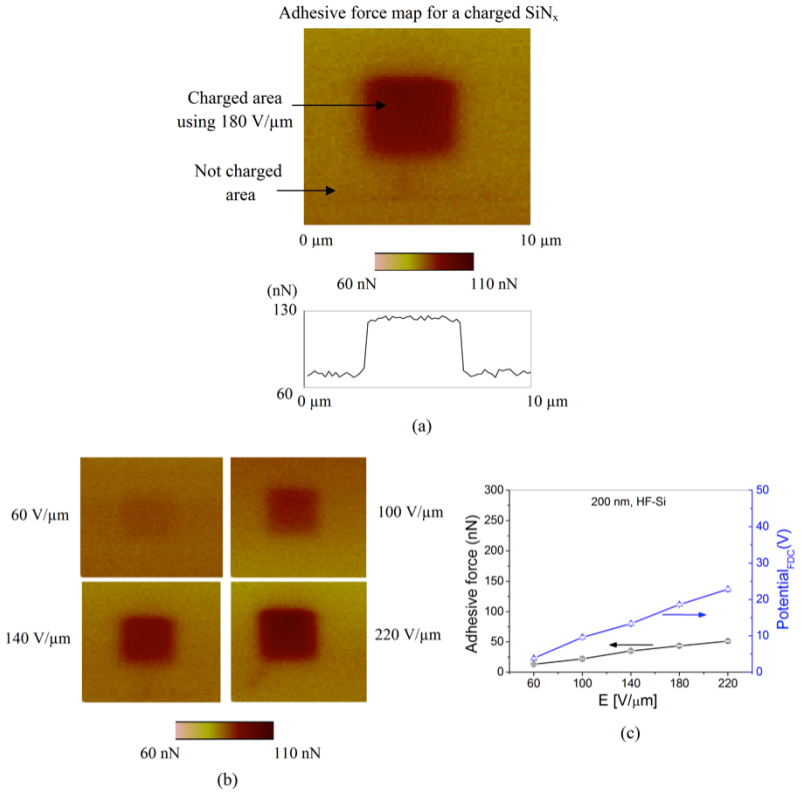

Figure 2.22: Example of adhesive force maps measured by FDC-TF for: (a) HF-SiNx film charged using E=180V/μm; (b) same film but charged using different values of electric field; (c) the induced adhesive force and surface potential corresponding to these latter bias conditions.

In the FDC-MIM, both the charge build-up with time as well as the discharging process of SiN_x films implemented in MIM capacitor was studied. Force-volume method here is used to map the adhesive force between the AFM tip and MIM top electrode continuously with time during both the charging and discharging experiments. Similar to the FDC-TF, the charging experiment is performed first while the AFM tip is biased. Then, the voltage difference between the AFM tip and the MIM bottom electrode is removed, and then the discharging adhesive force is measured continuously with time. As with the FDC-TF method, the bottom MIM electrode is kept grounded during the discharging process. In the FDC-MEMS technique, the adhesive force between the AFM tip and a charged SiN_x film implemented as the dielectric layer in a capacitive MEMS switch is monitored with time, similar to the KPFM-MEMS method.

Before charging the SiN_x films in the abovementioned FDC-based characterization techniques, the adhesive force map was first measured between the AFM tip and the SiN_x surface in the case of FDC-TF and FDC-MEMS, and between the AFM tip and the MIM top electrode in the FDC-MIM method. This adhesive force represents the adhesion due to meniscus formation, and is subtracted from the resulting induced adhesive force from the charge injection experiments. Therefore, the adhesive force data presented here related to the study of the dielectric charging phenomenon represents mainly the induced attractive force between the AFM tip and the sample surface that results from trapped charges in the dielectric film. The FDC has been used as well to investigate different stiction mechanisms (as adhesion due to friction)[106].

[106] U. Zaghloul, B. Bhushan, P. Pons, G.J. Papaioannou, F. Coccetti, and R. Plana (2011), "Nanoscale characterization of different stiction mechanisms in electrostatically driven MEMS devices based on adhesion and friction measurements," *J. Colloid and Interface Science* **358**, 1-13

Control of the Test Environment

Before to present some major achievement obtained with the AFM based techniques applied to dielectric charging a special attention need to be paid to the role of the testing environment. The relative humidity has a very high influence on charging/discharging processes in SiN_x dielectric films as will be explained later on. Also, the removal of the water-related layer from both surfaces of the sample and the AFM tip was reported to be very important for improving the reliability of the KPFM measurements[95].

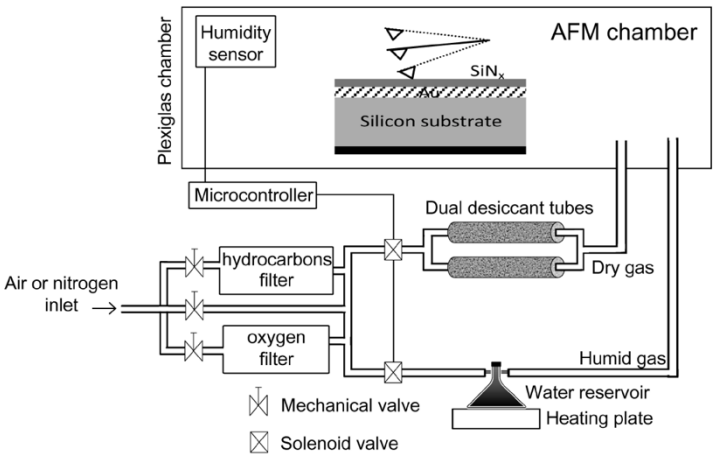

Figure 2.23: The environmental control system used for the Multimode AFM.

In addition, larger humidity levels and thicker adsorbed water film over the sample surface results in larger adhesive force between the AFM tip and the sample. This **adhesive force increases remarkably when voltage is applied** between the tip and the sample **due to the formation of electric field induced meniscus** (see later on Figure 2.34d). For these reasons, both the SiN_x samples and in the reported experiments the AFM tips went through two thermal cycles (heating up to 150 °C and cooling steps under vacuum) before each measurement in order to avoid the influence of humidity and the adsorbed water film over the dielectric surface on both KPFM and FDC measurements. Moreover, the KPFM and FDC measurements were performed in a controlled environment chamber under dry air flow (relative humidity ≈ 0.02%[107]) except for the experiments conducted to study the influence of environment parameters on both charging and stiction.

The environment control system used in this study is shown in Figure 2.23. The AFM was enclosed in a Plexiglas chamber with two inlet feed pipes: one for dry gas and another for moist gas. These two inlets carried the required environment gas and were mixed together inside the AFM chamber in order to obtain the desired relative humidity. The lab-air or nitrogen lines used were connected to the inlet of the system. Dry gas was obtained by passing the gas through a line purifier containing a desiccant while humid gas was obtained by bubbling air through water. The relative humidity in the controlled chamber was monitored with a humidity sensor. This sensor was connected to a microcontroller which controls solenoid valves in order to adjust the ratio between dry and humid gas to reach the desired humidity and maintain it at a constant level during the experiment. The environment control system includes also two types of gas purifiers (hydrocarbon filter and oxygen filter), which are used to purify the used gas.

[107] This value corresponds to the RH value provided by the dry air provider.

Major differences between KPFM and FDC

The dielectric charging assessment based on FDC has several advantages over KPFM-based methods.

First, FDC takes into account the influence of meniscus formation between the AFM tip and the dielectric surface which cannot be measured using KPFM. The meniscus formation resulting from the adsorbed water film between the MEMS switch bridge and the dielectric layer and its related electric field-induced meniscus constitutes major force components which contribute heavily to the final measured adhesive force especially at larger relative humidity levels.

Second, the potential levels which can be measured using FDC is much larger compared to KPFM. These higher surface potential levels often exits over charged MEMS dielectrics due to the large actuation voltage used to actuate MEMS switches, and are usually larger than the maximum potential which could be measured by KPFM.

Finally, the FDC can measure the surface potential accurately at larger relative humidity levels while KPFM cannot due to the potential shielding effect[94]. In this study, both KPFM and FDC measurements were performed using a commercial AFM from Bruker (MultiMode™ with NanoScope® IIIa controller and Extender™ Electronics Module).

Major achievements in AFM based dielectric charging investigations:

The most relevant findings generated by the aforementioned approaches are reviewed in the present section, while for a complete and exhaustive description see U. Zaghloul's PhD Manuscript (see detailed reference in Annex 4.3).

As already mentioned given the structural complexity of dielectric material typically used in microelectronics and MEMS devices, the study has been restricted to the silicon nitride. Besides being one of the most commonly used material in microelectronic silicon nitride is also one of the material on which LAAS has got more (process) experience. This has permitted to benefit from background knowledge and to have full control of the in-house deposition techniques. It is important to remind that a variation in the deposition material may yield a quite significant modification of the material properties and hence it can be considered *de facto* as a different material. All of them[108] have been submitted to physical characterization (FTIR and XPS) by means of which structural properties (e.g. stoichiometry), have been monitored.

One of the earliest and most significant results the AFM-based technique (KPFM and FDC) have allowed to reach is to demonstrate the validity of MIM test vehicles as replacement of MEMS device to carry out studies of dielectric charging. This represents a great achievement since it simplify and speed up the testing without any lost of information. As shown in Figure 2.24 indeed the two techniques be it KPFM or FDC, when applied to MIM and MEMS test vehicles yield the same results in terms of relaxation time (τ) and stretch exponential constant (β) in each technique. Noteworthy is that the two graphs depict two different charge induced phenomena: surface potential for the KPFM and adhesion force for the FDC which are described by different analytical expression (stretch exponential for the KPFM surface potential and square of the stretch exponential for the FDC adhesive force). The differences in value of τ and β are due to the fact that different injection conditions (amplitude and duration) and read-out conditions (start, duration) apply.

[108] U. Zaghloul**,** G. Papaioannou, H. Wang, B. Bhushan, F. Coccetti, P. Pons, and R. Plana, "Nanoscale characterization of the dielectric charging phenomenon in PECVD silicon nitride thin films with various interfacial structures based on Kelvin probe force microscopy," *Nanotechnology* **22**, Art. # 205708, (2011).

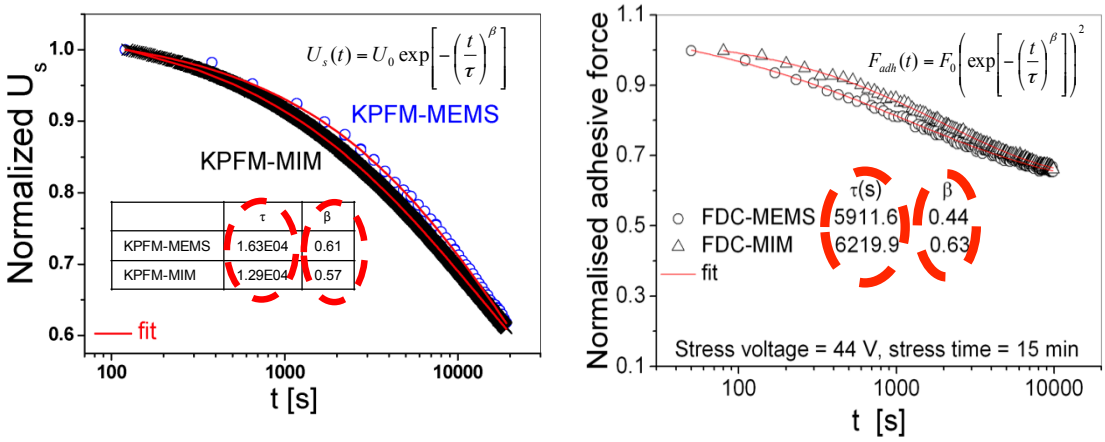

Figure 2.24: Comparison of the experimental results on two different test vehicles MEMS and MIM obtained with the two different techniques along their respective analytical fitting expression and parameters: (a) surface potential by KPFM-TF and (b) adhesive force by FDC-TF.

Another **important improvement with respect to the state of the art has been to demonstrate the limited validity of more conventional investigation methodologies such as the C/DCT** done on MIM test vehicle. As matter of fact the results of experiment done with KPFM have demonstrated that the discharging over increasing observation time window may differ significantly between these techniques. In particular it is found that the decay time constant increases much more for KPFM-MEMS and KPFM-MIM, which remains in the same order of magnitude, while for C/DCT it lays one order of magnitude below[109]. This indicate that the calculated discharge time constant is strongly affected by the duration of the observation time windows and more importantly that the C/DCT method provides always smaller decay time constants with respect to the KPFM based techniques.

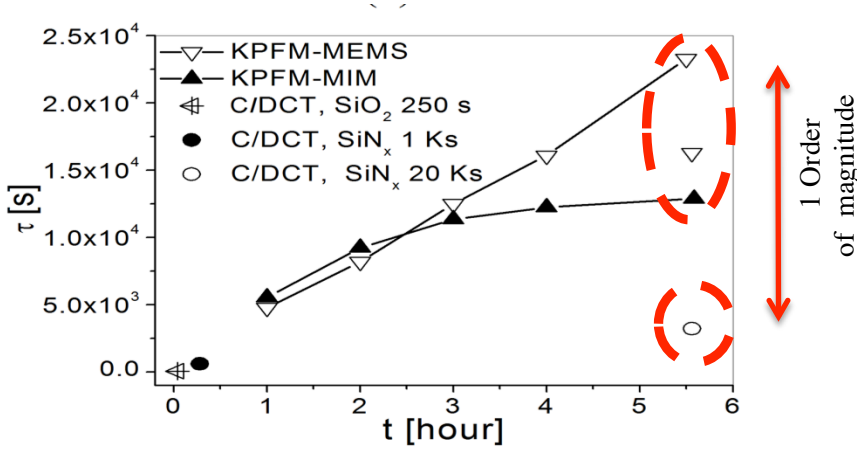

Figure 2.25: Comparison of charge discharging delay constant versus observation time window duration for different technique of KPFM (on MIM and MEMS) and different C/DCT experimental results.

This difference obviously arises from the difference in charge collection mechanisms in both methods, the collection by the two electrodes (injection and opposite one), in C/DCT and the single opposite electrode in the KPFM based methods. Thus, in these latter the discharge occurs through currents crossing the dielectric film. The associated current is expected to be much

[109] U. Zaghloul, G. Papaioannou, F. Coccetti, P. Pons and R. Plana, "Dielectric charging in silicon nitride films for MEMS capacitive switches: Effect of film thickness and deposition conditions," *J. Microelectron. Reliab.* **49**, (2009) 1309-1314.

smaller than the one measured in C/DCT method because of the successive trapping and emission of charges and the charge percolation due to potential fluctuation caused by inhomogeneities in the nonstoichiometric material.

Role of the material parameters:

An important achievement concerns as well the role of the deposition technique. The proposed techniques have indeed allowed to discriminate some deposition parameters as most relevant with respect to the final objective. For instance among the recipes typically used at LAAS for the synthesis of silicon nitride, for the first time it has been clearly demonstrated that the so called High Frequency nitride (HF-SiNx) yields a far lower charging (lower value of surface potential in the KPFM experiments and lower adhesive force in the FDC ones) with respect to the LF-SiNx counterpart, as shown in Figure 2.26a and Figure 2.26b.

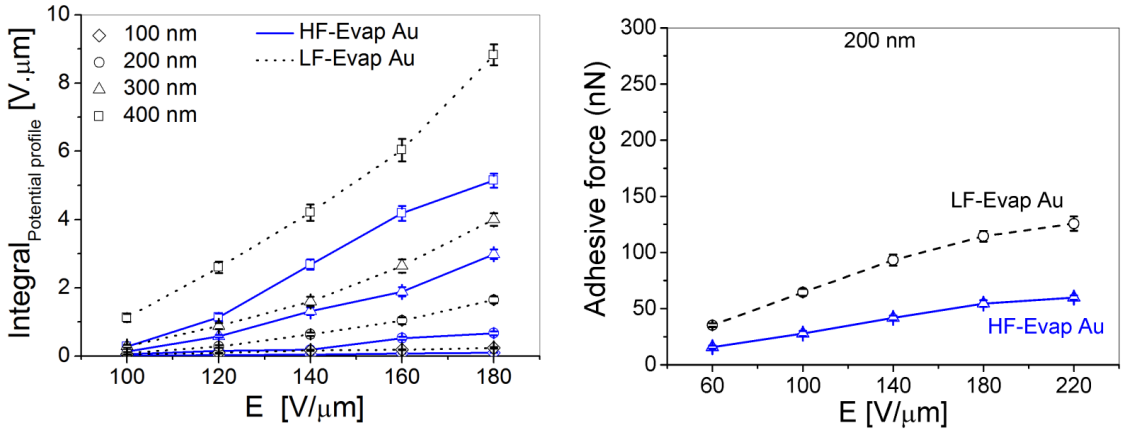

a) b)

Figure 2.26: Results comparison for two different deposition recipes HF and LF SiNx: (a) the integral of surface potential by KPFM at different values of thicknesses and (b) for the adhesive force with FDC for a single value of thickness (200 nm).

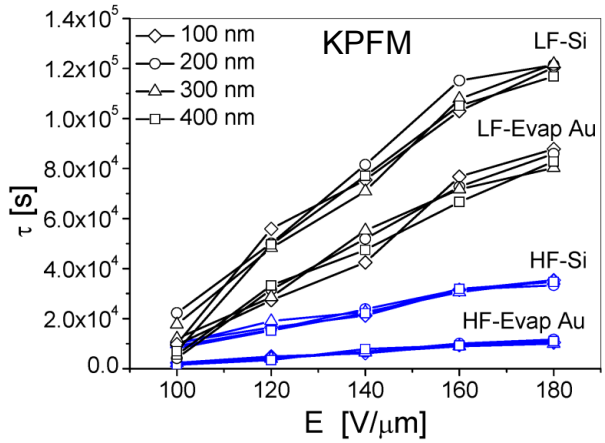

Figure 2.27: Comparison of the decay time constant results for two different deposition recipes HF and LF SiNx and different thicknesses.

The results for the KPFM show as well how the increased thickness at constant value of electric field, give rise to larger charge accumulation[110]. A further benefit of HF-SiNx is the characteristic to yield faster discharge as demonstrated in Figure 2.27. In this latter case the thickness seems to play no significant role. The faster discharge is attribute to the richer content of silicon in HF SiNx (as demonstrated by XPS tests[108]) which is well know to increase the material conductivity.

The larger the amount of silane, (hence the larger the ratio r of the amount of SH_4 over the amount of NH3 as indicated in Figure 2.28, the smaller the charging accumulation and the fast the discharging process. These results are clearly depicted in Figure 2.28, where these findings are consistently proven by KPFM-TF and FDC-TF at different values of bias voltage.

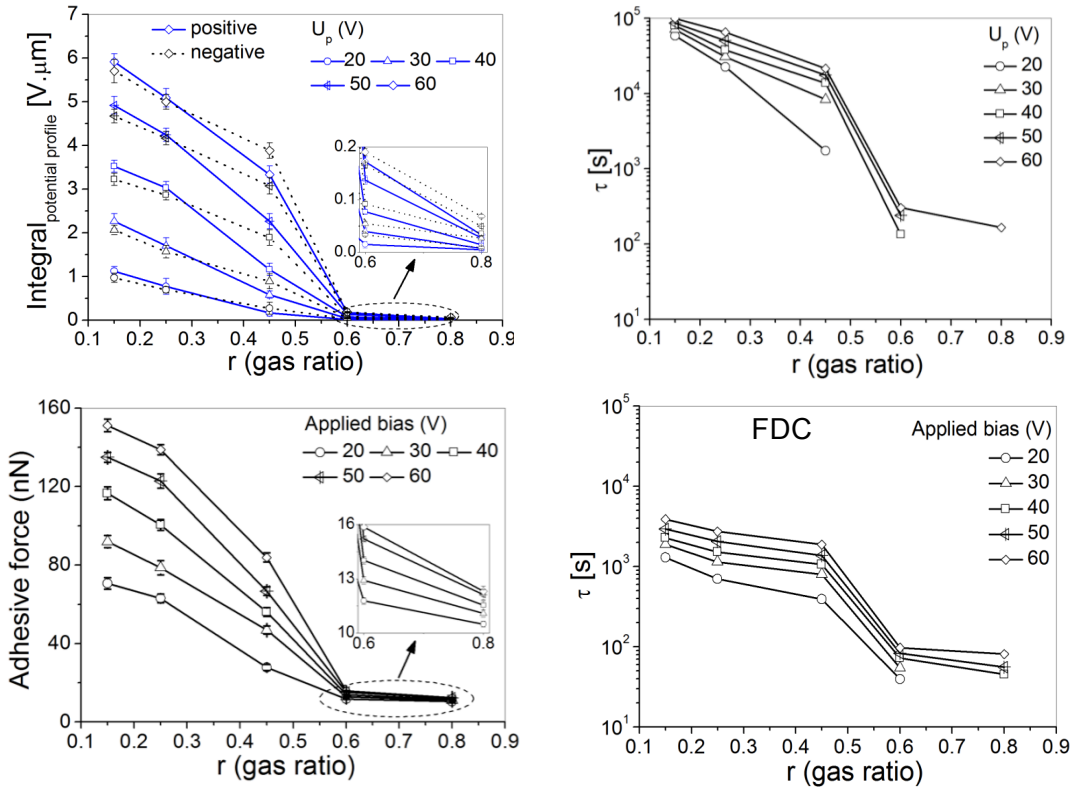

Figure 2.28: Effect of the deposition gas composition, *r* being the ratio between the amount of silane and ammonia: upper graphs are obtained by KPFM-TF and lower ones by FDC-TF. They provide the results for charge accumulation (right) and decay time (left).

One of the major achievement enabled by the AFM-based investigation techniques has been in the study of the working environment conditions, which are well know to have a critical impact on the functioning of MEMS devices. **In particular by means of these techniques it has been possible to observe for the first time phenomena associated to the amount of relative humidity (RH) content, and nature (composition) of the environment (atmosphere) in which the device is eventually working.** Considering that to date there are no whatsoever techniques to assess exactly the environmental condition (e.g. RH, gas composition) in such extremely small volumes as those enclosed in MEMS packaging ($\sim 10^{-14} \div 10^{-11}\ m^3$) the availability of a technique that allows to study preventively phenomena that can arise there in by easily emulating a large variety of environmental condition is paramount.

[110] At constant applied bias larger thickness yield smaller charging (Integral potential at 100 V/µm for 400 nm is smaller than at 200 V/µm for 200 nm thick SiNx independently from HF and LF).

The first results obtained at different level of RH and on two gases such as air and nitrogen (which are the common choice for MEMS packaging) regards the spreading of the injected charge. The parameter that measures these phenomena is the FWHM and as depicted in Figure 2.29, the larger is the RH the larger is the FWHM hence the spreading of the charge over the surface. This is attributed to the increasing of adsorbed water at the wafer and AFM tip surface which affects the geometry and the electrical properties of the AFM-sample interaction[95,111]. From Figure 2.29(b) it is apparent that nitrogen enhances the confinement (smaller FWHM) and yields better reproducibility of the experiments (smaller error bar) with respect to air. The impact of the relative humidity on the surface potential distribution can be directly related to the difference in conductivity of the adsorbed water film, hence the amount of the surface charge which exists on the dielectric surface as the humidity changes[112].

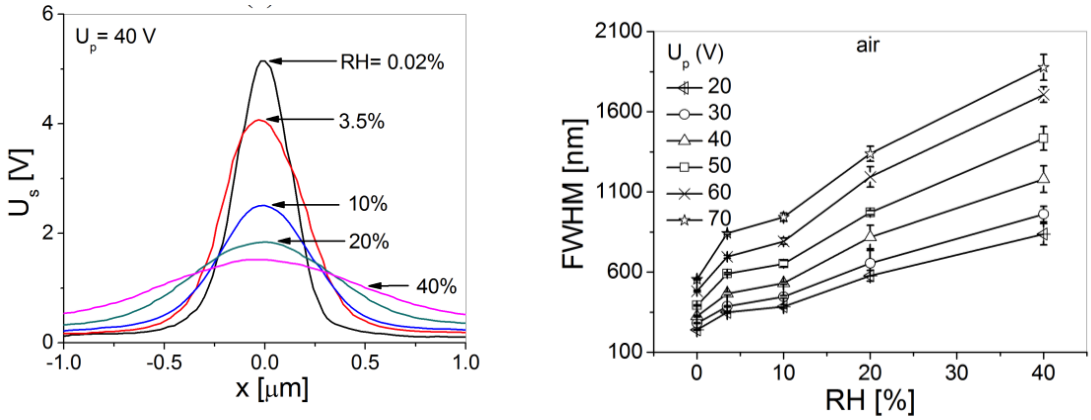

Figure 2.29: Comparison of surface potential spreading effect obtained by KPFM-TF at different values of RH for 40 V of injected potential: (a) spatial distribution and (b) FWHM for the same values of RH and for air and nitrogen.

The decreasing of the surface potential with increasing RH (Figure 2.29a) could be attributed to the fact that as it will be shown below, higher values of RH yields faster discharging and hence to a faster decreasing of the maximum value of surface potential taking place in the constant interval between injection and start of the reading (30 sec).

Since increasing the RH results in reducing the potential amplitude, U_s and increasing the FWHM (Figure 2.29a), area integration was performed for the induced surface potential profiles in order to estimate the impact of humidity on the injected charge density[113]. The results are plotted in Figure 2.30a) and b) and highlight that the potential integral, consequently the injected charge density inside the SiN_x film, increases remarkably with the relative humidity. These results show as well that the charging is more pronounced in air than in nitrogen.

The difference between the injected charge density in air and nitrogen might be attributed to the difference in charging due to gas discharge between the AFM tip and the underlying electrode through the SiN_x film. According to Wibbeler et al.[53], gas discharges in the capacitive air gap of silicon cantilever actuators were observed although their electrodes were covered with a PECVD SiO_2/Si_3N_4. Thus, when a discharge occurs in the gap between the AFM tip and the dielectric surface, an avalanche of free electrons and ions is generated. They traverse the gap and are stopped and neutralized by charge exchange at the dielectric surface instead of reaching the

[111] K. Ohara and Y. Cho (2004), "Effect of the surface adsorbed water on the studying of ferroelectrics by scanning nonlinear dielectric microscopy," *J. Appl. Phys.* **96**, 7460-7463.

[112] P. Mesquida, (2002), "Charge Writing with an Atomic Force Microscope Tip and Electrostatic Attachment of Colloidal Particles to the Charge Patterns", Doctor of Technical Sciences, ETH, Zurich, Swizerland

[113] U. Zaghloul, G. Papaioannou, B. Bhushan, F. Coccetti, P. Pons, and R. Plana (2011), "On the reliability of electrostatic NEMS/MEMS devices: Review of present knowledge on the dielectric charging and stiction failure mechanisms and novel characterization methodologies," *Microelectron. Reliab.* **51**, 1810-1818

underlying electrode resulting in accumulation of the generated free electrons and ions at the dielectric surface. The gas discharge phenomenon was reported to depend on the gap environment[114]. Gas discharge measurements performed in air and nitrogen at atmospheric pressure indicate that the Paschen's law is not applicable at an electrode gap spacing smaller than 4 μm[115]. Moreover, the difference between air and nitrogen gas discharge has not been investigated in a gap below 0.5 μm.

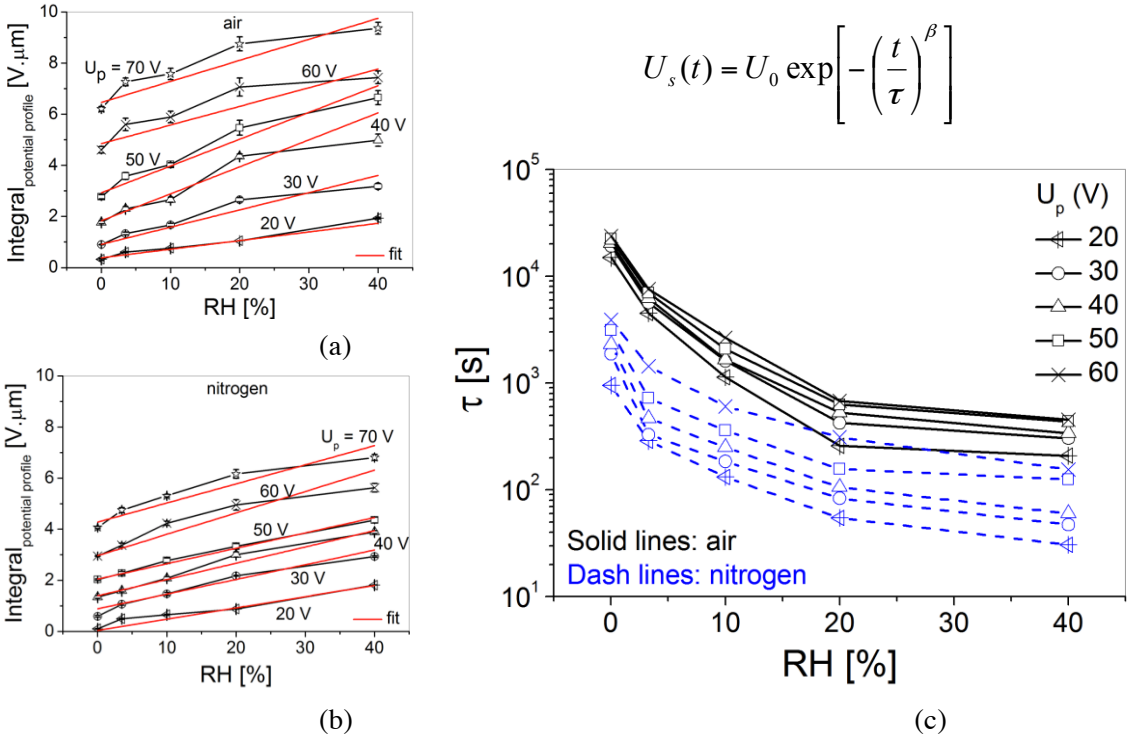

Figure 2.30: Comparison results for KPFM-TF study on RH effect under different bias values: Integral of the potential profile as function of the RH for (a) air and (b) nitrogen; and decay time constant for air and nitrogen (c).

A typical example of this small gap is a MEMS switch with the movable electrode in the down position is in contact with the dielectric layer, which is simulated in our study by the AFM tip which comes almost in contact with the SiN_x surface during the charging step. A special note deserves the background surface potential, which is the measured by KPFM when no charge is beforehand injected. The measured background surface potential was found to increase with the relative humidity in both air and nitrogen environments. This agrees with the previously reported KPFM measurements in air for InAs thin films[95] and further indicates that surface charges increase with increasing relative humidity level. This is attributed to the polarization in the adsorbed water layer, which cancels the DC bias applied between the sample and the AFM tip. It was found that the background potential in air is larger than in nitrogen under all investigated relative humidity. Finally, for nitrogen the background potential starts to saturate at 40% RH while in air the measured potential tends to increase[108].

The decay time constants τ, is plotted as a function of the relative humidity as shown in Figure 2.30c. This value is calculated from fitting the surface potential decay to the usual stretch

[114] F. Strong, J. Skinner and N. Tien (2008), "Electrical discharge across micrometer-scale gaps for planar MEMS structures in air at atmospheric pressure," *J. Micromech. Microeng.* **18**, Art.# 075025.

[115] Dhariwal, R., J. Torres and M. Desmulliez (2000), "Electric field breakdown at micrometre separations in air andnitrogen at atmospheric pressure," *IEE Proceedings-Science, Measurement and Technology* **147**, pp. 261-265.

exponential formula given therein[116]. The decay time constant τ decreases with the relative humidity indicating that injected charges decay faster as the humidity increases as shown in Figure 2.30c. This could be observed for both air and nitrogen environments and for charges which were injected under different U_p. There are several reasons for charge decay, which are usually classified into two main groups: internal and external decay. The internal decay takes place through tunneling towards the injecting metal electrodes and further through transport and diffusion[117]. The external decay is due to the neutralization of surface charges, which can be caused by the adsorption of counterions[118] from the surrounding medium or by charge loss due to its electrical conductivity. In the case of air and nitrogen environments the amount of available counterions and the electrical conductivity of the medium are both influenced by the relative humidity. **Since the internal charge decay is not affected by a change of the environmental conditions, the observed decrease in τ with increasing RH in both air and nitrogen is attributed mainly to the surface charge decay**. As the RH increases, the surface charge decays faster for two reasons. The first reason is the **faster neutralization of surface charges with the external medium**. Second, as humidity increases, the thickness of adsorbed water film over the SiN_x surface increases too, resulting in a **faster charge loss due to the larger conductivity of the water film**.

The decay time constant, τ, for nitrogen environment is smaller compared to air as shown in Figure 2.30c), which indicates faster charge decay in nitrogen for all observed RH level and applied bias.

The reason behind the observed difference in τ between air and nitrogen could be attributed to the difference in the amount of available counterions and the electrical conductivity of the medium for both environments. The number of available ions is expected to be higher in air than in nitrogen. Such ions are attracted by the external electric field of the charged sample and are randomly trapped over the SiN_x surface.

Influence of oxygen organics and hydrocarbon contaminants.

The measurements indicate that there is a big difference between air and nitrogen environments regarding both the charging and discharging processes, as shown in the previous section. Since the main difference between air and nitrogen is the oxygen, it becomes essential to completely remove this component from the employed nitrogen environment. The possible presence of hydrocarbons contaminants in MEMS packaging provide a further investigation target to the present study. In order to do so two types of gas purifiers have been used in a dedicated measurement set up[119] already shown in Figure 2.23.

To minimize the impact of the relative humidity for this set of measurements, the KPFM experiments were performed under the lowest possible relative humidity level in our environmental setup which is 0.02%.

Under the different environmental conditions taken into account the measured results (Figure 2.31a and b) show that the variations are barely noticeable for the surface potential so as for the spreading of the charge. On the contrary (Figure 2.31c) plugging the hydrocarbon filter the reduction of the decay time constant is apparent. A reduction of the discharging time constant is also evident on nitrogen with and without oxygen filter. This confirms the results given earlier about the better performance of nitrogen versus air.

[116] Note that for what concerns reliability of the device the important parameter of this fitting function is τ and not β.

[117] G.M. Sessler, (1987), *Electrets*, second edition, Springer topics in applied physics Vol.33, Springer-Verlag, Berlin, Germany.

[118] A counterion is the ion that accompanies an ionic species in order to maintain electric neutrality.

[119] The engaged oxygen trap is designed to remove the oxygen from non-oxidizing gas streams such as He, Ar, N_2, H_2 or CH_4, and it cannot be used with an air line. The trap consists of a high-capacity filter filled with copper-based adsorbent which forms copper oxide in the presence of oxygen, and no gas is generated. The employed hydrocarbon filter (www.chromres.com) is filled with activated charcoal, one of the most effective adsorbents for organics and hydrocarbons. It is used in these experiments with both air and nitrogen streams to remove the organic and hydrocarbon contaminants at room temperature except methane.

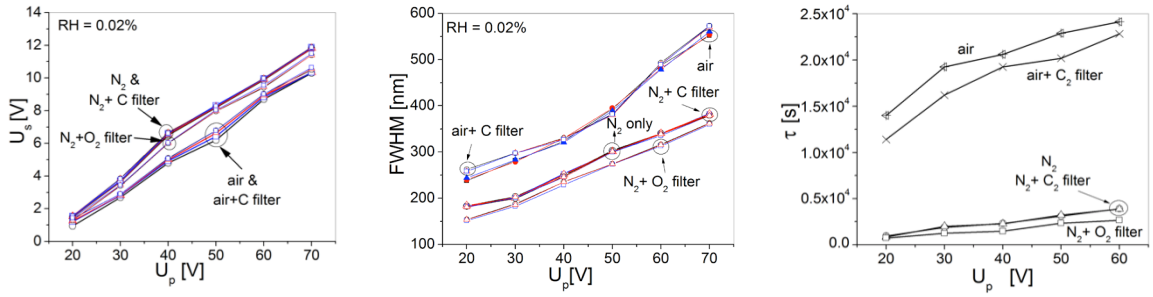

a) b) c)

Figure 2.31: Results of KPFM-TF measurements under oxygen and hydrocarbon contaminants controlled environment: surface charge potential (a), spreading of the surface potential (b) and decay time constant (c).

From these results becomes apparent that a well-purified nitrogen gas could reduce considerably the dielectric charging phenomenon in electrostatic MEMS switches and consequently increases the lifetime. These results are in line with previous investigations by Van Spensen et al from IMEC[85] (see Figure 2.32), done under cycling test conditions. This study gives a significant contribution to the state of the art since it provides a powerful investigation platform to carry out comprehensive evaluation of packaging conditions.

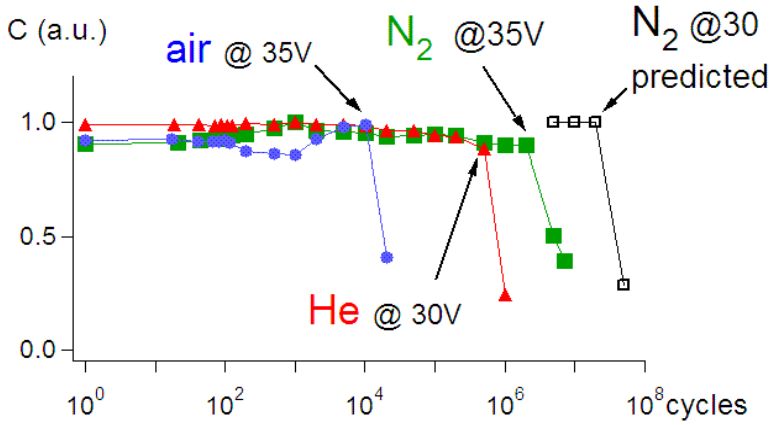

Figure 2.32 [Source IMEC]: Effect of environmental gasses on an electrostatically actuated MEMS performance.

Stiction mechanisms: Tribology applied to RF-MEMS

The concept of tribology, first enounced in the 60's, encompasses the interdisciplinary science and technology of interacting surfaces in relative motion[120]. The application of this science to the study of mechanical contact in RF-MEMS devices is a relatively recent topic (Patton 2005)[121]. In this work Patton et al, carried out the study of a Au-SiNx contact with a micro/nan adhesion apparatus at room condition (RH 45%). The authors observed an increasing adhesion and attribute it to the charging and enhanced Wan der Walls interactions associated with increasing bias and surface smoothening, respectively. In spite of the originality, the approach did not account for humidity. As already mentioned in a MEMS device where very

[120] B. Bhushan, "Introduction to tribology," Jhon Wiley & Son New York, 2002.
Quote from the same source "The economic implications of tribology are significant. Investigation by a number of countries arrived at the figure of savings of 1-1.4 % of the GNP obtainable by appling tribological principles".

[121] S.T. Patton, and J.S. Zabinski, "Failure mechanisms of capacitive MEMS RF switch contacts," Tribology Letters, Vol. 19, No. 4, August 2005

irregular and tiny surfaces come in contact by means of weak forces a quite complex tribology may take place. The most severe consequence beside contact degradation is the appearance of local stiction mechanisms, which added constructively (main contribution is attractive) over the entire actuation area, may yield a resulting force comparable with the actuation/release one. Any two surfaces with asperities (roughness) moving vertically with respect to each other could have two main contributions of stiction forces, friction and adhesive. However the influence of friction is usually neglected since there is there is no (or negligible) sliding motion between the two surfaces (bridge-dielectric).

The FDC-MEMS technique has been applied to this study so that arbitrary levels of RH and extremely small forces (nN) could be applied and monitored along with different values of applied bias. The investigated samples consist of actual RF-MEMS devices[122] (see Figure 2.33a) , and the environmental control was provided by the same setup presented earlier (Figure 2.23)[123]. The piezo travel distance used in these experiments was 500 nm, which is comparable to the air gap of actual MEMS switches. The FDC scan of the device actuation region (done after having applied a bias of 40 V for 2 min and removed the suspended membrane – see Figure 2.33b), generate an adhesive force map which clearly show a pronounced contrast between regions which underwent electric field and those which did not.

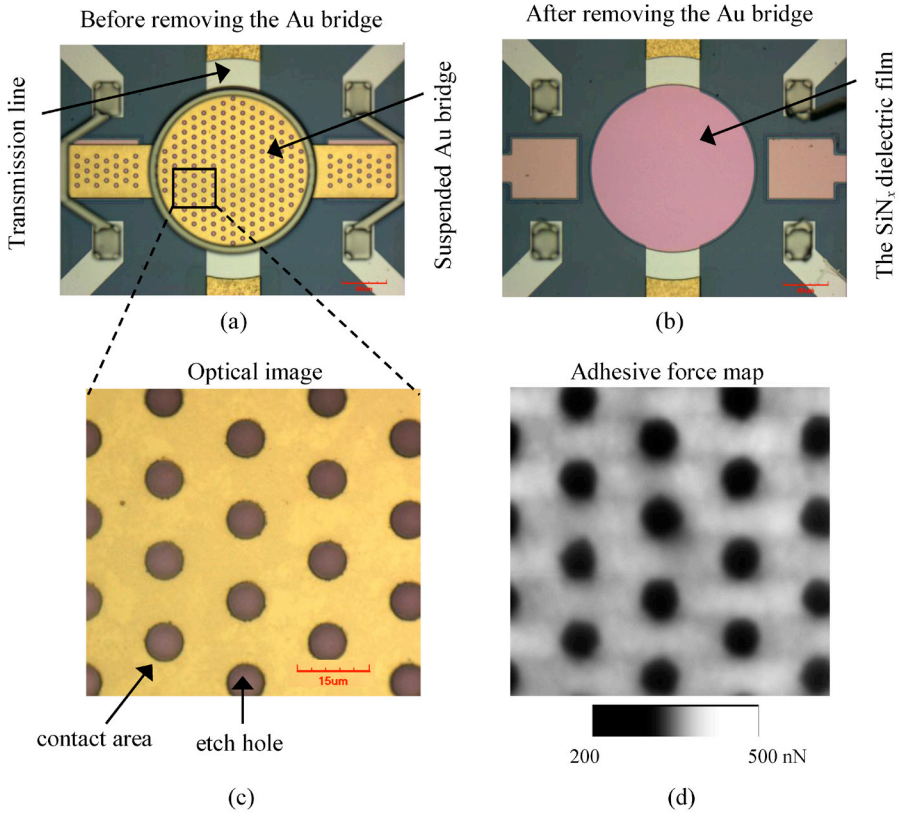

Figure 2.33: MEMS device used for the FDC-MEMS experiment (Source: AMICOM NoE): optical image of the device before (a) and after (b) removal of the suspended bridge; close up of the scanned region optical image (c) and FDC-MEMS (d).

In particular there are more than 200 nN difference between the area below the bridge and the one facing the opening (hole) in the membrane (see Figure 2.33c and d).

These results present a very impressive picture of the underlying physics and inspired a number of further tests where the role of RH and surface thermal treatments (dehydration) were

[122] PECVD SiN_x films with 300 nm thickness deposited over Au/Ti (200 nm/50 nm) layers, which were evaporated on Si substrates.

[123] The adhesion and friction measurements were conducted using highly doped Si tips (FORTA-10).

studied. In fact beside the electrostatic force another stiction mechanism have been identified, and attributed to the meniscus formation[124].

The separate and combined effect of the two stiction mechanisms induced by the electrostatic force and by the meniscus force, were studied by using three different groups of samples (A, B, and C). Group A and B were dehydrated[125]. Then, group A was measured under a very low relative humidity level (1%), while group B was stored under high relative humidity (60%) for 60 min, and then was measured under 60% RH. Group C was not dehydrated, and was measured under a low humidity level (1%) similar to group A. The thickness of the adsorbed water layer for group A is therefore smaller than groups B and C.

As RH increases, the adsorbed water film thickness (measured by FDC) also increases as depicted in Figure 2.34a, which in turn enhances the meniscus formation and hence the associated adhesion force.

So when no bias is applied (Figure 2.34b) the adhesive force is larger for group B than A and C. Due to the storage step of group B under higher relative humidity (60%), the thickness of the adsorbed water film is higher compared to group A. This results in larger meniscus formation, and hence larger meniscus force in group B compared to group A. In addition, the higher RH employed in group B leads to stronger attractive capillary force compared to groups A and C.

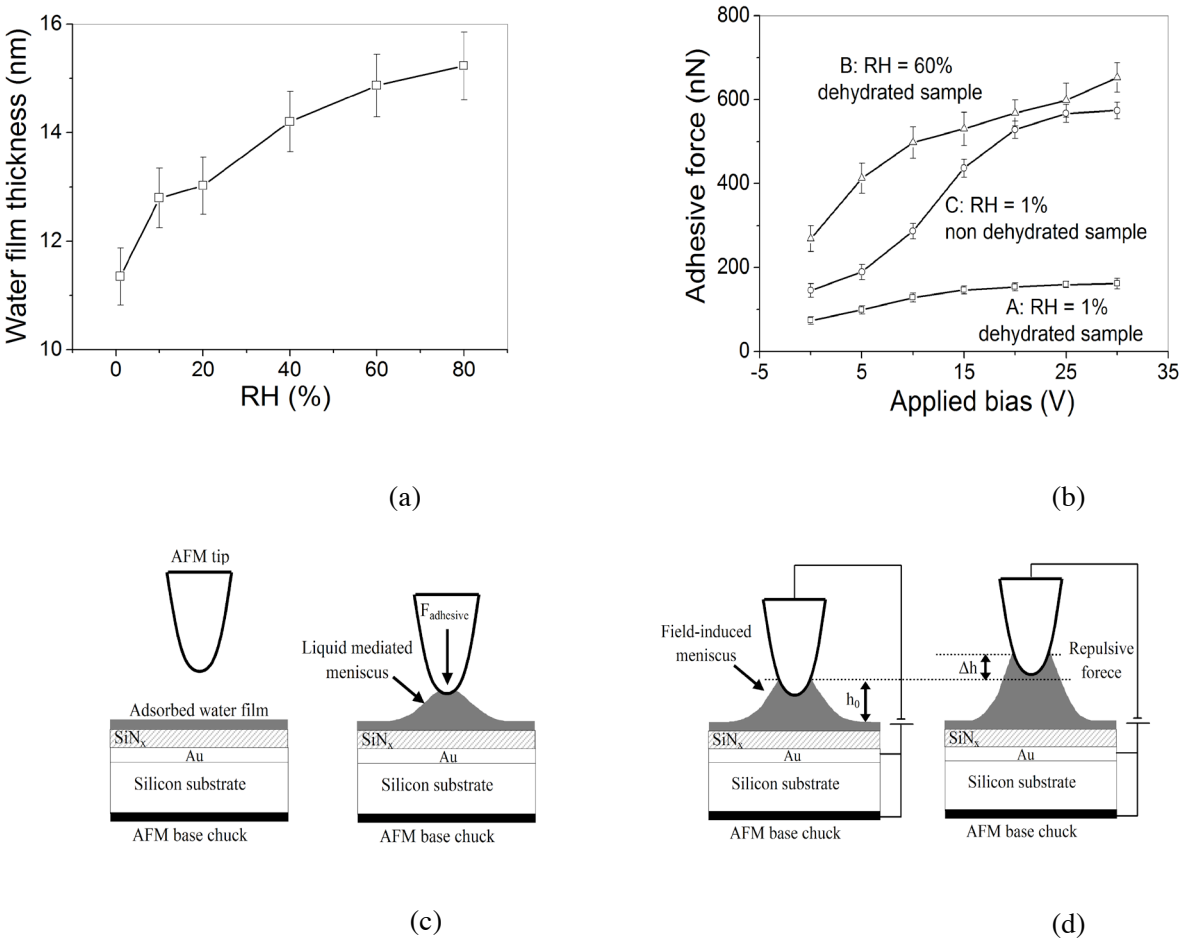

Figure 2.34: The interaction of AFM-tip and water film adsorbed on the dielectric surface: adsorbed water film thickness versus RH (a); Adhesive force for the three sample conditions A, B and C versus applied bias (b); schematic of the meniscus formation and evolution without (c) and with bias (d).

[124] Liquid mediated meniscus: bridges or interconnection made of liquid between two surfaces due to their proximity and the affinity of these surfaces for condensing liquids (Source: B. Bushan).

[125] Dehydration was performed through two cycles of heating (150 °C) separated by a cooling step under vacuum. This operation removes a considerable amount of the adsorbed water over the dielectric surface.

For the three groups the adhesive force is found to increase with the applied bias due to the additional contribution of the electrostatic force on the meniscus formation. The considerable increase in the water film volume surrounding the tip (asperity in actual MEMS), will result in a significant increase of the adhesive force between the AFM tip and sample surface (membrane and the electrode). The influence of the field-induced meniscus on the adhesive force is expected to be much higher compared to the liquid mediated meniscus formed, when no bias is applied.

With normal operating conditions of MEMS switches, the actuation time is much larger than the one used in the experiments reported here (2 min), and hence the induced surface potential is expected to be even higher[92]. Therefore, in the long term the induced surface potential for switch-C will be much higher than switch-A resulting in a much larger impact of the field-induced meniscus in the former. Based on this analysis the stiction between the switch bridge and the dielectric film for switch-C will be much faster compared to switch-A. These results confirm the need of annealing in MEMS switches in order to increase the device lifetime as reported by Czarnecki et al[126]. Furthermore, it is concluded that the main reason behind the stiction of MEMS switch-C is not the dielectric charging itself, but it is the field-induced meniscus formation enhanced by the dielectric charging.

This newly failure mechanisms discovered thanks to this work, was called field-induced meniscus, and was for the first time added to the official FMEA list of failure mechanisms (see Table 2.1).

2.2.3 Contact degradation in resistive (DC) metal-to-metal contact switches

The second important failure mechanism that has been considered is the degradation of the ohmic resistance in metal-to-metal contact based devices. These components are typically used for swicthing functions in the DC up to few tents of GHz range (RADANT, OMRON).

The activities in this area have been carried out within collaborative project (in particular FAME ANR-PNANO 2008-2012, and ESA-REDS 2008-2013).

Note that my personal contribution has been in managing these projects and interacting with the PhD student and their advisors.

In this case study the contact resistance is the most representative parameter to be observed in order to track possible degradation mechanisms. In the framework of this research activities innovative methodologies have been developed by colleagues at Novamems (now Fialab) in Toulouse and **École Nationale Supérieure des Mines de St-Étienne** (EMSE) at Gardanne with the aim to carry out a systematic study if micro contact issues from MEMS processes. Both techniques, based on commercial nanoindeters equipment aimed to monitor the contact resistance as function of the applied force, under different working condition (applied voltage and current across the contact). In spite of the common aim they differ significantly form each other **in terms of methodology**. The main difference resides in the implementation of the contact which is in both case measured by a four-point method[127], but while in one case (PhD from A. Broue[128] **with Fialab-LAAS**) is used a true MEMS test vehicle **issued** by the same MEMS process as for the final device, in the second (PhD P.Y. Duvivier[129] **with** EMSE at

[126] P. Czarnecki, X. Rottenberg, P. Soussan, P. Ekkels, P. Muller, P. Nolmans, W. De Raedt, H. Tilmans, R. Puers and L. Marchand (2009), "Effect of substrate charging on the reliability of capacitive RF MEMS switches," *Sens. Actuator A-Phys.* **154**, 261-268.

[127] M. Finetti, A. Scorzoni, G. Soncini ,"Lateral current crowding effects on contact resistance measurements in four terminal resistor test patterns," *IEEE electron device letters,* 5, (1984) 524-526.

[128] A. Broue, "Analyse multi physique des sources de défiabilisation du microcontact électrique à destination des interrupteurs MEMS," PhD Thesis Université de Toulouse 3 Paul Sabatier, June 2012.

[129] P. Y. Duvivier, "Ètude expérimentale et modelisation du contact électrique et méchanique quasi statique entre surfaces rugueses d'or: application aux micro relais MEMS," PhD Thesis from the Ecole Superieur de Mines Saint Etienne, March 2010.

Gardanne) two contact bars with the same metals **as for the former technique,** are separately fabricated **and used**.

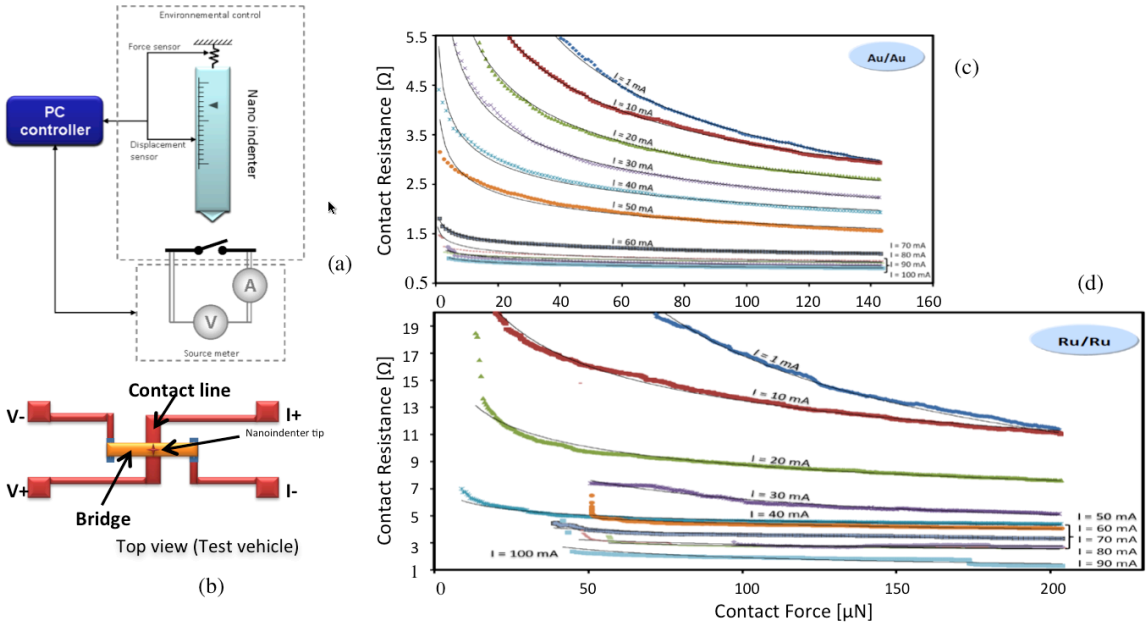

Figure 2.35[Source: A. Broue PhD 2012]: Micro contact characterization platform at Fialab: schematic of the experimental setup (a), test vehicle (b), Contact resistance results for two type of contacts Gold-Gold (c), and Ruthenium-Ruthenium (d), for different level of DC current (1 – 100mA).

Results have highlighted the role of temperature (softening temperature) induced by working conditions (voltage and current) as one of the most critical parameter to rule the interaction physics at the contact surface. The electro-mechanical responses of different contact configurations have been investigated. Au/Au and Ru/Ru contacts have been fully characterized demonstrating good performances (see Figure 2.35c and d) with contact resistances which may fall below 1 and 2 Ohms respectively for force larger than 100 μN and current above 90 mA . These tests are very flexible and allow a quite extensive study of metal types and combination of them. Experiment on bimetallic contact in fact, show larger power handling capability due to the intrinsic electro thermal properties of this contact configuration. The variation of the contact resistance is indeed determined by the concurrent effect of asperities flattening, which lowers the contact resistance, and heating, which affects the topography of the contact surface by the activation of thermal failure mechanisms[130].

Similar conclusions have been obtained with the other technique from EMSE (see Figure 2.36 where the results for the Gold-Gold contact are reported). The main difference between the two approaches resides in the very fine nature of the metal surface of the contact. While for the Fialab test the contact is identical (same manufacturing process history, hence all chemical and physical aspects, like for instance type of contaminants and roughness are the same) to the actual device, the EMSE test implements a contact between the metal surfaces of two parts manufactured in two separate processes. In this latter case, the advantage of a simpler fabrication process (no MEMS involved) is counterbalanced by a contact which is not exactly the same as in the real device. Given the importance of even smallest surface and material features in the contact physics this may introduce significant deviation from the real device.

[130] A. Broue,J. Dhennin, P.L. Charvet, P. Pons, N. Ben Jemaa, F. Coccett, R. Plana, « Multi-physical characterization of micro-contact materials for MEMS switches, » IEEE Holm Conference on Electrical Contacts, Charleston (USA), 4-7 Octobre 2010, 10p.

The metal-to-metal contact has been also the object of further investigation, this time at device level within the framework of an ESA project (REDS[131] where the device under study was a ohmic switch based on the LETI in-house process[132]) and the PHD thesis of N. Torres LAAS-ThalesAleniaSpace[133].

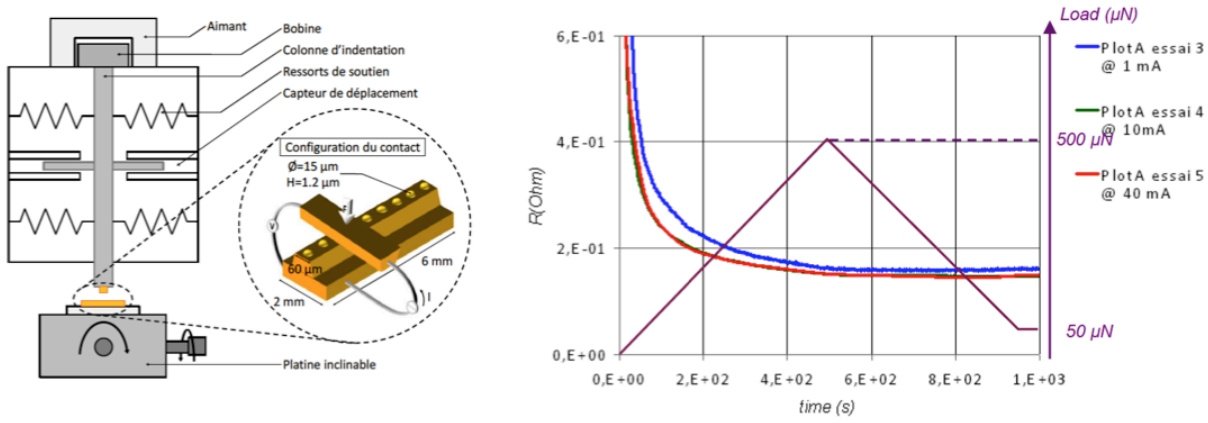

Figure 2.36 [Source: P. Y. Duvivier ANR-FAME project][129]: Micro contact characterization platform at ESMSE at Gardanne: Schematic view of the experimental set-up along with the test bars containing the contact dimples (a), and the results for the contact resistance in case of Gold-Gold contact (b).

The study was carried out by means of a semi empirical approach were equivalent circuit modeling and RF measurements (S-parameters) were combined in order to extract the contact resistance as function of the applied bias (hence force), and RF power (hence current)[134]. The equivalent circuit fitting to experimental measurements of actual device and deembedding test vehicles is a very effective technique to accurately extract the electrical parameters of the device, even when they are not directly accessible by measurements. The contact resistance is a very good example of this since it is not directly accessible (normally embedded within some structural part such as the membrane or the transmission line and protected by a packaging). In particular the interest has been devoted to the study of the contact resistance as function of the applied actuation voltage. Test done on Ru-Ru contact switches have validated the results obtained previously on contact test structures and allow to identify optimal operational region (see Figure 2.37a). Two different operational regions were identified with respect to the dispersion of the contact resistance. The same regions were observed in A. Broue PhD Thesis work[128]. This effect is due to the hardness of the contact material, which needs higher contact forces comparing with gold contacts in order to achieve the same contact resistance. Very interesting study highlighted the importance of a stable contact.

For the specific study of LETI switches it was demonstrated that a resistive behavior could be observed in in range $30\ V < V_{act} < 45\ V$ (weak force region), but at the costs of a high contact resistance dispersion (12-20 Ω) between identical devices. Above 45 V the contact resistance gets more stable and dispersion drops (0.4 Ω between identical devices). In order to enhance the contact force, so to obtain better RF performance (Figure 2.37b), the device has to be driven at least at high enough actuation potentials (> 50 V in this case) above which the minimum

[131] REDS Project ESA Grant 2008 - 2012.

[132] LETI process is based on a 200mm semi-automated MEMS foundry.

[133] N. Torres Matabosh, "Design for reliability applied to RF-MEMS devices and circuits issued from different TRL environments," Université de Toulouse – LAAS-CNRS – Januray 2013 Advisors: Dr. J.L Cazaux and Dr. F. Coccetti.

[134] PhD N. Torres-Matabosch January 2013.

asymptotic value of resistance is reached (here 1.5 Ω). Finally a value 40% higher than the V_{PI} (30V for the devices presented here) is a good compromise between good performances and safe operation with respect to break-down and charging (which in this case could be outruled since the switch was of dielectricless type[135]).

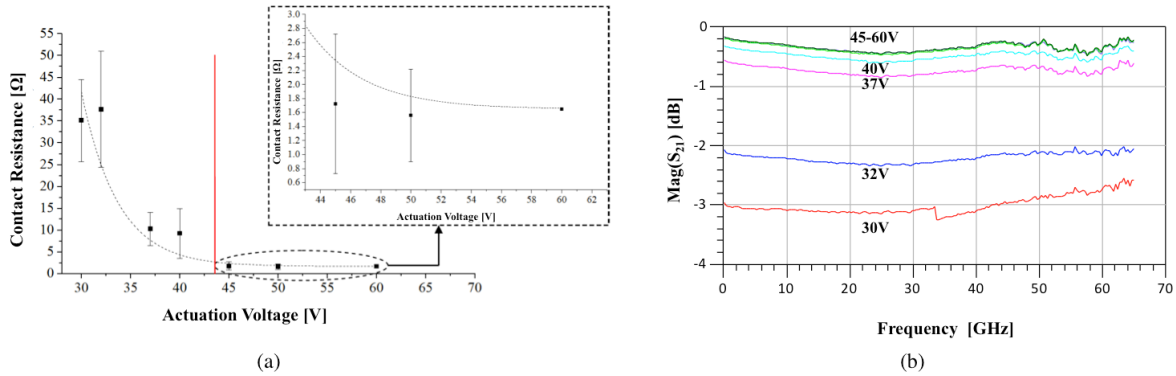

(a) (b)

Figure 2.37: Contact (Ru-Ru) device study versus applied voltage (bias). a) Contact resistance dispersion (error bar for 3 identical devices under test) versus applied bias; b) corresponding RF performances (insertion losses).

Noteworthy is that the for the specific studies done on LETI devices, the extracted minimum contact resistance value (1.5 Ω) was much smaller than the one reported for dedicated test setup (Figure 2.35d), for dedicated test structure, for the same material Ru-Ru and comparable working conditions (input current level of 2mA corresponding to an input RF power on the DUT of -10 dBm) but very close to the values reported in literature[136]. In the same reference, the failure signature of Ru-Ru contacts was clearly identified as a sudden increase of the contact resistance (fail to close). This in contrast with gold contacts which due to micro welding tends to remain closed (fail to open) (see Figure 2.38a).

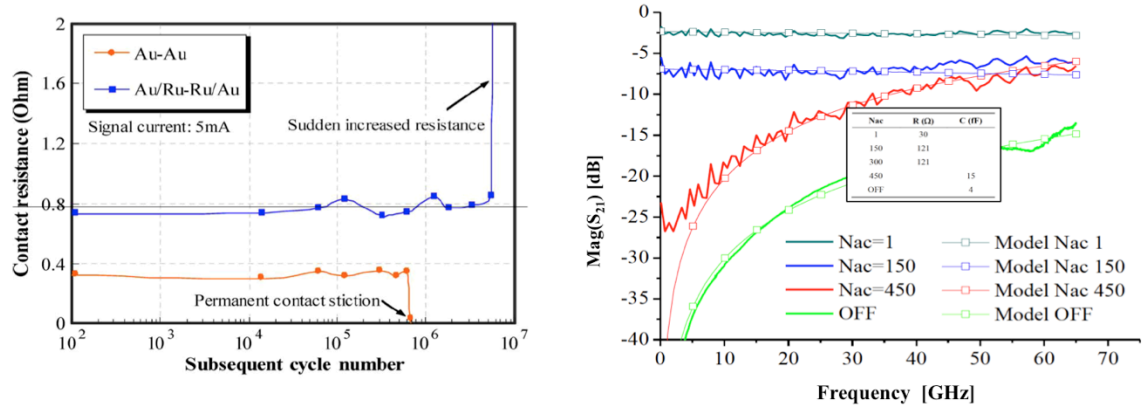

(a) (b)

Figure 2.38: Degradation of the ohmic contact: a) [Source: Ke et al. at KTH[136]] Lifetime behaviors of two different contact metals, Au-Au and Ru-Ru from; b) Effect of Ru-Ru contact degradation on the RF performance (Insertion loss) during the device lifetime. The difference between the OFF state and the working state at 450 actuations show the possible formation of a dielectric film covering the entire contact dimple. This is evident already at lower value of actuation where the high values of contact resistance for Nac<400 above 100 Ω, is due to the

[135] B. Reig, F. Souchon, N.Torres Matabosch, F.Coccetti, M. Koutsoureli, G.Papaioannou, C. Dieppedale, H. Sibuet, O. Vendier, B. Espana, F. Deborgies, "High Reliability RF MEMS Switch Fabricated with a Dielectric-Less Technology for DC-50 GHz Applications," Proceedings of Microwave Technologies & Techniques Workshop, 21 – 23 May 2012 ESA/ESTEC, Noordwijk, The Netherlands.

[136] F. Ke, J. Jianmin, J. Oberhammer, "A Ruthenium-Based Multimetal-Contact RF MEMS Switch With a Corrugated Diaphragm", Microelectromechanical Systems, Journal of, vol.17, no.6, pp.1447-1459, Dec. 2008

beginning of the contamination phenomena. The inset table indicates the contact resistance (Down state) and the open contact capacitance (up-state), extracted from the equivalent circuit.

Based on this the results two different conclusions can be drawn for the Ru-Ru contact. Either there is a very high resistance that builds up with the actuation duration and/or cycles, or there is a mechanical failure, which impedes the switch to close. In order to discard the mechanical failure, the actuation voltage can be increased (up to 60V) and by observing whether the contact switch resistance recovers (even though not to the optimal values). From Figure 2.38b it becomes evident how the build up of a resistance at the contact, degenerates into a capacitive contact (fail to close).

It was concluded that this contamination is likely due to the carbon residues present into the environment (outgassing from polymer ring sealing package) and the catalysis occurring on the ruthenium contact surface which is triggered by current and temperature rise (ruthenium is know to be an excellent catalyzer for carbon based organic materials[137]). These results stressed also the importance of controlling and knowing the working environment in packaged RF-MEMS switches.

[137] R. H. Grubbs, T. M. Trnka, "Ruthenium in Organic Synthesis", 2004 Wiley-VCH Verlag GmbH & Co. KGaA

2.2.4 Thermal induced elasto-plastic creep and/or fatigue in suspended membranes

A third failure mechanism on which lot of research efforts have been focusing are those associated to suspended membranes undergoing electromechanical workload. In these circumstances the dominant failure physics is dominated by internal forces or stress. Stresses in thin films and multilayers have three primary origins: intrinsic, thermal and mechanical. Intrinsic and thermal stresses are often referred to as residual stresses[138]. These latter are also called build-in stresses and come from fabrication process. Thermal stresses can be directly induced by a thermal treatment or temperature gradient along the structure consequence of electrothermal phenomena (Joule effect), while mechanical stress are generated by mechanical load. In both cases, process residual stresses or working induced stresses, temperature and mechanical load play a significant role in controlling or triggering elasto-plastic deformation which may eventually lead to healing or failures (creep/fatigue). Thermal process steps (annealing) have been largely investigated and exploited in order to control the residual stress of fabricated MEMS devices[139], while theoretical and experimental investigation of multilayered thin films have been done to predict mechanical properties and behavior of thin membranes[140,141] The final aim of all these studies was **to control mechanical stresses (be it gradient or biaxial stresses), so to optimize membrane shape and contact quality in cantilever and bridge type MEMS**.

The knowledge gathered at LAAS on thin film stress control have been very important in the investigation of a MEMS technology issued from BiCMOS integration process provided by the Innovation for High Performance Microelectronics (IHP) in Frankfurt Oder Germany[142]. The devices based on this technology (capacitive switches for the millimeter wave range) are intrinsically robust with respect to the failures mechanisms associated to the mechanical contact as dielectric charging (electrostatic actuation through separate dielectricless actuators) and contact degradation (physical RF contact through ceramic-like material TiN-TiN). In addition to this, technological solutions were adopted in the IHP early development of this device for the stress compensation. In fact symmetric multilayer metal stack, and a minimal membrane displacement (contact achieved far from pull in on actuation electrode) were implemented to optimize membrane planarity and hence control the value of the down state capacitance during lifetime. In spite of all these precautions and a well-stabilized fabrication platform, the devices with thickness below 1 μm suffered of planarity control due to creep and fatigue.

These devices have been therefore a perfect case study for addressing problems associated with fatigue and creep failure mechanisms. For these studies the combination of real time membrane shape monitoring and electrical behavioral modeling has been successfully applied in defining an efficient failure identification and selection methodology, which is briefly presented hereby. This work was part of Ms. Nuria Torres-Matabosch's PhD thesis I had the opportunity to co-advise along with Dr. J.L Cazaux from ThalesAleniaSpace.

Device and technology description and Lumped element EC with Technology dispersion

[138] A.G. Evans, J.W. Hutchinson, "The thermomechanical integrity of thin films and multilayers", Acta Metal!. Mater. 43, (1995), pp. 2507- 2530.

[139] C. Villeneuve, P. Pons, V. Puyal, R. Plana, "Planarization optimization of RF MEMS switches with gold membrane", Journal of Micromechanics and Microengering Volume 20 , N°6 (June 2010)

[140] H. Achkar, « Etude de l'actionnement piézoélectrique et électrostatique : Application aux micro commutateurs RF, » PhD Thesis Universite de Toulouse – July 2009.

[141] H. Youssef, « Caractérisations mécaniques de matériaux déposés en films minces utilisé dans la fabrication des systèmes micro électromécaniques, » PhD Thesis Universite de Toulouse – November 2011.

[142] IHP belongs to the Leibniz-Institute für innovative Mikroelectronik (http://www.ihp-microelectronics.com)

The MEMS device considered here is shown in Figure 2.39 and consists of a surface micromachined switched capacitor based on the IHP 0.25µm SiGe BiCMOS process (SG25H1) issued from the 5 aluminum metal layers of the back end of line process (BEOL)[143]. The capacitive switch is built between the two metal layers (M2 and M3), while another metal layer (M3) is used for the membrane and it is realized using a stress controlled Ti/TiN/AlCu/Ti/TiN stack. The RF line is built by means of a further metal layer (M2) and the separate actuation electrodes (called high-voltage electrodes to distinguish them from the CMOS technology supply potential V_{dd}), are formed using the bottom metal layer (M1). The entire RF-MEMS process requires only one additional mask (release step) to the standard IHP BiCMOS flow. This further step has a no significant impact on the cost and especially on the characteristics of the entire BiCMOS process.

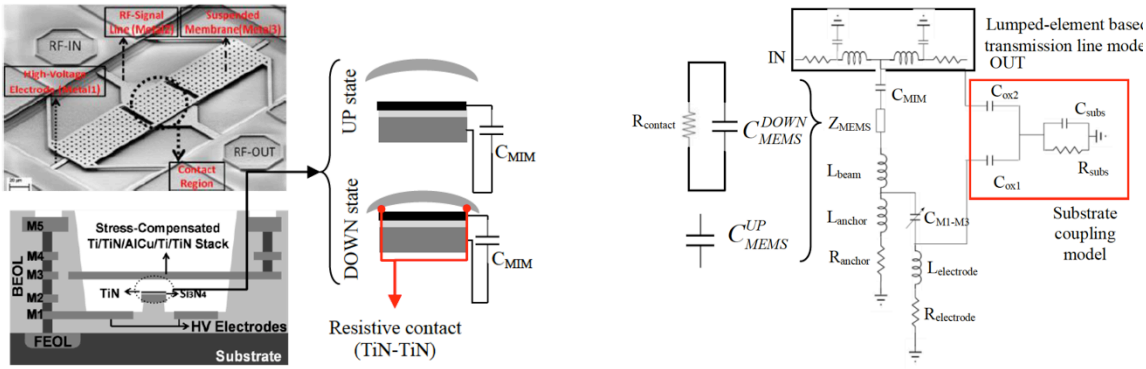

a) b)

Figure 2.39: IHP switch issued from a BiCMOS-MEMS fabrication process: a) [Source: M.Kaynak - IHP][143] Switch (top) and cross section (bottom) with a zoom of the contact region of the device, b) Lumped-elements based model of the switch with the substrate coupling network (red) and the model of the transmission line (black). Z_{MEMS} is the contact zone model in UP and DOWN state

All the fabricated devices use the same contact region[144]and the target operating frequency is tuned by adding series inductances at the anchors of the switch[145]. The main advantage of this solution is that the membrane is mechanically optimized only once in order to yield high reliability, while the switch can be designed to work at different frequencies. On the other hand, the bandwidth of the switch is reduced at lower frequencies because of the higher values of inductances that are needed (this at the cost of higher losses and lower Q-factor). For this reason these switches are typically suitable for applications at frequencies higher than 40GHz. Concerning the actuation voltage, 40V represents the optimal value with respect to the RF performance. Although the pull-in occurs around 30V, 40V actuation voltage is applied in order to ensure a stable contact of the membrane in down position and hence a stable value of isolation at the working frequency.

In order to model this device a scalable lumped-elements equivalent circuit was proposed for the different frequency versions of the device by a combination of fullwave simulation and experimental LF measurements of reference test structures[146,147]. The importance of the proposed

[143] M. Kaynak et al. , "BiCMOS embedded RF-MEMS switch for above 90 GHz applications using backside integration technique", *Electron Devices Meeting (IEDM), 2010 IEEE International* , vol., no., pp.36.5.1-36.5.4, 6-8 Dec. 2010

[144] M. Kaynak. et al., "RF-MEMS switch module in a 0.25 µm BiCMOS technology", Silicon Monolithic Integrated Circuits in RF Systems (SiRF), 2012 IEEE 12th Topical Meeting on , vol., no., pp.25-28, 16-18 Jan. 2012

[145] M. Kaynak et al., "Packaged BiCMOS embedded RF-MEMS switches with integrated inductive loads" Microwave Symposium Digest (MTT), 2012 IEEE MTT-S International , vol., no., pp.1-3, 17-22 June 2012

[146] N. Torres Matabosch et al. "Accurate and Versatile. Equivalent Circuit Model for RF-MEMS Circuit. Optimization in BiCMOS. Technology", Microwave Integrated Circuits Conference (EuMIC), 2012 European , October. 2012

model is that each lumped-element is associated to a constitutive part (shape and size) of the device. This provides a complete and detailed electrical description of the same and allows to trace back (or detect) possible manufacturing flaw or deviation due to technological dispersion so to provide information about the quality of the fabricated device.

In Figure 2.39b the schematic of the switch is presented. This equivalent circuit is based on two parallel resonant circuits. The RF performances are given in Figure 2.40. The main resonance which determines the working frequency is due to the down state capacitance and the inductors in the arms of the switch (Z_{MEMS} and L_{anchor}). The secondary resonance is associated to the capacitance between the membrane and the electrodes, and the inductance of the bias lines ($C_{M1\text{-}M3}$ and $L_{electrode}$). In both cases, an additional series resistor is added in order to compute the losses of the inductors (R_{anchor} and $R_{electrode}$).

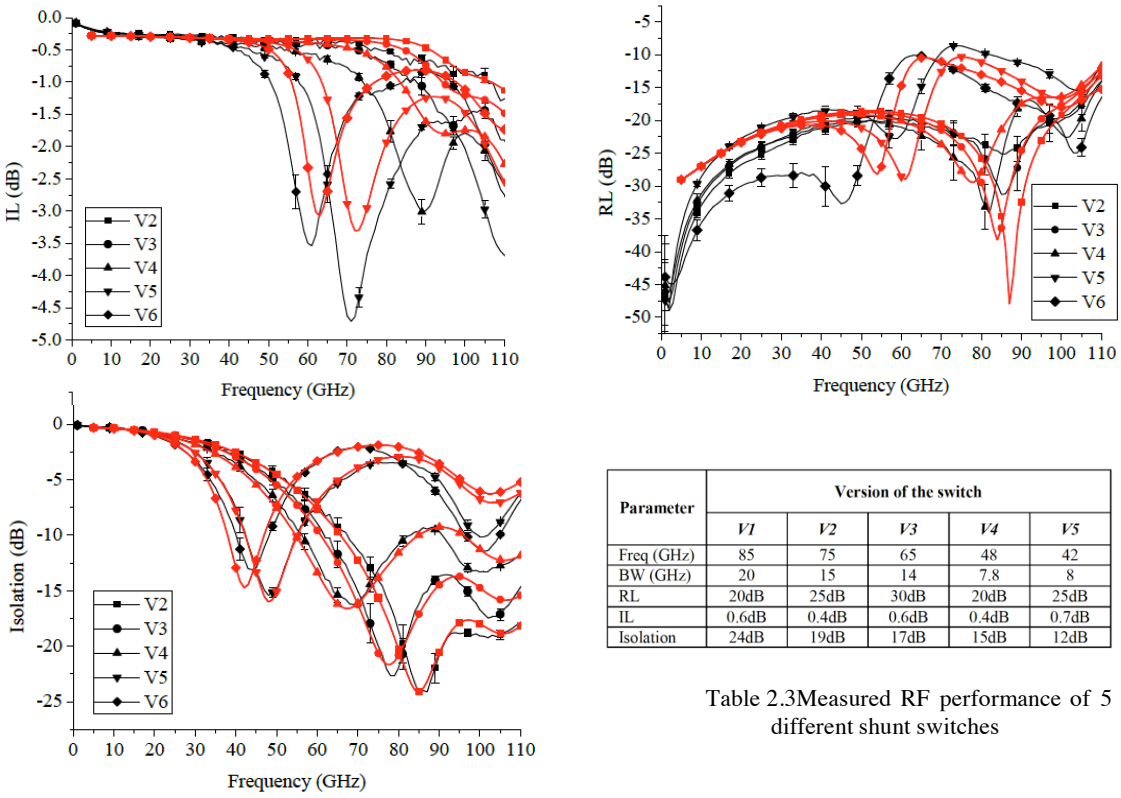

Parameter	Version of the switch				
	V1	*V2*	*V3*	*V4*	*V5*
Freq (GHz)	85	75	65	48	42
BW (GHz)	20	15	14	7.8	8
RL	20dB	25dB	30dB	20dB	25dB
IL	0.6dB	0.4dB	0.6dB	0.4dB	0.7dB
Isolation	24dB	19dB	17dB	15dB	12dB

Table 2.3Measured RF performance of 5 different shunt switches

Figure 2.40: Comparison between the measurements of each version (black) with the model (red). The errors bars represent de dispersion over the wafer (measurements of 50 devices of each version) and summary table.

Noteworthy about this device is that the major failure mechanisms have been carefully addressed. In order to avoid dielectric charging the actuation is done on separated lateral electrodes. By this way, the metals in the contact region (suspended membrane and RF-Signal line) have the same electrical potential (see Figure 2.39a). Reliability studies demonstrate successful operation up to 50 billion switching cycles under 45V actuation voltage[148]. The other major reliability issue, namely the mechanical contact repeatability between the membrane and

[147] N. Torres Matabosch, M. Kaynak, F. Coccetti, M. Wietstruck, B. Tillack, J. L.Cazaux, "Estimation of RF performance from LF measurements: Towards the Design for Reliability in RF-MEMS," Microelectronics Reliability, Special issue 23rd ESREF Symposium, Volume 52, Issues 9–10, September–October 2012, Pages 2310–2313

[148] M. Kaynak, F. Korndorfer, F.; Wietstruck, M.; Knoll, D.; Scholz, R.; Wipf, C.; Krause, C.; Tillack, B.; ,"Robustness and reliability of BiCMOS embedded RFMEMS switch," Silicon Monolithic Integrated Circuits in RF Systems (SiRF), 2011 IEEE 11th Topical Meeting on , vol., no., pp.177-180, 17-19 Jan. 2011

the signal line, has been tackled by using the floating TiN electrode on top of the SiN dielectric layer (MIM capacitor) and underneath the membrane[149]. Owing to some residual curvature of the membrane during contact, this metal contact between TiN and TiN occurs at the edges of the signal line guarantying an extremely stable and repeatable ohmic contact. Although the resistance associated to this contact is quite high (~ 5kOhm), this turns out to have not significant effect since it is in parallel with the down state air (MEMS) capacitance formed by the curved membrane and the RF line (see Figure 2.39a).

In terms of UP/DOWN capacitance (Z_{MEMS}), this value is extracted from C(V) measurements (=20fF and =128fF) while the MIM capacitor (C_{MIM}) has a measured value of 2.5pF. On the other hand, the inductor L_{anchor} is modeled using a pi-network[150]. The transmission line is a RLCG model combined with a substrate coupling network well-known in the BiCMOS process modeling. The reason of using this approach is due to its simplicity in being used in network simulators (Spice) and the substrate losses already known can be easily added. The values of each parameter of the substrate coupling network (C_{ox2}, C_{ox1}, R_{subs} and C_{subs}) are deduced from the process specifications by the following equations:

$$C_{oxi} = A_{line} \cdot C_{Mi-subs} \quad i = 1,2$$
$$R_{subs} = \frac{\varepsilon_r \varepsilon_0 \sigma_{Si}}{C_{subs}} = 405\Omega \qquad (2.9)$$

where $C_{Mi\text{-}subs}$ is the coupling from Metal i (M1 or M2) to substrate per mm^2 (defined by the process), A_{line} is the surface of the line, C_{subs} is measured and s_{Si} is the resistivity of the substrate. R, L and C are deduced from standard modeling of CPW.

In Figure 2.40 the measured RF performance of all the presented switches (V1 to V5) is compared with the model adapted with its corresponding L_{anchor} value. The measurement results were taken over an 8-inch wafer for more than 50 samples.

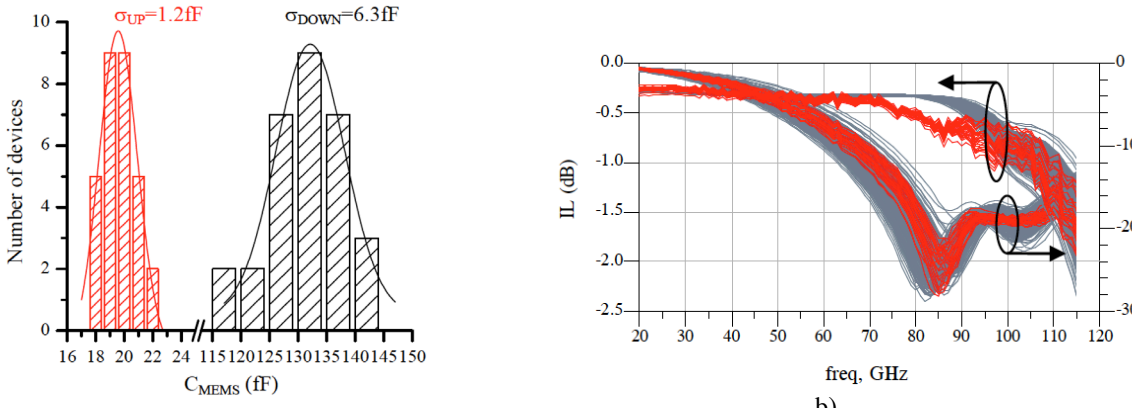

a) b)

Figure 2.41: a) LF measurements of C_{MEMS} in UP and DOWN state on more than 50 samples on a 8-inch wafer; b) and comparison between measured (red) and model (grey) RF performance with the computed fabrication process deviations

[149] TiN is a ceramic material known to be an extremely hard and typically used for mechanical hardening or as diffusion barrier layer. In the IHP BiCMOS process Ti Nis indeed used as such on top of the MIM capacitor and on the bottom of the metal layer used for the bridge.

[150] R.N. Simons, "Coplanar Waveguide Circuits Components & Systems", *John Wiley & Sons*, April 2012

The same figures show also the dispersion of the RF performance over the wafer. These results show very good agreement between model and measurements within the entire frequency band (30-110GHz).

In fact owing to nm-range thickness variations and the tolerances in the deposition of the metals, the stress gradient of the suspended membrane varies over the wafer. This turns out to yield a variation on the distance between metals (4%), which yields significant variation (5-6%) on the MEMS capacitance (C_{MEMS}) in both states. The same stress variation affects as well directly the capacitance between membrane and the actuation electrode ($C_{M1\text{-}M3}$), itself responsible for the bandwidth. It is therefore important to monitor and understand the variation of these two capacitances so to predict and control the device RF behavior.

In order to verify the relationship between RF deviation and C_{MEMS} variation, LF measurements (at 1MHz) using an impedance analyzer (Agilent 4294A Precision) of the UP and DOWN state capacitance (C_{MEMS}) have been carried out. The parasite capacitances of substrate and C_{MIM} are de-embedded by means of specific test structures (identical devices without the bridge part). These measurements show a Gaussian distribution from the mean value in both states (Figure 2.41a). By **applying the computed deviations to the lumped-elements circuit model shown above, the effect of the fabrication tolerances can be reproduced in the entire band**. A Monte Carlo analysis of the model with 50 trials is done and compared with the measurements of the 50 devices under test showing very good agreement (Figure 2.41b).

Noteworthy is that the relation between, $C_{M1\text{-}M3}$ and the RF performance can only be established by using the equivalent circuit since this capacitance cannot be measured experimentally. In fact, in order to measured it, an extra test structures would be needed to de-embed the coupling effects with other metal layers. These extra structures and additional measurements would hamper any fast (real time) device testing. For this reason, a rough first estimation of $C_{M1\text{-}M3}$ is extracted from the model by exploiting the parallel plate capacitance formula followed by more accurate identification based on curve fitting of the isolation around the secondary resonance (at 100 GHz in Figure 2.41).

The model obtained by introducing the technology dispersion give excellent fitting of the measurement results also if used for synthesis of new component based on the same device. An example of it is the series switched capacitance version of the same device which was design and realized upon this model[146].

Reliability: Failure analysis and study based on non intrusive monitoring and reverse modeling

From the manufacturer point of view, the availability of an accurate and time effective screening procedure is paramount, especially when some costly steps need yet to be carried out (e.g. packaging). For any device the definition of the selection criteria depends from the capability of the component to satisfy the targeted working conditions for a given application. In the present work the use of failure criteria provided by an industrial partner (ThalesAleniaSpace) have been considered[151]. According to them, a maximum deviation of 10% in V_{PIN} and V_{POUT} and an increase of 1dB in IL for 1h of continuous stress are assumed as the threshold upon which the failure is detected (failure criteria). The actuation profile has been monitored through $S_{12}(V)$ measurements since the DOWN state (contact) position is reached below the mechanical pull-in. In fact the contact is achieved on the signal line through a gap which is smaller than the gap between the membrane and the actuation electrode ($g_c<g_0/3$ in a)

b)

Figure 2.42 a and b).

The 8-inch wafer is divided in cells (reticule) within which the switches are replicated. The availability of a large number of devices (here taken on a quarter of wafer) allows a fair monitoring of the process dispersion and it is essential to assess the reliability of the device. The reliability study presented here was extended to any device based upon the same MEMS part.

Several devices of each cell have been held in DOWN position during 1h measuring the IL and the pull-in/out voltage every 10 min. An example of the results obtained is given in Figure

[151] O. Vendier, "RF-MEMS for Space Applications", *Microwave Integrated Circuits Conference (EuMIC), 2012 European*, RF-MEMS for Mm-wave Reconfigurable ICs Workshop, November 2012.

2.43, which plots the deviation after stress of the pull-out voltage for several (14) identical devices with respect to the their initial V_{POUT}. Note that this initial value can span over a quite large span of values due to the technology dispersion and/or failure mechanisms under study. As expected it is demonstrated that the higher the V_{POUT}, the lower is the deviation after stress. Moreover, also the difference between V_{PIN} and V_{POUT} plays an important role and should remain as low as possible. By applying the aforementioned industrial requirements (10% deviation in V_{POUT}) the only devices which succeeded the tests where those having a

$$V_{POUT} > 36V \quad \text{and} \quad |V_{PIN} - V_{POUT}| < 1.$$

Hence these values could have been taken as selection criteria to carry out wafer screening.

In particular the condition ($V_{PIN} - V_{POUT} < 1$) is imposed by the small gap between the membrane and the transmission line. In this device the contact is indeed achieved in the quasi-linear region, far below pull-in, where the actuation is reversible[152]. It must be pointed out that the values indicated above as V_{PIN} and V_{POUT} do not correspond to actual pull-in and pull-out occurrences. They rather represent the value of potential at which mechanical contact of the membrane with the underneath signal line is achieved. Now, since this contact is obtained far below the pull in of the actuator (the actual electrostatic driving force is on the laterals electrodes), these two values should be coincident, in a well functioning device. If this is not the case this deviation can be used to detect a failure mechanism likely associated to the membrane actuation.

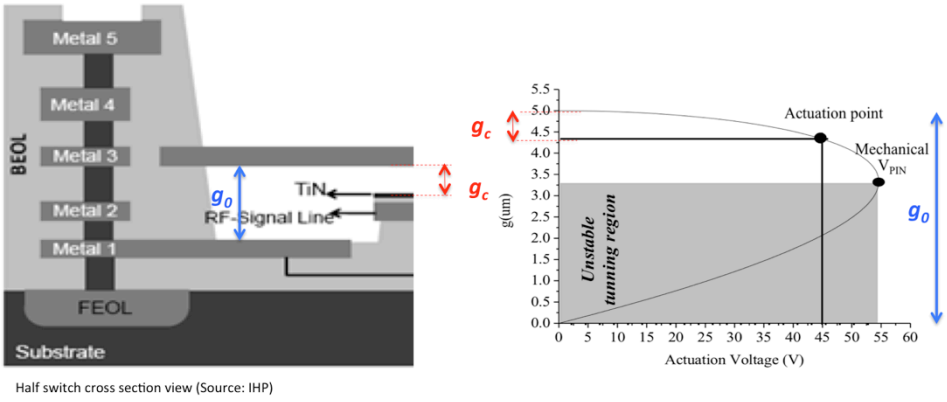

a) b)

Figure 2.42: Actuation principle based on far below pull in for the IHP MEMS devices: a) [Source: M.Kaynak - IHP][143] Half switch cross-section, b) Separation gap versus actuation voltage

Similarly these failure mechanisms show up on the V_{POUT} for value below 36V. The monitoring of the membrane by means of a light interferometry has allowed to relate the membrane shape to these electrical signatures. The results have been extremely useful since the failing device had a very characteristic mechanical profile easily detected by white light interferometry. The failure analysis has been based on the equivalent circuit described above, which has been able to describe accurately the specific defect, namely an undesired deformation of the membrane at the contact region (Figure 2.44a) and even reproduce specific failure mechanisms such as the breaking of an anchoring point likely due to fatigue (Figure 2.44c).

This method represents a cost-effective and non-intrusive reliability monitoring technique such to predict creep and/or fatigue induced phenomena.

[152] G. M. Rebeiz, *RF MEMS: Theory, Design, and Technology*. New York: Wiley, 2003, pp. 87–104.

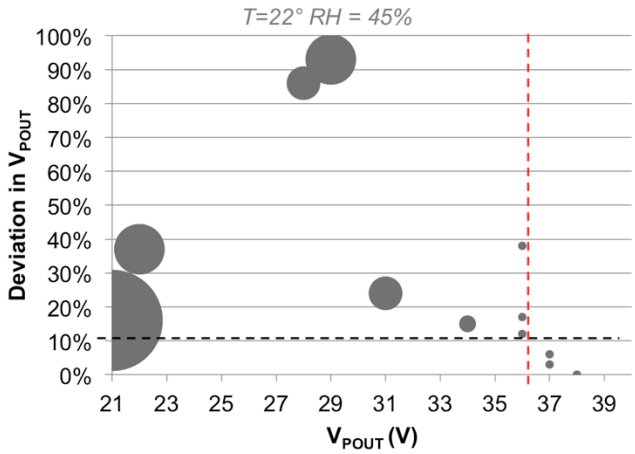

Figure 2.43: Relation between the deviation after 1h of stress and the initial VPOUT. The size of the disk represents the difference between VPIN and VPOUT. The vertical dashed line defines the selection criteria for the VPOUT. The successful devices are those that lie beyond this limit and have smallest radius (<1V).

The proposed reliability approach has demonstrated its validity and effectiveness in observing and analysing the MEMS process yield, be it within the same wafer or wafer to wafer for the IHP 0.25µm BiCMOS process. It could be extended and adopted as functional yield monitoring technique for other MEMS technology. The essential aspects are the availability of: a stable fabrication process (low fabrication process dispersions and variability) and of a clear failure criteria (typically associated to a given application).

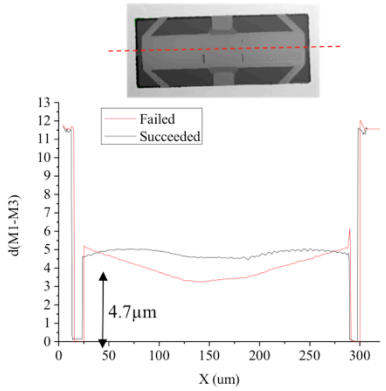

a)

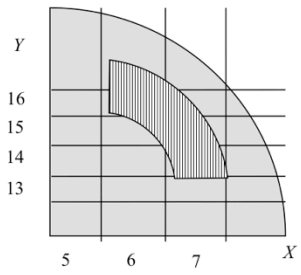

b)

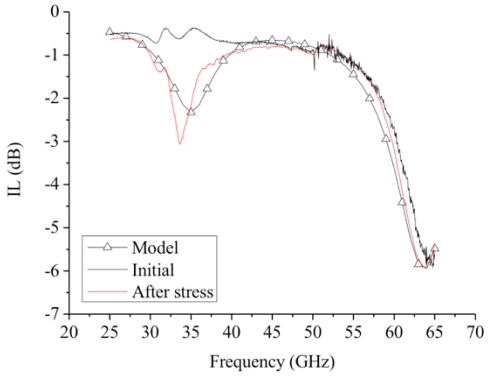

c)

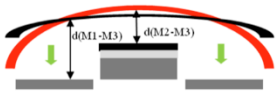

$$C_{MEMS}^{failed} = C_{MEMS} \cdot \frac{d_{M2-M3}^{initial}}{d_{M2-M3}^{final}}$$

$$C_{M1-M3}^{failed} = C_{M1-M3} \cdot \frac{d_{M1-M3}^{initial}}{d_{M1-M3}^{final}}$$

Figure 2.44: Profilometr analysis of IHP switches: a) On the left a typical profilometr results for a good (black) and failing (red) device with rough indication b) of the correspondent wafer area where good device are located; c) effect of the membrane deformation and likely failure mechanism (breaking of one suspension anchoring point) on the RF performance. The value of capacitance given therein are extracted from the profilometer measurement and used in the equivalent circuit.

Nowadays thanks also to these work in order to avoid failure mechanisms associated with fatigue and creep, the foundry (IHP) has opted for increased value of the membrane thickness.

2.2.5 Conclusions on RF-MEMS reliability study

MEMS switches failure mechanisms are a difficult **multiphysics / multidisplinar** challenge. Their study by means of "**ad-hoc**" experimental methodologies such to target **separately each phenomena**, has allowed to advance in the **fundamental understanding** of the underlying physics.

As main remarks on the maturity and adoption of these devices the conclusions can be as follows:

- CMOS foundries appears today as the most suitable solution for consumer electronics (co-integration of analog and digital electronics/functionalities). In this case, due to limited flexibility on the process option (especially materials) **only switched varactor** have been implemented to realize tuning matching network and antenna matching.
- MEMS foundries are well suited for pick-and-replace solutions, where more flexibility on material choice and process steps is possible. At the moment all metal-contact switches available commercially are issues from such environment and, due to high production costs, they are typically targeting medium to high-end niche applications (ATE, aerospace). This may change if market pressure increases and more cost effective manufacturing solutions are found.
- MEMS Research laboratory are essential for supporting both (R&D proof of concept and failure analysis), in particular in order to carry out fundamental failure mechanisms investigation. Although this conclusion is quite obvious nowadays, it was not few years ago, when RF-MEMS manufacturing was carried out in research level clean rooms (mainly by manual processes). Even for high-end niche markets, process variability and costs are way too large to match industrial product quality standards, and process transfer and industrialization is too hard and unreliable (often need to be started from scratch on a semiautomatic industrial platform).

Finally it must be highlighted that MEMS technology timeline demonstrate that product development may take longer than expected. An analysis made by R. Grace associates (Figure 2.45), indicates an average of 20-25 years of development from initial idea to commercialization, for most common MEMS devices such as accelerometers, gyroscope, ink-jet nozzle, … etc[153]. All these devices took advantage of the impressive progresses done earlier for the development of MEMS pressure sensors which more than 35 years. These latter, introduced in the middle 50's, paved the way of modern micromachining and solved several of the problems that make today MEMS technology an extremely successful category of products. The only exception to this success are still RF-MEMS. In spite of the maturity of MEMS technology RF-MEMS development stretched over 30+ years (more than 10 years more than late MEMS devices). It is my personal view that in RF-MEMS switches or relay, a functionality never encountered in other MEMS device takes place. As mentioned earlier, this is the electric energy transfer through a micro/nano electro-mechanical contact, which introduces a completely new class of multiphysics and multi-scale challenges. Consequently this yielded a longer time to market elapse time (see Micro-relays in Figure 2.45). The engineering community was confronted with new and yet more tedious physics of failure, which today are in large part understood and circumvent, also thanks to the work done at LAAS. In spite of this however, many further improvements are expected to be found in new materials (with superior electrical and mechanical performances)

[153] Roger H. Grace, « Barriers to the Successful Commercialization of MEMS: The 2011 MEMS Industry Commercialization Report Card, » Roger Grace Associates, (2012) www.rgrace.com commercial micro manufacturing international pp. 5.

and in the better understanding of surface physics contact interaction or proximity phenomena (nanotribology)[54,154].

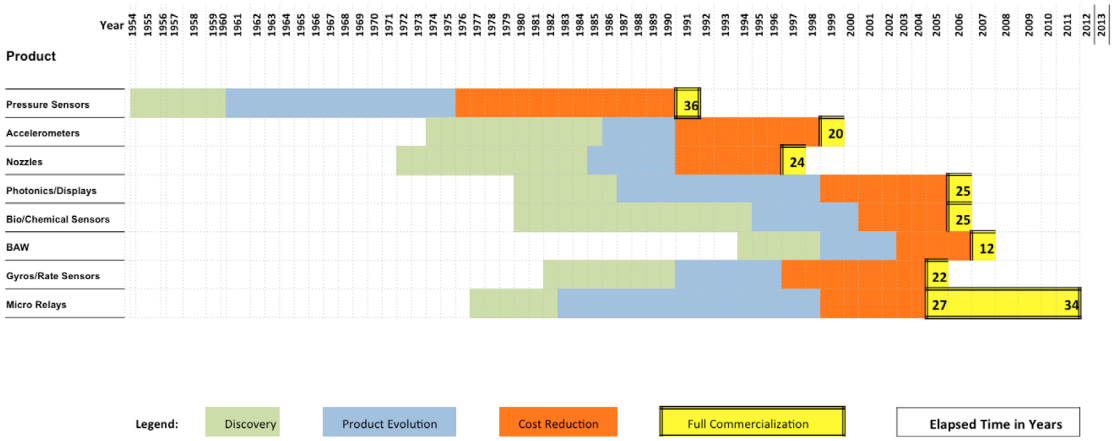

Source: R. Grace Associates (2012)

Figure 2.45: Adapted version of the timeline evolution for the major MEMS product from their discovery to full commercialization (Source: R. Grace Associated 2012). The milestone for RF-MEMS micro relay are the discovery attributed to K. Petersen toward the end of 70's and the first successful commercialization such as Radant (2005) and Wispry (2011).

Worth of note is that although the discovery of Micro Relays is attributed to Petersen 1979, this early realisations did not consist in a truly RF device. Moreover no further development can be associated to this early works until early 90s. Hence the actual start for the evolution of the RF micro relays should be moved forward to this period.

In spite this would considerably reduce the evolution window given above for this technology, on the other hand it should be stresses that what has been considered as full commercialisation in 2011 is, in reality, only partial (in terms of market share and penetration) and it is expected to become as such only in the years to come. Under this consideration the analysis made above, about the difficult evolution of RF MEMS switches, can still hold valid.

[154] B. Gotsmann and M. A. Lantz, « Quantized thermal transport across contacts of rough surfaces, » Nature Materials, vol 12, January 2013, pp. 59-65.

2.3 Conclusions on past Research activities: Lessons learned

The research activity on RF-MEMS taught a lot to me about science and the individuals dealing with that. In particular how essential is the thinking-out-of-the-box (electromagnetic box in my case) and consider the full picture by learning from different and past experiences while dealing with a new not "only-electrical" device.

From the reliability people I learned the very basic principle of "**no reliability with variability**". This principle could have spared the RF-MEMS community a lot of money if more efforts had been first devoted to establishing "stable" manufacturing platform/technology. As matter of fact the development of a MEMS process in a foundry lacking process control and stability can be risky since industrialization of such a complex process may be very problematic (even the simplest MEMS process becomes complex when repeatability is at stake). Device variability is an enemy also in research level where manufacturing platform with too large dispersion in material and geometry specifications hampers systematic and consistent experimental studies. Few group implemented their RF-MEMS concept on CMOS foundries from the very beginning, however prohibitive development costs and lack of critical mass in dealing with the entire device development has hindered (see Baolab) or delayed (see Wispry) their success. Not to mention that final success on the market depends from the delicate balance between price acceptance and added value in performances.

Naturally variability is not an issue in fundamental research (e.g. exploration of exotic material and sophisticated manufacturing process), where fundamental discoveries are more likely to happen even with single experimental prototypes/exemplars. Given the maturity of RF-MEMS technology today there is still room for improvement through this type of research.

In particular a lesson we learned about reliability in these sense is that it is useless and overwhelming to solve all problems at once on a final device.

In order to deal with reliability, we learned that the "**devide et impera**" approach, consisting in isolate and separately study each failure mechanism needs to be enforced, to understand and solve the underlying physics of failure. Undesired masking effects due to coupled physics typically occurring in MEMS may render this task impossible at device level.

In addition to this the working conditions play a fundamental role. Application conditions may be even very different from one case to another[155], and they determine which failure mechanisms will prevail. Hence the same working conditions should drive the optimization up front starting from the initial design. This introduced us to the need and importance of design for reliability, today widely adopted in the RF-MEMS community.

In fact at design stage, the knowledge gathered through separate studies need to be used collectively through what is called concurrent design (or co-design) approach. In this field still much need to be done to encompass all physics in a consistent and fully coupled numerical model, allowing a comprehensive analysis. Present software packages are good enough for separate or weakly coupled modeling, but not (yet) enough to embrace fully coupled physics. An ultimate tool able to do this is essential in introducing the further level of innovation in RF-MEMS technology and application.

As consequence of this awareness on environment and working condition effects, one of today still open and critical issues is the packaging. Not treated here at all, since it deserves considerable focused efforts by itself, the packaging issue in RF-MEMS can be summarized by the well known riddle "**hermetic package or die**". This in spite of the fact that today there is no cost-effective MEMS packaging solution that can guarantee a given (targeted) environmental specification with extreme accuracy and over the device lifetime. As matter of fact there are not even technique to know accurately (within few % of RH and ppm of gas composition) what is going on in such small volume packages. Therefore concurrent design not only of the micro-

[155] See Tx/Rx switching versus redundant channel switching where several millions of actuations versus one or none occur in their lifetime respectively.

electro-mechanical part but also at packaging level from the very early stage of the design is necessary. Yet more needed are stable and robust packaging processes.

Finally after so many years of research and development on RF-MEMS, few trends seems to be clear. Having in mind the perils laying ahead (see dielectric charging, metal contact degradation, membrane creep and fatigue and packaging leakages or deterioration) the options to counteract them are, either to remove the cause (e.g. dielectricless actuated device) or overdrive the device (e.g. large contact force actuation) or by dedicated and costly packaging solutions (e.g. glass frit type). This is what is happening in most mature RF-MEMS device available today. However only more advanced studies on novel dielectric materials (endowed of low/quick charging mechanisms), on contact surface physics-metallurgy, and on innovative low-cost process development are expected to push yet further the present level of miniaturization and device performances at affordable production costs.

Research in high frequency engineering is certainly yet possible especially by finding new design topologies or more accurate electrical descriptions (possibly combined within reliability models). However, from this quick to-do list of most serious issues mention above, it looks apparent, that actual breakthroughs are in the hand of physicists and process engineers.

Aware of this and asking myself what's next, I came to the personal conclusion that with RF-MEMS we reached the lower limit of what we could do in microelectronics by following a top-down approach, i.e. by trying to miniaturize macroscopic electro-mechanical principles through the mighty combination of photolithography and micromachining. It was in the 70's, the tiny "microscale" machines came to motion and the MEMS revolution began. Today, in 2013, the MEMS industry is worth turnovers of several billion dollars and it is steadily growing. Though RF-MEMS represents a very small part of this (less then 1% if but BAW are excluded), and competition is fierce (SOS, SOI, BST, …) I am sure their time will come.

Said that, I came to another important conclusion. Today progress in material science and nanscience gives the opportunity to actually practice the other way around of conceiving research in microelectronics and in particular the bottom-up approach. Today extremely sophisticated and powerful tool such as e-beam lithography and scanning probe microscopy are becoming available in microelectronic laboratory, empowering scientist with unprecedented opportunities.

One above all the possibility to fabricate and experimentally study device so small which introduce to completely new class of functionalities. A glance of how this translates in the RF realm is given in the next chapter dedicated to the personal research perspectives.

3 Research Outlook

This part of the document provides a personal outlook on future research directions. In large part this activity have been inspired by the activity carried out in the field of RF-MEMS reliability. In fact most of the studies in the physics of failure of a MEMS device were linked by a common bottom line. The behavior of a microdevice is strongly dominated by phenomena which take place at lower scale, e.g. at the nanoscale, where surface interaction dominate on volume's requiring a switching paradigm in how functionalities (electrical, mechanical, chemical, …) are studied and eventually exploited.

Hence the part which follows is influenced by the lesson learned in RF-Microsystem technology and encouraged by the continuous and impressive progresses in nanoscience.

In particular the focus will be devoted to what is called 2D and 1D electronics more recently made popular by the availability of carbon based materials. As one of the most promising technology to bridge present needs with future solutions, graphene and CNT are becoming accessible with increasing quality and acceptable prices. This perspective will be therefore divided in a shorter to medium term vision based on recent and ongoing activity on graphene ballistic electronics, and in a second part projected over a medium to long term period exploring NEMS as cornerstone to implement the next generation of integrated RF systems.

3.1 The way forward: RF Nanotechnology

Today's electronics is moving toward faster, smaller, more efficient, yet cost effective, solutions. In doing so, the limits of what currently used materials and processes may offer is frequently reached. Examples of this are appearing at the most critical building blocks of modern electronics most emblematically represented by the **transistors**. As for the past and now outdated technologies such as vacuum tubes (popular until late 50's), and bipolar transistors (70's), nowadays prodigious silicon CMOS technology is reaching the physical limit imposed on the one hand, by the maximum tolerable temperature rice (power density > 100 W/cm^2)[156], and on the other by the parasitic resistance and capacitance of gate length below 20 nm, which are starting to dominate the intrinsic resistance and capacitance values of the device[157]. These trends may imply the inevitable end of the Moore's law and with that the end of silicon technology, with its 60 years of undisputable domination.

As far as future integration approaches are concerned the ITRS roadmap bets all on **heterogeneous integration in order to achieve miniaturization and function diversification**. However the path toward the implementation of this approach is hampered by the very natural limit of conventional material (such as metals) at the very basic level of practical implementation, as for instance in case of interconnects. In their case crucial parameters namely, the electrical transport (conductivity and maximum allowed current density), becomes increasingly affected by surface scattering, be it at the grain boundary or on the side walls, which start dominating on bulk scattering (conventional conduction in metal) as soon as the wire width becomes smaller than the mean free path of the bulk scattering itself[158,159]. These results for

[156] Source: Intel Developmer Forum Spring 2044 – Pat Gelsinger

[157] S. E. Thompson and S. Parthasarathy, « Moore's law: the future of Si microelectronics, » Material Today, June 2006, Vol. 9, No, 6, pp. :20-25.

[158] K. Fuchs, "The conductivity of thin metallic filmsaccording to the electron theory of metals," Proc. Cambridge Philos. Society, 34 (1938) 100.

copper show that below the 100 nm diameter range, conductivity and current density starts to be strongly affected by surface scattering with a contribution that is 2.6 time lower than the corresponding bulk value[160]. These findings highlight the decisive role of grain boundaries and surface roughness. Likewise, these structural features are essential in determining also the mechanical properties (elasticity and plasticity) of nanoscale narrow materials[161].

In general the lower is the size of an object the larger the effect of the surface physics with respect to the volume and bulk phenomena in determining the overall (electrical, mechanical, …) behavior. Since few years this fundamental principle paved the way toward the exploitation of nanoscale geometry and material to enhance present capabilities (e.g. supercapacitance made with nanostructured material[162]) or introduce novel functionality such as ballistic transport devices for zero-bias detection[163,164] and nanoresonators for communication (nanoradio[165]) and sensing[166].

Hence, the quest for new materials endowed with disruptive, enhanced properties and possibly compatible with standard processes, has become essential.

Carbon based materials and most prominently carbon nanotube (CNT) and graphene, are becoming the emblematic protagonists, of this quest. Characterized by superior electric and mechanical performance, and considered to be compatible with conventional manufacturing techniques, graphene may become a key enabling material, for a new generation of high-speed nanoscale electronics. In order to understand and project the potentialities of carbon based material into practical microwave applications, it is necessary however to encompass the evolution of this fascinating material, beginning with early observations and moving through the underlying complex physics (relativistic and quantum physics) and the most cutting edge technologies (electron beam lithography, Raman spectroscopy, …).

By the same token on the wake of graphene discovery an entire class of two-dimensional crystal based materials each endowed with specific properties are now becoming popular and are believed to be at the cornerstone of a new class of so called 2D nanoelectronics devices[167,168]. Example of this is the molybdenum disulphate (MoS2), that similarly to graphene is a 2D crystal, but much differently from it, it has an energy bandgap and hence a semiconductor behavior (excellent candidate for digital 2D nanoelectronics with demonstrated impressive ON/OFF ratio above 10^7) [169].

The consequences associated to these on-going research activities are expected to open new perspectives for electronics similar to what silicon did in the last six decades.

---

159 E.H. Sondheimer, “The mean free path of electron in metals,” Advances in Physics Philosophical Magazine, Vol. 1, January 1952, No. 1.

160 W. Steinhögl, G. Schindler, G. Steinlesberger, and M. Engelhardt, “Size-dependent resistivity of metallic wires in the mesoscopic range,” PHYSICAL REVIEW B 66, 075414, 2002.

161 C. Seguineau “Caractérisation micromécanique de matériaux en couche mince destines aux micro et nano technologie,” PhD Thesis INP Grenoble.

162 D. Pech, M. Brunet, H. Durou, P. Huang, V. Mochalin, Y. Gogotsi, P.L. Taberna, P.Simon, “Ultrahigh-power micrometre-sized supercapacitors based on onion-like carbo,” Nature Nanotechnology, Vol.5, N°9, pp.651-654, Septembre 2010.

163 S. Bollaert, A. Cappy, Y. Roelens, J. S. Galloo, C. Gardes, Z. Teukam, X. Wallart, J. Mateos, T. Gonzalez, B. G. Vasallo, et al., “Thin Solid Films,” 515, 4321 (2007).

164 G. Deligeorgis, F. Coccetti, G. Konstantinidis, and R. Plana, “Radio frequency signal detection by ballistic transport in Y-shaped graphene nanoribbons,” Appl. Phys. Lett., vol. 101, no. 1, pp. 013502–013502–3, Jul. 2012.

165 K. Jensen, J. Weldon, H. Garcia, and A. Zettl, “Nanotube Radio,” Nano letters 2007 Vol. 7, No. 11 3508-3511

166 A. K. Naik, M. S. Hanay, W. K. Hiebert, X. L. Feng and M. L. Roukes, “Towards single-molecule nanomechanical mass spectrometry,” Nature Nanotechnology Vol. 4, July 2009, pp. 445-450.

167 K.S. Novoselov, “Graphene: Materials in the Flatland,” (Invited) plenary Talk at the European MMicrowave Week, October 2011, Manchester UK.

168 F. Bonaccorso, A. Lombardo, T. Hasan, Z. Sun, L. Colombo, A.C. Ferrari, “Production and processing of graphene and 2d crystals,” Materials Today December 2012, Vol. 15, No. 12, 564-589.

169 H. Wang, L. Yu, Y-H. Lee, Y. Shi, A. Hsu, M.L. Chin, L-J. Li, M. Dubey, J. Kong, T. Palacios, « Integrated Circuits Based on Bilayer MoS2 Transistors, » Nano Letter, 2012, 12, 4674-80.

Encouraged by these brilliant perspectives and motivated by the huge scientific challenge lying ahead research activities in the field of RF transport and exploitation of the same for carbon based devices was initiated and conducted in CNRS-LAAS starting from 2005 within the exploratory research topics launched by the AMICOM NoE and intensified within the following initiative of the LEA-SMARTMEMS common laboratory (2009-12), involving LAAS (R. Plana), IMT Bucarest - Romania(M. Dragoman) and FORTH Heraklion – Greece (G. Konstantinidis).

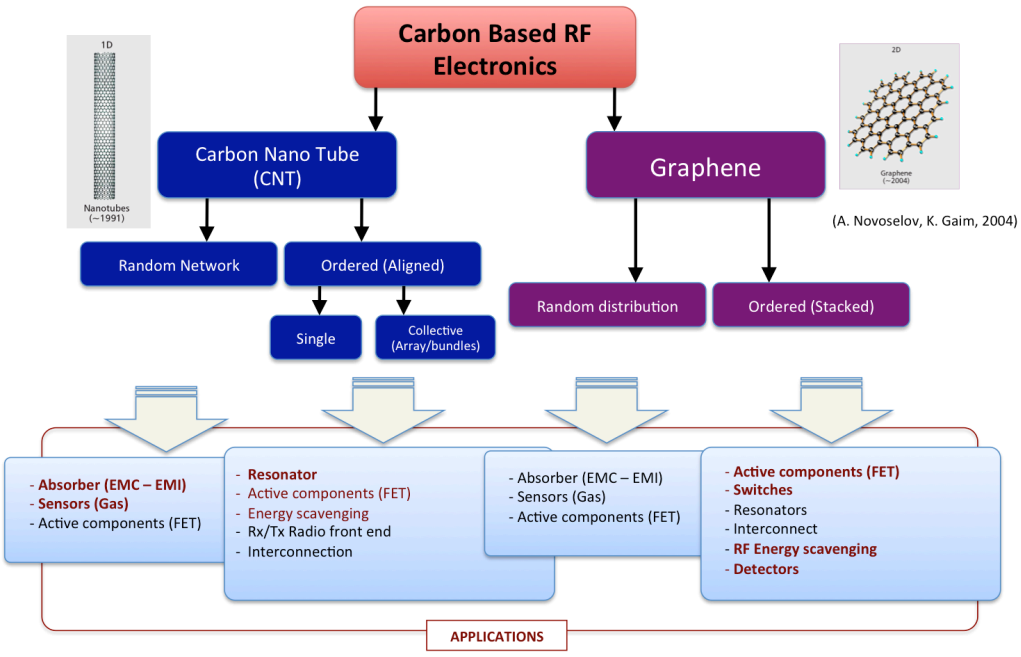

Figure 3.1: Overview of carbon based electronics for RF applications (in red the application/devices realized and investigated at LAAS)

The focus initially held on CNTs and more precisely DWCNT produced by the French material laboratory CIRIMAT (E. Flahaut), moved on graphene as early as these material became available from the first provider (Graphene Industry in Manchester). **Electromechanical properties** and **microwave transport** on these materials were identified as the main scientific scope in line with still on going RF-MEMS activities or the new strategic directions drawn by the recently funded research group on Micro and Nanosystems for Wireless Communication.

3.1.1 Brief introduction to Carbon based Electronics

The research on carbon based material covers many different application domains (material science, biology, construction engineering, …) and was triggered by the early discovery and availability of these carbon allotropes. Carbon nanotubes (CNT) discovered in 1991[170], have been immediately considered as key building element owing to their extremely promising electrical and mechanical properties. The insertion into actual electronics application has been however slow due to the difficulties in quality control in manufacturing and accurate handling by means of large and cost effective processes. More recently in 2004 the first successful isolation of a monoatomic thick aggregate of carbon atoms best known as graphene, has generated an unprecedented convergence of studies especially from the physicist community. Beside extraordinary properties already demonstrated in CNT such as the mechanical strength and

[170] S. Iijima, "Helical microtubules of graphitic carbon," S. Nature 354, 56-58 (1991)

record high thermal conductivity, other unique properties such as the zero bandgap, ambipolar transport and linear dispersion characteristics, along with a planar geometry and process compatibility with CMOS technology make of graphene a truly « wonder material » also in practical electrical engineering applications[171,172,173].

CNTs are 1D carbon allotrope obtained by rolled sheets of graphene to form single or multiple wall cylinders-like geometries. The CNT properties are strongly dependent from size[174], the way they are obtained from rolled sheet of graphene[175] and the number of walls. While single wall (SWCNT) may be conductive or semiconductive depending from the chirality, the multiple wall (MWCNT) type are always conductive. Since they may exist and be manufactured by the same (collective) process, for sake of application their separation is necessary. Most of the experimental studies conducted at LAAS have focused on double wall CNT (DWCNT). This choice was suggested by the peculiar properties of this nanotube to be very close in properties to the SWCNT (conductive or semiconductive depending from chyrality), easily functionalize on the outer shell while preserving the transport properties of the inner one (this is practical in application where they are used in liquid suspensions as for instance to fabricate inks), and finally they are available in large quantity thanks to cost effective fabrication processes [176].

Initial work done at LAAS was essentially on this type of "randomly" distributed CNT (deposed through drop-off, spincoating or inkjet printing). This sort of layer of CNT networks implied a simpler technology and aimed to explore the benefits of the large surface/volume ratio and the high dielectric constant sensitivity to maximize adsorbed gas (used then as sensing principle[177]), or by mixing CNT within a polymer (e.g. BCB) or dielectric (e.g. Silicon Nitride) to introduce loss mechanisms in order to realize electromagnetic shielding material[178], or to synthesize charging immune dielectrics in electrostatically actuated MEMS[179] respectively. An activity on which I was involved directly for the electromagnetic modeling aspects, was the study of carbon interconnects based on inkjet printed CNT network in collaboration with Dr. De Paolis and Dr. Pacchini and reported in the Annex 4.2.7.

For what concerns the studies on "ordered" CNTs (fabrication by external companies through controlled CVD growth on silicon substrate), the aim was to explore possible applications in miniaturization of other basic RF building blocks. For the locally growth aligned CNT this included the investigation of variable tunable NEMS (cantilevers) capacitors[180],

[171] L. Pierantoni, F. Coccetti, P. Russer, (Invited guest editors) "Nanoelectronics: The Paradigm Shift [From the Guest Editors' Desk]" IEEE Microwave Magazine, Vol.11, N°7, December 2010, pp.: 8-10.

[172] L. Pierantoni, F. Coccetti, P. Lugli and S.M. Goodnick (Invited guest editors) "Guest Editorial of the special issue on Radio Frequency Nanoelectronics," IEEE Transaction on Microwave Theory and Technique, Vol.59, N°10, October 2011, pp.: 2566-2567.

[173] T. Palacios, A. Hsu, and H. Wang, "Applications of Graphene Devices in RF Communications," IEEE Communications Magazine • June 2010, pp. 122-128

[174] In particular the diameter controls the bandgap according to $E_g = 4\hbar v_F / 3d$, with $\hbar v_F$ the product between the modified Planck's constant and the Fermi's velocity and which end up being $E_g(eV) \cong 0.9 / d(nm)$

[175] Specified by the chirality or chiral vector which indicated by a pairs of integer number defines the conductive or semi-conductive nature of the CNTs

[176] Flahaut, E.; Bacsa, R.; Peigney, A.; Laurent, Ch.: Gram-scale CCVD synthesis of double-walled carbon nanotube. Chem. Commun., (2003), 1442–1443.

[177] M. Dragoman, K. Grenier, D. Dubuc, L. Bary, and R. Plana, E. Fourn, E. Flahaut, "Millimeter wave carbon nanotube gas sensor," Journal of Applied Physics 101, 106103 2007

[178] S. Pacchini, T. Idda, D. Dubuc, E. Flahaut, K. Grenier, 'Carbon nanotube-based polymer composites for microwave applications', International Microwave Symposium, IMS'08, Atlanta, USA, June 2008.

[179] C. Bordas, K. Grenier, D. Dubuc, E. Flahaut, S. Pacchini, M. Paillard, J-L. Cazaux, «Carbon nanotube based dielectric for enhanced RF MEMS reliability, » IEEE International Microwave Symposium, Honolulu, Hawaii, June 3-8, 2007

[180] T. Ricart, S. Pacchini, D. Dubuc, K. Grenier « Multiphysic modeling and design of carbon nanotubes based variable capacitors for microwave applications, » IEEE European Microwave Week, Amsterdam, Netherlands, October 2008

micromechanical NEMS (carpet type) resonators for filter purposes, or CNT bundle active channel region in FET devices.

These preliminary results (2005-2010) could be considered as a mere proof of concept, since they highlighting quite clearly a number of practical difficulties essentially due to the accuracy in manufacturing, selecting and handling the desired CNTs within a planar photolithographic process platform.

For this and other reasons, which will be given below, the research focus was moved to an emerging carbon based material such as the graphene. Being flat, hence more compatible with conventional planar technologies, and commercial availability[181], it provided a very fertile ground for the investigation of its high frequency capabilities. Noteworthy is that although CNT are derived from graphene and therefore share quite few similarity, most of the electrical properties that characterize this two carbon allotrope are completely different since dimensionality, 1D or 2D, plays a fundamental role. By the same token it is clear that graphene won't replace or dwarf CNT in future applications since they will require the specific properties of the one or the other.

Brief introduction to graphene.

Theoretical existence of graphene is known since the late 40's. Considered (thermodynamically) unstable, as for any other 2D crystal with thickness <20 nm, from theoretical physicist[182]over the past century, it became the central focus of scientific community only in 2004, when researchers at University of Manchester succeeded in isolating first sample of it and published an extensive experimental analysis[183].

Table 3.1: Most remarkable properties of graphene

Parameter	Value	*Comment*
Current density	>10^8 A/cm^2	*100 x higher than best metals*
Thermal conductivity	~5000 W/mK	*2.5 x Diamond*
Young modulus	~1.1 TPa	*10 x Silicon (130 MPa)*
Mobility @300K (on SiO2 / suspended)	~10.000 / ~200.000 $cm^2V^{-1}s^{-1}$	*10 x higher than Silicon*
Mean free path (ballistic transport) (on SiO2 / suspended)	300-400 / ~1000 nm	*10 x higher than Silico*

Ever since this material has became the subject of very advanced studies[184] and the undisputed central topic in applied physics. Just for indication, the annual count for publication on graphene went from few hundreds in 2004 to almost 10 thousand in 2012[185]. In spite of this

[181] « Graphene Industries » Contact : Dr. Peter Blake - First commercial supplier of micro-mechanically cleaved graphene type. www.grapheneindustries.com.

[182] Peierls, R. E. Quelques proprietes typiques des corpses solides. Ann. I. H. Poincare 5, 177–222 (1935) - Landau, L. D. Zur Th eorie der phasenumwandlungen II. Phys. Z. Sowjetunion 11, 26–35 (1937).

[183] K. S. Novoselov, A. K. Geim, S. V. Morozov, D. Jiang, Y. Zhang, S. V. Dubonos, I. V. Grigorieva, and A. A. Firsov, "Electric field effect in atomically thin carbon films," Science, vol. 306, no. 5696, pp. 666–669, Oct. 2004.

[184] A. H. Castro Neto, F. Guinea, N. M. R. Peres, K. S. Novoselov, and A. K. Geim, ''The electronic properties of graphene,'' Rev. Mod. Phys., vol. 81, pp. 109–162, 2009.

[185] Count done on Number of papers published per year and listed in Web of Science the search terms ''graphene'' - Web of Knowledge. [Online]. Available: http://apps.webofknowledge.com

enthusiasm, only more recently graphene has entered the stardom of electrical engineering[186] where an overwhelming >70% of overall scientific work is done in the area of FET transistors[187].

Besides high frequency electronics, which will be developed hereafter, other application include advanced sensors, transparent electronics, low power switch, solar cells and even battery storage.

Why graphene has attracted such a wide and deep interest from fundamental physicists to industrial stakeholders?! The reason resides in the very nature of this material. As matter of fact this is the only material on earth that is a single atom thick (carbon atom thickness 0.3-0.5 nm) made of hexagonal honeycomb lattice of sp^2 hybridized carbon atoms, bonded each other by a covalent bond (distance between atoms 0.142 nm) and one free electron on the hybridized $2p_z$ orbital, which is perpendicular to the lattice plane. The covalent bond between these atoms (similar to diamond) endows graphene with the strongest mechanical properties known (Young's modulus ~1.1 TPa, i.e. 10x than silicon's) while the free electrons on its surface allow record high thermal conductivity (~5000 W/mK, i.e. 2.5x larger than diamond's), record high current density (>10^8 A/cm^2 x10 larger than conventional conductors used in electronics, e.g. copper). The most extraordinary properties of graphene (the main are listed in Table 3.1), regards however its electronic bandgap structure (found by Wallace in 1946)[188]. This exhibits unique properties such as symmetric linear (cone-like) dispersion characteristic with continuity (zero-bandgap) between the valence and conductance bands (which touch each other in a single point called Dirac's point).

Table 3.2: Comparison (not exhaustive) for various Graphene fabrication processes. The numerical value provided here correspond to typical ones given for comparison and reference purposes.

Fabrication Process	Quality (defects contents)	Typical Mobility [cm^2/Vs]	Scalability	Relevance	Comments	Applications
Expholiated	Highest (only few small flakes in random location	>100,000 (on SiO2) >200,000 (suspended)	Low (only few flakes on SiO2/Si wafer)	Fundamental Research	Flake size of few square hundreds μm	Proof of concept (any possible RF and photonic application)
Epitaxy from SiC	Medium (terrace effect and few layers)	< 5000	Medium	Industrial CMOS compatible	>1000 °C wafer level process, Difficult to remove from substrate, high cost of SiC	High end FET
CVD	Medium (few layer)	<10000	High	Industrial CMOS compatible	Deposition at 700-1000°C on large surface (>30 inches) Easy transfer to host substrate	High end FET, transparent electrode (touch screens)
Solution based Processing	Low	< 100	Very high (Inkjet or roll-to-roll transfer)	Industrial low cost	RT	Large scale flexible electronics

As consequence of these features this material allows ambipolar (electron and hole) transport and massless particles propagation. Electrons effective mass going to zero in the proximity of the Dirac point means that electrons behave like photons (obeying to relativistic transport law described by Dirac's equation -1929), and travel at so called Fermi's velocity $c_0/300 = 10^6$ m/s. These transport characteristics translate in record mobility (in excess of 200,000 cm^2/Vs

[186] P. Avouris, ''Graphene: Electronic and photonic properties and devices,'' Nano Lett., vol. 10, pp. 4285–4294, 2010.

[187] F. Schwierz, ''Graphene Transistors: Status prospects and problems'' in Proceedings of the IEEE Vol. 001, No. 7, July 2013, pp. 1567-1584

[188] P.R. Wallace, "The band theory of graphite, " Phys. Rev. 71, 622–634 (1947).

@T=5K[184] and in excess of 100,000cm^2/Vs@240K[189] in suspended graphene), record high mean free path (between 300-400nm@300K i.e. 10x silicon's, up and above 1µm for intrinsic suspended and in vacuum), and finally an extraordinary high saturation velocity (of $\approx 5\ 10^7$ cm/s which means 10x Silicon's, 2x GaAs's). To complete the list of "superior" features, the extremely thin thickness allows unprecedented electrostatic confinement (useful to realize active device and sensor) and endows graphene of extreme flexibility (25% elastic stretchability) and optical transparency (2-3% loss in transmittance per atom layer).

All these features are of course theoretical or extrapolated in ideal conditions. In the reality the very same characteristics, which make graphene the "wonder material", are also responsible of major practical limitations. In the real world, where the material needs first to be manufactured, patterned and eventually connected with the surrounding electronics or devices, many things can go wrong. Going in order, the manufacturing of graphene can be done according to different techniques, which include micromechanical cleavage (or exfoliation) of bulk graphite, chemical vapor deposition (CVD) on catalyst metals, epitaxial growth from SiC wafers, and finally solution based on graphene flake suspension used for selective transfer (e.g. inkjet). The detailed description of these techniques goes beyond the purpose of the present manuscript but plenty can be found in lieterature[168]. Here for sake of synthesis in the following table (Table 3.2) only a classification based of the typical fabrication outcomes are listed.

Although graphene electric features make it an excellent candidate for fast (owing to high mobility and high saturation velocity) and efficient (low losses due to ballistic transport) analog electronic, its use in digital electronics is strongly hampered by the lack of band gap. The zero bandgap and the lack of current saturation and pinch-off (graphene transistors do not switch off) make this material very unsuitable for digital electronics where high ON/OFF current ratio is at stake. Many attempt based on graphene nanoribbon (GNR), graphene bilayer, graphene barristors, …., have been made to curb this problem. In spite of this, present solutions are limited in ON/OFF current ratio (typical value 10^5, falls short from standard CMOS electronics which reach 10^6). As already mentioned for this specific applications (digital electronics) graphene is being gradually abandoned at the benefit of new emerging 2D semiconducting crystal such as molybdenum disolphite[169].

On the contrary, high motilities, high saturation velocity and long mean free patch means ballistic electronics e.g. high speed and high efficiency or low energy (thermal) losses, and represent the actual "wonder *high frequency* material".

3.2 Ballistic electronics (Short-to-Medium term Research outlook)

Exploring ballistic transport to introduce new functionalities and enhanced speed and energy efficiency. The way toward future THz electronics?

Progresses in nanolithography[190] have recently enabled the fabrication structures with dimension smaller than the electron mean free path at room temperature. In devices based on these structures the carrier can travel unimpeded (without scattering or transfer of energy) offering by this way a unique combination of high-speed and low-power loss performances[191].

[189] K. Bolotin et al., "Ultrahigh Electron Mobility in Suspended Graphene," Solid State Commun., vol. 146, June 2008, pp. 351–55.

[190] Nanolithography is the branch of nanotechnology concerned with the study and application of fabricating nanometer-scale structures, meaning patterns with at least one lateral dimension between the size of an individual atom and approximately 100 nm.

[191] S. Datta, "Electronic Transport in Mesoscopic Systems," Cambridge University Press - Cambridge Studies in Semiconductor Physics and Microelectronic Engineering, 1995.

Electric transport in this nanoscale presents completely different behavior with respect to its macroscopic bulk counterpart. In these latter, the electric transport is dominated by diffusive transport, described by empirical relations such as the Ohm's law (1825) in conductive media, or the Fik's law (or law of diffusion - 1855), for semiconductors.

On the contrary the former, are characterized by and overall structure/device dimension *L* (through which the carriers flow), with is comparable or smaller than the carrier mean free path (often called λ knowing that its value is function of the carrier energy E, hence λ = λ(E)[192]). In this case any reduction below these size features implies a higher probability that this transit, through the entire structure/device, will take place without any collision hence loss of energy. This kind of transport is called ballistic transport.

In 1988 a group of researcher from Philips, TU Delft, and University of Surrey made a sensational experimental by practically measuring the resistance associated ballistic conductors[193]. In this experiment the device was made of a two-dimensional electron gas (2DEG GaAs-AlGaAs heterostructure). The width *w* of the channel was controlled between 0 and 360 nm by biasing the gate on top of the heterostructure (Figure 3.2a).

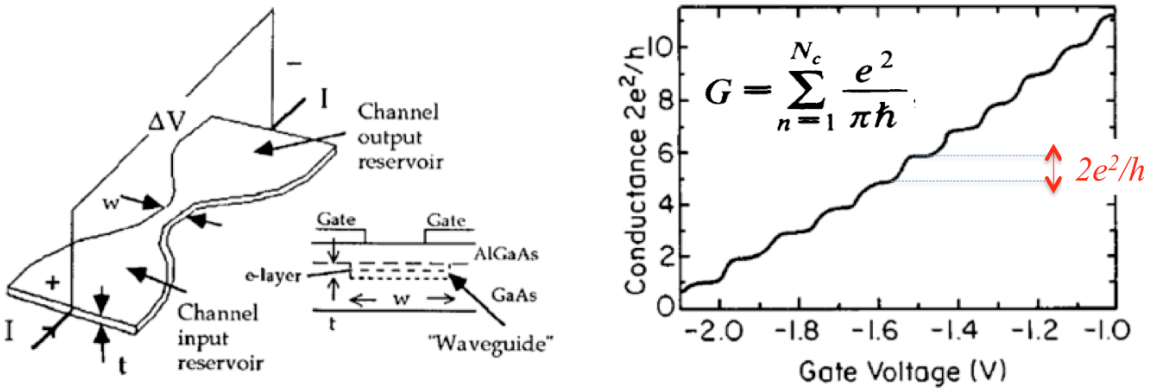

a) b)

Figure 3.2 [Source: B.J. van Wees – 1988][193]: (a) View of the experimental test structures used for the ballistic transport investigation. (b) Measured conductance as function of the gate voltage, hence of the width. Conductance shows plateau at integer multiple of e^2/h (corresponding to as many value of gate voltage).

A number of very fascinating considerations arose from this experiment.

- First of all, contrarily to the macroscopic case (Ohm's law) results showed that although the channel width varies continuously, the **conductance changes in discrete steps**, each of fixed height (e^2/h =38.7 *mS*). This can be equivalently seen by the inverse quantity h/e^2 =25.8 *KΩ* as ***the resistance quantum***.
- Second, again contrarily to the macroscopic case, this value of **conductance is independent from the length** of the channel.

These results represent very exciting and fascinating findings since they clearly reveal the evidence of conduction modes, occurring into nanoscale confined structure/devices, in all similar to what happens in electromagnetic waves propagating in waveguides.

For the explanation of this phenomenon some notion of quantum physics is necessary. Based on the quantum physics electrons can be described by wave functions, which measure the probability of these electrons to exist in a given part of the space. Be λ_B the wavelength associated to the electron ($\lambda_B = h/p$ with p electron momentum is known as the De Brogli

[192] The wavelength of an electron (mass = 9.11 x 10^{-31} kg) traveling at 5.31 x 10^6 m/s hence kinetic energy $E_K = (1/2)mv^2$ → $\lambda_B = h/\sqrt{(2E_K m)} = 1.37 \times 10^{-10}$ m.

[193] B.J. van Wees, H. van Houten, C. W. J. Beenakker, J. G. Williamson, L. P. Kouwenhoven, D. van der Marel, C. T. Foxon, "Quantized Conductance of Point Contacts in a Two-Dimensional Electron Gas," Physics review Letter, 60, 848.

wavelenth - 1829)[194], then for a given conductor of width *W* the structure behaves as an electron waveguide where the role of frequency is assumed by the energy so that increasing the energy of these electron a discrete number of modes become propagative. Or equivalently, for a fixed value of energy, by increasing the width *w* the number of propagating modes increases.

The relation which needs to be satisfied in order to obtain the number of propagating modes is:

$$M(E) = \frac{W}{\lambda_B(E)/2}$$

with $E = \hbar^2 k_y^2 / 2m^*$ energy of the electron (m^* its effective mass)

and $\psi(x,y) \propto e^{i(k_x x)} \sin(k_y y)$ is the electron wave function

with $k_y = m\pi / W$ for m=1,2, …

The transversal propagation constant of the electron "plane wave" [195].

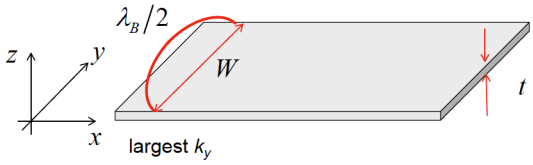

Figure 3.3: [Source: NanoHub][195] Nanometer wide conductor as an electron waveguide.

It is evident that when the width of the conductor becomes much larger than the electron wavelength $w >> \lambda_B$ then there are an infinity of propagating modes and the resulting conductance converge to the conventional continuous relation of Ohm's law.

Noteworthy is that based on the wave nature of electrons, various electron waveguide devices such as the directional coupler[196], the quantum stub transistor[197], and the electron **Y** - branch switch (YBS)[198], have been proposed and analyzed. The YBS in particular, has been considered a candidate for future low-power, high-speed electronics[199].

An interesting proposal is to use the YBS as a THz oscillator operating in the nonlinear response regime. This proposal was made based on a self-gating mechanism[200]. However, experiments motivated by the proposal have shown no clear sign of the self-gating effect, but strong nonlinear behavior instead[201]. Owing to these features and other interesting phenomena associated to the ballistic transport, the three branch junction has become a focus in our research activity and will be described later on in this chapter.

The Wees et al. findings showed above agreed perfectly with the more general formulation of electric transport, introduced with the Landauer's equation of conductivity (1957)[202].

This equation predicts the conductance of 1D, 2D and 3D conductors as the contribution of 3 terms involving the nature of the transport (whether ballistic or diffusive), the number of propagation modes and the gradient of the occupation level (better described below) and can be written as follows:

---

[194] M. Alonso and E.J. Finn, «Fundamental University Physics Volume III Quantum and Statistical Physics » Addison-Wesley Publising Comapany Inc 1968.

[195] Source: Lecture on "Near-Equilibrium Transport: Fundamentals and Applications" from Prof. M. Lundstrom, Perdu University Available under NanoHub (http://nanohub.org/resources/11763)

[196] J. A. del Alamo and C. C. Eugster, Appl. Phys. Lett. 56, 78 (1990)

[197] F. Sols, M. Macucci, U. Ravaioli, and K. Hess, J. Appl. Phys. 66, 3892 (1989).

[198] T. Palm and L. Thylen, « Analysis of an electron-wave Y-branch switch, » Appl. Phys. Lett. 60, 237 (1992).

[199] T. Palm and L. Thyle´n, J. Appl. Phys. 79, 8076 (1996).

[200] J.-O. J. Wesstro¨m, Phys. Rev. Lett. 82, 2564 (1999)

[201] L. Worschech, H. Q. Xu, A. Forchel, and L. Samuelson, (unpublished) NOTE: Around the year 2000 a research group led by L. Samuelson at Lund University has observed the effects predicted in this paper in various small TBJs made from InGaAs quantum well materials. The group has also observed the effects at room temperature and has built a frequency doubler with the effects.

[202] R. Landauer, IBM J. Res. Dev. 1, 223 (1957); R. Landauer, Phys. Lett. 85A, 91 (1981)

$$G = \frac{2q}{h}\int T(E)\,M(E)\left(-\frac{\partial f_0}{\partial E}\right)dE$$ Landauer's Equation of Conductivity

where q is the charge of the electron (1.60×10^{-19} C), h is the Planck's constant (6.62×10^{-34} m^2kg/s) and the three terms are respectively[195]:

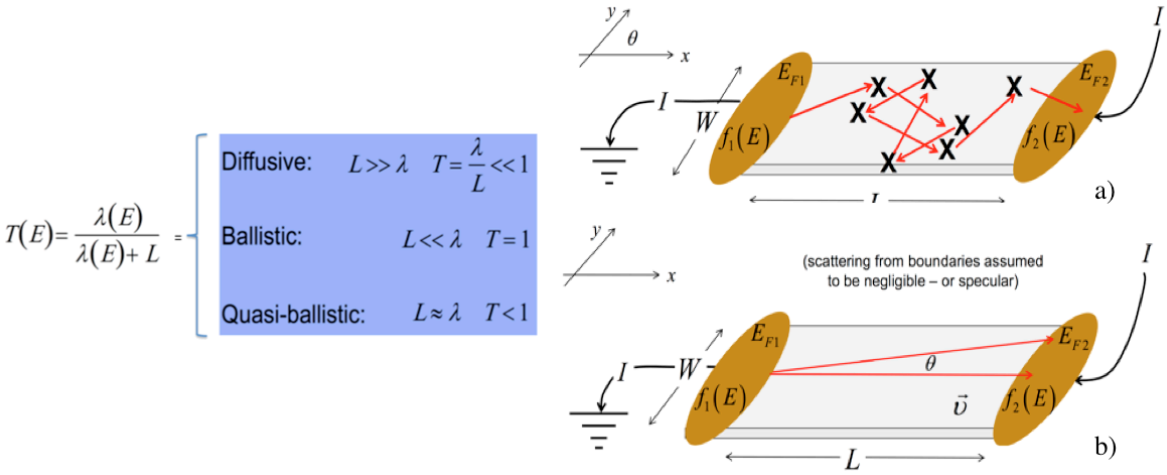

Figure 3.4 : [Source: NanoHub][195] Schematic view of the different transport: a) diffusive and b) ballistic.

T(E) is the transmission coefficient (or the **probability** that an electron injected in the contact 1 reaches contact 2) in the two possible transport mechanisms, diffusive (e.g. propagation taking place through sequence of collisions with scattering centers), or ballistics (e.g. the propagation of the carrier takes place without any collision between the two contacts). This probability goes from 1 to 0 and decreases down as much as the channel length L dominate the mean free path (λ).

$$M(E) = \begin{cases} M_{1D}(E) = \frac{h}{4}\langle \upsilon_x^+ \rangle D_{1D}(E) \\ M_{2D}(E)W = W\frac{h}{4}\langle \upsilon_x^+ \rangle D_{2D}(E) \\ M_{3D}(E)A = A\frac{h}{4}\langle \upsilon_x^+ \rangle D_{3D}(E) \end{cases}$$

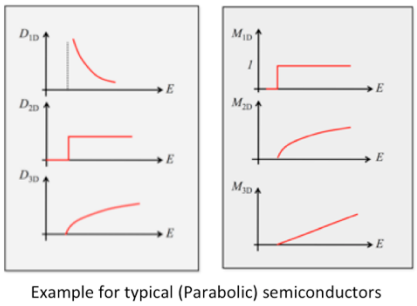

Figure 3.5: [Source: NanoHub][195] Density of states and conduction modes for typical (Si, Ge, called also parabolic) for the 1D, 2D, and 3D semiconductors.

The second term is *M(E)* which represents the number of conduction channels at energy E. M depends from dimensionality (1D, 2D, and 3D), the average velocity $\langle v^x_+ \rangle = 2v(E)/\pi$ and the density of states (which also depends from dimensionality as indicated in the figure above).

The last term of the Landaur 's equation finally is the derivative of the Fermi-Dirac distribution:

$$f_0(E) = \frac{1}{1+e^{(E-E_F)/k_BT_L}}$$

For T→0 $$\left(-\frac{\partial f_0}{\partial E}\right) \approx \delta(E_F)$$

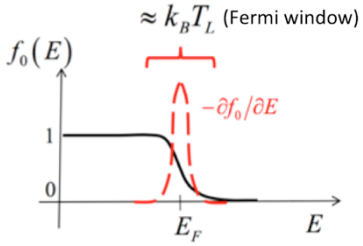

Figure 3.6: [Source: NanoHub][195]Example of Fermi-Dirac distribution for a given temperature (T > 0 K). The Fermi window, where the derivative function is not zero, is indicated.

which for $T \rightarrow 0$ becomes a step function and hence its derivative (contained in the Landauer's equation) becomes a delta functions. The meaning of this term is that the current may flow only if there is a gradient in the occupation levels (or Fermi-Dirac distribution).

In this case the original Landauer's equation becomes the following:

$$G = \frac{2q}{h}\int T(E)\,M(E)\left(-\frac{\partial f_0}{\partial E}\right)dE \xrightarrow{T\longrightarrow 0K} \frac{2q}{h}T(E_F)\,M(E_F)$$

which for T=1 (ballistic transport), is exactly verified in the 1988 Wees et al. experiments presented above (see Figure 3.2b).

Hence, due to the unimpeded propagation and low energetic losses ballistic transport is extremely promising for a variety of applications.

Owing to its record long mean free path even at room temperature, graphene is perfectly suited to open a number of application opportunities.

Much interest is associated with this material and its application in active devices. Besides the technological challenges, several questions remain open about how to model ballistic devices/structures.

Preliminary investigation of this devices were carried out at LAAS within the PhD thesis of G. Vincenzi[203] which essentially focuses on the one hand on the extension of ballistic DC transport into the diffusive limit and on the other on the microwave propagation in graphene and through graphene-metal transitions. **The focus on microwave was the original aspect of our research direction back in 2010, since most of the interest worldwide was rather devoted to the DC and the optical properties**, and information about microwave behavior of graphene were scarce.

Hence the reasoning behind these activities developed at LAAS was to apply the electrical high frequency engineering approach to the study of nanoscale phenomena and structures by extending the validity of lumped element model and computational electromagnetic tools. This implied to bridge the gap between nanoscale phenomena (e.g. ballistic transport) and the larger scale (e.g. diffusive propagation) with conventional analytical and numerical high frequency modeling tools.

In a work done at LAAS a model that can correctly predict both ballistic as well as diffusive transport and thus describe a large range of graphene FET devices has been presented and

[203] Bourse contrat doctorale du Ministère de la recherche et de l'Industrie sur thématiques prioritaires – Septembre 2010 – Aout 2013

validated[204]. It is based upon a simplified lumped element electrostatic model (called « Top-of-the-barrier" model[205]) introduced earlier for graphene nanotransistors but uniquely used in their ballistic limit[206], it was originally extended to the diffusive nature of transport on longer channels, without altering its simplicity. The original contribution has been to introduce a factor T, in all similar to the transmission probability used in the Landauer equations, indicating the number of transmitted and reflected (1-T) carriers, and to use it to cast a modified value of drain barrier potential from which to compute the Fermi pseudo-potential use in the Landauer's equation.

The model retains the simplicity of a lumped element approach and is able to correctly describe the I-V characteristics of both ballistic and diffusive devices, and was validated by describing the behavior of two different graphene FETs of 15 nm and 3μm channel length.

At LAAS the studies on FET have been limited to these work as the focus was rather on alternative concepts, such to explore the exciting potentialities of ballistic transport. In the following section an example of ballistic electronic device based on the so-called three terminal junctions will be discussed and introduced. Differently from FET these devices present intrinsic non-linearity residing in the very nature of the ballistic transport. **Owing to the zero or low scattering of this transport this non-linearity is virtually unlimited in frequency, hence can be exploited for a variety of functions, one above all, the zero-bias and the very large band (theoretically from DC up to the THz) detection**.

3.2.1 Graphene Three terminal Junctions

Since the early 90's three terminal junctions combined with concept of ballistic transport and electron waveguides have attracted considerable interest[207].

The T- branch junction (TBJ) called also Three Terminal Junction (TTJ), is a three terminal device with a T shaped conductive area typically implemented by a 2-dimentional electron gas (2DEG) realized in III-V technology[208].

Owing to its strong non linear input-output transfer function and its simple design TBJs are considered as promising candidates to implement low loss and fast nanoelectric devices[209], as for instance NAND and NOR gate[210,211].

Several theoretical works have been done trying to explain the non-linear transport mechanisms observed in TBJs. They include quantum mechanical scattering effects[212], the Landauer-Büttikker formalism[213], and ballistic transport, however a consistent interpretation is still missing.

Commonly TBJs are measured in a push-pull (pp) fashion (see Figure 3.7), meaning that the voltage with identical amplitude and opposite sign are applied to the left and right branches (V_L=-V_R=V_0, see Figure 3.7a) while, the central branch voltage V_C is measured keeping zero

[204] G. Vincenzi, G. Deligeorgis, F. Coccetti, M. Dragoman, L. Pierantoni, D. Mencarelli, R.Plana, "Extending ballistic graphene FET lumped element models to diffusive," Solid State Electronics, Vol.76, October 2012, pp.8-12

[205] A. Rahman, S. Datta, M. Lundstrom, Theory of ballistic nanotransistors, IEEE Transactions on Electron Devices 50 (2003) 1853-1864.

[206] G. Liang, N. Neophytou, D. E. Nikonov, M. S. Lundstrom, Performance Projections for Ballistic Graphene Nanoribbon Field-Effect Transistors, IEEE Transactions on Electron Devices 54 (2007) 677-682.

[207] H. Irie, Q. Diduck, M. Margala, R. Sobolewski, and M. J. Feldman, « Nonlinear characteristics of T-branch junctions: Transition from ballistic to diffusive regime, »Appl. Phys. Lett. 93, 53502 (2008).

[208] I. Iñiguez-de-la-Torre, J. Mateos, T. González, D. Pardo, J. S. Galloo, S. Bollaert, Y. Roelens, and A. Cappy, "Ballistic nano-devices for high frequency applications," Semicond. Sci. Technol. 22, 663 (2007).

[209] H. Q. Xu, "Electrical properties of three-terminal ballistic junctions," Appl. Phys. Lett. 78, 2064 (2001).

[210] H. Q. Xu, I. Shorubalko, D. Wallin, I. Maximov, P. Omling, L. Samuueson, and W. Seifert, "Novel Nanoelectronic Triodes and Logic Devices With TBJs," IEEE Electron Device Lett. 25, 164 (2004).

[211] C. R. Müller, L. Worschech, P. Höpfner, S. Höfling, and A. Forchel, "Monolithically Integrated Logic NOR Gate Based on GaAs/AlGaAs Three-Terminal Junctions," IEEE Electron Device Lett. 28, 859 (2007).

[212] D. Csontos and H. Q. Xu, "Quantum effects in the transport properties of nanoelectronic three-terminal Y-junction devices," Phys. Rev. B 67, 235322 (2003).

[213] A. N. Jordan and M. Büttiker, "Gap theory of rectification in ballistic three-terminal conductors," Phys. Rev. B 77, 075334 (2008).

current on it (open circuit). Another possible measurement scheme is called push-fixed (pf) and consists in applying the voltage to only one lateral branch and grounding the other one ($V_L=0$ $V_R=2V_0$, see Figure 3.7b). One of the first groups to demonstrate these results on graphene TBJs, has been the one led by F. Schwierz et al Univ. Ilmenau Germany [214].

Their measurements results on epitaxial graphene TBJs show that in both modes a clear voltage rectification[215] at room temperature takes place (see Figure 3.7c). Results for the best rectification efficiency plotted for the central branch voltage and its first derivative with respect to the bias voltage, i.e., dVC /dV0 , versus V0 clearly show two working regimes, a nearly quadratic behavior for abs(V0) < 1V and a linear region for abs(V0) > 1V (see Figure 3.7d). Similar characteristics have been reported for III-V TBJs[207].

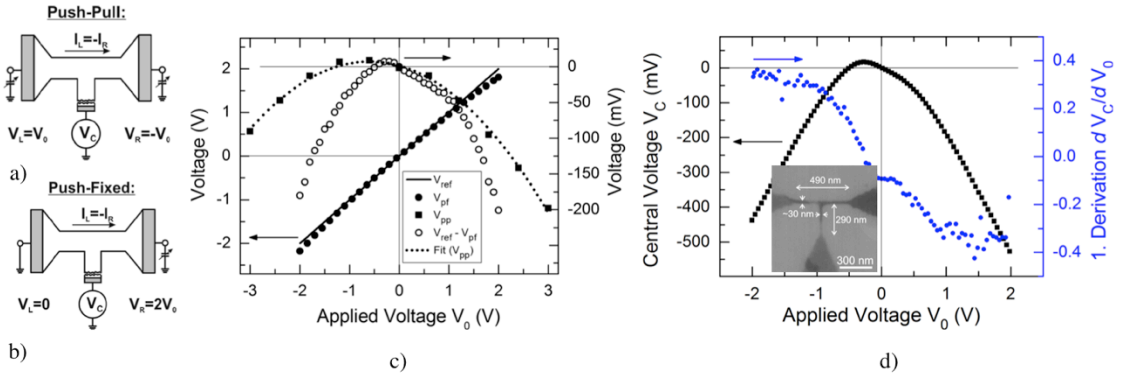

Figure 3.7 [Source: . Göckeritz et al., APL 2011][214]: Electrical characterization principle scheme of TBJs in (a) push-pull and (b) push-fixed; (c) Central branch voltages in pp and pf modes versus bias voltage V0 for the TBJ, along with the reference voltage and a quadratic fit. Note that to compare both modes, the central branch voltage of the push-fixed mode has to be subtracted from a reference voltage. To this end, the central branch voltage, V0 is used as reference. (d) Central branch (output) voltage and first derivative dVC/dV0 versus applied bias voltage for the device with the highest rectification efficiency.

The physical origin of the first regime is related ballistic transport (while the latter is attributed to intervalley scattering).

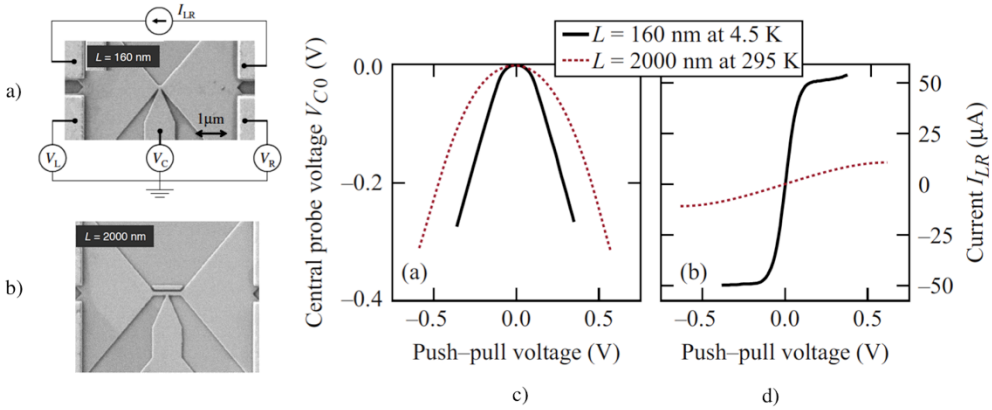

Figure 3.8 [Source: H. Iri et al., APL 2008] [207]: SEM images of TBJ devices with different nanochannel lengths a) 160nm measured at 4.5K (mostly ballistic transport) and b) 2000nm measured at room temperature (mostly diffusive). © The central probe voltage and (d) the device current vs the push-pull bias voltage for the two cases: mostly ballistic (solid line) and mostly diffusive (dashed line) modes of the TBJ operation.

[214] R. Göckeritz, J. Pezoldt, and F. Schwierz, "Epitaxial graphene three-terminal junctions," Appl. Phys. Lett. 99, 173111 (2011)

[215] The rectification efficiency calculated for the best device, as r = V_C/V_0 was 22% at V_0=1V.

This concept was earlier proved at the University of Rochester by H. Irie by using a III-V TBJ structure (see Figure 3.8)[207]. This latter was studied for different lengths of channel (Figure 3.8a and b) and measured in conditions such to enforce the ballistic and the diffusive operation modes. Results, reproduced in Figure 3.8a and b for the central voltage V_{C0} (defined as $V_{C0}=V_C-V_r$, with $V_r=(V_L+V_R)/2$, is the virtual zero reference potential) and crossing current I_{LR} vs input pp voltage ($V_{pp}= (V_R-V_L-I_{LR}R_{access}$, where the R access term allows to remove the drop on the access ports) respectively, show that a clear enhancement of the non linearity is observed in the former one.

For the low V_{pp} regime, the $V_{C0}(V_{pp})$ can be fitted by the following relation:

$$V_{C0} = -\frac{\alpha}{2}|V_{pp}|^2$$

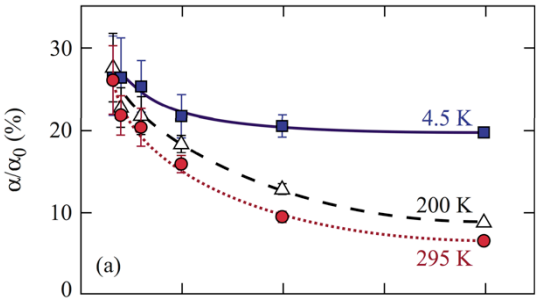

Figure 3.9 [Source: H. Iri et al., APL 2008] [207]: The channel-length dependence of α / α_0 the ballisticity factor α / α_0 where α_0 is the value of α_0 extracted from ideal ballistic condition at T=0K and found to be $\alpha_0=25\ V^{-1}$ for the given III-V device

Where α is a fitting parameter that represents the curvature and can be extracted from the derivative of the curves in Figure 3.8c) as the value of the slope in the vicinity of the origin. The **quadratic behavior $V_{C0}(V_{pp})$ suggests that the non linear ballistic effect is responsible for the electron transport in this regime**. The latter conclusion is supported by the fact that the value of α becomes closer to zero as the channel becomes more diffusive (Figure 3.9).

3.2.2 YBJ Ballistic rectifier

At LAAS the focus was in particular on a particular kind of TBJ ballistic devices where the Y-junction instead of a T's was used. YBTs have been studied in past as electron wave guide for low power high speed electronics[216].

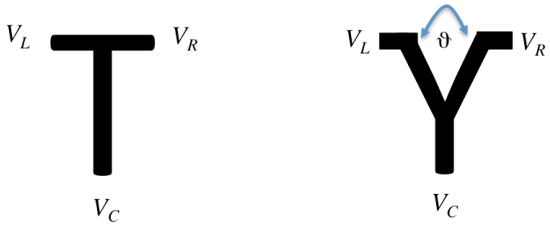

Figure 3.10: T- and Y- three terminal Junctions

The ballistic rectifier represents an example of such devices and addresses in particular the opportunity to have zero bias high speed devices capable to bridge the THz gap (where the lack of sources and detectors is apparent).

[216] T. Palm, L. Thylén, « Analysis of an electron-wave Y-branch switch Appl. Phys. Lett. 60, 237 (1992)

The ballistic rectifier exploits the fact that the electron travels straight until reaching a geometrical border where it undergoes a specular reflection. The rectification of electron flow is carried out by a downward deflection at the triangular barrier. Based on this principle the aforementioned group at the University of Rochester proposed the ballistic deflection transistor (BDT) [217] shown in Figure 3.11. BDT has the same geometry as the ballistic rectifier (Figure 3.11b) except for two additional gates on both sides of an electron injection channel. Depending on the direction of the electric field created between the gate electrodes, the gates actively switch the path of electron flow to either right or left drains. The very same principle of ballistic transport and geometrical scattering propagation is responsible for the detection principle called Ratched effect occurring in a 2DEG surface patterned with a matrix of asymmetric antidots. Exposed to an impinging electromagnetic plane wave this latter yields an asymmetric charge accumulation at the extreme of the surface, hence producing a detected signal[218,219].

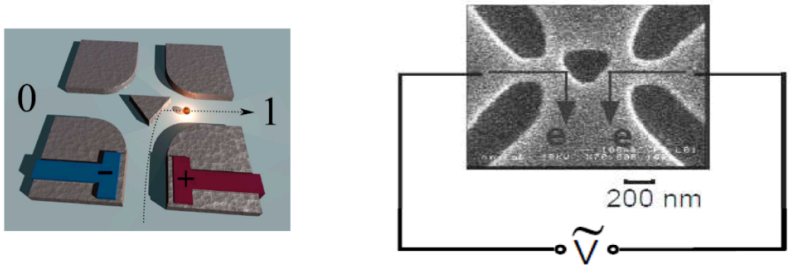

a) b)

Figure 3.11 [Source: D. Diduck IMS 2006][217]: Examples of ballistic devices: (b) ballistic deflection transistor (BDT) (c) ballistic rectifier

Monte Carlo based simulations of ballistic devices done by University of Salamanca and IEMN, have been able to demonstrate that this simple working principle, may work up to the **unprecedented high-frequencies** of 1 THz, with low power consumption, consequence of the ballistic electron transport[220].

The same studies clearly highlighted the difference between T- and Y- junctions. The decrease of the opposite branches angle (ϑ) from the 180 value of the TBJ to lower values, enhances the injection of carriers into the central branch hence the negative values of V_C and as consequence of α (rectification efficiency) (see Figure 3.12a).

Always using III-V heterogeneous junctions technology, the same group has experimentally demonstrated TBJ rectifying effects up to 94 GHz at room temperature[208]. Although THz frequency performance has been demonstrated by Monte Carlo simulation (Figure 3.12b,c), the high impedance of the nano-device combined with the parasitic capacitances is a limiting factor.

At LAAS the activity on ballistic rectifier has focused on the novelty to use (exfoliated) graphene combined with RF CPW technology, and the use of an YBJ-array in (parallel) shunt

[217] Q. Diduck, M. Margala, and M. J. Feldman, "A terahertz transistor based on geometrical deflection of ballistic current"in Microwave Symposium Digest, 2006. IEEE MTT-S International (2006), p. 345.

[218] A. D. Chepelianskii, M. V. Entin, L. I. Magarill, and D. L. Shepelyansky, "Ratchet transport of interacting particles," Phys. Rev. 5, vol. 78, no. 4, pp. 11271 -11278, Oct. 2008,

[219] D. Medhat, A. Takacs, H. Aubert, J.-C. Portal , "Comparative Analysis of Different Techniques for Controlling Ratchet Effect in a Periodic Array of Asymmetric Antidots" , in Proc. of Asia-Pacific Microwave Conference (APMC'2009) , Singapore, 7-10 Dec 2009, pp. 1711 – 1714.

[220] J. Mateos, B. G. Vasallo, D. Pardo, T. Gon´zalez, J.-S. Galloo, S. Bollaert, Y.Roelens, and A. Cappy, "Microscopic modeling of nonlinear transport in ballistic nanodevices," IEEE Trans. Electron Dev., 50, 1897, (2003).

configuration such to **exploit collectively the single YBJ non-linearity and alleviate the aforementioned high impedance limitation**.

TBJ based on exfoliated graphene have been already demonstrated at ETH Zurich[221], where the interest was on rectification efficiency tuning by means of a gate potential, rather than on RF performances.

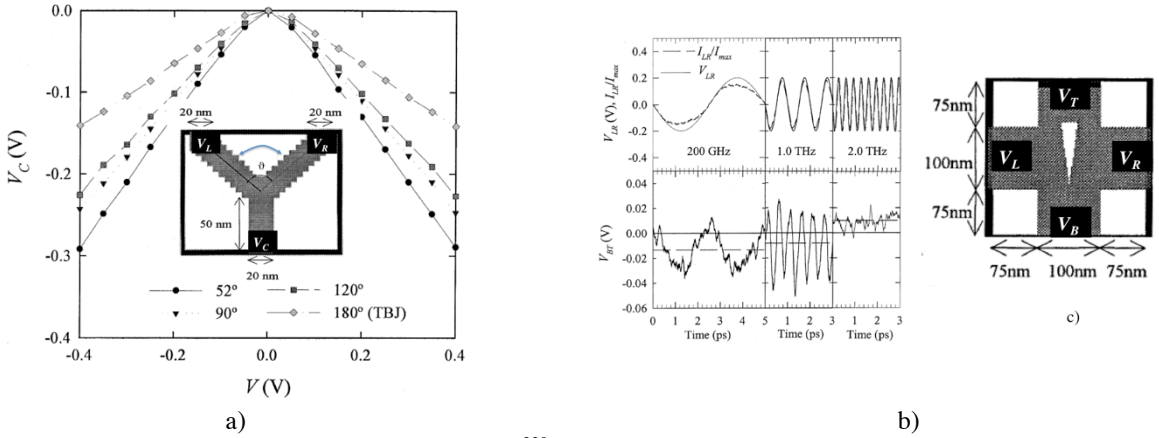

Figure 3.12 [Source: J.Mateos etal., TED 2003][220]: Montecarlo simulation of Y- junctions : a) V_C as a function of the biasing ($V = V_L = -V_R$) and different opening angles. The YBJ (depicted in the inset) has the following characteristics: 20-nm-wide and 50-nm-long branches with active area doping of $0.1x10^{12}$ cm^{-2}. b) V_{BT} response to periodic signals with amplitude of 0.2 V and frequencies of 200 GHz, 1 THz, and 2 THz applied to V (potential difference between left ad right electrodes) in the ballistic rectifier depicted in c).

The ballistic detector developed at LAAS (by G. Deligeorgis), is based upon a (2/250nm Cr/Au) CPW transmission line structure realized on a *$Si0_2$/HR Silicon 0.3/500μm*. The CPW slots are taped down to 2μm, a compromise between the accuracy of the optical lithography used to fabricate the device and the mean free path within which a ballistic transport occurs. The graphene YBJs are patterned within each CPW slot. Their size and number represent two design parameters, which can be used to optimize the device. For the first prototype, 50 identical YBJs are e-beam patterned on each of the two CPW slots. The width of these Y-shape graphene flakes is between 300nm, and it represents a trade off, such to reduce edge scattering (if too narrow), and to minimize drift transport (if too large). An angle below 90° and an overall length of the three branches such to fit in the 2μm wide slots complete the graphene flakes design. The CPW ground electrodes are continuous between the two ports, while the central signal line is interrupted in order to disconnect the RF input signal from the output's. The YBJs are positioned in the CPW slots such that the transversal branches are electrically connected with the ground and the signal line respectively. This configuration allows them to be exposed to the transversal RF field or equivalently to a push-pull electric signal as indicated above (Figure 3.7). Each of the YBJ's central branch (aligned along the longitudinal direction of the CPW) is contacted by an U-shaped collector electrode, which eventually leads to the output port. After the graphene flakes this collector is the second very important part of the device since it ensures the electrical contact between each YBJs and the output, while at the same time, should minimize the interference with the electric field. In order to this, the U-collector part is realized by a tiny (600nm wide, 300nm thick) gold airbridges (300nm high airgap) as shown in the inset of Figure 3.13).

The parallel connection of the YBJs through the U-shape airbridge collector is supposed to enhance the detection by collectively gathering the contribution on each junction. In fact for what explained earlier, each YBJ behaves as a strong non linearity.

[221] A. Jacobsen, I. Shorubalko, L. Maag, U. Sennhauser, and K. Ensslin, « Rectification in three-terminal graphene junctions,"Appl. Phys. Lett. 97, 32110 (2010).

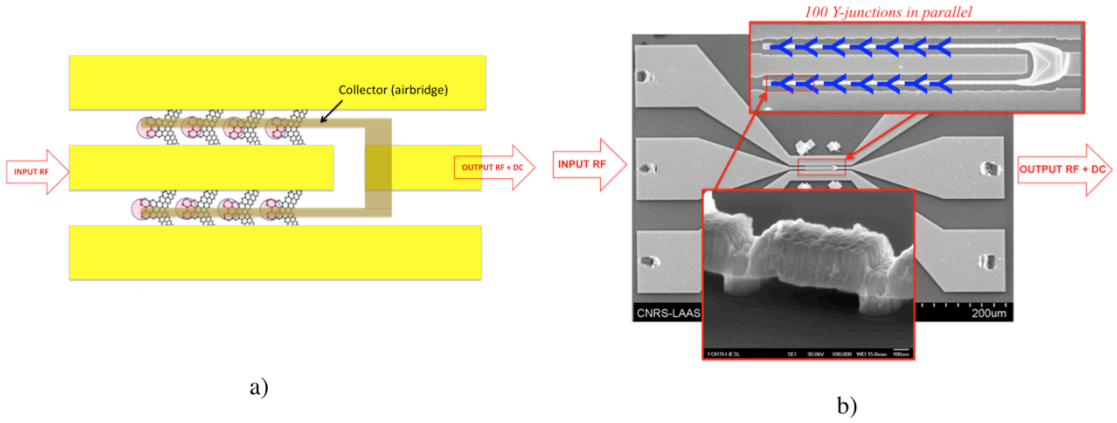

Figure 3.13: View of LAAS ballistic detector : a) principle schematic view of the detector ; b) Top view of the entire structure showing the CPW tapering from the GSG probe contact area, the active area with the simplified view of the YBJs disposition (top inset)

The measurements of this structure were performed on a GSG probe station at room temperature (23-25°C) and ambient conditions (35-45% RH). The device input was connected to a CW source generator (Agilent 8257D) while the output a spectrum analyzer (R&S FSU) was connected to a digital multimeter (Keithley DMM4200), through a T-bias in order to to separate the RF from the DC contribution. The input power on DUT (after deembedding of input access losses) was swept between -40 and 0 dBm, while the frequency span was set from 50 MHz to 50 GHz.

Since no specific cleaning treatment was carried out on the device (no thermal nor current annealing nor post-processing treatment), possible pollution and adsorbed humidity could have affected the device overall performance. These effect need to be better addressed.

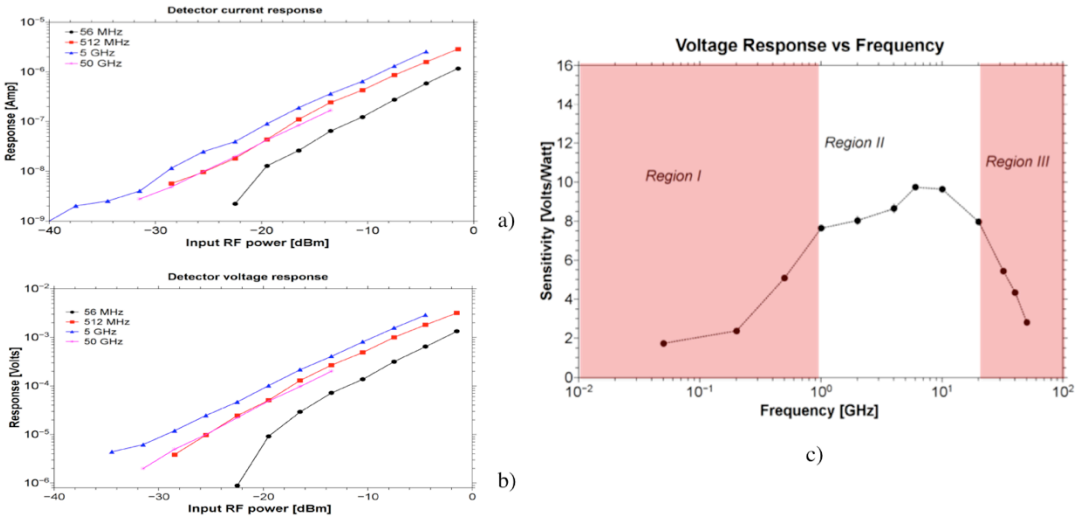

Figure 3.14: Experimental results of LAAS ballistic detector : a) short circuit current and (b) open circuit voltage response at different value of frequency and as a function of input power ; c) Sensitivity as a function of input frequency. A maximum that corresponds to 10Volts/Watt was measured for 10 GHz and a drop below 20% of this value was observed below 1 GHz and above 20 GHz.

The measured current and voltage response of the device is shown in a log-log plot for four different frequencies (Figure 3.14a,b)). From the slope in the log-log plot a quite obvious linear response can be observed for an input CW power level range which covers four orders of magnitude. This is verified for all measured frequencies. Plotting the data shown in (Figure

3.14a,b) in a linear plot (response as a function of the input power), the sensitivity of the device can be calculated. A response as high as 10Volts/Watt (@10 GHz) was obtained.

As explained earlier this very interesting response is likely attributed to the ballistic transport of carriers in the junction. In fact carriers forced to move by the transversal electric field present in the CPW slots are accelerated towards the YBJ where they will either pass through scattering and drift diffusion toward the opposite branch or proceed without scattering and end up in the bottom branch, where they may be collected by the output electrode. This process does not depend from the sign of the field so that a rectification effect is developed. Such explanation is supported by the fact that the size of the YBJ core is similar or smaller than the mean-free-path measured in graphene monolayers (1μm @RT). To accurately evaluate the frequency response of the device, the response of the detector (sensitivity) was extracted for several frequency values and is reported in Figure 3.14c). The graph shows a central region (region II) between 1-20 GHz where the response is almost flat around 8-10 V/W, while it drops below 20% of this value outside this range (region I and III).

The device is operating efficiently as a detector exhibiting a linear response as high as 10 V/W over a large dynamic range and is able to detect signals at least as low as -40dBm (100 nW).

Even though in terms of sensitivity few orders of magnitude separate this device from the commercial state of the art, these measured performances are superior in terms of frequency bandwidth and response to any carbon based passive RF detector presented so far.

In order to explain the drops in the lower and upper frequency regions, RF measurements and FEM simulations[222], have been performed on the « device » and on a « reference » one (same as the final device but without graphene). The results shown in Figure 3.15, have allowed to highlight a number of relevant information[223].

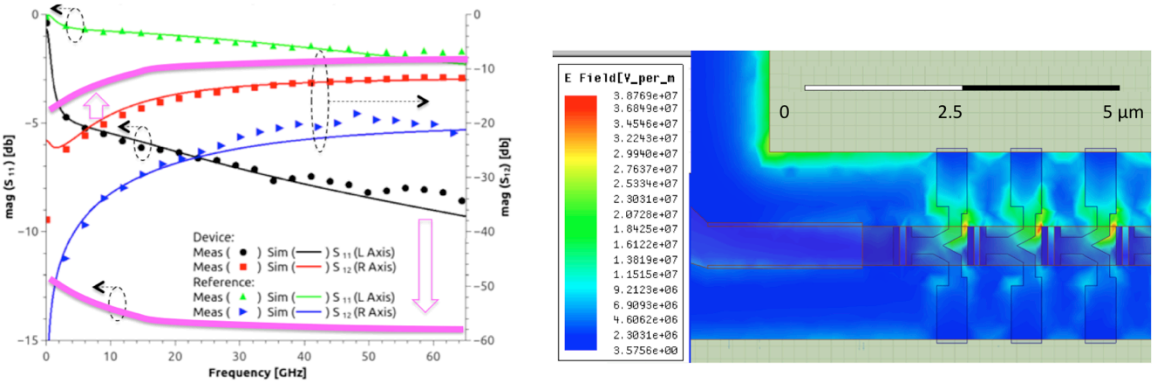

a) b)

Figure 3.15: RF investigation of the ballistic detector: a) Comparison of the measured and FEM simulated scattering parameters for the actual device and the reference (no graphene). Continuous thick purple curves represents the performances improvement after the device optimization (graphene sheet resistance from 1900 to 700 Ω/sq, which include the contact resistance); b) Electric field distribution in a corner of the device core (only 3 out of 50 YBJs are visible).

First of all the comparison between the device and the reference (Figure 3.15a) makes clear the shunting resistive role played by graphene, which introduces a clear improvement on the input matching (RL from better than -1 dB to better than -6 dB) and of the transmission (IL increases for more than 10 dB all over the band). It must be clear out that this improved transmission does not translate directly in higher detection efficiency since this latter is related only to the ballistic part of the transport, while the RF transmission is a contribution of conductive (diffusive) and displacement current flowing in the device. In fact the presence of the

[222] Ansys Ansoft HFSS v14

[223] F. Coccetti, R. Plana, G. Deligeorgis, "Modeling and optimisation of a RF ballistic graphene demodulator", 2013 International Microwave Symposium (IMS), Microwave Symposium Digest (MTT), Seattle, WA, USA, June 4-6, 2013

U-shaped collector within the slots introduces a capacitive coupling between input and output and prevent the electric field to be applied on the YBJ (see the field enhancement at the air bridge region in Figure 3.15b). This latter effect may be responsible for the low detection efficiency at higher frequency (Region III). Second important element is the degradation at the graphene to metal overlapping which is clearly visible through a capacitive (instead of resistive) contact and clearly visible through the high IL value at low frequencies (Figure 3.15a). This is attributed to a very thin residues (few nm) of patterning resin[224] (here PMMA) which turns out to behaves like a leaky capacitor[223]. This problem is likely responsible of the bad device response in region I of Figure 3.14c.

The RF studies of the device have be furthermore completed by an equivalent circuit model which has allowed us to clearly separate each contribution such as reference structure (device without graphene), graphene, and graphene-metal contact. This approach enabled not only a full understanding of the RF performances but also to perform a device optimization, which may be based on an improved design or on the evaluation of possible material and contact improvement.

Contrarily from other detector device, this one present several degree of freedom which can be exploited to enhance its performance (see example of material improvement in Figure 3.15a)[223].

In all these the modeling of the graphene deserves a special attention.

As a matter of fact, the graphene surface impedance depends on its intrinsic conductivity that, in turns, depends on the electric doping of the material, e.g. provided by biasing graphene by using an electric field. This value of conductivity has been deeply investigated by means of theoretical[225], and experimental[226] approaches.

In a simplified scenario where, zero external (static) bias, external magnetic fields, doping, edge effects, and interaction with underlying SiO_2 substrate are neglected, graphene can be modeled by means of a dispersive complex surface conductivity (of equivalently a surface impedance) [227].

The graphene conductivity depends on graphene unique band structure and on a number of

parameters including temperature, scattering rate, Fermi energy, electron velocity, pre-doping (not all these parameter are independent), as well as electrical and magnetic field bias. In general, this conductivity is frequency dependent, and can have completed different behavior from microwave to THz[225], however, in the millimeter waves range it can be considered quite independent on frequency and essentially dominated by the real part. Depending from the parameters mentioned above, typical values may range from few hundreds of ohms/sq to few KΩ/sq[228] (see table in Figure 3.16). In the present modelling the fitting with measurements has allowed to extract value around 1.9 KΩ per square, which is an overestimation since it includes as well a significant contribution of the graphene metal contact resistance (exfoliated graphene is rather in the lower hand of the above indicated range).

In general FEM simulation combined with lumped element equivalent circuit extraction have demonstrated a very effective way to handle overall device performance and optimization.

The critical aspects which need yet more investigation are the extraction of the intrinsic graphene

[224] Y.-C. Lin, C. Jin, J.-C. Lee, S.-F. Jen, K. Suenaga, and P.-W. Chiu, "Clean Transfer of Graphene for Isolation and Suspension," ACS Nano, vol. 5, no. 3, pp. 2362–2368, Mar. 2011.

[225] G. W. Hanson, "Dyadic green's functions and guided surface waves for a surface conductivity of graphene," J. Appl. Phys. 103, 064302, (2008).

[226] P. Sharma, J.S. Gomez-Diaz, A. M. Ionescu, J. Perruisseau Carrier, "Determination of Minimum Conductivity of Graphene from Contactless Microwaves Measurements", IEEE NANO 2012, 12th International Conference on Nanotechnology, Birmingham, UK, 2012.

[227] J. S. Gomez-Diaz, J. Perruisseau-Carrier "Microwave to THz Properties of Graphene and Potential Antenna Applications", 2012 International Symposium on Antennas and Propagation (ISAP2012), Nagoya, Japan, 2012.

[228] D. Mencarelli, M. Dragoman, L. Pierantoni, T. Rozzi, F. Coccetti, "Design of a Coplanar Graphene-Based Nano-Patch Antenna for Microwave Applications", 2013 International Microwave Symposium (IMS), Microwave Symposium Digest (MTT), Seattle, WA, USA, June 4-6, 2013.

and the metal-to-graphene contact. This part has been the partial focus of a PhD thesis at LAAS (G. Vincenzi) where the role of technology and design options have been considered.

In these studies the objective is to extract an electrical model for a generic graphene based device, by accounting for the material an its surrounding environment be it the dielectric layers, or the contact with metal to realize interconnections. So as for individual CNTs or nanowires, owing to their high intrinsic impedance, measurements on nanostructured graphene flakes represent a very delicate operation, which deserves special precautions if done with conventional instrumentation[229]or specialized setup if dedicated approaches are used (e.g. the high impedance one port test setup based on Wheatstone bridge developed at IEMN[230]).

The analysis carry out at LAAS had the intent to draw some guideline on how to model graphene structure within a hosting RF structures. In this case the RF structures realized to build a graphene nanodevice are typically such to form few micrometer wide slots CPW transmission line. In this case a 50Ω characteristic impedance CPW only few 100's nanometer tick (limit of the lift-off photolithographic technology) presents already few ohms of series DC resistance.

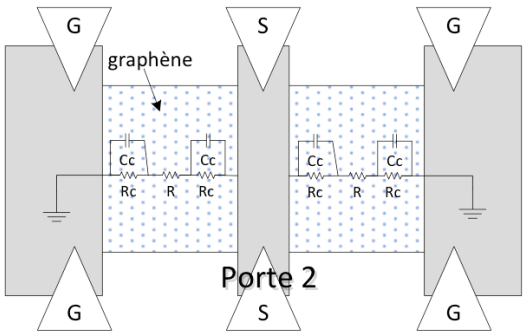

a)

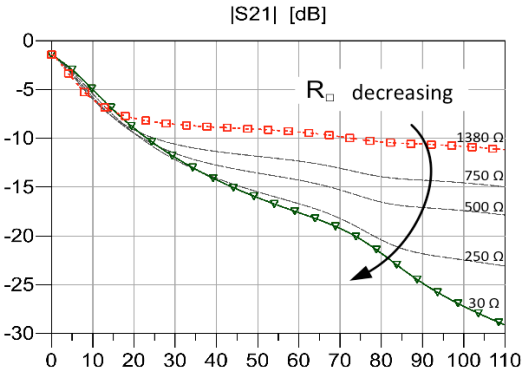

b)

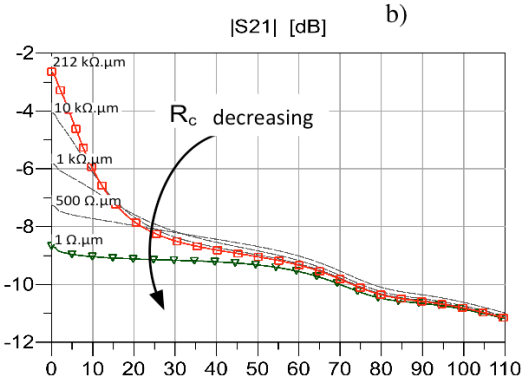

c)

Graphene	Metal Contact	R□ [kΩ]	R_C [kΩ.µm]
Exfol. (LAAS)	**Ti/Au**	**1.38**	**211**
CVD	Ti/Au	1.1÷1.3	//
SiC	Cu	1.6	0.19
CVD	Ti/Pd/Au	//	0.21
Exfol.	Ni, Cr/Au	3.8	0.5÷200

Source: K. Nagashio and A. Toriumi *Japanese Journal of Applied Physics*, vol. 50, no. 7, p. 070108, Jul. 2011.

Figure 3.16: a) Schematic view of a CPW test structure and the equivalent lumped element model (extracted from measured data from DC to 110GHz); Measured and fitted transmission magnitude over the same band with parametric sweep of the key parameter graphene-metal contact resistance (R_C) and the intrinsic sheet resistance ($R_□$) within a range of expected possible values. The table indicates the comparison with some typical value from literature. The value for C_C extracted from measurement is 8.87 fF/µm.

The extracted lumped element equivalent circuit needs to model the graphene-metal contact resistance R_C and the intrinsic sheet resistance $R_□$. Besides these two key parameters an

[229] T. Mitch Wallis, Atif Imtiaz, Hans T. Nembach, Paul Rice, and Pavel Kabos, « Metrology For HighFrequency Nanoelectronics, » AIP Conf. Proc. 931, 525 (2007).

[230] Nougaret L., Dambrine G., Lepilliet S., Happy H., Chimot N., Derycke V., Bourgoin J.P. "Gigahertz characterization of a single carbon nanotube" , Appl. Phys. Lett., 96, 4 (2010) 042109-1-3

additional shunt capacitance is put in parallel to the contact resistance in order to account for a charge accumulation due to different transport mechanisms between metal and graphene (the value for C_C extracted from measurement is C_C=8.87 fF/µm). As in the detector showed above residual of photolithographic resins may affect this value hence needing further investigation currently ongoing.

As mentioned above when talking about the graphene conductivity, these values can be very sensitive to working conditions and technology. A simple schematic view of a CPW test structure used to extract the equivalent lumped element model for a continuous graphene layer deposed beneath the CPWTL is given in Figure 3.16a).

The reported RC model is extracted from measured data from DC to 110GHz (after deembedding - planes positioned at the level of the graphene) in red in the plot of Figure 3.16b,c). The transmission performance for a parametric sweep of the key parameter R_C and $R_{\square}$, is indicated in the same graphs. The values extracted from LAAS sample are in agreement with values given in literature (see table in Figure 3.16)[231].

These preliminary results are being further investigated by means of a design of experiment approach in which different graphene type (exfoliated, CVD and epitaxial SiC growth) are tested in different configuration (shunt and series), and for different sizes of the contact and flake region. These results are expected to shed some light on how to model graphene in a typical nanodevice and from DC up to the millimeter frequency range[232] and support the development of ballistic transport based devices such as the YBJ detector introduced earlier.

[231] K. Nagashio and A. Toriumi, "Density-of-States Limited Contact Resistance in Graphene Field-Effect Transistors," Japanese Journal of Applied Physics, vol. 50, no. 7, p. 070108, Jul. 2011.

[232] G. Vincenzi, G. Deligeorgis, F. Coccetti, R. Plana2, « Modèle de propagation large bande (DC à 110 GHz) du graphène, » Proceedings of 18 èmes Journées Nationales Microondes Paris Mai 2013.

3.3 NEMS RF Electronics: Medium-to-long term research outlook

Exploring the electromechanical and electromagnetic energy coupling through self-oscillating NEMS to introduce new functionalities and miniaturization.

The next paradigm shift toward smart RF nanosystems?

A research direction that in my opinion is worth of focus in future activity is the one concerning the coupling of electromechanical and electromagnetic energy by means of vibrating or self-oscillating nanowires or nanotubes. The emblematic example of this working principle is represented by the all nanotube nanoradio. This concept brings to the farthest extend the idea of coupled electromechanical physics and was first demonstrated by different groups around the same time (A. Zettl from Univ. of Berkley[233], P. Burke, Univ of California in Irvine[234]).

3.3.1 NEMS Radio

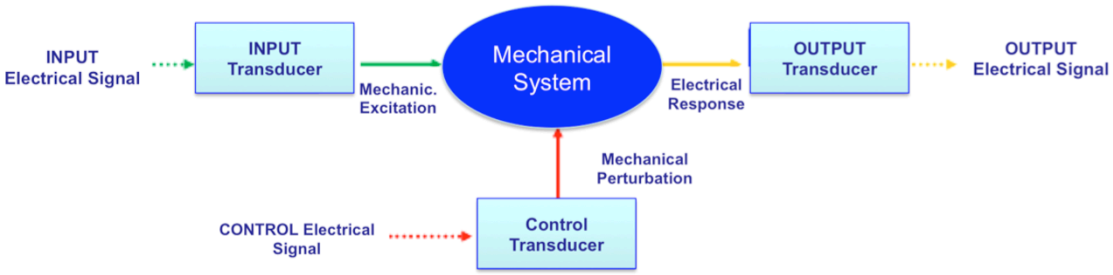

Figure 3.17: Principle of an electromechanical transducer (see also M. Rouke et al.[235]).

The idea behind these preliminary experiments is the basic principle of electromechanical transduction. The results and the associated buzz have gone far beyond the NEMS community and have been largely publicized by the spectacular results such as the atomic scale sensing[236] (by Zettl at Berkley) or the nanometer scale electrometer[237] (by Roucke group at Caltech).

Owing to the extreme small size and form factor of nanowire and NTCs, phenomena that could not be observed before are starting to appear with extraordinary potential applications. In particular the fact that these nanoobject can be engineered to yield vibrating and /or oscillating natural frequencies in the range of microwave is an unprecedented fact and remarkable achievement which opens the way to a number of nanoelectronic applications.

It must be clear that here the intention is not to focus on nanomechanical resonator, which extreme miniaturization by means of CNT[238] and more recently graphene[239], are largely used in chemical sensing, but rather explore the potentiality to implement electrical functions useful for applications in wireless RF communications and RF sensing. Hereby follows an overview of what it is meant with this.

---

[233] Jensen, Burke et al., "Nanotube Radio," Nanoletters Vol 7 No 11 3505, (2007)

[234] Rutherglen, Burke, et.al.. Nanoletters.7, 3005. (2007)

[235] K.L. Ekinci, M.L. Roukes, « Nanoelectromechanical systems ,» Rev. Sci. Instrum. 2005, 76.

[236] K. Jensen, A. Zettl et al,. "An atomic-resolution nanomechanical mass sensor," *Nature Nanotechnology* **3**, 533 - 537 (2008)

[237] A.N. Cleland and M.L. Roukes, "A nanometer scale mechanical electrometer", Nature 392, 160 (1998).

[238] A.M. van der Zande, R.A. Barton, J.S. Alden, C.S. Ruiz-Vargas, W.S. Whitney, P.H.Q. Pham, J.Park, J.M. Parpia, H.G. Craighead, and P.L. McEuen, Nano Letters 10, 4869-4873 (2010).

[239] D. Garcia-Sanchez, A.M. van der Zande, A. San Paulo, B. Lassagne, P.L. McEuen, A. Bachtold, "Imaging Mechanical Vibrations in Suspended Graphene Sheets," Nano Letters 8, 1399 (2008)

Let's consider a conducting nanowire fixed at the extreme of an electrode and facing a second electrode on the other extreme. By applying a DC potential between these two electrodes a charge accumulation at its open ends arises. The higher the form factor and the applied potential (bias), the larger is the accumulated charge. Now if this device is exposed to an electromagnetic plane wave, which frequency corresponds to the self-oscillating (resonance) frequency of the one-end-fixed nanowire, the coulomb force exerted from the plane wave on the charge accumulated at the extreme of the nanowire may become large enough to induce self-oscillations in the nanowire. This is the very fundamental principle of the RF NEMS receiver. By the same principle if stimulus are inverted the same device can be used to radiate electromagnetic waves becoming at the same time a RF NEMS transmitter[233]. In 2007 Zettl's group gave a very astonishing experimental demonstration of this concept baptized "nanoradio", and schematically represented in Figure 3.18.

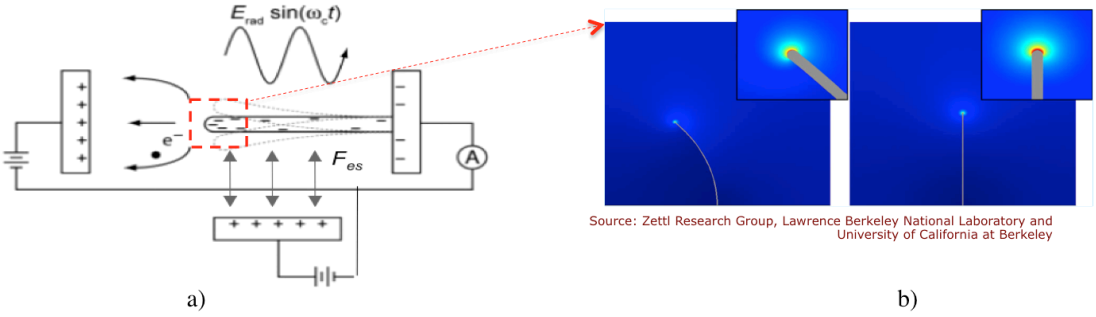

Figure 3.18: [Source: A. Zettl et al. Berkelay] [233]: All-in-one nanotube Nanoradio: a) schematic principle; b) modeling of the charge accumulation at the free end tip.

The origin of this principle are dated back to (1999) when Poncharal et al. first demonstrated that the charge and hence the electrical force exerted on a CNT, is located entirely on its tip, and that the CNT cantilever deflection is proportional to the square amplitude of the applied signal[240,241].

The **amount of charge at the tip** is the critical quantity determining the performance of this electromagnetic-electrostatic coupling principle. According to the Zettl's experiments[233], nanotubes with typical dimensions (L ≅ 500 nm, r ≅ 5 nm), accumulate, for an external electric field of $E_{ext} \cong 10^2$ V/μm, approximately $3\text{x}10^{-17}$ C of charge (almost 200 unbalanced electrons) at their tips. The **amplitude of the vibrations** of the tip of the nanotube is shown in Figure 3.18 and is given by the equation:

$$|y| = \frac{qE_{rad}/m_{eff}}{\sqrt{\left(\omega^2 - \omega_0^2\right)^2 + \left(\omega\omega_0/Q\right)^2}}$$

where q is the charge on the tip, E_{rad} is the amplitude of the electric field of the incoming transmission[242], $m_{eff} \cong 0.24\ m_0$ is the effective mass of the nanotube determined from Euler-Bernoulli theory, and Q is the quality factor.

[240] P. Poncharel, Z. L. Wang, D. Ugarte, and W. van der Heer, "Electrostatic Deflections and Electromechanical Resonances of Carbon Nanotubes »Science 283, 1513 (1999).

[241] Z. L. Wang, R. P. Gao, P. Poncharal, W. A. de Heer, Z. R. Dai, and Z. W. Pan, "Mechanical and electrostatic properties of carbon nanotubes and nanowires,"Mater. Sci. Eng., C C16, 3 (2001).

[242] Note that for a radio FM signal this value could span between far field intensity (as low as 10^{-8}V/m) up to the maximum power exposure limits (in the range of 10 V/m).

To estimate the resonant frequency shifts we can resort to classical *Euler-Bernoulli beam theory* and the *Rayleigh-Ritz theorem*. Solving the equation gives the fundamental **resonant frequency for the MWNT cantilevered beam** (see Figure 3.19a):

$$f_0 = \frac{0.56}{L^2}\sqrt{\frac{YM}{\rho A}} = 0.56\sqrt{\frac{YM}{L^3 m_{cnt}}}$$

where Y is the Young's modulus, M is the areal moment of inertia[243], ρ is the mass density, and A is the cross-sectional area m_{cnt} is the mass of the MWNT.

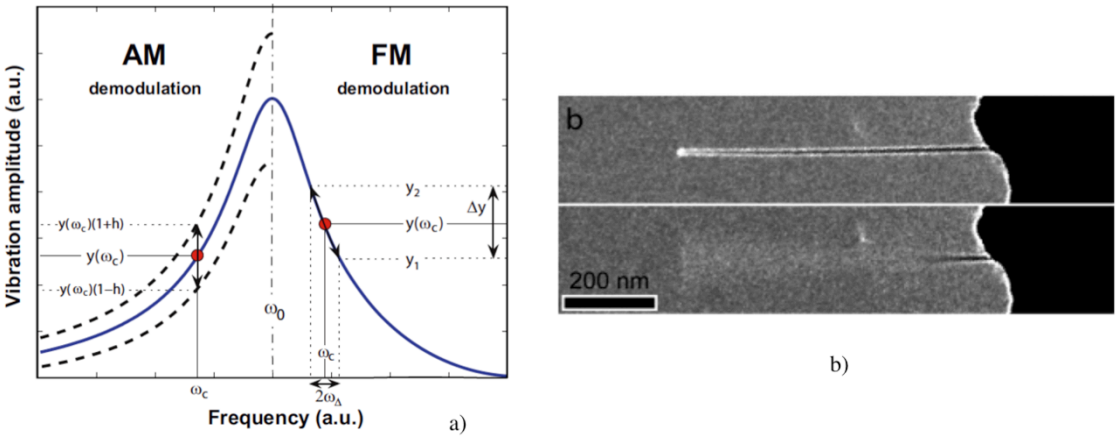

Figure 3.19 [Source: A. Zettl et al. Berkelay][233]: a) Amplitude of the oscillation as function of the frequency. In the same graph the demodulation process across the mechanical resonance of a CNT is shown. The solid line (blue) traces the linear mechanical amplitude versus the excitation frequency. Left (right) schematizes the AM (FM) demodulation process. The AM and FM signals result in low frequency variations of the oscillations that cause in turn variations of (y); b) Transmission electron micrographs of a nanotube radio off and on resonance during a radio transmission.

The minimum detectable electric field amplitude while maintaining a bandwidth B is:

$$E_{rad} = (1/q)\sqrt{4k_B T m_{eff}\omega_0 B/Q},$$

which in typical experiments (Zettl et al.) was 1 V/m/√Hz or equivalently 60 dBmV/m/√Hz.

A further feature of this simple NEMS device resides in the opportunity to exploit the non-linearity associated with the field emission occurring at the extreme of the nanowire open end.

In fact the applied bias combined with the elevated form factor and the proximity of the tip to the electrode give rise to a field emission (FE), which is well described by a Fowler-Nordheim conduction law[244]:

$$I_{FE} = I = c_1 A(\gamma E_{ext})^2 \exp\left(-\frac{c_2}{\gamma E_{ext}}\right)$$

whereas A is the area from which the nanotube emits, E_{ext} is the external applied electric field, and γ is the local field enhancement factor[245]. The constants c_1 and c_2 take the values 3.4 x 10^{-5} A/V^2 and 7.0 x 10^{10} V/m.

The field enhancement factor, a measure of the concentration of the local electric field by the nanotube's geometry[245], distinguishes carbon nanotubes as excellent field emitters and also plays a critical role in the operation of the nanotube radio. To a good approximation, the field enhancement factor for a nanotube is $\gamma = 3.5 + h/r$, where h is the height of the tip of the

[243] For a cylinder with outer and inner radii respectively r_o and r_i: $I = (\pi/4)(r_o^2 - r_i^2)$

[244] R.H. Fowler, L. Nordheim, "Electron emission in intense electric fields," Proc. R. Soc. London, Ser. A, 119, 173-181 (1928).

[245] Wang, X. Q., Wang, M., He, P. M., Xu, Y. B., Li, Z. H., "Model calculation for the field enhancement factor of carbon nanotube," *J. Appl. Phys.*, 96, 6752-6755 (2004).

nanotube above the cathode and r is the radius of the nanotube[246]. As the nanotube vibrates, the height of its tip oscillates resulting in a time-varying field enhancement factor: $\gamma(t) = \gamma_0 + \Delta\gamma(t)$. The response of the field emission current to the vibrations is determined by substituting this $\gamma(t)$ in the above equation for I_{FE}. Furthermore expanding to second order in powers of $\Delta\gamma(t)/\gamma_0$ and filtering out the zeroth and first powers of $\Delta\gamma(t)/\gamma_0$, which correspond to DC and radio frequency terms, yields :

$$\Delta I(t) = I_0\left(1+\alpha+\frac{\alpha^2}{2}\right)\left(\frac{\Delta\gamma(t)}{\gamma_0}\right)^2, \qquad \text{with } \alpha = \frac{c_2}{\gamma_0 E_{ext}}$$

which accounts for both amplification and demodulation. Amplification occurs because the output of the radio, $\Delta I(t)$, is proportional to the field emission current, I_{FE}, which is powered by the battery voltage source. The power gain, given by the ratio of the power dissipated by the signal current through a load resistor, $P_{out} = \Delta I_{rms}^2 RL$, to the power absorbed by the nanotube from a radio signal on resonance is given by $P_{in} = m_{eff}\,\omega_0^3\,abs(y)^2\,/2Q$, and it is easily adjustable over a wide range. Demodulation occurs because $\Delta I(t)$ is proportional to the square of the input signal $\Delta\gamma(t)$, effectively mixing the input signal with itself. In this manner, a field-emitting nanotube operates similarly to standard diode detectors. On this regard it is worth of mention that other detection principle which consist in exploiting the tunnel effect taking place exactly at the same location (CNT facing the electrode and under bias) have been proposed predicting lower bias voltages (tens instead of hundreds of volts) and larger tuning range (4 fold)[247].

Today's progress in nanotechnology make possible to adjust the electromechanical properties (geometry and mechanical properties) of the nanowire or CNT in order to prove this concept. The consequences of this basic principle are paramount. **The most emblematic is the fact that this phenomenon allows to break the well known relation linking the size of an electrical resonator or of an antenna to the electrical wavelength of the radiated signal**

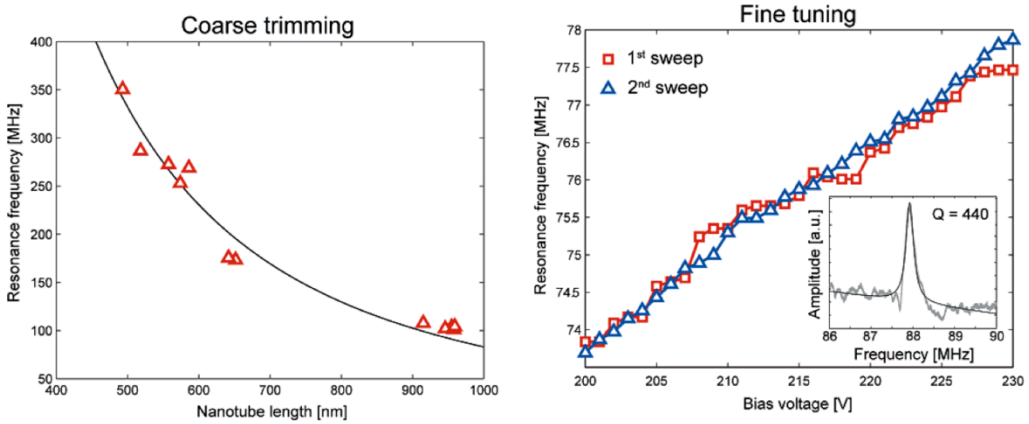

Figure 3.20 [Source: A. Zettl et al. Berkelay][233]: Oscillation frequency adjustment: a) During coarse tuning or "trimming", the nanotube is controllably shortened thus increasing its resonance frequency. Its resonance frequency closely follows the $1/L^2$ dependence predicted by Euler-Bernoulli beam theory; (b) During fine-tuning, a bias voltage is used to adjust tension on the nanotube. Multiple sweeps of the bias voltage demonstrate the reversibility of the process. Inset is a typical resonance peak with a Lorentzian fit.

If miniaturized electrical resonator through electromechanical or piezoelectric principle exists since long time (see MEMS resonators, SAW, BAW or quartz), electrically radiating

[246] Wang, X. Q.; Wang, M.; He, P. M.; Xu, Y. B.; Li, Z. H. Model calculation for the field enhancement factor of carbon nanotube. J. Appl. Phys. 2004, 96, 6752-6755.

[247] D. Dragoman and M. Dragoman, "Tunneling Nanotube Radio," J. Applied Physics, vol. 104, no. 7, Oct. 2008.

resonators, (or electrically small antenna) theory, imposes a hard lower bound to any possible solution (Chu limit[248]).

Therefore this transfer, or coupling, between the electromagnetic wave energy to electromechanical energy is a unique and fundamental principle, which may represent an alternative to conventional antenna miniaturization approaches. The further functionalities described above and culminating in the full operational nanoradio, complete this paradigm of extreme integration.

In addition to what already explained about the fundamental functioning principle, by trimming the length of the cantilever (Figure 3.20a), these electromechanical resonances can be defined or fine-tuned in case where a lateral electrode (control electrode in Figure 3.17 and as shown in Figure 3.18) is added. By applying a bias to it, an electrostatic force is exerted laterally to the oscillating cantilever so that the resonating frequency can be adjusted. The larger the applied bias, thus the electrostatic force, the higher the oscillating frequency (Figure 3.20b).

Early study on exploitation of Electromagnetic – Electromechanic energy coupling principle at LAAS

A quite similar principle was also introduced at LAAS by M. Dragoman et al. in 2006 to perform RF filter functions[249]. In this case the self-oscillating nanowire or CNT were used to create a transmission zero in the transfer function of an RF guiding structure.

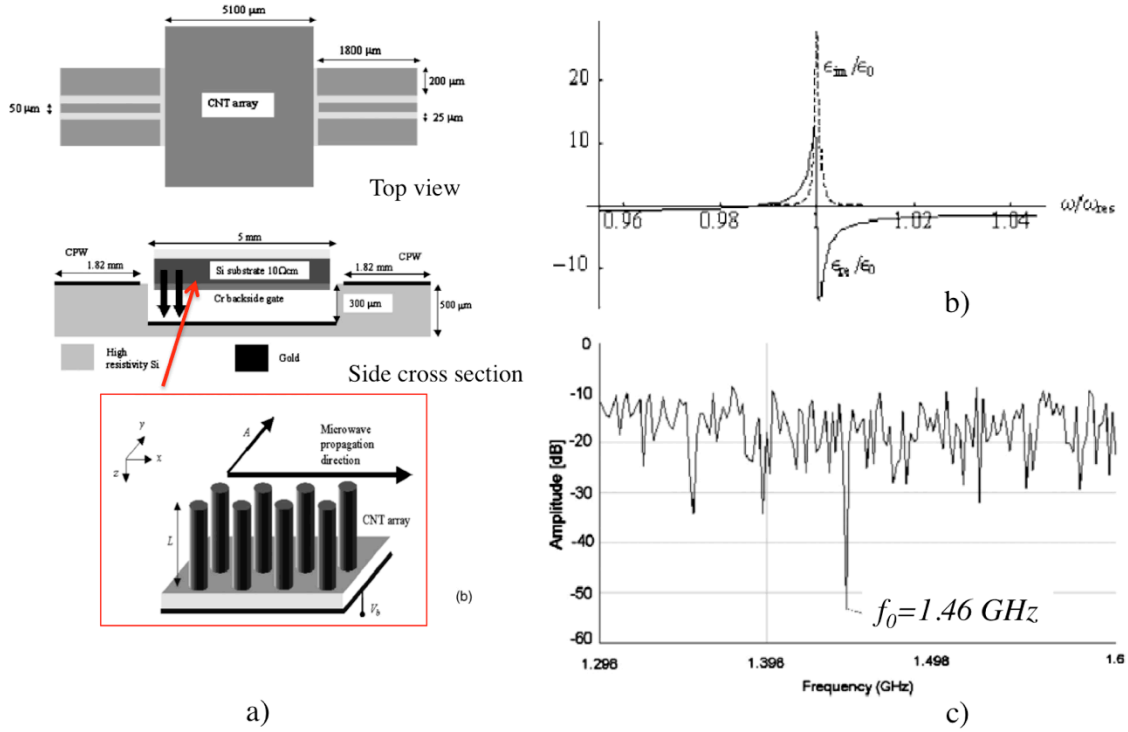

Figure 3.21 [Source: M. Dragoman et al. LAAS-IMT] [250]: CNT based NEMS notch filter : a) Schematic representation of the device based on a CPW transmission line where the CNT carpet (109 CNTs/cm^2) is mounted within a bulk micromachined cavity5x5 sqmm. A slight misalignment translates in loss of coupling; b) Frequency dependence of the real (solid line) and imaginary (dotted line) parts of the electric permittivity of the CNT array modeled by the Drude-Lorentz theory; c) The transmission mod(S_{21}) of the CNT array as a function of frequency (high uncertainty and low value value of transmission are due to dispersion on the CNT length and low coupling between

[248] L.J. Chu, « Physical limitations on omni-directional antennas, » Dec. 1948, J. Appl. Phys 19, pp. 1163-1175

[249] D. Dragoman M. Dragoman, "Electromagnetic wave propagation in dense carbon nanotube arrays,"JAP 99, 076106 2006

electromagnetic energy and CNTs). A clear notch is visible at the resonance frequency (f_0=1,46GHz computed from the Euler-Bernoulli formula with a CNT length of 300nm, a diameter of 40nm).

In fact since the charge, is located entirely on the tip of a very large number of vertically aligned cantilever beams (e.g. a carpet of vertically ordered CNTs) positioned within a waveguide the cantilever deflects (oscillate) only when the incoming RF field frequency equals the resonant mechanical frequency of the CNT cantilevers (Figure 3.21a). In case of metallic CNT array, at the mechanical resonant frequency, the carpet behaves as a dielectric material endowed of very high losses. This turns out to create the transmission notch behavior at that oscillation frequency. The metallic-dielectric transformation can be described by the classical *Drude-Lorentz* theory which is used usually to estimate the electric permittivity contribution of electronic vibrations in a crystal (in this case the oscillators are the charged tips of the cantilevered CNTs, arranged in a two-dimensional pattern) (Figure 3.21b). In spite of the fact that experimental results have demonstrated several limits due to the fabrication difficulties[250] (limited coupling due to poor alignment of the CNT carpet free-tip surface with the maximum electromagnetic field intensity within the planar waveguide - CPW), they could still provide a proof of concept for this original and fascinating concept (Figure 3.21c).

3.3.2 Critical analysis of the NEMS radio: science or fiction.

In spite of the simple working principle several limitations hampers the present exploitation of this NEMS radio.

As matter of fact the mentioned coupling between electromagnetic and electromechanical energy is extremely sensitive to atmospheric conditions, electrostatic discharges, and any possible mechanical or electrical perturbation in the surrounding area.

Moreover the self-oscillations of the nanocantilevers are very sensitive to possible inhomogeneity (structural defects) which may induce multiple resonating modes[251]. The role of technology is therefore essential in fabricating regular and defect-free nano-objects which moreover need to be accurately manipulated and positioned within the hosting structures (e.g. bias electrodes).

The working frequency range as well is limited by the electromechanical resonance frequency which defined by the Euler-Bernoulli formula given above, lay today below few GHz.

The most comprensive understanding of the underlying physics has been carried out in 2002 by the group of S. Purcel (at the Laboratoire de Physique de la Matière Condenseé et Nanostructures, Université de Lyon). Their study on field emission and self-oscillating nanowire[251] paved the way toward a sound interpretation of the previous work, providing a critical analysis and identifying the limitation of practical implementation of the NEMS radio or nanoradio[252].

In this analysis they demonstrated that the estimations of the excitation efficiency of a charged CNT for capturing RF signals is possible but shown however that this new type of antenna works very poorly in the open FE geometry (i.e. for a CNT on a tip without facing electrode). In other words this new type of mechanical reception does not circumvent the basic difficulty of the mismatch between the RF wavelength and CNT length. A better optimization taking into account the electrostatic, electromagnetic, mechanical and FE is an engineering

[250] M. Dragoman, D. Neculoiu, A. Cismaru, D. Dragoman, K. Grenier, S. Pacchini, L. Mazenq, R. Plana – High quality nanoelectromechanical microwave resonator based on a carbon nanotube array, Appl. Phys. Lett. 92, 063118, 2008.

[251] S. Purcell, P. Vincent, C. Journet, V.T. Binh, « Tuning of nanotube mechanical resonances by electric field pulling, » Phys Rev Lett. 89(27):276103 (2002).

[252] P. Vincent, A. Ayari, P. Poncharal, T. Barois, S. Perisanu, V. Gouttenoire, and S.T. Purcell, "Carbon Nanotube Nanoradios: The Field Emission and Transistor Configurations, » Comptes Rendus Physique Advances in nano-electromechanical systems Elsevier, Volume 13, Issue 5, June 2012, pp.: 395–409.

problem that must be tackled before the real capabilities and characteristics of this nanoradio are known.

Finally it must be pointed out that all these tests (Zettl's, Purcell's, Burke's) have been conducted in extremely low noise condition (e.g. TEM chambers, hence in UHV conditions (pressure lower than about 10^{-7} Pa or 10^{-9} mbar, ~10^{-9} torr) and low temperature.

Another possible limitation is the electrostatic issues related to high voltage excitation (to reach a critical quantity of charge accumulation), and the electromagnetic wave "access" to the accumulated charge. The tip is indeed very close to the electrode whereupon the field effect takes place and where the electric field needs to exist in order to apply his effect. In spite of the fact that the presence of these conductor can reduce the electric field at the tip of the nanowire/CNT, there may be still enough energy to excite excitation and there may be other geometrical configuration which allows more exposure to electromagnetic field (e.g. vertical CNT with only one side bias –though in this case no FE could be achieved).

Also the modeling of this fascinating principle is at the moment hampered by several open challenges. One for all is again the need to account for the all involved physics (electromagnetic electromechanic field electron emission, …) which, being closely coupled (they have similar time constants), need to be considered consistently. Given the experience from the MEMS multyphysics modeling this challenge is hard to accomplish with present tools. Finally as further consideration the quantum limits for an electromechanical device need to be mentioned. The ultimate limit for nanomechanical devices is to operate at, or even beyond, the quantum limit. In fact, as for the electrical properties of nanoscale confined conductor mentioned earlier in this chapter, giving rise to the concept of ballistic transport and resistance quantum, in NEMS the notion of mechanical quanta needs to be considered. The mechanical quantum, given by $\hbar\omega_0$, (ω_0 mechanical oscillation) represents discrete jump in the displacement (in the order, or greater than the thermal energy, k_BT). Hence the quantum theory needs to be brought in to understand and optimize force and displacement measurements[253]. All this goes far beyond the purpose of the present document, but it confirms the need for a new paradigm in "thinking at the nanoscales".

3.4 Conclusions on the Research Outlook: RF Nanotechnology

The nanotechnology implies to face the very limits of matter. Down to the nanoscale metals insulator and semiconductors behave differently from their bulk counterparts. One of the most emblematic examples of this is the "resistance quantum" which appears in very narrow conducting material where ballistic transport occurs. At these scales Landauer's equation for conductivity replaces Ohm's law. Although nanoobjects (CNT, nanowire, nanribbons) are therefore individually endowed by large numerical value of impedance, their collective use (ordered or randomly organized) allow to reach impedance value compatible with the RF applications. **The critical issue in this sense is that individual nanostructures have very high impedance (~KOhm) which intrinsically translates in a severe RF mismatch, possibly solved by collective use of single nanostructure.**

The technology which allows to manufacture and organize them in large number represents the fundamental link between the nanoscale realm, dominated by quantum electrodynamics (QED), where impedances are ruled by the resistance quantum *(h/e^2 =25.8 KΩ),* and the RF realm dominated by classical electrodynamics and where the impedance values are governed by another natural physical constant, the free space impedance *($\mu_0 c_0$ = 376.73 = 120 π)*[254]. In order to

[253] C.M. Caves, K.S. Thorne, R.W.P. Drever, V.D. Sandberg, and M. Zimmerman, "On the measurement of a weak classical force coupled to a quantum mechanical oscillator. I. Issues of principle", Rev. Mod. Phys. 52, 341 (1980).

[254] P. Burke, invited talk on "CNT for RF nanoelectronics" at IMS Workshop, Baltimore June 2011.

bridge the nanoscale realm to the RF one (e.g. use in actual RF applications), new paradigms in how nanobjects are handled (fabricated) and modelled (understood) need to be found.

Two dimensionals (one atom/molecule thick crystal) based nanotechnology[255] seems to provide a viable solution toward the next generation of nanoelectronics which combines enhanced performances (miniaturization, energy efficient and speed), with planar technology compatibility[167].

Among all 2D crystals, graphene is by far the most investigated. In fact owing to its unusual electronic properties, "graphene has led to the emergence of a new paradigm of 'relativistic' condensed-matter physics, where quantum relativistic phenomena, some of which are unobservable in high-energy physics, can now be mimicked and tested in table-top experiments"[256].

It is most certain that we will see many efforts to develop various approaches to graphene electronics. Whichever approach prevails, there are two immediate challenges. First, despite the recent progress in epitaxial growth of graphene, high-quality wafers suitable for industrial applications still remain to be demonstrated. Second, individual features in graphene devices need to be controlled accurately enough to provide sufficient reproducibility in their properties.

Graphene based ballistic electronics represents a very promising approach to implement high speed and low losses devices. Speed and low losses are indeed peculiar properties of ballistic transport and the opportunity to implement them by means of planar photolithographic technology has open the door to several experiments. At LAAS the interest was devoted to detectors based on the strong non-linearity introduced by ballistic transport in three-terminal junctions and more specifically in YBJs. Although this detection principle has potential application up to the THz, practical implementation limitations (i.e. fabrication and large band design of the entire device) remain the major challenge.

On the longer term another nanotechnology-enabled area could emerge, the NEMS radio. Although several groups have carried out a quite spectacular practical demonstration, this subject has been fading down in the last few years due to the implementation difficulties. Although for the moment it remains a lab proven concept, the coupling of radiated electromagnetic energy with electromechanical one through NEMS may represent the next paradigm shift toward extreme integration of RF nanoelectronics.

In fact if the question "What will be the future offering in 10-20 years ?" is asked, it will be very difficult to answer since actual progress occurs through groundbreaking discovery or indeed paradigm shifts.

Present achievements in nanosciece lead us however to anticipate a likely scenario where energy and spectrum optimization will become the major driving needs. Traditional communication technologies are not suitable for nanonetworks mainly due to the size and power consumption of transceivers, receivers and other components. The use of nanosystems (NEMS, molecules, …) to encode and transmit the information represents a possible new communication paradigm that demands novel solutions[257].

P. Burke from University of California in Irvine was the first to propose his vision on possible future RF architectures. He did this by bridging information communication technology (ITC) with nanoscale biosensor network (NBSN). In his outlook he talks about « single cell implantable RF systems[258]», as the next generation of intelligent and wireless sensor network made of autonomous « Nano »-node capable to interface with a biological ecosystems (Figure

[255] K.S. Novoselov, D. Jiang, F. Schedin, T.J. Booth, V.V. Khotkevich, S.V. Morozov, A.K. Geim, "Two-Dimensional Atomic Crystals, " Proc. Natl. Acad. Sci. U. S. A. 2005, 102, 10451–10453.

[256] A. K. Geim, K. S. Novoselov, "The rise of graphene,"*Nature Materials* 6, 183 - 191 (2007), Quote from:

[257] I. F. Akyildiz, F. Brunetti, and C. Blazquez, "Nanonetworks: A New Communication Paradigm," Comp. Net., vol. 52, no. 12, Aug. 2008, pp. 2260–79.

[258] P. Burke and C. Rutherglen "Towards a Single-Chip, Implantable RFID System: Is a Single-Cell Radio Possible?," Biomedical Microdevices, Jan. 2009.

3.22). Similar approach always based on NEMS based radio, was proposed at METU in Turkey through the Carbon nanotube-based nanoscale Ad hoc NETworks (CANETs)[259].

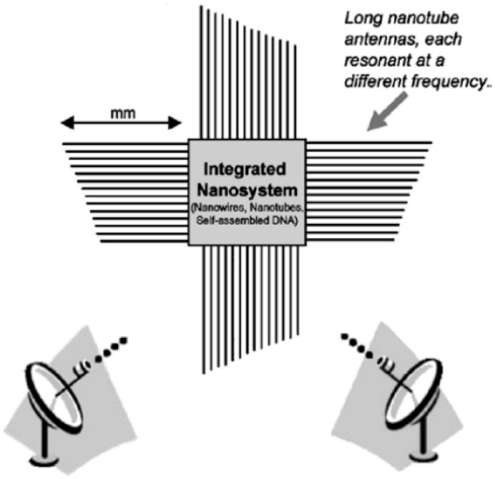

a)

	Circuit size (m^3)	Antenna size (m^3)	System size
Hitachi	1E−14	1E−08	1E−08
UCI CNT Radio	1E−23	1E−05	1E−03
France-Telecom	1E−09	1E−09	1E−09
Smart Dust	3.125E−09	1E−06	1E−06
SMS	NA	NA	1E−06
BioRasis	NA	NA	5E−09
ISSYS	NA	NA	1E−06
Potential single-chip radio			1E−14
Volume of single cell			1E−18
Potential nano radio			1E−21

These are estimates only, as most literature does not specify complete system volume

b)

Figure 3.22 [Source. P. Burke – UCI 2010]: Long term vision for integrated RF architectures : a) Possible architecture based on NEMS (CNTs) Rx/Tx ; b) Table with estimated circuit, antenna, and system size for various radios complied from the literature.

These predictions may appear too ambitious or even hazardous if compared with the several but still application-limited results. In spite of this, the bottom-up approach enabled by nanotechnology is becoming a reality and will be the protagonist of many achievements to come.

Today we only start to scratch the surface of the "*Feymaninan realm*" but many idea on how to build a nano-machine[257,260]are already a reality

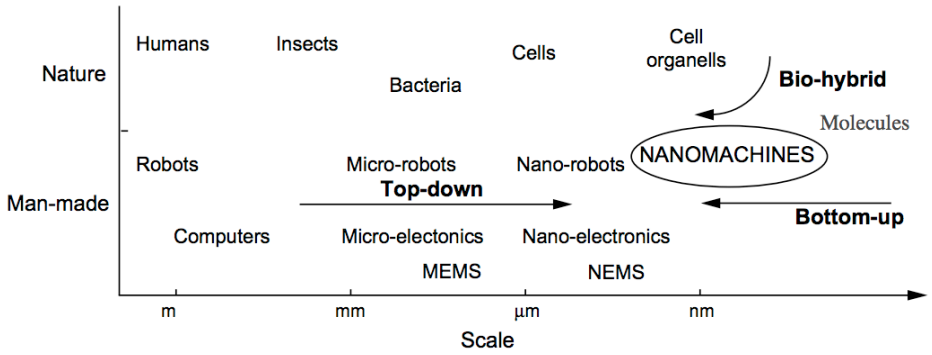

Figure 3.23: [Source: I.F. Akyildiz et al. (2008)[257]]: Approach for the development of a nano-machine

Much work lays ahead in understanding nanoscale phenomena (multiplysics) and mastering nanoscale manufacturing, however the experimental appearance of first nanoscale and molecular devices combined with recent successfully achievements in precise handling of atoms to create atomic scale systems (memories)[261] is attracting an unprecedented level of interest within the

[259] B. Atakar, O.B. Akan, « Carbon Nanotube-Based Nanoscale Ad Hoc Networks, »IEEE Communications Magazine • June 2010, pp. : 129-135.

[260] See example of bottom-up nano-machine manufacturing by nano 3D-printing (of a microscopic Car: http://www.youtube.com/watch?feature=player_embedded&v=5y0j191H0kY) and the more science-fiction atom-by-atom molecular factory (Source: - Dr. K. Eric Drexler. Nanofactory: http://www.youtube.com/watch?feature=player_embedded&v=vEYN18d7gHg)

[261] Source: IBM « The boy and his atom » Dr. A. Heinrich http://www.research.ibm.com/articles/madewithatoms.shtml (**Today memory: 10^6 atoms/bit, IBM record: 12 atoms/bit)**

physics and engineering community. This is likely to reach soon a critical mass of competences and motivations that will trigger the next breakthroughs. If the past century has undoubtedly seen the most impressive technical breakthrough of human history, nanotechnology will be for sure the protagonist of the next one yet to come.

RF nanotechnology will have a big role in all this, so better to stay tuned.

4 Annexes:

4.1 Global overview of research activities

In this annex some complements with respect to the main flow of activities and described in the main body of this document will be given and briefly discussed. A graphic overview which covers the period 1999 (MSc) until 2015, is depicted in Figure 4.1. This overview embraces the whole set of research topics (above timeline) along with collaborative projects and industrial collaborations (below timeline) unfolded during this time span. The research activities showed as interrelated by means of arrows, represent the backbone of my personal research interests and form in good part the main part of this manuscript. The remaining topics concern advisory and management involvement within PhD thesis and collaborative projects, only loosely related with this latter.

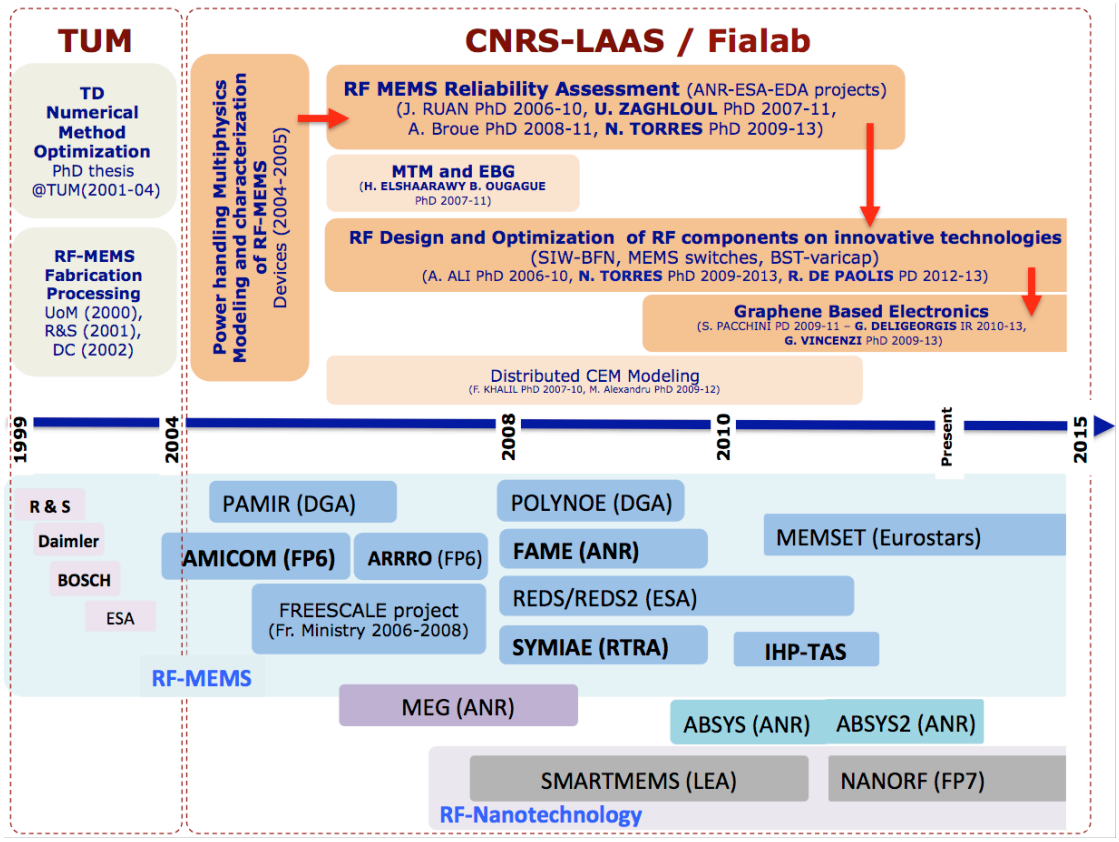

Figure 4.1: Activity synopsis for the period 1999 - 2015. The plot is divided in research activity subjects (above the timeline) and project participation (below the timeline). Main involvement (advisor in PhD and PI/management in project) is marked in boldface. The red arrows relate the topics described in the main document.

For sake of completeness these topics are reported in the following paragraphs with the aim to provide a synthetic and not-exhaustive overview. They cover from distributed computational electromagnetic for the modeling of complex electromagnetic problems (F. Khalil – PhD, and M. Alexandru – PhD) to more pragmatic issues such as the investigation of ESD in RF-MEMS (J. Ruan - PhD), or design approach of reconfigurable RF circuits based on the electromagnetic

bandgap structures (EBG) (H. El-Shaarawy - PhD), and metamaterial approach (B. Oaugague - PhD), to eventually close with material and technological aspects, such as the study of ferroelectric materials (such as barium strontium titanate - BST) to implement innovative variable capacitors (R. De Paolis - PD), multilayered substrate integrated waveguides (SIW) for beam forming networks (BFN) (A. Ali - PhD), and inkjet printed CNTs for application in RF interconnections (S. Pacchini – PD, R De Paolis – PD). Owing to the heterogeneity of these topics it was not possible to include these subjects in the main body of this document. In spite of this, they all contributed to widen the perception and the understanding of the challenges toward heterogeneous integration of smart RF micro and nano systems.

For what concerns the collaborative projects and the industrial collaborations mentioned in Figure 4.1 they have been instrumental for supporting the aforementioned research activities and more detailed about them can be found in the Appendix 4.3.

4.2 Complementary Research Topics

4.2.1 Distribute Computational Electromagnetics

Fadi Khalil *PhD Thesis INP - Université de Toulouse (2006-09).*
Advisors: Prof. H. Aubert, Dr. F. Coccetti
Mihail Alexandru *PhD Thesis INP – Université de Toulouse (2009-12).*
Advisors: Prof. H. Aubert, Prof. T. Monteil
In collaboration with: Grid 5000
IMAG Lab in Grenoble (Prof. Y. Denneulin), Lorenz Solution in Munich (Dr. P. Lorenz).
Personal involvement[262]: 10-20% (Mentoring on TLM method and network oriented modeling)
Publications: 5 Int. Journals; 10 Int. Conferences; 2 National Conferences.

These research activities faced the challenging scenario of the numerical modeling of complex electromagnetic problems. A dual approach based on the exploitation of distributed computing resources (computing cluster and/or computing grid technology) and known electromagnetic solvers was followed. These latter were available in LAAS as open source tools: the Transmission Line Matrix method (TLM[263] - available through the distribution pack YATPACK[264]) and the Scale Changing Technic (SCT)[265]. This activity has unfolded with a first phase targeting the optimal deployment of parametric TLM and SCT models over the French national test grid called Grid5000[266]. This topic was developed within Mr. F. Kahlil PhD thesis (2007-2010). A second phase was more dedicated to the deployment on computing clusters, of large electromagnetic problems where the parallelization and hybridization was at stake. This part was the topic of internal collaboration at LAAS and was carried out through the PhD thesis of M. M. Alexandrou (2009-2012). These two studies have been the core of an ANR project called "Multiscale modeling: from Electromagnetism to the GRID" (MEG – ANR-BLAN), which has given the initial pulse to these activities at LAAS and that eventually addressed not only the modeling of the miniaturized RF microsystems but also large electromagnetic problems such as the radio propagation channel within airplane fuselages[267] and tunnel networks[268].

This two-fold approach allowed first the validation and exploitation on GC of the intrinsic performance of the TLM and SCT methods.

- In the case of the TLM arbitrary scalability of the grid resources is allowed by the possibility to have arbitrary decomposition of the simulation domain (i.e. the domain can be arbitrarily partitioned in the 3 directions as more convenient with the grid resources availability of free nodes and connection speed).
- For the SCT adaptive scalability of the grid resources is enabled by the intrinsic scalability of the method. The computation of each domain can be mapped to an equivalently large set of computing nodes and solved accordingly.

Another central aspect was the hybridization of the two techniques (TLM and SCT). In this case the objective was to use each technique to a portion of the entire problem (domain decomposition) where its computational efficiency is maximal (in this case SCT for the 2D multiscale domains, and the TLM to the remaining 3D parts). This operation represented an ambitious objective, as hybridization of numerical technique is still today the ultimate numerical modelling goal toward the modeling of arbitrary complex problems. The most serious obstacle

---

[262] The personal involvement is indicated as indicative calculation of the fraction of time spent on the project/thesis with respect to the overall development/advisor time.

[263] F. Coccetti " Application of System Identification (SI) to Full–Wave Time Domain Characterization of Microwave and Millimeterwave Passive Structures" PhD Thesis TUM Munich Germany 2004

[264] TLM open source solver from the YATPAC distribution, developed at the High Frequency Institute of Prof. P. Russer at the Technische Universität München.

[265] The SCT solver was early developed by Prof. H. Aubert and available (Matlab) open source.

[266] Grid5000 – National test grid - www.grid5000.fr

[267] Only preliminary study on actual size model used only as case study.

[268] Investigation done for the Agence National por la gestion de Déchets Radioctifs (ANDRA).

consists in the interfacing of the different solution domains (e.g. the 3D time-domain for the TLM and 2D frequency domain for the STC), so that energy conservation and causality are satisfied. The most elegant approach to face this challenge, and used in this work, is the *Network Oriented Modeling theory,* introduced by Russer, Mongiardo, Felsen[269].

This approach was implemented in these activities through the hybrid electromagnetic simulation of large and complex electrical structures, such as airplane cabins, tunnels, etc. In particular it combined the TLM (applied to homogeneous volumes), and the mode matching, (applied to planar structures).

As an example of this an electromagnetic simulation of a downscaled (1:300 see Figure 4.2a) airplane cabin (the structure included seat and finely meshed resulted in more than 150 millions TLM SCN nodes or more than 1 billion unknowns) with closed between termination planes modeled by mode matching (see P51. in bibliography).

The measured results have demonstrated that the higher is the number of parallel processes the larger the speedup deviation from the optimal values (upper limit is the ideal scalability). This was found to be essentially due to the fact that communication time between the processes is larger than network latency. Consequently, in order to launch efficient simulations the size of the structure needs to be matched with the number of computational nodes.

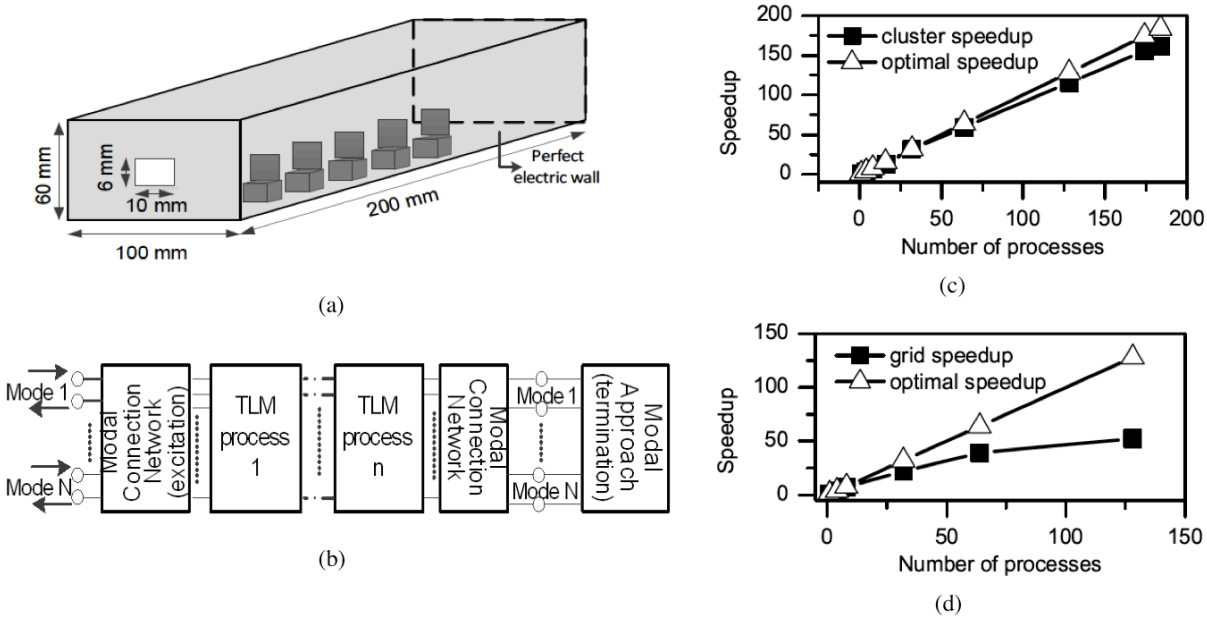

Figure 4.2: Example of distribute electromagnetic modeling: a) Model of a downscaled airplane cabin (1:300, compared with a regular one) with seats, having perfect electric walls and a rectangular aperture antenna, b) Schematic view of the TLM/modal hybrid modeling approach. Parallel computation speedup showing the role of the number of processes and the role of the communication between computing nodes on a cluster (several nodes in the same location) and (d) a grid computing test bed (several nodes in sparse locations).

For this reason a prediction model, based on a hybrid approach, which combines a historic-based prediction and an application profile-based prediction, was developed in collaboration with Prof. T. Monteil (from the Advanced Informatics Network Architecture group at LAAS). The analysis of the simulation performances allows to extract practical rules for the estimation of

[269] P.Russer, M.Mongiardo, andL.B.Felsen, Electromagnetic field representations and computations in complex structures III: Network representations of the connection and subdomain circuits, Int. J. Numer. Modeling 15 (2002), 127–145.

the required resources, and for the task duration for a given structure on a given grid GC platform (see P49. in bibliography).

My personal involvement was in the support and understanding of numerical technique (in particular the TLM) for adapting it to the distributed computing environment.

4.2.2 Investigation of ESD on capacitive RF-MEMS switches

Junyu Jason Ruan *Thesis UPS – Université de Toulouse (2007-10).*
Advisor: Prof. R. Plana (UPS-LAAS), N. Nohlier (UPS-LAAS).
In collaboration with NKUA Athens (Prof. G. Papaioannou).
Personal involvment[262]: 20-30% (Mentoring on RF Design and modeling, physics of failure analysis)
Publications: 6 Int. Journals; 10 Int. Conferences; 3 National Conferences

The aim of this work was to investigate the electrostatic discharging (ESD) in RF-MEMS. The activity combined successfully the in-house expertise on RF-MEMS technology of the MINC group, the experimental and theoretical background on ESD available within the group ISGE (Prof. N. Nolhier) and finally the knowledge on dielectric charging physics, brought in through the collaboration with Prof. G. Papaioannaou from NKUA Athens.

Two major achievements are worth of note, the first investigation of ESD induced failure mechanisms in capacitive RF MEMS switches, and the development of an original accelerated test method for electrostatically driven MEMS devices.

Regarding the ESD, study on in-house RF-MEMS were carry out by means of most relevant stress protocols (transmission line pulsing – TLP, and human body model - HBM). The tests with TLP stresses allowed to find out for instance, that by increasing the stress voltage and the number of stress pulses, electric arching occurs at the electrostatic actuator over an increasing number of spots/locations, inducing a progressive degradation of the capacitive contact (Figure 4.3a) (see P5 in bibliography).

On the other hand the experimental observations carried out during the ESD investigations with the HBM technique have allowed to come up with an original and innovative acceleration method based on pulse-induced stresses. In fact the results have shown a clear speed up in the charge accumulation originated by pulsed stress with respect to conventional (square waveform) cycling tests (Figure 4.3b). This means that by playing with the field intensity and duration the charging mechanisms can be stimulated over a shorter test time. This principle was exploited to introduce an accelerated stress test (called pulse induced charging or PIC) that was finally implemented directly on a dedicated test-bench (see P41 in bibliography). The test procedure was implemented through and hardware board which could be finally mounted directly of the GSG-probe access within an environmental controlled test chamber.

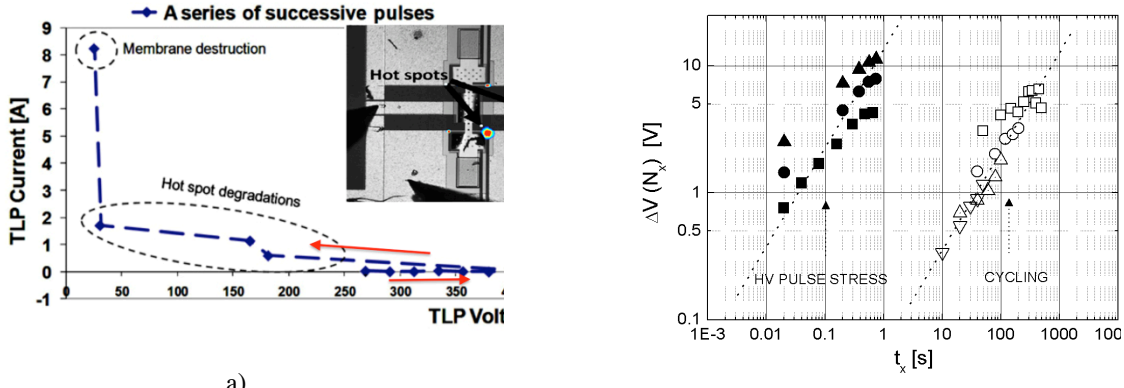

a) b)

Figure 4.3: ESD investigations on RF-MEMS: a) TLP I–V characteristic of an AlN-based TF-MEMS switch from LAAS. In the inset are shown the hot spots generated at 420 V; b) Measured shift of bias voltage for the two ageing methods, the pulses based stress (using and HBM-ESD test equipment – black filled marker) and the cycling one (using square waveform – empty marker). The plot shows an excellent correlation between the two trends (same slope) but with the former occurring much earlier than the former. The different marker indicates different switches used for the tests.

4.2.3 EBG Structures for Filtering Applications

Heba El-Sharaawy *PhD Thesis UPS - Université de Toulouse (2007-09).*
Advisor: Prof. R. Plana.
In collaboration with: Cairo University (Prof. M. ElSaid, Prof. E.A. Hashish).
Personal involvement[262]: 50% Thesis co-advisor.
Publications: 2 Int. Journals; 6 Int. Conferences; 2 National Conferences.

The aim of this activity was to explore planar periodic structures in order to miniaturize filters and eventually, study possible ways to implement frequency reconfigurability/tuning.

Electromagnetic bandgap (EBG) structures have many interesting features for this aim. The most important features are the presence of frequency "bandgap", and the slow wave behavior, which were exploited to introduce frequency selectivity and miniaturization respectively. A second design, which was explored for the same aim, were the defected ground structures (DGS). Different equivalent circuits have been proposed to introduce and model reconfigurable dumb-bell DGS structures on CPW technology eventually used to design reconfigurable multi-stopband and band-pass filters, which have been fabricated and successfully tested (see Figure 4.4).

The structure was analyzed by RLC lumped element model and using the slotline closed form expressions while configurability was implemented through PIN diodes (see P25 in bibliography).

A second part of this thesis was dedicated to miniaturization and higher order harmonics suppression of ring resonators in microstrip technology (presciently studied at Cairo University). A final design based on optimized location and geometry of folded stubs has allowed to achieve 72% of overall size reduction, while the additional EBG patterning on the ground plane pushed the reduction down to 85% (see P10 in bibliography).

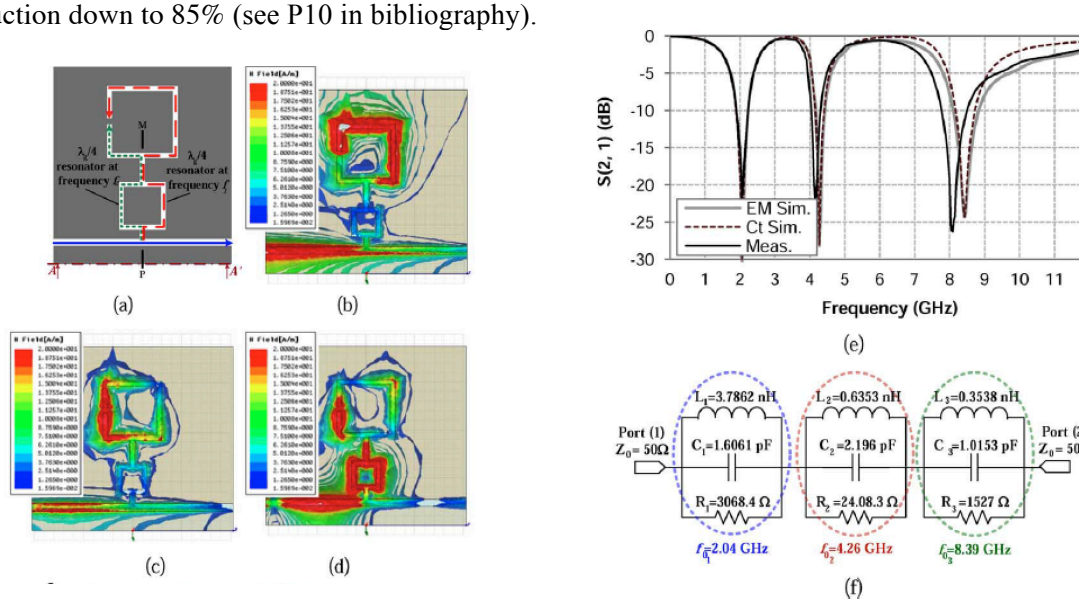

Figure 4.4: Example of DGS structure: (a) Layout (half-view) of the DGS for configuration four (S1 and S2 are OFF, and S3 is ON). (b) Magnetic current distribution at 2.04 GHz, (c) at 4.26 GHz, (d) at 8.4 GHz. (e) EM, and circuit simulated and measured S-Parameters. (f) Equivalent circuit model.

4.2.4 Investigation of metamaterial for reconfigurable microwave circuits

Badredine Ouagague *PhD Thesis UPS – Université de Toulouse (2007-13)*
Advisors: Prof. R. Plana and Dr. F. Coccetti.
Personal involvment[262]: 50% (Design and modeling of SIW)
Publications: 8 Int. Conferences; 4 National Conferences.

This work was devoted to the investigation of metamaterials (MM) for the possible use in RF circuit miniaturization and, eventually made reconfurable by the insertion of variable element (MEMS and BST varactors). For this purpose the composite right left handed (CRLH) configuration was chosen for its simple implementation on CPW technology and the in-house silicon based manufacturing process. As an example of results a reference CRLH cell composed of two series interdigital capacitors (IDC) with a shunt stub-inductor has been modified by adding a new stub capacitor that provides a new degree of freedom on the definition of the LH and RH branches by opportunely fixing the lower and higher cut-off frequencies[270]. The reconfigurability is introduced by replacing the IDC with a MEMS switchable capacitor that allows a variable value of series capacitance (Figure 4.5a and b). The dispersion diagrams covering all the configurations are extracted from equivalent circuit models (Figure 4.5c). The results show up to 15 % of frequency tunability while adding the stub capacitor and up to 150 % while changing the MEMS capacitor state. This approach proves the feasibility of reconfigurable network based on this concept.

Further part of this work have focused on the use of the MM to implement miniaturized circuits. Designs combining the CRLH structure with split ring resonators (SRR)[271], have proven the validity of this approach especially in the low frequency bands and allowed the design of compact bandpass filter for space application (example: 4x2 sqcm for 300MHz bandwidth centered around 150MHz and with 50dB rejection at 20MHz out of band).

The activity on MM have been interesting as exploration but have also demonstrated the serious limitation of this approach which suffers of significant losses introduced in actual implementations.

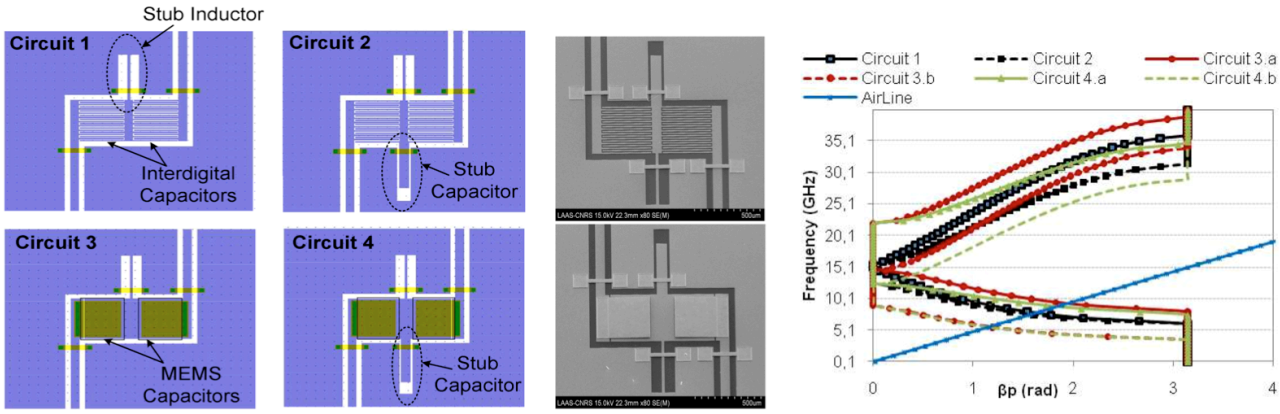

(a) (b) (c)

Figure 4.5: Example of investigated CRLH unit cell: a) Four different implementations based on: IDC capacitor and closed stub inductor to realize the elementary cell (circuit 1), addition of the open stub capacitor to introduce a design degree of freedom in reaching the balanced case (circuit 2), introduction of the MEMS variable capacitor instead of the IDC to introduce frequency reconfigurability (circuit 3) and final design with open stub capacitor and MEMS capacitor (circuit 4); b) Actual implementation on LAAS silicon technology for the fixed case (top) and MEMS version (bottom); c) measured dispersion diagram characteristics extracted from the lossless equivalent circuit model of the different structures (a and b indicate up and down position in the corresponding MEMS implementations).

[270] C. Caloz and T. Itoh, Electromagnetic Metamaterials, Transmission Line Theory and Microwave Applications, A John Wiley & Sons, 2006

[271] F. Martin, F. Falcone, J. Bonache, R. Marques, and M. Sorolla, "Miniaturized coplanar waveguide stop band filters based on multiple tuned split ring resonators," IEEE Microwave and Wireless Components Letters, vol. 13, Dec. 2003, pp. 511-513.

4.2.5 Development of novel compact wideband Butler matrix in SIW technology

Ahmed Ali *PhD Thesis INP - Université de Toulouse (2007-10).*
Advisor: Prof. H. Aubert. In collaboration with: CNES (Dr. N. Fonseca) and Ecole Politechnique de Montreal (Prof. K. Wu).
Personal involvement[262]: 10-20% (Mentoring on design and modeling of SIW).
Publications: 1 Int. Journal; 5 Int. Conferences; 1 National Conferences.

This study concerned the development of microwave components in Substrate Integrated Waveguide (SIW) technology. This is a relatively new technology, is attracting considerable attention because it combines the advantage of rectangular waveguides (such as low losses), with those of PCB technology (manufacturing simplicity, low costs, reduced size and weight). For this reasons it suites perfectly with the heterogeneous integration approach of future smart RF front-end. The work reported here tackles the innovative implementation on SIW of beam-forming feeding network, such as the Nolen and the Buttler matrices (see Figure 4.6). These solutions have been proposed and implemented o SIW technology. These networks make use of basic components, such as directional couplers and phase shifters which design was originally optimized through a compact multilayer approach (leading to the so-called Substrate Integrated Circuits, or SICs).

An important aspect of this thesis has been the tide collaboration with the end user (the French national space agency - CNES), which has provided a valuable expertise and practical feedback and the other academic partner, namely the Ecole Politechnique de Montreal and in particular with the Poly-GRAMES group of Prof. K. Wu who has been instrumental in the practical manufacturing of the final prototypes.

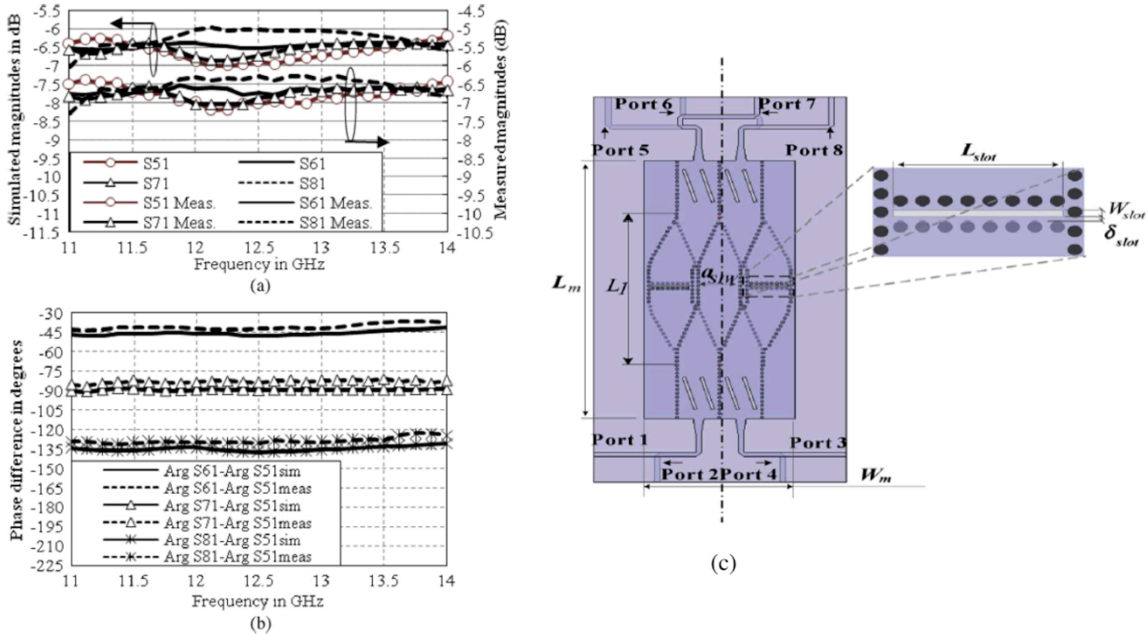

Figure 4.6: Novel wideband two layer 4x4 Butler matrix designed and realized by SIW. Isolation characteristics better than 15 dB with input reflection levels lower than 12 dB are experimentally validated over 24% frequency bandwidth centered at 12.5 GHz. Measured transmission magnitudes and phases exhibit good dispersive characteristics of 1 dB, around an average value of 6.8 dB, and 10 with respect to the theoretical phase values, respectively, over the entire frequency band. The impact of the measured transmission phases and magnitudes on the radiation pattern of a 4-element antenna array is also investigated. a) Scattering parameters versus frequency for the optimized Buttler matrix (case feeding from port 1), simulated (left axis) and measured (right axis) coupling magnitudes, b) Simulated and measured phase at the output ports with respect to that of port 5, c) Complete layout of the developed 4 x 4 two-layer SIW Butler matrix, including microstrip to SIW transitions.

4.2.6 Reconfigurable RF circuits based on ferroelectric Materials

Dr. Rosa De Paolis *(CNRS - Post Doctoral contract)*
In collaboration with: CNRS-ICMCB Bordeaux (Dr. M. Maglione and Dr. S. Payan) and ST-Microemectronics Tour (Dr. G. Guegan).
Personal involvement[262]: 10-20% (RF design-modeling and characterization advisor)
Publications: 1 Int. Journals; 1 Int. Conferences; 1 National Conference.

Owing to their characteristic to tune the dielectric permittivity under applied electric field ferroelectric materials represent valid candidate for tunable variable capacitors and an interesting counterpart to MEMS technology. Driven by the need of tunable component (especially capacitors) to enhance capabilities and miniaturization of future agile hand held wireless communication equipment the research activities (explored within the ANR project ABSYS2), have been focusing on two cornerstones, the development of low loss ferroelectric material compatible with industrial production standards, and the definition of innovative capacitance design respectively. The material development (synthesis done essentially by ICMCB and ST Microelectronics with full RF test at LAAS), has hinged on $Ba_xSr_{1-x}TiO_3$ (BST) as key material and it has investigated the benefit of doping elements (such as manganese and or copper) to control and eventually reduce the contribution of charged defect on leakage current. Results have allowed to reach state of the art material properties with loss tangent below 1% (See example in Figure 4.7). For what concerned the design of innovative variable capacitors the activities have been lead by LAAS with an approach combining BST with standard lower losses dielectric (example SiO2) and by adopting multilayer high-density capacitor design and suitable topological scheme (series and parallel connection). In this case the challenge was to accurately extract the material parameters (ε_r and *tan* δ) over wide working conditions range (frequency DC-60GHz, bias -20 to +20V, and temperature -40 to 80°C) and to optimize tunability by keeping high overall quality factor. The manufacturing process optimization was a challenging issue since material stacking by means of an industrial process was at stake. The variable capacitance designed at LAAS was exploited to design reconfigurable RF circuit (modeled and characterization done at LAAS) (Figure 4.8– see P50 in bibliography). The activities carried out at LAAS on ferroelectric tunable capacitance profit from the experience in material characterization (DC and RF) on the one hand and on the other from the know-how in design and modelling gathered on reconfigurable circuit and RF-MEMS in the past years. They show in synthesis a way forward on how to capitalize a rich multidisciplinary background to handle emerging technologies and materials.

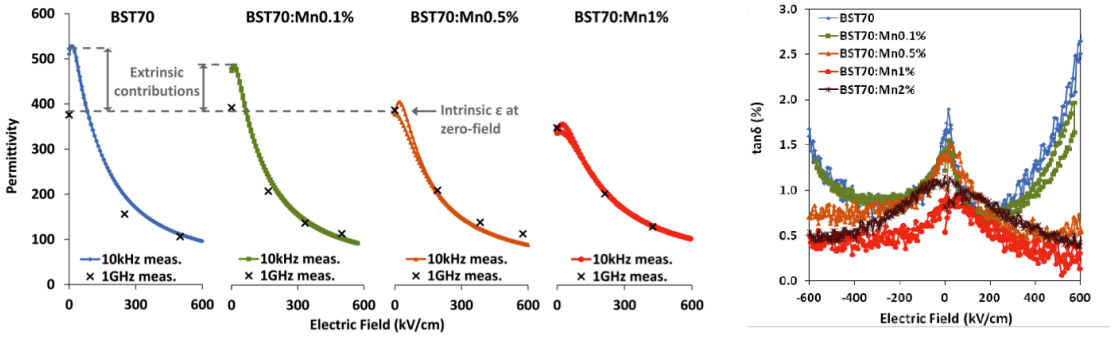

(a) (b)

Figure 4.7: Dielectric measurements: a) Comparison of the low and high frequency permittivity under electric field (respectively 10 kHz and 1GHz) for the undoped BST, and Mn0.1%, Mn 0.5%, and Mn1% doped samples. The vertical scale is the same for each chart. The extrinsic contribution to the low frequency permittivity is observed for

the undoped and Mn0.1% samples. b) dielectric losses *vs* electric field plot measurements at 10kHz as a function of electric field for undoped and doped BST70 from Mn 0.5%, and Mn 2%.

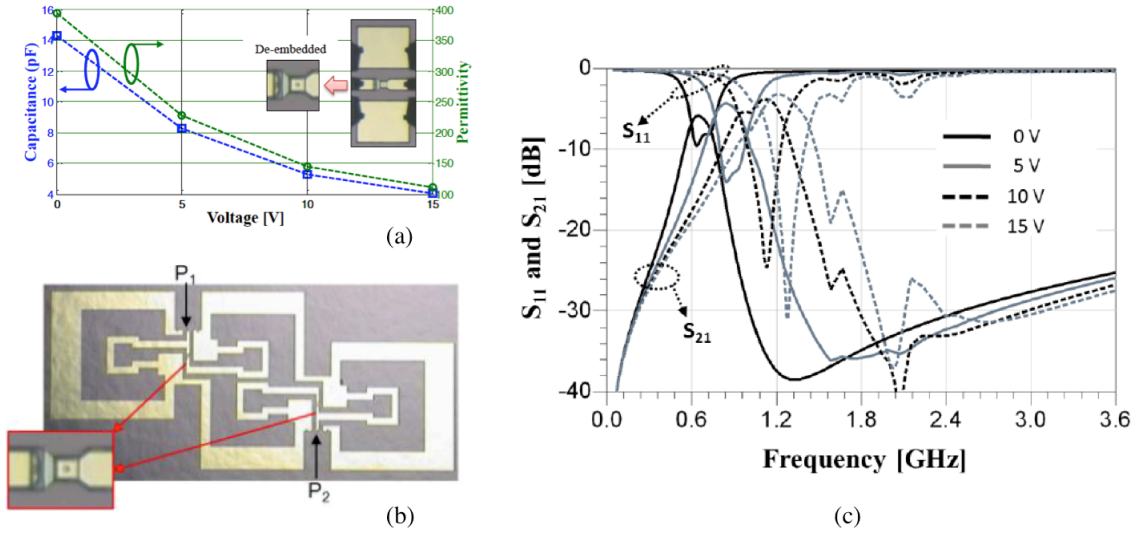

Figure 4.8: Example of manufactured and tested devices. a) BST variable capacitor performances (design and test structure given in the inset). The voltage-dependent material properties (capacitance, tunability) have been extracted and used in the development of a specific MIM capacitor that, after a first fabrication test, shows a measured tunability of 72% under 0-15 V bias. b) tunable band pass filter implemented by using lumped elements coupled resonators, thus allowing a compact size (total size 2.53 x 5.88 mm^2) with respect to conventional λ/4 resonator lines. The analysis of some preliminary experimental results shows a tuning of 88% (657 MHz-1235 MHz) of the filter center frequency and an almost constant fractional bandwidth of 30% upon the application of a 0-15 V bias. The insertion loss is between 5.8 and 3.2 dB, and the return loss is better than 9 dB, c) Band pass filter performances based on measured variable capacitor ($|S_{11}|$ (dotted line) and $|S_{21}|$ (solid line) of the filter at different voltages).

4.2.7 Investigation of inkjet printed CNTs RF interconnects.

Dr. S. Pacchini *(CNRS - Post Doctoral contract), and* ***Dr. R. De Paolis*** *(CNRS - Post Doctoral contract)*
In collaboration with: CNRS-CIRIMAT (Dr. E. Flahaut) and Georgia Institute of Technology (Prof. M. Tentzeris).
Sponsoring projects: NATI (MP Region 2009) NANOCOMM (ANR NANO-INNOV/RT)
Personal involvement[262] (2009-12): 10-15% (RF design-modeling and characterization)
Publications: 1 Int. Journals; 3 Int. Conferences; 2 National Conference.

The purpose of these studies was to explore the potentialities of CNT networks deposed by selective transfer (inkjet printing), for the implementations of RF interconnects.

Double Wall Carbon Nanotubes (DWNTs synthesized at CIRIMAT by Dr. E. Flahaut) network layers have been patterned using inkjet transfer printing process developed at LAAS (Dr. N. Fabre – group TEAM). The conductive characteristics of carbon nanotubes (CNTs) are considered as promising candidates for transmission line as well as microelectronic interconnects of arbitrary pattern. In these activities, the understanding of the transmission properties in DC and RF of interconnects made of inkjet printed network of DWCNT were at stake. The structures consisted in DWNTs patterns deposited in a CPW hosting test vehicles and then characterized through 2 ports current-voltage measurements, low frequency and high frequency from 40 MHz up to 40 GHz. Results showed that the increasing number of inkjet overwrites, results in a adjustable and possibly arbitrarily low value of resistance (Figure 4.9, see P23. in bibliography).

An electrical model for the DWCNT structures was also extracted from measured structures demonstrating the presence of electrical resonances likely attributed to, curled CNTs and electrical coupling between the different overwritten layers (Figure 4.10, see C86. in bibliography).

These studies and the extraction of equivalent lumped element models were further extended to samples coming from GTECH and used for implementation of RF sensing structures (see C97. in bibliography).

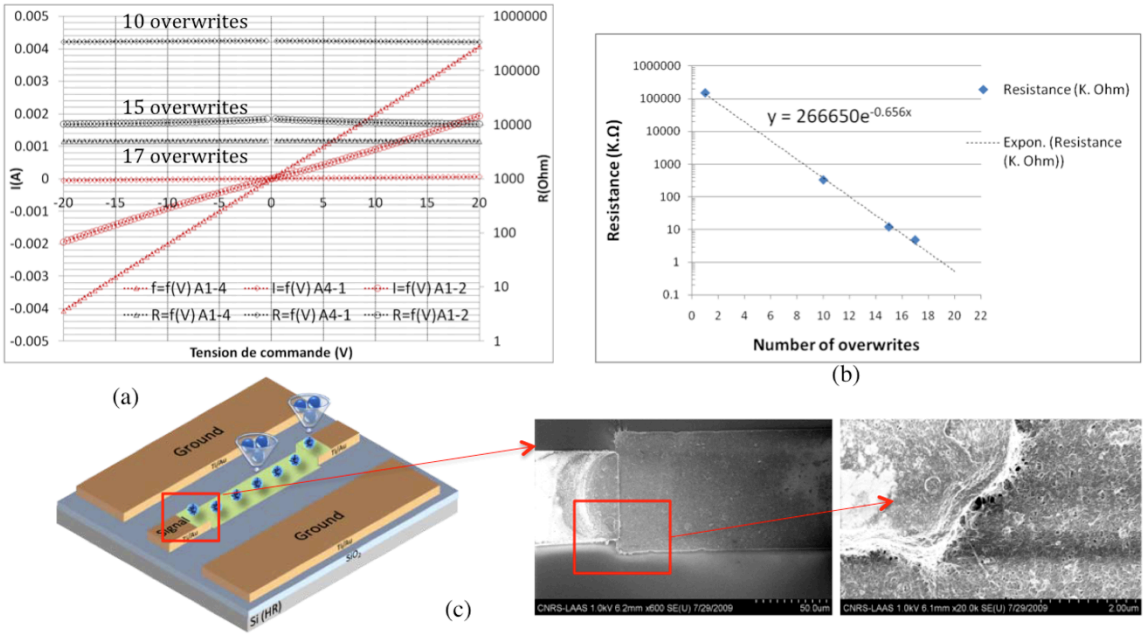

Figure 4.9: Measured electrical characteristic of DWCNT interconnects: a) I-V characteristics for increasing number of overwrites, b) extracted resistance characteristics for increasing number of overwrites, c) schematic view of the test structure and close up (SEM view) on the metal-CNT network transition.

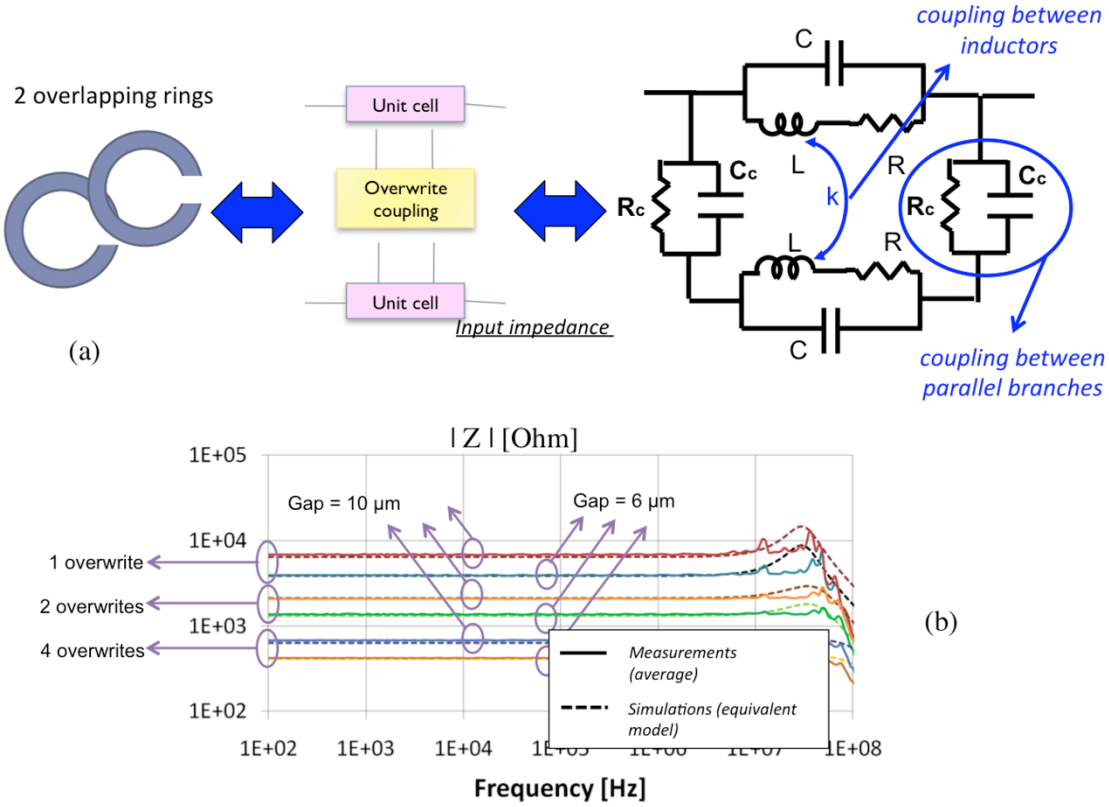

Figure 4.10: Modeling of DWCNT interconnections: a) schematic view of two partially overlapping curled CNT, and its possible interpretation by lumped element circuits, modeling the resonance and the coupling interlayers, b) Comparison results between measurements and model up to 100MHz for different CPW gap distance and number of overwrites.

4.3 Curriculum Vitae:

Fabio Coccetti, PhD Foligno (Italy) on October 19th 1972

Work address:	Fialab / CNRS-LAAS 7, avenue du Colonel Roche F-31077 Toulouse Cedex 4 France
Phone:	+33 (0)5 61 33 79 00
Mobile:	+33 (0)6 73 53 78 55
Fax:	+33 (0)5 61 55 69 69
Email:	coccetti@laas.fr fabio.coccetti@fialab.eu
Web:	http://homepages.laas.fr/fcoccett/
Skype:	fabio.coccetti

Qualifications - Professional experience

- MS Degree (Electronic Engineering Laurea), Università di Perugia, Perugia – Italy (Prof. M. Mongiardo) - November 1999
- Postgraduate Scholarship at the University of Michigan (UoM), Ann Arbor – USA (Prof. L. Katehi) February 2000 – July 2000
- Postgraduate Scholarship at DaimlerChrysler (DC) AG (Dr. F. Luy) - February 2002 – May 2002
- Ph.D. degree in Electrical Engineering and Information Technology Technische Universität München, Munich, Germany (Prof. P. Russer) July 2001 July 2004
- Research Scientist and teaching assistant at Technische Universität München (TUM), Munich, Germany (Prof. P. Russer) - July 2000 - July 2004
- Postdoctoral position at the Laboratoire des Analyse et Architecture des Système (LAAS – CNRS) goup Micro and Nanosystems for wireless communications MINC (Prof. R. Plana), Toulouse - France - September 2004 – September 2005
- R&D project manager at Fialab (former Novamems) Toulouse France (Dr. X. Lafontan)
- Associated research scientist within the group MINC at LAAS-CNRS) - September 2005 – Present

Scientific production / Publications: (see Bibliography in appendix 4.4)

- Book chapters (5),
- Journals (50)
- International conferences (100)
- National Conferences (18)

R&D activities:

- Project management (coordination):
  - **European Commission** (FP6 2005 – 2007) - Project title: European Network of Excellence on RF-MEMS and RF-Microsystems" (AMICOM) - Consortium of 25 organizations from 12 EU countries for a total investment of 7.5 M€ of which 5.5 M€ funded by the European Commission under the 6th Framework Program – FP6).

- **National Research Agency (ANR PNANO Program** 2008-2011) - Project title „Reliability of RF-MEMS ohmic and capacitive switches“ (FAME Ref.: ANR/PNANO2007/059-05). Involving 4 French organizations: ARMINES, Thales Alenia Space, Novamems, CEA-LETI). Budget 1.3M€ with 56% funding from ANR
- **RTRA (Fondation STAE** 2008-2011) Project title: “Miniaturized smart systems for aeronautic and space applications” Involving 2 french laboratories (LAPLACE and CIRIMAT Toulouse) and 2 external organizations (NKUA Greece, and University of Toronto Canada). Total budget 1.2M€ with 50% funding from RTRA
- **Regional Grant (Région Midi-Pyrénées** 2008-2010) - Project title (FITMEMS): “Fiabilité et test de MEMS RF pour les applications de systèmes embarqués”. Other regional MP organization included: Novamems, Epsilon, Freescale-Toulouse and Thales-Alenia-Space.

▪ Project involvement (PI):

- ***Rhode & Schwarz GmbH***, Munich – Germany (2000 – 2002), Center of Competence for Microwave Development and Production led by Mr. C. Evers. Topic: RF-MEMS switches for application in step attenuators: from the proof of concept for novel design to fabrication process development by means of in-house R&S facilities.
- ***Robert Bosch GmbH***, Stuttgart – Germany (May 2002 – October 2003) FV/FLO Department led by Dr. O. Riuss. Topic: Automotive radar systems front-end in SOI technology in the 70-140 GHz frequency range.
- ***Siemens AG***, Munich – Germany (March 2003 – October 2003) Corporate Technology Materials & Manufacturing Division Ceramics led by Dr. R. Matz. Topic: Design and optimisation of HiPERLAN Front-End at 5GHz in LTCC technology.
- ***European Space Agency*** *(ESA)*, (2003 – 2004) Project title: Microwave Electrostatic Micro-machined devices for On-Board Applications (0-40GHz). Other involved organizations: Universita di Perugia (Italy), FBK (Italy), TUM (Germany). ESA project contact: F. Deborgies.
- **European Commission FP6** (2006 – 2007)**:** European Specific Support Action project title: “Applied Research Roadmaps for RF Micro/Nano-systems Opportunities” (ARRRO) Consortium of 4 EU organizations, funded by FP6 and coordinated by Wicht Technology Consulting, Munich – Germany.
- ***French Ministry of Industry*** (2006 – 2009) Project title: “Development of Piezoelectric-Based MEMS Binary-State Capacitors for Application to Reconfigurable RF Networks”, (SPRINT). Other 2 partners involved: CEA-LETI and Freescale (Tempe – USA, scientific coordinator).
- ***European Space Agency*** (ESA) (2007-2012) project title “High reliability MEMS for redundancy switches in space application” (REDS - Ref.: AO/1.5288/06/NL/GLC). Other 3 organizations involved: Thales Alenia Space, CEA-LETI (scientific coordinator) and NKUA (Gr). ESA project contact: F. Deborgies.
- ***European Defence Agency*** (EDA - CAPTECH01 Program) (2007-2011) Project title: “Manufacturing sensitivity analysis of RF-MEMS Switches” (POLYNOE - Ref: 2006-74165-4-DCR/STI). Other 7 organizations involved: MEMSCAP, MBDA, EADS (scientific coordinator) Epsilon (from France), QinetiQ, Univ. of Warwick and Univ. of Loughborough (from UK).
- ***ANR Program Blanc*** (2007-2009) Project title: “Multiscale modeling: from Electromagnetism to the GRID” (MEG - Ref.: Projet ANR-06-BLAN-0006-01). In collaboration with ID Lab (Grenoble).
- ***ANR VERSO Program*** (2011-2013) Project title „ Advanced BST based systems: new RF designs “ (ABSYS2 Ref.: ANR/VERSO 2010). Involving 3 French

organizations: CNRS-ICMCB, ST Microelectronic, CNRS-LAAS). Budget 1.92M€ with 43% funding from ANR

- **ThalesAleniaSpace** Toulouse France, "Absortive switches in V band based on CMOS RF-MEMS" (2011-2012) In collaboration with IHP Germany and TAS. Budget: 22K€ entirely from TAS.

Educational activities

- **Teaching activities in Germany** (2001-04): more than 100hr teaching (10% CM, 60% TD et 30% TP) in English for International master of science on High Frequency engineering at TUM Munich.
- **Teaching activities in France** (from 2013): 16hr CM (conference on RF nanotechnology) (etudiantes 2e and 3e anneé microonde INP-ENSEEIHT et 14hr TD 1er année EM INP-ENSEEIHT).
- **Teaching in International Schools (from 2007)**: 2-4hr course on « RF-MEMS technology (modeling, design and reliability) » at the annual "International Summer School on RF-MEMS and RF-MST" (from 2013 belonging to to the EUMA European School of Microwave).
- European Microwave Lectures on "From RF-MST to RF Nanotechnology, the way toward nano enabled RF intelligence" appointed by EUMA in April 2013 for a duration of 3 years.
- More than 30 oral (invited) talks at international conference and workshops (see Bibliography).

Involvement in PhD Thesis

- Co-direction:
  - **Mr. Fadi Kahlil** (June 2006 - December 2009) - Thesis title: „_Multi-scale modeling: from electromagnetism to grid",Université de Toulouse – LAAS-CNRS – December 2009 http://tel.archives-ouvertes.fr/tel-00448305. Advisors: Prof. H. Aubert and Dr. F. Coccetti
  - **Ms. Heba Badr-El-Din-Shaarawy** (Octobre 2007 - December 2009) - Thesis title: „Electromagnetic bandgat structure for filter applications",Université de Toulouse – LAAS-CNRS December 2009 http://tel.archives-ouvertes.fr/tel-00446721 Advisors: Prof. R. Plana and Dr. F. Coccetti.
  - **Mr. Usama Heiba-Zaghloul** (October 2007 – September 2011) : Thesis title: „Nanoscale and macroscale characterization of the dielectric charging phenomenon in electrostatically driven MEMS devices",Université de Toulouse – CNRS-LAAS – September 2011 (URL: http://thesesups.ups-tlse.fr/1428/1/2011TOU30085.pdf). Advisors: Prof. R. Plana and Dr. F. Coccetti.
  - **Ms. Nuria Torres Matabosh** (October 2009 – January 2013) – Thesis Title: "Design for reliability applied to RF-MEMS devices and circuits issued from different TRL environments", Université de Toulouse – LAAS-CNRS – Januray 2013 Advisors: Dr. J.L Cazaux and Dr. F. Coccetti.
  - **Mr. Badredine Ougague,** (October 2008 – December 2011) – Thesis Title: "Etude théorique et expérimentale des métamatériaux pour la conception des circuits microondes reconfigurables", Université de Toulouse – LAAS-CNRS – Defence foreseen on December 2013 Advisors: Prof. R. Plana and Dr. F. Coccetti.

- **Mr. Giancarlo Vincenzi** "Investigation of microwave transport in graphene based devices", Université de Toulouse – LAAS-CNRS – Defence foreseen on Janvier 2014 Advisors: Prof. R. Plana and Dr. F. Coccetti.

- **Mentoring/Collaboration:**
  - **Mr. Ahmed Ali** (October 2006 - May 2010) – Thesis title: „ On the development of novel multi-layer passive components and the implementation of compact wideband two-layer butler matrix in SIW technology", University of Toulouse – LAAS-CNRS (May 2010) http://tel.archives-ouvertes.fr/tel-00542002. Advisor: Prof. H. Aubert.
  - ***Mr. Jinyu Jason Ruan*** (October 2006 - July 2010) – Thesis title: „ Investigation and modelling of the impact of electrostatic discharges on capacitive RF MEMS switches », Universite de Toulouse – LAAS-CNRS (July 2010) http://tel.archives-ouvertes.fr/tel-00512333 Advisors: Prof. R. Plana and Prof. N. Nohlier.
  - ***Mr. Mohamed Matmat*** (October 2006 - September 2010) Thesis title: „Pour une approche complète de l'évaluation de fiabilité dans les microsystèmes", University of Toulouse (September 2010), http://tel.archives-ouvertes.fr/tel-00538717. Advisors: Prof. J.Y. Fourniols.

- **PhD Thesis Jury member:**
  - Mr. Amir Rashid, Thesis title: „Electromagnetic modeling of large and non-uniform planar array structures using Scale Changing Technique (SCT)", University of Toulouse – LAAS-CNRS (July 2010) - http://tel.archives-ouvertes.fr/tel-00525070/fr/ Advisor: Prof. H. Aubert (INP).
  - Mr. Julien Givendraud, Thesis title: "L'étude, la conception et la fabrication des circuits et dispositifs micro-ondes à base des matériaux intelligents type VO2", University of Limoge – Xlim (April 2010). Advisors: P. Blondy (XLim), A. Crunteanu (XLim) and C. Champeaux (SPCTS).
  - Mr. Romain Stephanini, Thesis Title: "Commutateurs MEMS et leurs Applications aux Filtres Accordables Fort Q" University of Limoge – Xlim (Novembre 2011) – Advisors : M. Chatras matthieu.chatras@unilim.fr, P. Blondy (XLim).
  - Mr. Gang Li, Thesis title: "Physical model for charge accumulation and technology development for robust RFMEMS swicthes switches" - University of Oslo (April 2013). Advisor: Prof. X. Chen Xuyuan.Chen@hive.no (Vestfold University College).
  - Ms. Hong Lue, Thesis Title: "Modélisation par éléments finis du contact ohmique de microcommutateur MEMS", University of Toulouse – LAAS-CNRS (May 2013) - Advisor: Prof. S. Colin (INSA), D. Leray - dimitri.leray@insa-toulouse.fr (INSA).

Other Training and Mentoring activities:

- Master level: Vitale Ciabatta (TUM 2002) - Benoit Dufur (LAAS 2009) - Rosa De Paolis (LAAS 2010) - Laura Corchia (LAAS 2010) - Silvia Fabiani (LAAS 2010), Ruben Acevedo (LAAS 2012), Luciano Mariani (LAAS 2013).

- Post doc level: L. Hamelin (2009-10), H. Wang (2009-11), G. Deligeorgis (2010-11), R. Depaolis (2011-12).

Organization and scientific animation:

- Organization of Scientific Events:
  - Workshops and Focused sessions at international conferences (IMS, EUMW, ESREF, MEMSWAVE).
  - International Summer School on RF-MEMS and RF-MST (Responsible/Organizer – every 2 years at LAAS with 20-30 participant and 10-15 lecturers from worldwide)
  - European cluster meeting on RF microsystem technology (co-organizer with the European Commission from 2006)
  - Conference treasurer for the European Microwave Week Paris 2015
- Reviewing expertise activities:
  - Reviewer International journals: IEEE MTT-Transaction, IEEE-MWCL, JMEMS, IEEE-TED, EUMA-IJMWT, Elsevier-Microelectronic Reliability, ….
  - Guest Editor: IEEE-MTT-Transaction (Dec. 2010), IEEE-Microwave Magazine (Nov. 2010, Dec 2011), EUMA-IJMWT (Aug. 2011), IEEE-MCWL (Jan. 2012).
  - Research programs: ANR-P2N and ANR bourse cifre (France); NSERC (Canada) FP7-ICT (European Commission 2011-2013).

Technical Review Activities:

- Journal/Letters reviewer: IET Microwaves, Antennas & Propagation, IEEE IEEE Microwave and Wireless Components Letters, IEEE-ASME Journal of MEMS, IEEE Microwave Theory and Technology, EuMA Int. Journal of Microwave Wireless Technology, IEEE Electron Device Letter, Elsevier Microelectronic Reliability
- Conferences reviewers: EUMW (EUMA), MTT-IMS (IEEE), ESREF, MEMSWAVE, SiRF (IEEE).
- Program Evaluator: Project reviewer for the European Commission 7th Framework Program (http://cordis.europa.eu/fp7/home_en.html)- Fond de Recherche Nature et Technologie Quebec (http://www.fqrnt.gouv.qc.ca)

Affiliations:

- Member of the Institute of Electrical and Electronic Engineers (IEEE)
- Member of the European Microwave Association (EUMA)
- Member of the Technical Program committee of the „European Microwave Week“ since 2009 (Sub-committee chairman in 2010, 2011, 2012)
- Member of the Technical Program Committee of the International Microwave Symposium (IMS) (since 2010)
- Technical Program Committee member of the “European Symposium on Reliability of Electron Devices, Failure Physics and Analysis” (ESREF) (since 2010).
- Technical Program committee member of the “Journée National Microondes” (since 2007).

Special achievements:

- Co-founder of the EUMA Topical Group on „RF MEMS and RF-MST“ on Janvier 2010.
- Co-founder and Chairman (from october 2013) of the IEEE MTT-S Technical committee on „RF Nanotechnology“.
- EUMA European Microwave Lecturer “From RF-MST to RF Nanotechnology, the way toward nano enabled RF intelligence” 2013-2015.
- Member of the « Observatoire des Micro et NanoTechnologies » (OMNT unité mixte de service du Commissariat à l’Energie Atomique de Grenoble et du Centre National de la Recherche Scientifique) from June 2013.

4.4 Bibliography

4.4.1 Review and Journal Articles (peer reviewed):

P1. F. Coccetti, W. Dressel, P. Russer, L. Pierantoni, M. Farina and T. Rozzi, "Accurate modelling of high frequency microelectromechanical systems (MEMS) switches in time- and frequency-domain", *Advances in Radio Science*, vol.1, pp.: 135-138, 2003

P2. M. Exarchos, V. Theonas, P. Pons, G.J. Papaioannou, S. Melle, D. Dubuc, F.Coccetti, R. Plana "Investigation of charging mechanisms in metal-insulator-metal structures", Elsevier Journal of Microelectronics Reliability, Vol.45, N°9-11, pp.: 1782-1785, September-November 2005

P3. D. Lukashevich F. Coccetti and P.Russer, "System Identification and Model Order Reduction for TLM Analysis", International Journal of Numerical Modelling: Electronic Network, Devices and Fields – John Wiley & Sons, Ltd. Jan-Apr, 2007, pp.: 75-92

P4. J. Ruan N. Nolhier, M. Bafleur, L. Bary, F. Coccetti, T. Lisec, R. Plana,"Electrostatic discharge failure analysis of capacitive RF MEMS switches", Elsevier Journal of Microelectronics Reliability, Vol.47, N°9-11, November 2007, pp.: 1818-1822

P5. J. Ruan, G. Papaioannou, N. Nolhier, N. Mauran, M. Bafleur, F. Coccetti, R. Plana, "ESD failure signature in capacitive RF MEMS switches," Elsevier Journal of Microelectronics Reliability, Vol.48, N°8-9, November 2008, pp.: 1237-1240

P6. F. Coccetti, R. Plana, "Simultaneous electro-thermal experimental analysis of RF-MEMS switches for high microwave power handling",Physica Status Solidi (a). Applications and Material Science, Vol.205, N°11, pp.: 2647-2650, December 2008

P7. F. Coccetti, D. Peyrou, M. Al-Ahmad, V. Puyal, P. Pons, H. Aubert, R. Plana, "RF MEMS: status and perspectives »,(Invited paper) 3rd International Conference on Micro-Nanoelectronics, Nanotechnology and MEMS, Physica Status Solidi C, Vol.5, N°12, pp.: 3822-3827, November 2008

P8. M. Dragoman, G. Konstantinidis,A. Kostopoulos, D. Dragoman, D. Necoloiu, R. Buiculescu, R. Plana, F. Coccetti, H. Hartnagel,"Multiple negative resistances in trenched structures bridged with carbon nanotubes", Applied Physics Letters, Vol.93, N°4, September 2008, doi: 10.1063/1.296336, pp.: 043117-1-043117-3

P9. H. El-Shaarawy, F. Coccetti, R. Plana, M.El-Said, E. Ahashish, "Defected ground structures (DGS) and uniplanar compact-photonic band gap (UC-PBG) structures for reducing the size and enhancing the out-of-band rejection of microstrip bandpass ring resonator filters", WSEAS Transactions on Communications, Vol.11, N°7, September 2008, pp.: 1112-1121

P10. H. El-Shaarawy, F. Coccetti, R. Plana, M. El-Said, E.A. Hashish, "Compact bandpass ring resonator filter with enhanced wide-band rejection characteristics using defected ground structures",IEEE Microwave and Wireless Components Letters, Vol.18, N°8, September 2008, pp.: 500-502

P11. J. Ruan, E. Papandreou. M. Lahmandi, M. Koutsoureli, F. Coccetti, P.Pons, G. Papaioannou, R. Plana, "Alpha particle radiation effects in RF MEMS capacitive switches", Elsevier Journal of Microelectronics Reliability, Vol.48, N°8-9, 2008, pp.: 1241-1244

P12. D. Girbau, L. Pradell, A. Lázaro, D. Peyrou, P. Pons, P. Calmon, R. Plana, F. Coccetti "A Method for Characterization of Intermodulation Distortion produced in MEMS switches," Microwave and Optical Technology Letters, Vol.51, N°2, pp.: 526-529, February 2009

P13. J.Y. Choi, J. Ruan, F. Coccetti, S. Lucyszyn "Three-dimensional RF MEMS switch for power applications,"IEEE Transactions on Industrial Electronics, Vol.56, N°4, pp.1031-1039, April 2009

P14. A. Ali, H. Aubert, N. Fonseca, F. Coccetti, "Wideband two-layer SIW coupler: design and experiment,"Electronics Letters, Vol.45, N°13, June 2009

P15. F. Khalil, H. Aubert, F. Coccetti, P. Lorenz, and R. Plana, "Grid- Based Global Electromagnetic Simulation Tool for Parametric Distributed Analysis of Array Antennas", Progress In Electromagnetics Research M/, Vol. 10, 1-12, 2009

P16. M. Matmat, F. Coccetti, A. Marty, R. Plana, C. Escriba, J.Y. Fourniols, D. Esteve,"Capacitive RF MEMS analytical predictive reliability," Elsevier Journal of Microelectronics Reliability *Vol. 49 Issues 9-11, Sept-Nov 2009 pp.:* 1304–1308

P17. U. Zaghloul, , G. Papaioannou, F. Coccetti, P. Pons and R. Plana, "Dielectric charging in silicon nitride films for MEMS capacitive switches: Effect of film thickness and deposition conditions," Elsevier Journal of Microelectronics Reliability Vol. 49 Issues 9-11, Sept-Nov 2009 pp.: 1309-1314

P18. M. Dragoman, D. Dragoman, F. Coccetti, R. Plana, and A. Muller, "Microwave switches based on graphene," Journal of Applied Physics, vol. 105, no. 5, p. 054309, 2009

P19. F. Khalil, C. J. Barrios-Hernandez, A. Rashid, H. Aubert, Y. Denneulin, F. Coccetti and R. Plana, "Parallelization of the Scale-Changing Technique in Grid Computing environment for the electromagnetic simulation of multi-scale structures," Int. J. Numerical Modeling, 2011; 24:57–76 (2010) in Wiley Online Library DOI: 10.1002/jnm.760

P20. M. Dragoman, D. Neculoiu, D. Dragoman, G. Deligeorgis,G. Konstantinidis, A. Cismaru, F. Coccetti, and R. Plana, "Graphene for Microwaves," IEEE Microwave Magazine, December 2010 pp. 81-86 DOI 10.1109/MMM.2010.938568

P21. A. Ali, N. Fonseca, F. Coccetti, H. Aubert, "Design and implementation of two-layer compact wideband Butler matrices in SIW technology for Ku-band applications," IEEE Transactions on Antennas and Propagation, Vol.59, N°2, February 2011, pp.: 503-512

P22. F. Khalil, E.B. Tchikaya, R. Sharrock, T. Monteil, F. Coccetti, and H. Aubert, "Grid-based SCT Approach for the Global Electromagnetic Simulation and Design of Finite-Size and Thick Dichroïc Plate," Journal of Applied Computational Electromagnetics Society (ACES Journal) Vol.25, N°11, (10pp), November 2010

P23. S. Pacchini, E. Flahaut, N. Fabre, V. Conédéra, F. Mesnilgrente, F. Coccetti, M. Dragoman and R. Plana, "DC and radio-frequency transmission characteristics of double-walled carbon nanotubes-based ink," International Journal of Microwave and Wireless Technologies, Cambridge University Press and the European Microwave Association, 2010 pp.: 471-477

P24. L. Pierantoni, F. Coccetti, P. Russer, (Invited guest editors) "Nanoelectronics: The Paradigm Shift [From the Guest Editors' Desk]" IEEE Microwave Magazine, Vol.11, N°7, December 2010, pp.: 8-10

P25. H. El-Shaarawy, F. Coccetti, R. Plana, M.El-Said, E.A. Hashish, "Novel reconfigurable defected ground structure resonator on coplanar waveguide," IEEE Transactions on Antennas and Propagation, Vol.58, N°11, November 2010, pp.: 3622-3628

P26. M. Dragoman, A. Muller, D. Dragoman, F. Coccetti, R. Plana, "Terahertz antenna based on graphene", Journal of Applied Physics, Vol. 107, 2010 pp.: 104313

P27. U. Zaghloul, G. Papaioannou, F. Coccetti, P. Pons and R. Plana, "A systematic reliability investigation of the dielectric charging process in electrostatically actuated MEMS based on Kelvin probe force microscopy " *J. Micromech. Microeng.* 20, (2010) 064016 (12pp) doi:10.1088/0960-1317/20/6/06401

P28. U. Zaghloul, M. Koutsoureli, H. Wang, F. Coccetti, G. Papaioannou, P. Pons and R. Plana, "Assessment of dielectric charging in electrostatically driven MEMS devices: A comparison of available characterization techniques," Elsevier Journal of Microelectronics Reliability, *Vol. 50 Issues 9-11, Sept-Nov 2010 pp.: 1615-1620*

P29. M. Matmat, K. Koukos, F. Coccetti, T. Idda, A. Marty, C. Escriba, J-Y. Fourniols, D. Esteve, "Life expectancy and characterization of capacitive RF MEMS switches," Elsevier Journal of Microelectronics Reliability, *Vol. 50 Issues 9-11, Sept-Nov 2010 pp.:* 1692-1696

P30. L. Pierantoni, F. Coccetti, P. Lugli and S.M. Goodnick (Invited guest editors) "Guest Editorial of the special issue on Radio Frequency Nanoelectronics," IEEE Transaction on Microwave Theory and Technique, Vol.59, N°10, October 2011, pp.: 2566-2567

P31. U. Zaghloul, G. Papaioannou, B. Bhushan, F. Coccetti, P. Pons, R. Plana, "On the reliability of electrostatic NEMS/MEMS devices: Review of present knowledge on the dielectric charging and stiction failure mechanisms and novel characterization methodologies," Elsevier Journal of Microelectronics Reliability, *Vol. 51 Issues 9-11, Sept-Nov 2011 pp.: 1810-1818*

P32. U. Zaghloul, B. Bhushan, F. Coccetti, P. Pons, and R. Plana, "Kelvin probe force microscopy-based characterization techniques applied for electrostatic MEMS/NEMS devices and bare dielectric films to

investigate the dielectric and substrate charging phenomena," J. Vac. Sci. Technol. A 29(5), Sep/Oct 2011 - American Vacuum Society p. (17pp) 051101

P33. U. Zaghloul, B. Bhushan, P. Pons, G.J. Papaioannou, F. Coccetti, and R. Plana, "On the Influence of Environment Gases, Gas Purification and Relative Humidity on Dielectric Charging/Discharging processes in Electrostatically Driven MEMS/NEMS Devices ", *J. Nanotechnology* 22 (2011) 035705 *(22pp)*

P34. G. Monti, L. Corchia, L. Tarricone, T. Idda, F. Coccetti, R. Plana, "Broadband Compact Planar Monopole", Microwave and Optical Technology Letters Vol. 53, No. 12, December 2011 , pp. 2838-2842

P35. L. Pierantoni, F. Coccetti, (Invited guest editors) "Microwave nanopackaging and interconnects," IEEE Microwave Magazine, Vol.12, N°7, December 2011, pp.: 14-18

P36. U. Zaghloul, B. Bhushan, F. Coccetti, P. Pons and R. Plana, "Kelvin probe force microscopy-based characterization techniques applied for electrostatic MEMS/NEMS devices and bare dielectric films to investigatethe dielectric and substrate charging phenomena," J. Vac. Sci. Technol. A 29, 051101 (2011); doi:10.1116/1.3611004 (*17pp*)

P37. U. Zaghloul, G. Papaioannou, B. Bhushan, F. Coccetti, P. Pons, and R. Plana, "New insights into reliability of electrostatic capacitive RF MEMS switches," *Int. J. of Microwave and Wireless Technologies, Cambridge University Press and the European Microwave Association, September 2011, pp.: 571-586*

P38. U. Zaghloul, G.J. Papaioannou, B. Bhushan, H. Wang , F. Coccetti, P. Pons, and R. Plana (2011), "Effect of deposition gas ratio, RF power and substrate temperature on the charging/discharging processes in PECVD silicon nitride films for electrostatic NEMS/MEMS reliability using atomic force microscopy," *IEEE/ASME J. Microelectromechanical Systems* December 2011, Vol. 20, Issue 6, December 2011, pp.: 1395-1418

P39. U. Zaghloul, B. Bhushan, P. Pons, G.J. Papaioannou, F. Coccetti, and R. Plana, "Nanoscale characterization of different stiction mechanisms in electrostatically driven MEMS devices based on adhesion and friction measurements", *J. Colloid Interface Sci.* 358, 2011, pp.: 1-13 (Selected for the cover page of the journal)

P40. U. Zaghloul, G.J. Papaioannou, H. Wang, B. Bhushan, F. Coccetti, P. Pons, and R. Plana, "Nanoscale characterization of the dielectric charging phenomenon in PECVD silicon nitride thin films with various interfacial structures based on Kelvin probe force microscopy," *Nanotechnology* 22, (2011) Art. # 205708 (25pp)

P41. J. J. Ruan, N. Monnereau, D. Trémouilles, N. Mauran, F. Coccetti, N. Nolhier, and R. Plana "An Accelerated Stress Test Method for Electro-Statically Driven MEMS Devices" - IEEE Transaction on Intrumentation and Measurements, Vol. 61, NO. 2, February 2012 pp. 456-461

P42. U. Zaghloul, B. Bhushan, G. Papaioannou, F. Coccetti, P. Pons, R. Plana, "Nanotribology-based novel characterization techniques for the dielectric charging failure mechanism in electrostatically actuated NEMS/MEMS devices using force–distance curve measurements," J. Colloid Interface Sci. Vol. 365, Issue 1, January 2012, pp.: 236-253

P43. J. Ruan, D. Trémouilles, F. Coccetti, N. Nolhier, G. Papaioannou, R. Plana, "Reliability assessment of electrostatically driven MEMS devices: Based on a pulse-induced charging technique," Journal of Micromechanics and Microengineering, April 2012, Vol. 22, no. 4, 045016 (10pp) http://iopscience.iop.org/0960-1317/22/4/045016

P44. A. Broue, J. Dhennin, P.-L. Charvet, P. Pons, N. Ben Jemaa, P. Heeb, F. Coccetti and R. Plana. "Comparative study of RF MEMS micro-contact materials," International Journal of Microwave and Wireless Technologies, 1(1), pages 1-8 (2012)

P45. G. Vincenzi, G. Deligeorgis, F. Coccetti, M. Dragoman, L. Pierantoni, D. Mencarelli, R.Plana, "Extending ballistic graphene FET lumped element models to diffusive," Solid State Electronics, Vol.76, October 2012, pp.8-12

P46. G. Deligeorgis, F. Coccetti, G. Konstantinidis and R. Plana, "Radio frequency signal detection by ballistic transport in Y-shaped graphene nanoribbons," Applied Physics Letters 101, 013502 (2012)

P47. N. Torres Matabosch, F. Coccetti, M. Kaynak, B. Espana, B. Tillack, and J. L. Cazaux, "Equivalent Circuit Model of Reliable RF-MEMS switches for Component Synthesis, Fabrication process characterization and Failure Analysis, "International Journal for Microwave Wireless Technologies (JMWT) – 2013

P48. N. Torres Matabosch, F. Coccetti, M. Kaynak, B. Espana, B. Tillack, J.L. Cazaux, "Failure Analysis and Detection Methodology for Capacitive RF-MEMS Switches based on BEOL BiCMOS Process, " accepted for publication on the Journal of Microelectronic Reliability Special issues ESREF 2013

P49. M. Alexandru, T. Monteil, P. Lorenz, F. Coccetti, H. Aubert, "Large electromagnetic problem on large scale parallel computing systems, "Wiley InterScience Journal of Concurrency Computat.: Pract. Exper. 2013; 00:1–15, DOI: 10.1002/cpe

P50. D. Levasseur et al, "Systematic tuning of the conduction mechanisms in ferroelectric thin films, " accepted for pubblication on the Journal of Physics: Condensed Matter 2013

P51. M. Alexandru, T. Monteil, P. Lorenz, F. Coccetti, H. Aubert, "Full-wave Electromagnetic Complex Structures Solving by Parallel TLM on Distributed Computing Systems," submitted at IEEE Antennas and Wireless Propagation Letters (AWPL) 2013

4.4.2 International Conference Articles (peer reviewed):

C1. L. Vietzorreck F. Coccetti and P. Russer, "A numerical study of MEMS capacitive switches", In 16th Annual Review of Progress in Applied Computational Electromagnetics Monterey 20.-25, March 2000, pp.: 580-586

C2. L. Vietzorreck, F. Coccetti, V. Chtchekatourov and P. Russer, "Modelling of MEMS Capacitive Switches by TLM", In 2000 IEEE MTT-S International Microwave Symposium Digest June 11-16 Boston USA, June 2000, pp.: 1221-1224

C3. F. Coccetti L. Vietzorreck and P. Russer, "Numerical Methods for the High-Frequency Analysis of MEMS Capacitive Switches", In Proceedings of the II. Topical Meeting on Silicon Monolithic Integrated Circuits in RF Systems 26 - 28. April 2000 Garmisch Germany, April 2000, pp.: 123-124

C4. V. Chtchekatourov, F. Coccetti and P. Russer, "Direct Y-parameter Estimation of Microwave Structures Using TLM Simulation and Prony´s Method", In 17th Annual Review of Progress in Applied Computational Electromagnetics Monterey 19.-23.3.2001, March 2001

C5. V. Chtchekatourov, F. Coccetti and P. Russer, "Full-Wave Analysis and Model-Based Parameter Estimation Approaches for Y- matrix Computation of Microwave Distributed RF Circuits", In 2001 IEEE MTT-S International Microwave Symposium Digest May 20-25 Phoenix USA, May 2001

C6. V. Chtchekatourov, F. Coccetti and P. Russer, "Time-Domain Analysis of RF Structures by Means of TLM and System Identification Methods", In 31th European Microwave Conference London England 25.-27.9.2001, September 2001

C7. L. Pierantoni, M. Farina, T. Rozzi, F. Coccetti, W. Dressel and P. Russer, "Comparison of the efficiency of electromagnetic solvers in the time- and frequency-domain for the accurate modelling of planar circuits and MEMS", In 2002 IEEE MTT-S International Microwave Symposium Digest June 2002, Seattle, USA, Vol. 2, pp.: 891-894

C8. M. Al–Ahmad, F. Coccetti, M. Tentzeris and P. Russer, "Parametric Model Generation Algorithm for Planar Microwave Structures based on Full–Wave analysis and Design of Experiment", In 19th Annual Review of Progress in Applied Computational Electromagnetics (ACES) - Monterey, 2003, pp.: 751-756

C9. L. Pierantoni, M. Farina, T. Rozzi, F. Coccetti, P. Russer, N. Bushyager, M. Tentzeris, "Comparison of Electromagnetic Solvers for the Analysis of LTCC Components", In IEEE AP-S Digest, June 2003 Columbus, Ohio, USA

C10. F. Coccetti and P. Russer, " A Prony's Model Based Signal Prediction (PSP) Algorithm for Systematic Extraction of Y– Parameters from TD Transient Responses of Electromagnetic Structures ", In Mikon 2004, Warszawa May 19th 2004

C11. F. Coccetti, W. Dressel, M. Burger, J. Hasch and P. Russer, “Analysis of SOI Cavity Resonator by means of a Fully Automatic Time–Domain Response Prediction Algorithm”, European Microwave Conference 2004, Amsterdam, Netherlands, October 7-9, 2004

C12. Y. Kuznetsov, A. Baev, F. Coccetti, and P. Russer, “The Ultra Wideband Transfer Function Representation of Complex Three-Dimensional Electromagnetic Structures”, 34-th European Microwave Conference, Amsterdam, Oct. 2004

C13. F. Coccetti, B. Ducarouge, D. Dubuc, K. Grenier, R. Plana, “Power Handling RF-MEMS Switches Optimization trough a Multiphysic Numerical Environment”, MEMSWAVE 2005 Lausanne June 23 – 24, 2005

C14. F. Coccetti, B. Ducarouge, E. Schied , D. Dubuc , K. Grenier , R. Plana, “Thermal analysis of RF-MEMS switches for power handling front-end”,13th Gallium Arsenide and other Compound Semiconductors Application Symposium (GaAs’2005), Paris (France), 3-4 Octobre 2005, pp.513-516

C15. R. Plana, F. Coccetti, “RF-MEMS in Europe: a review”, Invited paper. 9th International Conference on Electromagnetics in Advanced Applications, Turin (Italie), 12-16 Septembre 2005, 3p

C16. K. Grenier, L. Mazenq, D. Dubuc, F. Bouchriha, F. Coccetti, E. Ojefors, P. Lindberg, A. Rydberg, J. Berntgen, W.J. Rabe, E. Sonmez, P. Abele, H. Schumacher, R. Plana “IC compatible MEMS technology”, 13th Gallium Arsenide and other Compound Semiconductors Application Symposium (GaAs’2005), Paris (France), 3-4 Octobre 2005, pp.293-296

C17. M. Exarchos, V. Theonas, P. Pons, G.J. Papaioannou, S. Melle, D. Dubuc, F.Coccetti, R. Plana “Investigation of charging mechanisms in metal-insulator-metal structures”, 16th European Symposium on Reliability of Electron Devices, Failure Physics and Analysis (ESREF’2005), Arcachon (France), 10-14 Octobre 2005

C18. K. Grenier, D. Dubuc, F. Coccetti, A. Coustou, D. Dragomirescu, R. Plana, “MEMS IC for RF and millimeterwave communications”, (Invited Paper) Microwave Conference Proceedings, 2005. APMC 2005. Asia-Pacific Conference Proceedings Volume 2, Suzhou, China, 4-7 Dec. 2005, 2p

C19. F. Coccetti, R. Sorrentino ,”RF-MEMS and RF-MST for advanced communication in Europe”, Mediterranean Microwave Symposium 2006 September 19-21, 2006 Genova, Italy

C20. D. Peyrou, F. Pennec, H. Achkar, P. Pons, F. Coccetti, H. Aubert, R. Plana, “BCB Based Packaging for Low Actuation Voltage RF MEMS Devices”, Symposium W: Heterogeneous Integration of Materials for Passive Components and Smart Systems. Materials Research Society Symposia Proceedings (2006), Boston (USA), 27-29 November 2006, pp.: 131-142

C21. F. Khalil, H. Aubert, F. Coccetti, R. Plana, Y. Deunneulin, B. Miegemolle, T. Monteil, H. Legay, “Electromagnetic Simulation of MEMS-Controlled Reflectarrays based on SCT in Grid Environment” - 2007 IEEE Antennas and Propagation Society International Symposium, 10-15 June, 2007, Honolulu, Hawaii USA

C22. J. Ruan, N. Nolhier, M. Bafleur, L. Bary, N. Mauran, F. Coccetti, T. Lisec and R. Plana “Dielectric Charging and ESD stress of AlN-based Capacitive RF MEMS” - 8th International Symposium on RF MEMS and RF Microsystems, MEMSWAVE 2007, June 26-29,2007, Barcelona, Spain pp.: 179-182

C23. F. Khalil, H. Aubert, F. Coccetti, R. Plana, T. Vähä-Heikkilä, and T. Lisec, ”Distributed Parametric Simulation of Complex Electromagnetic Structures in Grid Computing Environment” - 8th International Symposium on RF MEMS and RF Microsystems, MEMSWAVE 2007, June 26-29,2007, Barcelona, Spain pp. 215-218

C24. J. Bouchaud, B. Knoblich, H. Tilmans, F. Coccetti, A. El-Fatatry, “RF MEMS Roadmap”, - 8th International Symposium on RF MEMS and RF Microsystems, MEMSWAVE 2007, June 26-29, 2007, Barcelona, Spain pp.: 237-240

C25. J. Ruan, N. Nolhier, M. Bafleur, L. Bary, N. Mauran, F. Coccetti, T. Lisec and R. Plana “Failure Mechanisms of AlN based RF-MEMS Switches under DC and ESD stresses” - 14th International Symposium on the Physical and Failure Analysis of Integrated Circuits IPFA 2007, 11-13 July 2007, Bangalore, India, pp: 120-123

C26. J. Ruan, N. Nolhier, M. Bafleur, L. Bary, F. Coccetti, T. Lisec and R. Plana ,"Electrostatic Discharge Failure Analysis of Capacitive RF MEMS switches" - 18th European Symposium on Reliability of Electron Devices, Failure Physics and Analysis, ESREF 2007 Arcachon , Bordeaux, France October 8-12 2007

C27. F. Coccetti, D. Peyrou, M. Al Ahmad, P. Pons, D. Dragomirescu, H. Aubert, R. Plana „MEMS/NEMS technologies for ambient intelligence," (Invited paper) Electronics' 2007, Sozopol (Bulgarie), 19-21 September 2007, p.6

C28. J. Bouchaud, B. Knoblich, H. Tilmans, F. Coccetti, A. El Fatatry, "RF MEMS Roadmap",Proceedings of the 2nd European Microwave Integrated Circuits Conference – EuMW October 2007, Munich Germany, pp.: 343-346

C29. D. Peyrou, H. Achkar, F. Pennec, F. Coccetti, M. Al Ahmad, P. Pons, R. Plana, „TCADMEMS Overview" (Invited) at the 2007 International Semiconductor Conference. CAS 2007, Sinaia (Roumanie), 15-17 Octobre 2007, pp.: 21-24

C30. F. Coccetti, R. Plana, "Concurrent Electrothermal Experimental Analysis of RF-MEMS Switches for High Microwave Power Handling", 3rd International Conference on Micro-Nanoelectronics, Nanotechnology & MEMs NCSR Demokritos, Athens, 18 – 21 November 2007

C31. F. Coccetti, D. Peyrou, M. Al Ahmad, V. Puyal, Patrick Pons, H. Aubert and R. Plana, „RF MEMS: Status and Perspectives", (Invited) at the 3rd International Conference on Micro-Nanoelectronics, Nanotechnology & MEMs NCSR Demokritos, Athens, 18 – 21 November 2007

C32. M. Al Ahmad, F. Coccetti, R. Plana, "Piezoelectric Materials for Advanced Integrated RF Components", MRS Spring Meeting, San Francisco (USA), 2008, (12pp) 1075-J03-01

C33. D. Peyrou, F. Coccetti, F. Pennec, H. Achkar, P. Pons, R. Plana, "A new methodology for RF MEMS contact simulation", 2008 International Conference on Thermal, Mechanical and Multi-Physics Simulation and Experiments in Micro-Electronics and Micro-Systems" at 9th. Int. Conf. on Thermal, Mechanical and Multiphysics Simulation and Experiments in Micro-Electronics and Micro-Systems, EuroSimE 2008, Freiburg (Germany), 21-23 April 2008, pp.: 66-69

C34. F. Kahlil, B. Miegemolle, T. Monteil, H. Aubert, F. Coccetti, R. Plana, "Simulation of micro electro-mechanical systems (MEMS) on grid",8th International Meeting High Performance Computing for Computational Science (VECPAR'08), Toulouse (France), 24-27 June 2008, 14p

C35. F. Kahlil, C.J. Barrios-Hernandez, H. Aubert, Y. Denneulin, F. Coccetti, R. Plana, "Electromagnetic simulations via parallel computing: an application using scale changing technique for modelling of passive planar reflectarrays in grid environment", IEEE International Symposium on Antennas and Propagation, San Diego (USA), 5-12 July 2008, 4p

C36. A. Ali, F. Coccetti, H. Aubert, N. Fonseca, "Novel multi-layer SIW broadband coupler for Nolen matrix design in Ku band", IEEE International Symposium on Antennas and Propagation, San Diego (USA), 5-12 July 2008, 4p

C37. H. El-Shaarawy, F. Coccetti, R. Plana, M.El-Said, E.A.Hashish, "Miniaturized extended-stopband microstrip ring resonator bandpass filter using uniplanar compact photonic bandgap (UC-PBG) structures", 8th International Conference on Applied Informatics and Communications (AIC'08), Rhodes (Greece), 20-22 August 2008, 5p

C38. H. El-Shaarawy, F. Coccetti, R. Plana, M. El-Said, E.A. Hashish, "A novel reconfigurable DGS cell for multi-stopband filter on CPW technology", Asia Pacific Microwave Conference (APMC 2008), Hong Kong (Chine), 16-20 December 2008, 4p

C39. A. Ali, N. Fonseca, F. Coccetti, H. Aubert, "Novel two-layer broadband 4X4 butler matrix in SIW technology for Ku-band applications", Asia Pacific Microwave Conference (APMC 2008), Hong Kong (Chine), 16-20 December 2008, 4p

C40. U. Zaghloul, A. Belarni, F. Coccetti, G. Papaioannou, R. Plana, P. Pons, "Charging processes in silicon nitride films for RF-MEMS capacitive switches: the effect of deposition method and film thickness," Microelectromechanical Systems-Materials and Devices II, MRS Spring meeting 2008, Proc. Vol. 1139, pp. 141-146, Material Research Society (MRS), Pennsylvania

C41. J. Ruan, E. Papandreou. M. Lahmandi, M. Koutsoureli, F. Coccetti, P.Pons, G. Papaioannou, R. Plana "Alpha particle radiation effects in RF MEMS capacitive switches", 19th European Symposium on Reliability of Electron Devices, Failure Physics and Analysis (ESREF), Maastricht (Pays Bas), 29 September - 2 October 2008, 6p.

C42. J. Ruan, G. Papaioannou, N. Nolhier, N. Mauran, M. Bafleur, F. Coccetti, R. Plana, "ESD failure signature in capacitive RF MEMS switches," 19th European Symposium on Reliability of Electron Devices, Failure Physics and Analysis (ESREF), Maastricht (Netherland), 29 September - 2 October 2008

C43. M. Dragoman, G. Konstantinidis, D. Dragoman, D. Necoloiu, A. Cismaru, F. Coccetti, R. Plana, H. Hartnagel, A. Kostopoulos, R. Buiculescu, "RF NEMS based on carbon nanotubes and graphene," CAS 2008. International Semiconductor Conference, Sinaia (Romania), 13-15 October 2008, 4p

C44. F. Coccetti, R. Sorrentino, "RF-MEMS and RF-MST for advanced communicationsin Europe," (Invited) at the XXIX General Assembly of the International Union Radio Science (URSI) Chicago August 2008

C45. G. Papaioannou, F. Coccetti, R. Plana, "Advanced dielectric charging characterization and modeling in capacitive MEMS," atSmart System Integration (SSI 2009), Brussels Belgique), 10-11 Mars 2009, 8p

C46. B. Ouagague, F. Coccetti, R. Plana, "A modified CRLH cell optimized for easy reconfigurability,"IEEE 2009 International Symposium on Antennas and Propagation (APS 2009), Charleston (USA), 1-5 June 2009, 4p

C47. H. El-Shaarawy, F. Coccetti, R. Plana, M. El-Said, E.A. Hashish, "Novel reconfigurable multiband bandpass filter using defected ground structure on CPW technology," IEEE 2009 International Symposium on Antennas and Propagation (APS 2009), Charleston (USA), 1-5 June 2009, 4p

C48. A. Ali, H. Aubert, N. Fonseca, F. Coccetti, "Novel impact waveguide-based composite right/left-handed phase shifter with arbitrary phase shift and broad bandwith: analysis and design,"IEEE 2009 International Symposium on Antennas and Propagation (APS 2009), Charleston (USA), 1-5 June 2009, 4p

C49. F. Kahlil, A. Rashid, H. Aubert, F. Coccetti, R. Plana, C.J. Barrios-Hernandez, Y. Denneulin, "Application of scale changing technique-grid computing to the electromagnetic simulation of reflectarrays," IEEE 2009 International Symposium on Antennas and Propagation (APS 2009), Charleston (USA), 1-5 June 2009, 4p

C50. U. Zaghloul, A. Belarni, F. Coccetti, G.J. Papaioannou, L. Bouscayrol, P. Pons and R. Plana, "A comprehensive study for dielectric charging process in silicon nitride films for RF MEMS switches using Kelvin Probe Microscopy, " The 15th International Conference on Solid-State Sensors, Actuators and Microsystems (Transducers 2009), Denver (USA), 21-25 June 2009, pp.: 789-793

C51. J. Ruan, G.J. Papaioannou, N. Nolhier, M. Bafleur, F. Coccetti, R. Plana "ESD stress in RF-MEMS capacitive switches: the influence of dielectric material deposition method, " International Reliability Physics Symposium (IRPS 2009), Montréal (Canada), 2630 April 2009, pp.: 568-572

C52. R. Sharrock, F. Khalil, T.Monteil, H.Aubert, F.Coccetti, P.Stolf, R.Plana, "Deployment and management of large planar reflectarray antennas simulation on grid," Challenges of Large Applications in Distributed Environments (CLADE), Munich (Allemagne), 9-10 June 2009, pp.: 17-26

C53. H. El-Shaarawy, F. Coccetti, R. Plana, M. El-Said, E.A. Hashish, "Analysis and design of a novel reconfigurable defected ground structure resonator on CPW technology,"Progress in Electromagnetics Research Symposium (PIERS 2009), Beijing (Chine), 23-27 March 2009, 2p

C54. B. Ouagague, F. Coccetti, R. Plana, "Novel CRLH cell based on robust planar design in CPW technology,» 3rd International Congress on Advanced Electromagnetic Materials in Microwaves and Optics (METAMATERIALS 2009), London (GB), 30 August - 4 September 2009, pp.: 713-715

C55. U. Zaghloul, G. Papaioannou, F. Coccetti, P. Pons and R. Plana, "Effect of Humidity on Dielectric Charging Process in Electrostatic Capacitive RF MEMS Switches Based on Kelvin Probe Force Microscopy Surface Potential Measurements," Microelectromechanical Systems-Materials and Devices III, MRS Fall Meeting Proc. Vol. 1222, Material Research Society(MRS), Pennsylvania, pp.: 39-44

C56. A. Ali, H. Aubert, N. Fonseca, F. Coccetti, "Novel compact three-layer wideband phase shifter in SIW technology," Progress in Electromagnetic Research Symposium (PIERS 2009), Moscow (Russia), 18-21 August 2009, 2p

C57. H. El-Shaarawy, F. Coccetti, R. Plana, M.El-Said, E.A. Hashish, "Novel compact defected ground structure based filters on coplanar waveguide,"Progress in Electromagnetic Research Symposium (PIERS 2009), Moscow (Russia), 18-21 August 2009, 3p

C58. J. Ruan, G.J. Papaioannou, N. Nolhier, D. Trémouilles, F. Coccetti, R. Plana, "Temperature dependence of ESD charging in RF MEMS capacitive Switch," Proceedings of the 4th European Microwave Integrated Circuits Conference 28-29 September 2009, Rome, Italy, pp.: 93-96

C59. M. Matmat, F. Coccetti, A. Marty, R. Plana, C. Escriba, J.Y. Fourniols, D. Esteve, "Capacitive RF MEMS analytical predictive reliability," European Symsposium on Reliability of Electron Devices, Failure Physics and Analysis October 2009 5th - 9th Arcachon – France

C60. U. Zaghloul, A. Belarni, F. Coccetti, G.J. Papaioannou, L. Bouscayrol, P. Pons and R. Plana, "Kelvin probe microscopy for dielectric charging assessment in silicon nitride films for RF MEMS switches," MicroMechanics Europe 2009, September 20-22, 2009, Toulouse, France

C61. A. Belarni, U. Zaghloul, G. Papaioannou, F.Coccetti, P. Pons, R. Plana, "Deposition Conditions on Charging Process in Silicon Nitride Films Based on Kelvin Probe Microscopy," Proceedings of the 10th International Symposium on RF MEMS and RF Microsystems (MEMSWAVE 2009) Trento – Italy July 6-8, 2009 pp.: 95-98

C62. U. Zaghloul, G. Papaioannou, F. Coccetti, P. Pons, R. Plana, "Investigation of Dielectric Charging in Low Frequency PECVD Silicon Nitride Films for MEMS Capacitive Switches," Proceedings of the 10th International Symposium on RF MEMS and RF Microsystems (MEMSWAVE 2009) Trento – Italy July 6-8, 2009 pp. : 125-128

C63. U. Zaghloul, G. Papaioannou, F. Coccetti, P. Pons, and R. Plana, "Dielectric charging in silicon nitride films for MEMS capacitive switches: effect of film thickness and deposition conditions," Proc. of the 20th European Symposium on Reliability of Electron Devices, Failure Physics and Analysis (ESREF 2009), 5-9 October 2009, Arcachon, France, pp. 1309-1314

C64. J.J. Ruan, G.Papaioannou, N. Nolhier, D. Trémouilles, F. Coccetti, R, Plana, "Charging and discharging studies in microwave capacitive switches under high field pulse discharges," 10th Topical Meeting on Silicon Monolithic Integrated Circuits in RF Systems (SIRF 2010), New Orleans (USA), 11-13 January 2010, pp.:140-143

C65. G. Papaioannou, F. Coccetti, and R. Plana, "On the Modelling of Dielectric Charging in RF-MEMS Capacitive Switches," 10th Topical Meeting on Silicon Monolithic Integrated Circuits in RF Systems (SIRF 2010), New Orleans (USA), 11-13 January 2010, pp. 108-111

C66. U. Zaghloul, F. Coccetti, G. Papaioannou, P. Pons and R. Plana, "A novel low cost failure analysis technique for dielectric charging phenomenon in electrostatically actuated MEMS devices," 2010 IEEE Int. Reliability Physics Symp., IEEE, New York pp. 237-245

C67. M. Matmat, K. Koukos, F. Coccetti, T. Idda, A. Marty, C. Escriba, J-Y. Fourniols, D. Esteve, "Life expectancy and characterization of capacitive RF MEMS switches," 21st European Symposium on Reliability of Electron Devices, Failure Physics and Analysis (ESREF 2010), 11th - 15th October 2010, Gaeta – Italy

C68. U. Zaghloul, M. Koutsoureli, H. Wang, F. Coccetti, G. Papaioannou, P. Pons and R. Plana, "Assessment of dielectric charging in electrostatically actuated MEMS devices: A comparison of available characterization techniques," 21st European Symposium on Reliability of Electron Devices, Failure Physics and Analysis (ESREF 2010), 11th - 15th October 2010, Gaeta – Italy

C69. G. Papaioannou, F. Coccetti, and R. Plana, "Modeling of Dielectric Charging in MEMS Capacitive Switches," Proceedings of the 11th International Symposium on RF MEMS and RF Microsystems MEMSWAVE - Otranto, ITALY June 28-29-30, 2010

C70. J. J. Ruan, C. Villeneuve, F. Coccetti, P. Pons, N. Nolhier, R. Plana, "Push-Pull Seesaw Principle Capacitive RF-MEMS Shunt Switch," Proceedings of the 11th International Symposium on RF MEMS and RF Microsystems Otranto, MEMSWAVE - ITALY June 28-29-30, 2010

C71. A. Mardivirin, S. Courrèges, P. Blondy, F. Coccetti, R. Plana, "Successive Conduction Modes in Si3N4 Capacitive RF-MEMS," Proceedings of the 11th International Symposium on RF MEMS and RF Microsystems Otranto, MEMSWAVE - ITALY June 28-29-30, 2010

C72. N. Torres Matabosch, F. Coccetti, R.Plana, B.Reig and JL. Cazaux, "High Isolation T-switch for reconfigurable switching Matrix, "Proceedings of the 11th International Symposium on RF MEMS and RF Microsystems Otranto, MEMSWAVE - ITALY June 28-29-30, 2010

C73. M. Dragoman, D. Dragoman, F. Coccetti, R. Plana, "Carbon Nanotube Based Microwave Resonators," USNC/URSI National Radio Science Meeting, July 11 - 17, 2010 Toronto, Ontario, Canada.

C74. B. Ouagague, F. Coccetti, C. Villeneuve, R. Plana, "Experimental Study of a Modified Silicon-Based CRLH Cell for Enhanced Reconfigurability," 2010 IEEE AP-S International Symposium on Antennas and Propagation, July 11 - 17, 2010 Toronto, Ontario, Canada

C75. A. Ali, N. J. G. Fonseca, F. Coccetti and H. Aubert, "Analysis and Design of a Compact SIW-Based Multi-layer Wideband Phase Shifter for Ku-band Applications," 2010 IEEE AP-S International Symposium on Antennas and Propagation, July 11 - 17, 2010 Toronto, Ontario, Canada.

C76. H.B. El-Shaarawy, F. Coccetti, and R. Plana, "A Novel Compact Reconfigurable Defected Ground Structure Resonator on Coplanar Waveguide Technology for Filter Applications," 2010 IEEE AP-S International Symposium on Antennas and Propagation, July 11 - 17, 2010 Toronto, Ontario, Canada

C77. Mardivirin, S. Courrèges, A. Crunteanu, A. Pothier, P. Blondy, F. Coccetti and R. Plana, "Evidence of Successive Fowler-Nordheim and Frenkel-Poole Conductions in Si3N4 Based RF-MEMS Capacitive Switches," Proceedings of the 40th European Microwave Conference 28-30 September 2010, Paris, France, pp: 513-516

C78. J. J. Ruan, G. J. Papaioannou, D. Trémouilles, N. Nolhier, F. Coccetti, R. Plana, "Pulse Induced Charging Tests in Capacitive RF-MEMS Switches," Proceedings of the 40th European Microwave Conference 28-30 September 2010, Paris, France, pp: 517-520

C79. B. Ouagague, F. Coccetti, C. Villeneuve, T. Idda, R. Plana, " Reconfi gurable CRLH Cells with New Open-End Stub and RF MEMS Switches on Silicon Technology, " Proceedings of the 40th European Microwave Conference 28-30 September 2010, Paris, France, pp: 1405-1408

C80. A. Broue, J. Dhennin, P.-L. Charvet, P. Pons, N. Ben Jemaa, P. Heeb, F. Coccetti, R. Plana, "Multi-physical characterization of micro-contact materials for MEMS switches," Electrical Contacts (HOLM), 2010 Proceedings of the 56th IEEE Charleston, SC - 4-7 Oct. 2010 pp.: 1 – 10

C81. U. Zaghloul, B. Bhushan, P. Pons, G.J. Papaioannou, F. Coccetti, and R. Plana, "On the Impact of Relative Humidity and Environment Gases on Dielectric Charging Process in Capacitive RF MEMS Switches Based on Kelvin Probe Force Microscopy," AVS 57th International Symposium & Exhibition October 17-22 2010 Albuquerque USA

C82. S. Pacchini, V. Conedera, F. Mesnilgrente, N. Fabre, E. Flahaut, F. Coccetti, M. Dragoman, R. Plana, "Tunability of Carbon NanoTubes Resistance Deposited by Inkjet Printing at Low Temperature," MRS Spring meeting 2010, Proc. Vol. 1258-R10-15

C83. U. Zaghloul, G. Papaioannou, B. Bhushan, F. Coccetti, P. Pons, R. Plana (Invited), "On the reliability of electrostatic NEMS/MEMS devices: Review of present knowledge on the dielectric charging and stiction failure mechanisms and novel characterization methodologies," 22nd European Symposium on Reliability of Electron Devices, Failure Physics and Analysis (ESREF 2011), 3rd-7th October 2011, Bordeaux – France

C84. U. Zaghloul, B. Bhushan, P. Pons, G. Papaioannou, F. Coccetti, and R. Plana, "Nanoscale characterization of different stiction mechanisms in electrostatic RF-MEMS switches", Proc. of the 41st European Microwave Conference, October 9-14 2011, Manchester, UK, pp. 478- 481

C85. S. Pacchini, V. Conedera, F. Mesnilgrente, N. Fabre, E. Flahaut, F. Coccetti, M. Dragoman, R. Plana, "Room temperature ink-jet printed carbon nanotube networks for high frequency flexible electronics," MRS Spring meeting & Exhibit 2011, Proc. San Francisco (USA) April 2011 (1p)

C86. R. De Paolis, S. Pacchini, F. Coccetti, G. Monti, L. Tarricone M.M. Tentzeris and R. Plana, "Circuit model of carbon-nanotube inks for microelectronic and microwave tunable devices," International

Microwave Symposium Digest (MTT), 2011 IEEE MTT-S International, 5-10 June 2011, Baltimore, MD pp.: 1-4

C87. U. Zaghloul, B. Bhushan, P. Pons, G. Papaioannou, F. Coccetti, and R. Plana, "Different Stiction Mechanisms In Electrostatic MEMS Devices: Nanoscale Characterization Based On Adhesion And Friction Measurements," the 16th Int. Conf. On Solid-State Sensors, Actuators and Microsystems (TRANSDUCERS 2011), IEEE, New York

C88. U. Zaghloul, G. Papaioannou, B. Bhushan, P. Pons, F. Coccetti and R. Plana, "Effect of working environment on stiction mechanisms in electrostatic RF-MEMS Switches," Proceedings of the 12th International Symposium on RF MEMS and RF Microsystems MEMSWAVE - Athens June 28-29-30, 2010, (4pp)

C89. M. A. Llamas, D. Girbau, M. Ribó, L. Pradell, F. Giacomozzi, S. Colpo, F. Coccetti, S. Aouba, "A highly-repeatable, broadband 180º phase switch for integrated MEMS processes," Proceedings of the 12th International Symposium on RF MEMS and RF Microsystems MEMSWAVE - Athens June 28-29-30, 2010, (4pp)

C90. D. Mencarelli, T. Rozzi, L. Pierantoni, F. Coccetti, "Self-consistent simulation of local potential in external-gate biased graphene nanoribbons," XXX General Assembly and Scientific Symposium of the International Union of Radio Science (GA-URSI) Istanbul, Turkey on August 13-20, 2011

C91. L. Pierantoni, D. Mencarelli, T. Rozzi, and F. Coccetti, "Analysis of the Electromagnetic/Coherent Transport Problem in Graphene Nanoribbons," XXX General Assembly and Scientific Symposium of the International Union of Radio Science (GA-URSI) Istanbul, Turkey on August 13-20, 2011

C92. M. Alexandru, T. Monteil, F. Coccetti, P. Lorenz, and H. Aubert ,"Efficient large electromagnetic problem solving by hybrid TLM and modal approach on grid computing" International Microwave Symposium (IMS 2012), Montréal (Canada), 17-22 Juin 2012, 4pp

C93. N. Torres Matabosch, F. Coccetti, M. Kaynak, W. Zhang, B. Tillack and J. L. Cazaux, "An Accurate Equivalent Circuit Model for RFMEMS Circuit Optimization and Fabrication Process Monitoring in BiCMOS Technology," Proceedings of the 13th International Symposium on RF MEMS and RF Microsystems Antalys, MEMSWAVE - Turkey July 2-4, 2012

C94. N.Torres Matabosch, F. Coccetti, B.Reig ,C.Dieppedale, H.Sibuet, C.Billard, F.Deborgies and J.L.Cazaux, "DC-50GHz RF-MEMS SPDT switch for High Reliability applications," Proceedings of the 13th International Symposium on RF MEMS and RF Microsystems Antalya, MEMSWAVE - Turkey July 2-4, 2012

C95. L. Pierantoni, D. Mencarelli, F. Coccetti, "Advanced modeling of graphene nanodevices: metal-carbon transition and patch antennas, " in proceedings of the 7th European Conference on Antennas and Propagation, 8-12 April 2013 Gothenburg, Sweeden

C96. F. Coccetti, R. Plana and G. Deligeorgis, "Modeling and optimization of a RF ballistic graphene demodulator, " in proceedings of IEEE International Microwave Symposium Seattle 1-7 June 2013

C97. R. De Paolis, T. Li, F. Coccetti, G. Monti, L. Tarricone, M. Tentzeris, R. Plana , "A Novel Circuit Model of Nanotechnology-Enabled Inkjet-Printed Gas Sensors Using Multi-Wall Carbon Nanotubes", in proceedings of IEEE International Microwave Symposium Seattle 1-7 June 2013

C98. N. Torres Matabosch, F. Coccetti, M. Kaynak, B. Espana, B. Tillack, and J. L. Cazaux, "Fast and Non Intrusive Failure Analysis of BiCMOS RF-MEMS, " in Proceedings of the MEMSWAVE 2013 Postadam, Germany 2-4 July 2013

C99. N. Torres Matabosch, F. Coccetti, M. Kaynak, B. Espana, B. Tillack, and J. L. Cazaux, "Fast and Non Intrusive Failure Analysis of BiCMOS RF-MEMS," in proceedings of the 24th European Symposium on Reliability of Electron Devices, Failure Physics and Analysis, 30 Sept. -4 Oct. 2013, Archachon, France

C100. R. De Paolis, F. Coccetti, S. Payan, A. Rousseau, M. Maglione, G. Guegan, "Microwave Characterization of Ferroelectric Thin Films for Novel Compact Tunable BST Filters, " in proceedings of the 43th European Microwave Conference Nuremberg 6-11 October 2013

4.4.3 National Conferences (peer reviewed):

N1. V. Chtchekatourov, L. Vietzorreck, W. Fisch, F. Coccetti and P. Russer, "Time-Domain System Identification Modelling for Microwave Structures," Kleinheubacher Berichte, Kleinheubach, Germany, Sep 25-29, 2000

N2. L. Pierantoni, M. Farina, T. Rozzi, F. Coccetti, W. Dressel and P. Russer, "Comparison of the Efficiency of E.M. Solvers in the Time-and Frequency-Domain for the Accurate Modeling of Planar Circuits and MEMS", in XIV Riunione Nazionale di Elettromagnetismo (RiNEM), 16-19 Settembre 2002, Ancona, pp. 464-467

N3. F. Coccetti, W. Dressel, P. Russer, L. Pierantoni, M. Farina, T. Rozzi, "An accurate Time and Frequency domain modeling of high frequency microelectromechanical (MEMS) swicthes," Kleinheubacher Berichte, Miltenberg, Germany, Sep 30 - Oct 2, 2002

N4. P. Russer and F. Coccetti, "Network Methods in Electromagnetic Field Computation", In Proceedings of the 2nd National Congress of URSI in Turkey, Bilkent University, Ankara, Turkey, 8 - 10 September 2004, September 2004, pages 2-18

N5. F. Coccetti, B. Ducarouge, E. Scheid, D. Dubuc, K. Grenier, R. Plana „Analyse thermique expérimentale de MEMS-RF de puissance", XIVe Journées Nationales Microondes (JNM'2005), Nantes (France), 11-13 Mai 2005

N6. B. Ducarouge, F. Coccetti, L. Mazenq,L. Bary, J. Rayssac, D. Dubuc, K. Grenier, R. Plana, „Conception et caractérisation de MEMS-RF de puissance", XIVe Journées Nationales Microondes (JNM'2005), Nantes (France), 11-13 Mai 2005

N7. J. Ruan, N. Nolhier, M. Bafleur, L. Bary, F. Coccetti, R. Plana, „Analyse des propriétés électriques de MEMS RF sous contraintes DC et décharges électrostatiques", 15èmes Journées Nationales Micro-ondes (JNM'2007), Toulouse (France), 23-25 Mai 2007, 4p

N8. F. Khalil, F. Coccetti, H. Aubert, R. Plana, Y. Denneulin, B. Miegemolle, T. Monteil, „Etude des potentialités du concept de grille de calcul pour la simulation électromagnétique de micro-systèmes complexes" 15èmes Journées Nationales Micro-ondes (JNM'2007), Toulouse (France), 23-25 Mai 2007, 4p

N9. J. Ruan, N. Nolhier, F. Coccetti, G. Papaioannou, R. Plana "Analyse de défaillance des MEMS RF capacitifs sous décharges électrostatiques », LAAS No08455 11e Journées Nationales du Réseau Doctoral en Microélectronique (JNRDM), Bordeaux (France), 14-16 Mai 2008, 3p

N10. H. B. El-Shaarawy, B. Ouagague, F. Coccetti, R. Plana, M. El-Said, E. A. Hashish, "Miniaturisation d'un filtre à résonateur en anneau en utilisant des stubs repliés et des « DGS » circulaires", 16èmes Journées Nationales Micro-ondes (JNM'2009), Grenoble (France), 27-29 Mai 2009, 4p

N11. H.B. El-Shaarawy, B. Ouagague, F. Coccetti, R. Plana, M. El-Said, E. A. Hashish, "Filtre multi coupe-bande reconfigurable utilisant un nouveau résonateur à base de structure à plan de masse usiné en technologie CPW", 16èmes Journées Nationales Micro-ondes (JNM'2009), Grenoble (France), 27-29 Mai 2009, 4p

N12. B. Ouagague, F. Coccetti, R. Plana, "Etude d'une structure CRLH optimisée", 16èmes Journées Nationales Micro-ondes (JNM'2009), Grenoble (France), 27-29 Mai 2009, 4p

N13. Ali, N. Fonseca, F. Coccetti, H. Aubert, "Nouvelles structures passives bicouches à base de GIS pour des matrices de répartitions multifaisceaux compactes", 16èmes Journées Nationales Micro-ondes (JNM'2009), Grenoble (France), 27-29 Mai 2009, 4p

N14. J. Ruan, N. Nolhier, G. Papaioannou, D. Tremouilles, F. Coccetti, R. Plana, "La fiabilité d'un MEMS-RF capacitif en bande W sous décharges électrostatiques", 16èmes Journées Nationales Micro-ondes (JNM'2009), Grenoble (France), 27-29 Mai 2009, 4p

N15. F. Khalil, C.J. Barrios-Hernandez, H. Aubert, Y. Denneulin, F. Coccetti, R. Plana, "Simulations Electromagnétiques Distribuées sur une Grille de Calcul", 16èmes Journées Nationales Micro-ondes (JNM'2009), Grenoble (France), 27-29 Mai 2009, 3p

N16. K. Makasheva, H. Wang, B. Despax, F. Coccetti, L. Boudou, G. Teyssedre "New materials versus new design: study on the physico-chemical and electrical properties of thin SiOxNy layers for their use in RF-MEMS switches," Conférence sur les Matériaux du génie Electrique, MGE 2010, Montpellier, France, Sept. 2010.

N17. S. Pacchini, V. Conedera, E. Flahaut, G. Droval, A. Rumeau, F. Coccetti, M. Dragoman, R. Plana, "Carbon nanotube networks for High frequency electronics," Colloque annuel du GDR-I GNT : Graphène et Nanotubes, Dourdan (France), 7-12 February 2011 (1p)

N18. R. De Paolis, F. Coccetti, S. Payan, A. Rousseau, M. Maglione, G. Guegan, R. Plana, "Filtre compact accordable en fréquence intégrant des capacités BST, " , in proceedings of18èmes Journées Nationales Microondes, 15-16-17 Mai 2013 - Paris

4.4.4 Book Chapters

B1. F. Coccetti and P. Russer "Application of System Identification to Time-Domain Modelling of Electromagnetic Structures" In Fields, Networks, Methods, and Systems in Modern Electrodynamics, Springer, Berlin, 2004, pages 143-156

B2. F. Coccetti, "Application of System Identification (SI) to Full–Wave Time Domain Characterization of Microwave and Millimeterwave Passive Structures", Dissertation an der Technischen Universität München, Lehrstuhl für Hochfrequenztechnik, München, 2004

B3. J. Bouchaud, B. Knoblich, H. Tilmans, F. Coccetti, A. El Fatatry,"RF MEMS Roadmap", Chapter of the book "Advanced RF-MEMS" - Editor Stepan Lucyskyn - by Cambridge Press (June 2010)

B4. F. Coccetti, R. Plana, "RF Power handling" Chapter of the book "Advanced RF-MEMS" - Editor Stepan Lucyskyn - by Cambridge Press – (June 2010)

4.4.5 Workshops and Seminars

W1. F. Coccetti, W. Dressel, L.Vietzorreck and P.Russer RF Theory and Modeling of Transitions and Interconnects In Workshop Proceedings EuMC 2003, Munich, October 2003

W2. F. Coccetti, W. Dressel, "Time-Domain Modeling of RF MEMS (Switches)" In Workshop Proceedings IMS - Philadelphia June 2003

W3. F. Coccetti, P. Russer, "Application of System Identification to Time Domain Modeling of Electromagnetic Structures" Workshop in honor of Prof. Leopol Felsen at TUM Munich Germany 1-2 June 2004

W4. D. Lukashevich, F. Coccetti, P. Russer, "System Identification and Model Order Reduction for TLM Analysis of Microwave Components", proceedings of the 2005 Workshop on Computational Electromagnetics in Time-Domain - CEM-TD 2005 Georgia Tech, Atlanta, GA, U.S.A, September 12 - 14, 2005 pp. 64-67

W5. K. Grenier, D. Dubuc, N. Do, J.P. Busquere, F. Coccetti, A. Coustou, D. Dragomirescu, R. Plana, "MEMS IC concept for advanced RF and millimeterwave communications", Radio-Frequency Integration Technology: Integrated Circuits for Wideband Communication and Wireless Sensor Networks, 2005. Proceedings. 2005 IEEE International Workshop on 30 Nov.-2 Dec. 2005 pp: 135 – 138

W6. F. Coccetti, B. Ducarouge, D. Dubuc, K. Grenier, and R. Plana, " Power Handling Optimisation of RF-MEMS Devices by means of a Multiphysic Numerical Environment", The AMICOM DTIP 2005 workshop May 31st, 2005 - Montreux, Switzerland

W7. F. Coccetti, "Micro and Nanosystems for Wireless communications", presented at Electronica 2006 Nov. 14-17, 2006 Munich, Germany

W8. F. Coccetti and R. Plana, "RF MEMS reliability under high power stress: characterization and modelling," at the RF-MEMS workshop on industrial applications : RF power MEMS : Reliability and Applications during the MEMSWAVE 2007 in Barcellona June 2007

W9. R. Sorrentino, F. Coccetti, "Advantages of RF-MEMS and RF Microsystemtechnology though AMICOM NoE" (R. Sorrentino invited talk) at The Second European Conference on Antennas and Propagation (EuCAP 2007) 11 - 16 November 2007, EICC, Edinburgh, UK

W10. F. Coccetti, "Metrology issues in RF-MEMS" round table at the NEXUSplus Experts Workshop on metrology and design-for-purpose 19 May 2008 Loughborough, UK

W11. F. Coccetti, "RF-MEMS Reliability" at MNT Reliability Workshop MAY 29-30 2008 CANEUS 2008 - CNES Toulouse, France

W12. F. Coccetti, G.J. Papaioannou, R. Plana, "New tool and methods to assess failure mechanisms in RF-MEMS," in workshop proceedings, European Microwave Week, Rome, 28th Sept. – 2cd Oct. 2009

W13. F. Coccetti, course on "Microwave and millimeter wave MEMS" at the NAMIS AUTUMN SCHOOL 14- 18 September 2009 LAAS-CNRS Toulouse France

W14. M.M. Jatlaoui, F. Chebila, P. Pons, H. Aubert, F. Coccetti, G.J. Papapioannou, M. Dragoman, D. Necoloiiu, D. Dragoman, A. Muller, G. Konstantinidis, R. Plana, "Micro and nanoengineering of electromagnetic energy: applications to sensors, communications, scavenger," Joint IFIN-HH, ICTP, IAEA Workshop on Trends in Nanoscience: Theory, Experiment, Technology, Sibiu (Romany), 23-30 August 2009, 1p

W15. M.M. Jatlaoui, F. Chebila, P. Pons, H. Aubert, F. Coccettti, "RF MEMS/NEMS technologies for advanced sensors and scavengers," Joint IFIN-HH, ICTP, IAEA Workshop on Trends in Nanoscience: Theory, Experiment, Technology, Sibiu (Romany), 23-30 August 2009, 2p

W16. G. Deligeorgis, S. Pacchini, M. Dragoman, G. Konstantinidis, F. Coccetti and R. Plana, "Carbon based devices for RF applications", European Symposium on Carbon-based Electronics, Aachen, 13-14 July, 2010

W17. L. Pierantoni, F. Coccetti, "The IEEE Microwave Theory and Techniques Technical Committee "RF Nanotechnology": Mission and Perspectives in the European Area", European Symposium on Carbon-based Electronics, Aachen, 13-14 July, 2010

W18. F. Coccetti, "Exploring nanostructured materials for sensing and communication applications" In Workshop Proceedings IMS 2010 – Anaheim June 2010

W19. A. Rumiantsev, F. Coccetti, L. Bary, S. Giessmann, F.M. Werner, "Wafer-Level Testing of MEMS Devices in Controlled Vacuum Environment," Microtech 2010 Conference & Expo, June 21-24, 2010, Anaheim, CA

W20. M. Alexandru, T. Monteil, F. Coccetti, P. Lorenz and H. Aubert, "Transmission-line modelling computational electromagnetic on grids, "Present challenges in computational electromagnetics: complexity management multi-scales multi-physics uncertainty management statistics, Saint Malo (France), 2-3 December 2010

W21. F. Coccetti, "Advanced Techniques for reliability assessment of RF-MEMS devices: focus on contact physics in resistive and capacitive switches," in proceeding of the EuMC/EuMIC WS on « Applications of RF MEMS », at the 41st European Microwave Conference, October 9-14 Manchester, UK

W22. A. Ali, F. Coccetti, H. Aubert, "Novel Wideband Microwave Components, Interconnects and Subsystems in Multi-Layer SIW Technology," in proceeding of the EuMC WS on « Substrate Integrated Waveguide (SIW) Technology and Applications », at the 41st European Microwave Conference, October 9-14, Manchester, UK

W23. L. Pierantoni, F. Coccetti, "Multiphysics Modeling of the Electromagnetic-Coherent Transport Phenomena in RF in Nanodevices", Proceedings of the 11th Intern. Workshop on Nanoscience & Nanotechnology, Frascati, Italy, pp. 60, Sept 19-23, 2011

W24. S. Pacchini, F. Coccetti, N. Fabre, E. Flahaut, R. Plana, “Printed CNT network and interconnects,” in the workshop proceedings of the International Microwave Symposium (MTT), 2011 IEEE MTT-S International, 5-10 June 2011, Baltimore, MD

W25. G. Delegeorgis, F. Coccetti, M. Dragoman, G. Konstantinidis, R. Plana, “Progress in graphene based devices and sensors,” in the workshop proceedings of the International Microwave Symposium (MTT), 2011 IEEE MTT-S International, 5-10 June 2011, Baltimore, MD

W26. F. Coccetti, ”News: IEEE TC ”RF Nanotechnology” in the proceedings of the European RF-MST CLUSTER WORKSHOP Athens, Greece, 27th of June, 2011

W27. F. Coccetti, ”Radio Frequency Nanotechnology: A New Paradigm in Electronic Systems Design,” at the SEMINARS on Emerging Micro-Nano Technologies for RF Applications 11 August 2011, Thursday, Middle East Technical University Dept. of Electrical & Electronics Eng., Ankara

W28. F. Coccetti, ”Tools and methodologies for RF-MEMS reliability assessment,”Workshop (Full Day) at the XXX General Assembly and Scientific Symposium of the International Union of Radio Science (Union Radio Scientifique Internationale-URSI) Istanbul, Turkey on August 13-20, 2011. Organizer(s): O. Aydin Civi (METU Ankara, Turkey), F. Coccetti (LAAS-CNRS Toulouse, France), G. Papaioannou (NKUA Athen, Greece)

W29. J. Dhennin, C. Seguineau, A. Broué, F. Coccetti, F. Courtade, ,” MEMS Switches: Status on reliability Issues and Characterization Techniques,” 8th ESA Round Table on Micro and Nano Technologies for Space Applications, 15-18 October 2012 at ESA/ESTEC, Noordwijk, The Netherlands

W30. F. Coccetti, ”Technologie MEMSRF: état d’avancement et commercialisation,” invited at the Le salon des radiofréquences, des hyperfréquences, du wireless et de la fibre optique, 10 & 11 avril 2013 Paris Expo - Porte de Versailles